Studies on Oil-Water Separation using Functionalized Magnetic Nanoparticle Dispersed Polymeric Membranes

Thesis Submitted in Partial Fulfilment of the Requirements

for the Degree of

DOCTOR OF PHILOSOPHY

by

Pankaj Boruah

(Roll No. 166107115)

DEPARTMENT OF CHEMICAL ENGINEERING

INDIAN INSTITUTE OF TECHNOLOGY GUWAHATI

GUWAHATI-781039

October 2023

Dedicated to

My Beloved Parents

for their

Endless Love, Sacrifice and Support

Department of Chemical Engineering
Indian Institute of Technology Guwahati

DECLARATION

I do hereby declare that the content embodied in this thesis entitled **"Studies on Oil-Water Separation using Functionalized Magnetic Nanoparticle Dispersed Polymeric Membranes"** is carried out by me at the Department of Chemical Engineering, Indian Institute of Technology Guwahati, under the supervision of Prof. Vimal Katiyar and Dr. Raghvendra Gupta. The results documented in this thesis are achieved by me and have not been submitted to any other University or Institute for the award of any degree or diploma.

Pankaj Boruah
Roll no.: 166107115
Department of Chemical Engineering
Indian Institute of Technology Guwahati
Guwahati -781 039, India

Department of Chemical Engineering
Indian Institute of Technology Guwahati

CERTIFICATE

This is to certify that the thesis entitled **"Studies on Oil-Water Separation using Functionalized Magnetic Nanoparticle Dispersed Polymeric Membranes"** is being submitted by **Pankaj Boruah** for the award of Ph.D. The degree has been carried out by him at the Department of Chemical Engineering, Indian Institute of Technology Guwahati, under our guidance and supervision. The work documented in this thesis has not been submitted to any other University or Institute for the award of any degree or diploma.

Dr. Vimal Katiyar
Professor
Department of Chemical Engineering
Indian Institute of Technology Guwahati
Guwahati-781039, India

Dr. Raghvendra Gupta
Associate Professor
Department of Chemical Engineering
Indian Institute of Technology Guwahati
Guwahati-781039, India

Acknowledgement

I would like to sincerely express my deepest sense of gratitude and appreciation to my thesis supervisors Prof. Vimal Katiyar and Dr. Raghvendra Gupta, for their inspiration and valuable guidance throughout the research period. I am indebted for their constructive criticism, encouragement, and advice to carry out and complete my research work. My ability to improve the calibre of my research work has been greatly aided by their genuine scientific attitude, support, and time-to-time suggestions. I consider it as a great privilege to be mentored by them. This research work carried out under their guidance helped me to generate a lot of fresh ideas and thoughts, which improved my aptitude for science. This would not have happened without their constant direction as well as their moral support.

I would also like to acknowledge my doctoral committee members, Prof. S Senthilmurugan, Dr. Uttam Manna and Dr. Amit Kumar, for their insightful advice, encouraging words and constructive criticism when evaluating my PhD programme, which helped me in improving the quality of the work. I would especially like to thank Prof. S Senthilmurugan for allowing me to carry out sample analysis in his lab and Mr. Priyamjeet Deka for assisting me in carrying out the sample analysis. I would like to thank the Centre of Excellence for Sustainable Polymers (CoE-SusPol), the Centre for Sustainable Polymers and Central Instruments Facility (CIF) for research and analytical facilities and Lakhminath Bezborua Central Library IIT Guwahati for facilitating various resources. I would like to thank all the staff of CIF IIT Guwahati for their support in carrying out the analysis using different instruments. Here, I would like to especially acknowledge Dr. Dolly Gogoi (Technical Officer, CIF IIT Guwahati) and Mr. Madhurjya Borah (Technical Superintendent, CIF IIT Guwahati) for offering their valuable time and support in carrying out the research work. I would also like to thank the present and past heads of the Department of Chemical Engineering for providing me with all the research and analytical

facilities required for my work. I am extremely thankful to the technical and non-technical staff of the Department of Chemical Engineering for their help and assistance in the successful completion of my work. I am also thankful to the Central Workshop of IIT Guwahati for helping me to fabricate parts of the experimental setup, which was essential to complete the research work.

I sincerely thank Prof. Shinichi Sakurai and Prof. Sono Sasaki of the Department of Biobased Material Science, Kyoto Institute of Technology, Japan, for providing the opportunity to work in their laboratories and for all the support provided during my stay in Japan. I am also thankful to Dr. Amit Pandey for his help during my stay at KIT Japan. I am deeply thankful to Mr. D.K. Phukan, my school teacher, for his unwavering motivation and encouragement, which played a pivotal role in inspiring me to successfully complete my PhD work.

I owe my sincere gratitude to lab seniors Dr. Arvind Gupta, Dr. Akhilesh Kumar Pal, Dr. Melaku Tesfaye, Dr. Narendren S., Dr. Prodyut Dhar, Dr. Surendra Singh Gaur, Dr. Gourhari Chakraborty, Dr. Siddhartha Mohan Bhasney, Dr. Shasanka Sekhar Borkotoky, Dr. Naba Kumar Kalita, Dr. Prasanta Baishya, Dr. Rahul Patwa, Dr. Monika, Dr. Neha Mulchandani, Dr. Purabi Bhagabati, Dr. Riddhi Mahansaria and Dr. Prasannavenkadesan V. for their support and guidance in carrying out the research work. I am fortunate to have excellent lab mates like Dr. Chethana, Dr. Munmi, Abhishek, Dr. Kona, Dr. Dolly, Dr. Bhanupriya, Dr. Sayan and others, whom I would like to thank for their timely assistance, friendly support and cooperation throughout my research. I would also like to acknowledge all the juniors, present and past members of CoE-SusPol, including Lakhya, Diganta, Partha and others, for making my stay more enjoyable by doing everything they could to assist me in the lab.

I am also privileged to have friends like Ms. Rumi, Mr. Amit, Dr. Adhiraj, Dr. Prerona, Dr. Nimisa, Dr. Gaurangi, Dr. Joyprakash, Mr. Sourav and Mr. Sunny, and I would like to thank them for their constant support and motivation during the period of my stay at IIT Guwahati.

I want to acknowledge the Ministry of Education (MoE), formerly the Ministry of Human Resource Development (MHRD), Government of India, for the scholarship, which helped me financially during my PhD research.

Finally, I would like to express my deep appreciation to my wife, parents, and in-laws for their unwavering support, unending love, and innumerable sacrifices that have enabled me to reach this point in my life. In the end, I owe everything to the Almighty, who is all-powerful and made it possible for me to finish the PhD work.

Pankaj Boruah

Abstract

The motivation of the current research work is to develop a suitable method for the separation of oil from oily wastewater. A bio dispersant and a polymeric membrane were developed for the treatment of oily wastewater. The dispersant was developed by using a biopolymer as a bio-dispersant to stabilize crude oil. The polymeric membrane was developed using polyvinylidene fluoride (PVDF) and a lab-developed bioderived nanofiller, cellulose nanocrystal (CNC). Oligo lactic acid conjugate chitosan (OCH) were used as a bio-dispersant, an alternative to the synthetic chemical dispersant, which reduces the toxicity associated with chemical dispersants used in oil spill remediation. Results from the research indicate that by applying Xanthan gum (XG) and OCH, a considerably stable crude oil-in-water emulsion was obtained, which remains stable for more than 3 weeks, as confirmed by the optical microscopic image. XG was used to increase the viscosity of water, which helps in further stabilizing the oil droplets. Degradation of these stabilized emulsion droplets was also carried out by isolated bacteria *Pseudomonas aeruginosa* CoE-SusPol3. The degradation percentage obtained from gas chromatography (G.C.) analysis for the stabilized emulsion is 74.31%, whereas the unstabilized emulsion is 34.06%. The in-situ production of biosurfactants from the isolated bacteria also assisted the degradation process by decreasing the surface tension of the crude oil. This research work addressed in this thesis also discussed the use of CNC as a bionanofiller, an alternative to the inorganic filler in the membrane. CNC was modified to form magnetic CNC (FeCNC) by single-step co-precipitation method, and a thin film membrane was prepared by adding FeCNC into the PVDF matrix. Detailed characterization for morphology, wettability, porosity and performance analysis was carried out for the composite membranes. For comparison, PVDF membranes with CNC were also prepared, and its detailed characterization and performance analysis were carried out. Further, the application of a magnetic field during

membrane formation gives a new dimension to understanding the magneto-responsive behaviour of FeCNCs for orientation at the surface of the membrane. More prominent finger-like structures were obtained for the PVDF/FeCNC membrane. This migration of FeCNCs to the surface improves the hydrophilic property of the membrane and thus results in superior antifouling properties. This current research helps in understanding the application of biomaterials for treating oily wastewater and how a bio-based material could be a potential and sustainable solution for treating oil spills instead of using harmful synthetic chemical dispersants. The reported findings also give an idea for the improvement of properties of the membrane by application of surface modification of the CNCs and how CNCs can be oriented at the surface of the membrane to improve the performance.

Table of Contents

List of Figures

Figure No. **Figure Caption** **Page No.**

List of Tables

Nomenclature

Abbreviations

MF	Microfiltration
UF	Ultrafiltration
RO	Reverse osmosis
NF	Nanofiltration
PAN	Polyacrylonitrile
PSf	Polysulfone
PVDF	Polyvinylidene fluoride
CA	Cellulose acetate
PES	Polyethersulfone
PVC	Polyvinyl chloride
CPVC	Chlorinated polyvinyl chloride
PEG	Polyethylene glycol
WCA	Water contact angle
GO	Graphene oxide
PDMS	Polydimethylsiloxane
BSA	Bovine serum albumin
TA	Tannic acid
PP	Polypropylene
CVD	Chemical vapour deposition
PET	Polyethylene terephthalate
GNs	Graphene nanoplatelets
HP	Phosphoric acid
PAA	Poly acrylic acid

AA	Acrylic acid
POSS	Polyhedral oligomeric silsesquioxane
DMF	N, N-dimethylformamide
DMAc	N, N-dimethylacetamide
NMP	N-methyl-2-pyrrolidone
CNC	Cellulose nanocrystal
PVP	polyvinylpyrrolidone
TEA	Triethylamine
PVP-VTES	Poly(vinylpyrrolidone-vinyltriethoxysilane)
NIPS	Non-solvent induced phase separation
TIPS	Thermally-induced phase separation
PTFE	Polytetrafluoroethylene
LBL	Layer-by-layer assembly
FRR	Flux recovery ratio
PVD	Physical vapour deposition
ALD	Atomic layer deposition
PLA	Polylactic acid
SMPLA	Superhydrophobic and magnetic poly(lactic acid)
NPs	Nanoparticles
PA	Polyamide
PVA	Poly(vinyl alcohol)
PVDF-HFP	Polyvinylidene fluoride-co-hexafluoropropylene
PVDF/PMMA	PVDF/poly (methyl methacrylate)
HMWPE	High-molecular-weight polyethylene
CCNC	Cationic CNCs

mNPs	Magnetic nanoparticles
OCH	Oligo lactic acid conjugate chitosan
XG	Xanthan gum
DCM	Dichloromethane
BSA	Bovine serum albumin
FeCNC	Magnetic cellulose nanocrystal
DHB	2,5-dihydroxybenzoic acid
FESEM	Field Emission Scanning Electron Microscopy
EDX	Energy Dispersive X-ray spectroscopy
FETEM	Field emission transmission electron microscopy
FTIR	Fourier transform infrared spectroscopy
ATR	Attenuated total reflectance
TGA	Thermal gravimetric analysis
XRD	X-Ray diffraction analysis
XPS	X-ray photoelectron spectroscopy
PWF	Pure water flux
POM	Polarised optical microscope
GC	Gas chromatography
MMMs	Mixed matrix membranes
VSM	Vibrating sample magnetometer
EWC	Equilibrium water content

Notations

d	Diameter
P_c	Critical pressure
$\gamma_{o/w}$	Interfacial tension between oil and water

θ	Contact angle
r_o	Radius of oil droplet
r_p	Radius of pores of the membrane
J_{w1}	Permeation flux
J_t	Instantaneous flux
J_o	Permeate flux before fouling
J_p	Oil permeate flux
C_i	Initial concentration
C_f	Final concentration
DR_r	Reversible flux decline ratio
DR_{ir}	Irreversible flux decline ratio
W_w	Wet weight
W_d	Dry weight
ρ	Density
γ	Surface tension of liquid
I_{CR}	Crystallinity index
CP_A	Crystalline peaks
AR_A	Amorphous regions
A	Effective membrane area

Chapter 1
Introduction and Literature Review

This chapter discusses the causes and effects of oily wastewater and the different methods available for its treatment. The toxicity associated with chemical dispersants used in oil spill remediation is highlighted, and the use of bio-dispersant as an alternative to chemical dispersants is being discussed. A detailed discussion on the use of the polymeric membrane for oil-water separation was presented. This chapter briefly summarises the fundamentals involved in membrane separation technology and a literature review of the polymer used to fabricate polymeric membranes. A brief review of the different fabrication techniques and the major problem associated with the polymer membrane during oil-water separation. This chapter also covers the state-of-the-art in the application of different nanomaterials with polymeric membranes to improve the properties of the membrane for application in oil-water separation. In the last section, the application of cellulose nanocrystals in the polymeric membrane is discussed, and lastly, the objectives of the present work and the outline of the thesis are highlighted.

Research Output: *A part of this chapter was published as a book chapter*

Pankaj Boruah, *Pradyut Dhar and Vimal Katiyar, Nanocellulose-based composites for applications as catalysts and pollutant remediation. Book: Cellulose Nanocrystals, (2020) 229–278.*

1.1 Oil-Water Separation: Introduction

Water pollution is a major issue all over the globe due to the input of pollutants from various sources like household works, industrial waste, and as well as petroleum industries; the level of contamination in water bodies is increasing day by day. The rapid growth of industries like mineral extraction and processing, dyeing, electroplating, petrochemicals, oil and gas production, etc., has led to the release of enormous wastewater every day, causing a severe shortage of freshwater. A considerable amount of oil/oily wastewater is being released into the water bodies from these different industries and from oil spill accidents during transportation and processing. Petroleum industries specifically generate a substantial amount of oily wastewater; treating this oily wastewater is still a major challenge. These also include produce water that comes from the oil well during drilling and production activities, which contains a wide range of pollutants like heavy metals, dissolved organic matter, and dissolved and undissolved oils [1]. Oils and petrochemical hydrocarbons can also contaminate water bodies by terrestrial runoff from industrial sources and municipal and automobile service stations. In general oil concentration of 600–1500 mg/L or higher in present in the effluent released from oil refineries [2]. The sources **(Figure 1.1)** also include waste products from agriculture and food processing facilities, such as edible oil refineries, restaurants and catering industries [2]. As a result of this runoff, rivers, lakes, and other water bodies may finally be contaminated with oil. It would be a serious concern for the environment and ecosystem if adequate measures were not taken to separate these oils from oily wastewater [3,4]. These residual oil pollutants obstruct sunlight from entering water bodies, decreasing dissolved oxygen concentration and making the water unsafe for habitation. Some chemical compounds associated with these wastewaters, if not treated properly, can persist in the aquatic environment for a prolonged period, leading to long-term and short-term environmental damage. Also, with the rapid

growth of the global population and deteriorating climate change, the availability of fresh water is increasingly scarce, causing a major challenge to meet the future demand for domestic and industrial water. As per the Central Pollution Control Board's Environment (Protection) Rules of 1986, regulations governing effluent discharge are differentiated for offshore and onshore activities. For offshore discharge, the stipulated limit for oil content in treated effluent stands at 40 mg/l for 95% of the observations, with a strict maximum threshold of 100 mg/l. This stringent control is designed to ensure that offshore discharges have minimal environmental impact. And, for onshore discharge, a more stringent restriction is imposed, with a concentration not exceeding 10 mg/l for Oil & Grease in the effluent. These regulations are established to uphold water quality standards and safeguard the environment, with the stricter onshore limits aimed at reducing the ecological footprint of industrial effluents on local ecosystems and surrounding water bodies. These rules underscore the commitment to maintaining a balance between industrial processes and environmental preservation in line with the principles of sustainable development.

Treating of the oily wastewater is crucial as it affects not only the aquatic ecosystem and wildlife but also human health and the economy. Public health may be impacted by exposure to such contaminated water, particularly in areas where residents depend on such sources of water for their daily requirements. Additionally, a decline in crop production, tourism, fishing, and other water-based industries can result from contaminated water bodies, which can have a negative impact on the economy of that region (source and the effects are oily wastewater summarized in **Figure 1.1**) [5]. Oily wastewater frequently produces stable oil-in-water emulsions, and the emulsified oil typically has particles that are between a few hundred nanometers to tens of microns in size. Additionally, these oil pollutions comprise complex organic solvents in addition to other types of oil-water mixtures. Hence, getting these emulsified oils to be separated out of water is challenging.

As a result, given the environmental and other issues created by oil pollution, developing better technologies for oil-water separation has emerged as a topic of growing importance in both the business sector and the scientific community. Currently, available separation/treatment methods include the combustion of oils [6], the use of dispersants [7], and the use of mechanical devices such as skimmers and booms [8]. Chemically coated mesh, different membranes and porous sponge-like materials are also ideal for separating oil from oily wastewater [9,10]. However, mesh and some membranes are capable of removing the large size droplets (>150 μm), and because of the hydrophobic nature of some of the adsorbents, it adsorbs water along with the oil. In order to overcome these limits, various methods are adopted, such as chemical modification, surface coating, and altering the surface texture by changing the surface chemistry of such adsorbent or membrane. Developing an environmentally acceptable method for treating and disposing of oily wastewater is a great challenge for E&P industries. Due to the hazardous nature of this oily wastewater, treatment is of utmost importance. Gravity settling, coagulation, skimming, coalescence, hydrocyclones, etc., are not effective enough to separate emulsified oil from water. Also, these conventional methods used for oil separation are not efficient enough to completely remove all the oil from the water [11]. Moreover, they have several inherent drawbacks, such as high manufacturing costs, high energy requirements, the release of a secondary pollutant, high maintenance and operating cost, and the presence of toxic chemicals.

Over the past decade, there has been a significant increase in research focusing on engineering, materials science, and chemical engineering to create different types of superhydrophobic and superhydrophilic materials, including nanofibers, nanomaterials, etc. These materials are intended for use in the fabrication of adsorbents, membranes, aerogels, meshes and a range of other porous materials. For large volumes of spilled oil,

which accumulates and remains in the water bodies, the application of chemical dispersant is the most widely and immediate method followed.

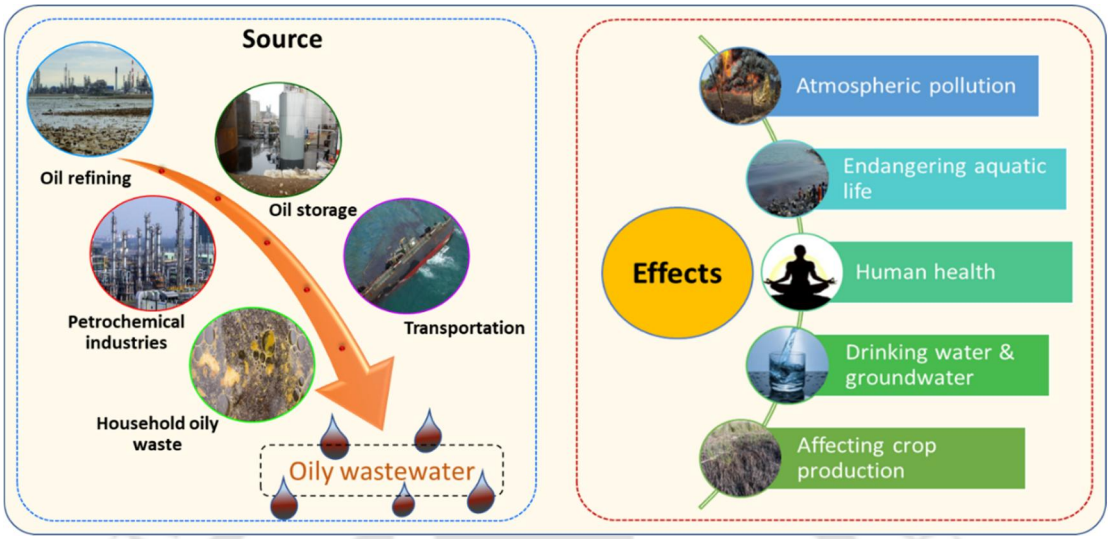

Figure 1.1: Source and effects of oily wastewater

Stabilization and treatment of oil droplets by chemicals have been in use for centuries, but the impact of such chemicals will pose chronic effects on the ecosystem [12,13]. Dispersants are generally surfactants that have both lipophilic and hydrophilic parts attached at the oil-water interface and reduce the crude oil-water interfacial tension [14]. However, chemical dispersants used are toxic for aquatic life, not readily biodegradable, and some by-products formed during their manufacturing are hazardous to the environment [15]. Literature suggests that the toxic effect of the most commonly used chemical dispersant is Corexit 9500A, and it is reported that it is highly toxic to marine life. The crude oil dispersed with Corexit 9500A is more harmful than raw crude oil [12,16]. More often, the droplets formed by the application of this dispersant are less stable and coalesce quickly due to an inadequate electrostatic repulsive barrier [7,17]. Another chemical dispersant, Corexit 9580, contains 2-butoxyethanol, which was known to be carcinogenic [18,19]. Peter G. Wells also reported that the chemical dispersant used in the 1967 Torrey Canyon oil spill was toxic to the aquatic species [20]. Moreover, the application of these chemical dispersants also inhibits the activity of oil-degrading microbes [21]. Hence, the

utilization of less detrimental dispersants is of great importance, and therefore there is a need for the development of eco-friendly bio-dispersants with good dispersion efficacy. The development of such environmentally benign alternatives holds immense significance in ensuring effective mitigation of environmental impacts while addressing the need for sustainable solutions for treatment of oily wastewater.

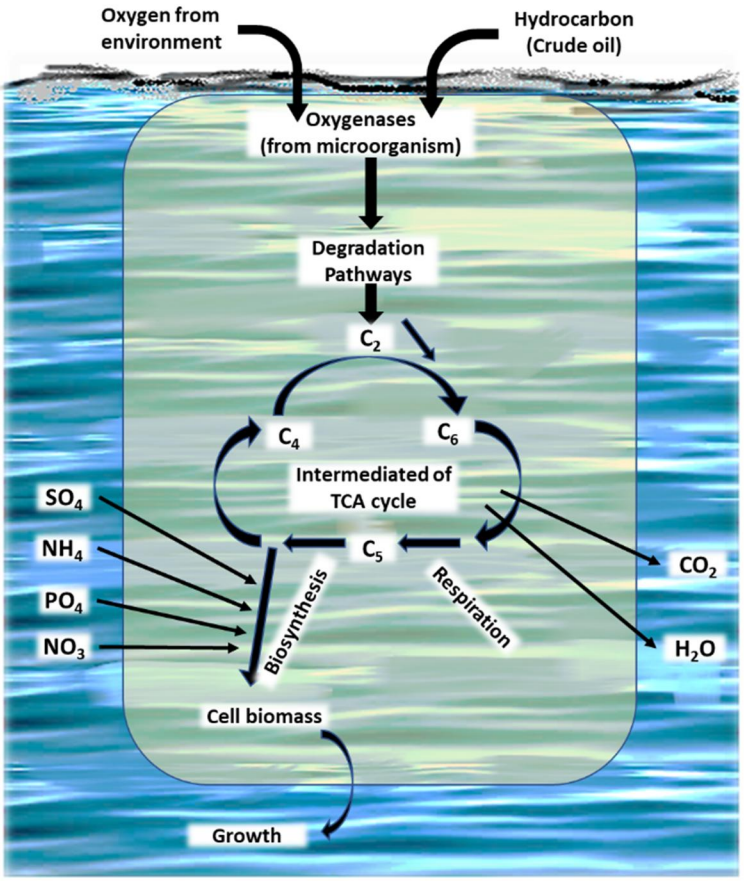

Figure 1.2: Schematic for the mechanism of degradation of hydrocarbons by microorganisms, adapted from [22,23]

Considering the acute and chronic effects caused by the chemical dispersants and spilled oil, the use of bio-dispersants and bioremediation plays a very important role and can replace the chemical remediation methods for such applications to retain the natural environment. Bioremediation is defined as the conversion of harmful chemicals, with the help of living organisms, into energy, biological waste products and biomass. The biodegradation also depends on the effect of temperature, change in physiochemical

properties, and rate of degradation of hydrocarbons by microorganisms [24]. Schematic for the mechanism of degradation of hydrocarbons by microorganisms is shown in **Figure 1.2** (adapted from E.S. Okeke et al. and N. Das et al. [22,23]). Organic pollutants were initially attacked by the microbes following an oxidative process; oxygenases and peroxidases are involved in the enzymatic reaction of activating and incorporating oxygen. Organic pollutants are gradually converted into intermediates, such as the tricarboxylic acid cycle (TCA), by peripheral degradation pathways (where C2, C6, C5, C4, etc. are the number of carbons in the intermediate products in the cycle). Some research demonstrated the capacity of some microorganisms to produce the bio-surfactant, which helps indirectly for the biodegradation of crude oil [15]. But for the removal of smaller droplets of oil remaining in the water, filtration is another approach that can separate oil from water based on droplet size and capillarity. Membrane filtration techniques are found to be more effective in such cases. Membrane separation technology for wastewater purification is gaining an additional reputation due to the low-cost and sustainable process of removing contaminants without producing harmful by-products [25]. Membrane-based separation has become the most anticipated and outstanding solution for treating emulsified oil in water. The membrane separation is highly attractive due to its efficiency in selectively separating oil from oily wastewater. It can offer numerous benefits, such as leaving zero or negligible oil in the water and reducing chemical usage. Apart from efficient separation, the membrane separation process can be easily scalable at a low cost compared to other conventional methods [26].

However, one of the major drawbacks associated with the membrane is its fouling results in a decline in flux with time, reduces the permeation rate, reduces the lifetime of the membrane and increases the energy required for operation [27]. In order to deal with such problems associated with the flux decline of the membrane, extensive research has been

carried out to improve the characteristics of membranes, which can be achieved through the development of new materials or surface modifications to conventional membranes [28,29]. The use of readily available, cost-effective hydrophilic materials is of research interest specifically applicable to separating oil from an oil-water mixture. As compared to other technologies, membranes in the microfiltration (MF) and ultrafiltration (UF) range can separate oil-water to a significant concentration and can even separate emulsified droplets [30]. It also has its intrinsic advantage, such as it does not require any additional chemical or thermal energy to break the emulsion.

1.2 Overview of Oil-Water Separation Technologies

In this section literature review of the oil-water separation problem and different techniques presently used are being discussed, including the use of dispersant and bioremediation techniques to remove the oil from water. Initially, this section discusses about different available methods for the separation of oil from oily wastewater followed by discussion on application of bio-dispersant for oil-water separation. In the subsequent section, the use of membrane separation processes to treat oily wastewater is discussed in details. Membrane separation processes is now becoming an emerging technology due to its high removal efficiency and ease of operation. Most importantly, the focus is on developing a new polymeric membrane type with desired hydrophilic or oleophobic or vice versa characteristics, which is becoming an attractive option. An attempt is being made to develop a comprehensive understanding of the properties of polymeric membranes to treat oily wastewater.

In order to address the problem of oil-water separation, there are many technologies and methods available, as presented in **Figure 1.3**. The key factor governing the use of methods lies in the size of oil droplets dispersed in the water bodies. Varieties of mechanical devices, such as booms and skimmers, are used to remove oil from water bodies; however, these

methods are only capable of removing larger oil droplets (>150 µm). These methods also require a high amount of energy and cost. Based on the diameter (d) of the oil droplets, Cheryana M. and Rajagopalan N. reported that oil-water mixtures can be divided into three categories [31]:

a) Free mixtures d > 150 µm

b) Dispersions 20 < d < 150 µm

c) Emulsions d < 20 µm

Emulsions can be further classified as oil-in-water (dispersed phase: oil, continuous phase: water) or water-in-oil (dispersed phase: water, continuous phase: oil). For the primary treatment of oily wastewater, gravity separation techniques are used, which are efficient for the removal of free oil from water. Other methods to remove free oil and oil in the emulsified form include coagulation, hydrocyclones, ceramic or polymeric membrane filtration, in situ burning, mechanical methods, chemical treatments, bioremediation, and adsorption [32]. The important parameters to be considered before choosing a method depend on the oil and particulate rejection, energy requirement and cost. All commonly available methods have their own advantages and disadvantages; a summary of different methods and their advantages and disadvantages is represented in **Table 1.1**.

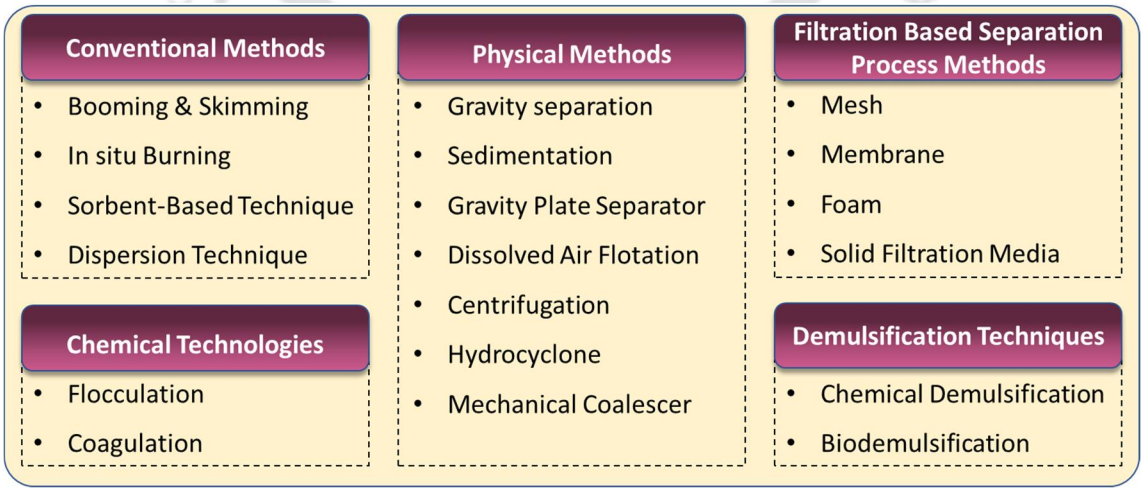

Figure 1.3: Some of the commonly available oil-water separation methods

Table 1.1: Comparison of various oil cleanup methods [33,34]

Classification	Examples	Advantages	Limitations	Environmental impact	Cost
In situ burning	Combustion	Effectively removes large volumes of oil	Environment and safety concerns	Formation of large quantities of harmful smoke and viscous residues after combustion	Cheapest
Mechanical methods	Skimmers, booms	Efficient	Labor-intensive, time-consuming	Friendly	Expensive
Chemical treatments	Use of dispersants or solidifiers	Simple operation, suitable to treat a large polluted area	Little effect on very viscous oil, ineffective in calm water, high initial and/or running costs	Being harmful to aquatic organisms	Expensive
Bioremediation	Microorganism degradation	Good oil-removal efficiency, low operation cost	Ineffective in spill with large coherent mass	Friendly	Cheap
Adsorption	Use of oil sorbents (fly ash, sand, exfoliated graphite)	Good oil-removal efficiency, simple operation, practically feasible, less secondary pollution	Labor intensive	Friendly, its biodegradation depends on the used sorbents	Cheap

A method for containing and cleaning up crude oil spills is in-situ burning. This method is comparatively cheap compared to other oil spill response techniques; it is frequently utilized as a last resort. Water density, oil kind, and weather are some of the variables that impact how effective it is. Despite its success, burning the spilt oil has raised questions regarding the emissions and residues that result, including how they will be transported and what will happen to them, also causing potential harm to the environment, biodiversity, and public health. Many developing nations lack the necessary legal frameworks and contingency planning to monitor in-situ burning properly, making the practice dangerous to society. Therefore, further research and development are required to develop an alternative method to lessen the harmful effects of oil spills on the environment and human health [35]. The mechanical method of removing oil from oily wastewater includes the use of specialized equipment like barriers, booms, and skimmers. Utilizing mechanical techniques has the benefit of retaining the characteristics of the oil. As a result, it can still be improved upon and used in the future, cutting down on waste and possibly averting financial losses. However, the efficiency of these techniques is based on variables including weather and sea conditions, the type of oil that has leaked, and the encounter rate. These methods also demand significant financial expenditure and logistical assistance. Moreover, if the recovered oil is not suitable for reuse, then disposal of it is also a major concern [36].

Moosai R. and Dawe R. A. [37] investigated gas flotation as a technique for treating oily wastewater. The experimental findings demonstrate how flotation may more effectively remove oil droplets from wastewater when gas bubbles are attached to them. The studies also demonstrate that the addition of surfactants can strengthen the bond between gas bubbles and oil droplets even further. The study examines the application of gas flotation for the treatment of oily wastewater and highlights the importance of gas bubble size and quantity in determining the effectiveness of the procedure. Gas flotation can maintain

effluent oil contents below 40 mg/l if it is correctly built and managed. The method, however, only works with oil droplets larger than 20 µm, and chemical additives are frequently needed for it to function properly. It is also challenging to extract dissolved oil using the gas flotation method, and emulsified oil is often removed via chemical pre-treatment. The production of smaller microbubbles needs more energy and materials, which might increase the cost of the procedure. Furthermore, it may be challenging for the microbubbles to bind to the oil and remove it from the wastewater if they are smaller than the oil droplets [38]. Hydrocyclone is another useful device for separating free oil and water because it has a high processing capacity, easy to use, and requires little maintenance. The hydrocyclone is an economically feasible option because of these benefits. However, both geometric and operational parameters, including the equipment's dimensions, fluid characteristics, solids concentration, high intake pressure, unsuitable for stable emulsions and heavy oils (small-size droplets) have an impact on the hydrocyclone's efficiency. Despite its usefulness, the hydrocyclone has been demonstrated to be inefficient when separating oil droplets with small diameters and low oil concentrations [39].

The chemical method is another option for cleaning up oil spills/oily wastewater or sometimes as a supplement to mechanical oil cleanup techniques. Chemical processes try to alter the chemical and physical characteristics of oil to make it easier to remove or manage. The use of chemical dispersants is the most common method, which is generally a surfactant mix that lowers the interfacial tension between oil and water [40]. The oil is subsequently broken down into tiny droplets and spread throughout the water column. However, the use of dispersants is a sensitive matter because it may harm the environment. Dispersants are typically utilized in big oil spills if the advantages of breaking down and dispersing outweigh any potential risks caused by it. Examples of other chemical methods include emulsion breakers, which are used to break water and oil emulsions, gelling agents,

bioremediation chemicals that accelerate the biological breakdown of oil, burning agents, neutralizing agents, and sinking agents. These substances are used to alter the physical and chemical characteristics of the oil and make it simpler to handle [41]. As discussed in section 1.1, the use of these chemical dispersants poses a significant threat to the environment, and few such non-toxic materials were explored as bio-dispersants for oil spills, such as biopolymers, cellulose nanocrystals (CNC) and lecithin [12,42,43]. The application of such bio-dispersants also assists the growth of oil-degrading bacteria for the biodegradation of crude oil. For example, microorganisms such as *Bacillus subtilis* and *Bacillus methylotrophicus* are capable of producing surfactants and are able to degrade crude oil [15,44]. So, the application of bio-dispersants and bioremediation is getting more attention as an alternative method to solve the oil spill problem as it has the advantage of being low-cost and environment friendly [45]. Therefore, there is increasing demand to explore green, facile, and eco-friendly bio-dispersants to treat oil spills. For this reason, the wise way is to explore the use of readily available bioderived materials with low toxicity as bio-dispersants that are easy to scale up for the removal of oil spills.

Venkataraman P. et al. [43] synthesised low molecular weight Hydrophobically Modified Chitosan (LHMC) and high molecular weight Hydrophobically Modified Chitosan (HHMC). LHMC was used to stabilize the crude oil droplets, significantly improving its stability and bacterial remediation. The study aims to reduce the use of chemical dispersant, which has a severe impact on the environment. However, the work does not talk about the complete abolition of chemical dispersants; LHMC and HHMC were used along with the chemical dispersant Corexit 9500A. HHMC was used to immobilize the oil droplets by increasing the viscosity of the dispersed phase. Tamer T. M. et al. [46] have developed an amphiphilic Chitosan-g-Octanal Schiff base material used for the adsorption of crude oil from seawater. Chitosan is reacted with octanal with varying amounts of octanal ranging

from 38% – 82% to form the desired compound. Compared to pristine Chitosan, the oil adsorption capacity for Chitosan-g-Octanal was improved by 167% and 110%.

Chen Z. et al. [47] developed a novel method for the removal of oil from oil-contaminated shorelines using a combination of chitosan and rhamnolipid complex (CS/RL) dispersion with a pH-responsive property. The developed method was found to be efficient in removing oil from sand, even at varying levels of oil content. Using rhamnolipid alone is less efficient compared to the CS/RL complex dispersion. CS/RL complex showed higher oil removal capabilities due to its improved emulsification abilities. However, the pH-responsive nature of CS/RL complex helps in separating oil and water at different pH. Chitosan aggregates and precipitates around oil droplets, facilitating oil-water separation. This novel complex shows promising characteristics for efficient and environmentally friendly oil spill response strategies.

Wang A. et al. [48] used xanthan gum (XG) as an additive with chemical dispersant for oil spill treatment. The dispersion efficiency of crude oil and the stability of the oil droplets were improved. Their results also indicate that the rate of biodegradation by bacteria also increased when XG was used along with chemical dispersant 9500A. Thus, this work suggested that the use of XG along with dispersant can be an effective solution to enhance the oil droplet stability and degradation of crude oil. XG was also used with silica nanoparticles for stabilization of oil droplets, which in turn helps in favourable degradation of oil droplets. A stable oil in water emulsion can be formed with a small amount of silica nanoparticle in the presence of XG [49].

1.3 Membrane-Based Separation of Oil-Water

Membrane separation techniques for the separation of the oil-water system have become increasingly attractive due to their ability to efficiently separate both the components along

with the other contaminants, their affordability, and the increase in the application for large scale. Several notable advantages include the following [50–52]:

- The simplicity of operation and maintenance, allowing for continuous separation with minimal effort and low cost
- Easy control and operation, low energy consumption, and a more compact overall system
- Environmental friendliness, as membranes are usually made of nontoxic materials
- Energy efficiency, since separation can be achieved at room temperature
- The ability to recycle substances without the need for additional chemicals

The application of membrane-based processes for oily wastewater treatment is widely used for oil-water treatment, with cost-effective polymeric MF/UF and reverse osmosis (RO)/nanofiltration (NF) membranes available [53,54]. However, efficient separation of oil-water requires a highly hydrophobic or hydrophilic membrane with robust mechanical properties and high thermal and chemical stability. The use of polymer membranes for oil-water separation is one of the deep-rooted interdisciplinary research areas with considerable challenges. Membrane-related research is being conducted to find an effective solution for the problem of oil-water separation and other contaminants removal from polluted water to make it usable.

1.3.1 Polymers Used for Fabrication of Membranes

A membrane can be fabricated from different types of materials; most commonly, it includes polymers and ceramics. Polymeric membranes are widely used in membrane separation processes because of the advantages of their ability to separate dispersed and emulsified oil particles with high efficiency. These membranes are flexible, tough, cost-effective and require less energy than ceramic membranes [55]. It has been widely used for

the separation of oil and water; some of the common polymers that have been used to prepare membranes are polyacrylonitrile (PAN) [56], polysulfone (PSf) [57], polyvinylidene fluoride (PVDF) [58], cellulose acetate (CA) [59], and polyethersulfone (PES) [60]. However, the polymeric membrane also has some disadvantages, like being prone to fouling more quickly; as a result, flux declines while treating oil and water systems and shows less stability for some volatile compounds. Therefore, several types of research are being carried out worldwide with different approaches to address these issues, such as altering the surface properties by physical or chemical methods and adding antifouling agents. For oil-water systems, it is evident that the addition of a hydrophilic component on the membrane reduces the adhesion of oil to the surface, which results in the reduction of fouling [61–64].

Liu et al. [65] prepared a membrane from polyvinyl chloride (PVC) and chlorinated polyvinyl chloride (CPVC), which was used for UF. To improve the permeability, polyethylene glycol (PEG2000) and polyethylene oxide-polypropylene oxide-polyethylene oxide triblock copolymer (Pluronic F127) were used as both pore-forming agents and surface modifiers. Blending with CPVC improves the water flux of the membrane, and Pluronic F127 have excellent antifouling property. PVC and CPVC are completely miscible and are lower priced than other common polymers like PAN and PSf. Zhang et al. [66], in another study, employed a salt coagulation bath, which enhances the morphological structures and properties of PVC membrane. In their study, Pluronic F127 was also blended with PVC, which improves the hydrophilicity of the PVC membrane, and the salt coagulation bath helps in pore-forming with a remarkable surface porosity of 7.2% and water flux of 1405 L/m^2h bar.

Ahmad et al. [67] prepared a low-cost PVC/bentonite blended UF membranes using different inorganic salts (i.e., NH_4Cl, NaCl, KCl, $MgCl_2$ and $CaCl_2$) in the coagulation bath

for the treatment of oilfield-produced water. The use of different inorganic salts helps in the improvement of surface pore density and hydrophilicity with a water contact angle (WCA) of 60.1° with antifouling characteristics. The maximum permeation flux of 421.3 L/m^{2}h is achieved using PVC-loading-15.01 g, bentonite-loading-1.37 g, membrane thickness-100 µm, pH-9 and TMP-250 kPa, while maximum oil rejection is 98.6% at PVC-loading-18.0 g, bentonite-loading-0.0 g, membrane thickness-250 µm, pH-5.1 and TMP-54.4 kPa.

Zhao et al. [68] modified the PVC UF membrane with graphene oxide (GO) via the phase inversion method. The incorporation of GO leads to an improvement in the hydrophilicity of the membrane, and it also improves the mechanical properties. With 0.1% of GO, the pure water flux (PWF) increased from 232.6 L/m^{2}h bar to 430.0 L/m^{2}h bar. This is mainly due to the presence of hydrophilic functional groups on the surface of GO. The flux recovery ratio of the hybrid membranes blended with 0.10 and 0.15 wt% GO were 70.4% and 75.9%, respectively, which is much higher than that of the pure PVC membrane (only 41.8%), representing the improved antifouling property.

Zhang et al. [69] blended an amphiphilic copolymer to PES to fabricate a low-oil fouling membrane through the phase inversion technique. The amphiphilic copolymer [poly (carboxyl betain methyl acrylamide-co-3,3,4,4,5,5,6,6,7,7,8,8,8-tridecafluorooctyl acrylate) P(CBMA-co-TFOA)] was synthesized by free radical polymerization and subsequent quaternization reaction. The membrane exhibits a flux recovery ratio of 99.3% and enhances the oil-fouling resistance as compared to the PES membrane. In another attempt, the same research group blended amphiphilic comb copolymer with mixed PEG and polydimethylsiloxane (PDMS) brush, which has mixed hydrophilic and low surface energy side chains. The antifouling property of the blend membrane improved by 31.3% as compared to the pristine PES membrane, with a flux recovery rate of 96.6%. The prepared

membrane was tested for three cycles of bovine serum albumin (BSA) filtration (a model fouling agent) and found to be stable after three cycles [70].

Mansourizadeh & Azad [71] blended PES with cellulose acetate to improve the hydrophilicity of the membrane and the structure to promote oil-water separation. A phase-inversion promoter PEG-400 was added to the solution, which also acts as a pore-forming agent to produce highly permeable membranes. The prepared membrane has a thinner skin layer and larger pore sizes. The optimum concentration of CA was found to be 17% for the PES/CA blend membrane, which shows higher water flux and lower fouling rate than the pure PES membrane.

Song et al. [72] reported a two-pot coating process with Tannic acid (TA) and ferric ion (Fe III), which transform polypropylene (PP) membranes into superhydrophilicity. PP membrane was first immersed in TA, and then Fe III, respectively, and this membrane also shows superoleophobicity underwater, having a water contact angle of 0° and water permeability up to 7092.6 ± 216.1 L/m^2h bar, which is significantly higher than the one-pot modified membrane. This membrane has an excellent oil-water emulsion separation ability, and it took about 15 min for the treatment. The presence of large amounts of massive hydroxyl groups on the membrane facilitates improving surface hydrophilicity. A dead-end filtration setup was used for measuring the separation performance.

Kansara et al. [73] modified the PP membrane to be superhydrophobic by a facile one-step dip-coating method in which the PP membrane was dipped in a coating solution for 10 min for optimal sorption uptake. The coating solution contained silica nanoparticles networked with alkyl siloxanes, where silica particles were dispersed in toluene solution and sonicated for a sufficient time at room temperature, followed by the addition of trichloro(alkyl)silane dropwise. The dipped PP membrane was removed from the solution and dried. They

claimed it to be a recycled membrane with a water contact angle of 150° with the efficacy of separating oil with 99% oil purity from the mixture. The separation is a simple gravity-induced separation process. The main reason behind the superhydrophobicity of the membrane is described as the arrangement of the silica nanoparticles on the PP substrate.

Yang et al. [74] demonstrated a membrane modification process in which the PP membrane exhibits superhydrophilicity and underwater superoleophobicity. The process involves decorating the membrane by silicification process where PDA/PEI-deposited membranes are dipped in silicification solution. This membrane shows a high-water permeation flux higher than 1200 L/m^2h under 0.04 MPa. A dead-end filtration apparatus (Millipore) was applied to measure the permeate flux (the diameter of the membrane is 25 mm), and the trans-membrane pressure was adjusted by a nitrogen tank. They claimed that this membrane has a high breakthrough pressure of up to 0.16 MPa, which can be applied for industrial applications.

Jiang et al. [75] developed a hydrophobic PP fibre membrane by chemical vapour deposition (CVD) technique, where hydrophobic silanes were deposited on the surface of commercially available PP fibres. The superhydrophobic surface of the PP surface shows a WCA of 156°, and this material selectively absorbs oil from water with good performance after repeated use. Prior to CVD, PP fibre was etched by H_2SO_4 and then immersed in SiO_2-GO suspension, where graphene GO sheets were used as a substrate for the deposition of SiO_2 nanoparticles. The prepared material also shows good stability towards high-temperature applications like oil separation from hot water. The authors claimed that it is inexpensive, reproducible, and suitable for different organic solvents.

Himma et al. [76] prepared a hollow fibre membrane from PP through the dip coating process. PP hollow fibre was immersed in a PP solution and withdrawn at a constant speed.

It follows a two-step dip coating process where PP hollow fibre is first immersed in a non-solvent solution and then in a PP solution. The solution concentration, dip time, temperature and other parameters were properly optimized to obtain a homogeneous coating. This process results in the development of a high hydrophobic PP membrane with a WCA of 151.3°. The modified membrane is capable of separating oil from water, but it gives a lower flux than the unmodified membrane.

Han et al. [77] applied a dip coating method of polyester, polyethylene terephthalate (PET) and PP membrane to make it a superhydrophobic and superoleophilic membrane for efficient separation of oil and water. The surface of PET and PP membranes was modified by the deposition of P-SiO_2 nanoparticles, and PDMS was used as a binding material. After the hydrophobic dip-coating process, the water contact angle of both PET and PP samples increased from 143° and 150° to 162° and 155°, respectively, due to the deposition of the P-SiO_2 nanoparticles on the surface. It was also observed that P-SiO_2 is more firmly adhered to the surface of PET than PP due to the strong chemical interaction between PET and PDMS. However, to increase the oil separation efficiency, the viscosity of the oil should be reduced for a given membrane thickness.

Zhang et al. [78] fabricated a membrane by coating PET fabric with graphene nanoplatelets (GNs) on one side and phosphoric acid (HP) grafted on the other side. The process employs high temperature and high pressure. This results in a heterogeneous wetting capacity of the membrane where the GN coating side is hydrophobic and the HP grafted side is hydrophilic. Thus, the water can pass through the membrane from the hydrophobic side to the hydrophilic side and prevent it from entering through the membrane from the hydrophilic side. The developed membrane has a high water flux of 2073 ± 207 L/m^2h with a separation efficiency of more than 99% for both oil and water with several repetitive

cycles. Thus, it claims that the obtained Janus membrane has excellent separation capability for separating the layered oil-water mixtures and possesses wonderful recyclability.

Several researchers also reported about the polymeric coating on different membranes, wire mesh, nonwoven fabrics, etc. or coating polymeric membranes with different organic or inorganic materials to obtain hydrophilic and oleophobic characteristics, which can be utilized effectively in separating oil-water mixtures. Chen & Xu [79] reported a superhydrophilic membrane prepared by depositing $CaCO_3$-based mineral coating on poly acrylic acid (PAA)-grafted PP membrane, which is capable of separating oil-water effectively. The prepared MF membrane can separate a range of oil-water mixtures with a high water flux of more than 2000 L/m^2 h with an efficiency greater than 99%. The mineral coating on the membrane surface traps abundant water in its rough surface and forms a hydrated layer on the pore surface, imparting low oil adhesion due to low fouling. PAA was grafted on a microporous PP membrane using a photoinitiated graft polymerization reaction, and $CaCO_3$-based mineral coating was done by dip coating alternately in $CaCl_2$ and Na_2CO_3 aqueous solutions for ten alternate soaking processes. Benzophenone in heptane was used as a photoinitiator solution for the polymerization reaction where the PP membrane was dipped for 2 h and then immersed in acrylic acid (AA) solution, followed by exposure to UV light to form PAA-grafted PP membrane. PAA and $CaCO_3$ (intrinsically hydrophilic) improve the hydrophilicity of the membrane [80].

Crick et al. [81] prepared a superhydrophobic polymer coating which was applied on a copper mesh that can be utilized as a membrane for efficient separation of oil-water. Silicone elastomer (PDMS) films were coated on the copper mesh by aerosol-assisted chemical vapour deposition. The WCA increases to 20° after coating, and it can easily handle large volumes of water. In another attempt, Guo et al. [82] reported coating of stainless-steel mesh by spray-coating polyhedral oligomeric silsesquioxane (POSS) hybrid

acrylic polymer. The coated mesh shows superhydrophobic-superoleophilic, which was utilized for the separation of an oil-water mixture. The coated mesh shows a water contact angle of 153° and can separate a series of oil-water mixtures, such as n-hexane, isooctane, petroleum ether, kerosene, and vegetable oil, with separation efficiency of nearly 99% and retain its efficiency even after use for 25 cycles. Chen et al. [83] also reported highly efficient and robust oil-water separation materials based on stainless steel wire mesh coated by reduced GO. First, the GO was coated on the commercially available wire mesh; after that, the GO-coated mesh was treated with O_2 plasma from the back side to open the pores. Further, the GO-coated mesh is subjected to thermal annealing at 200 °C for 2 h to form stable superhydrophobic reduced graphene oxide coating. The coated mesh shows stable superhydrophobicity under long-term storage and excellent resistance to high temperatures.

Among different types of membrane materials available, PVDF is considered as an ideal material due to its outstanding chemical resistance, thermal stability, mechanical durability and good membrane-forming ability. PVDF is semi-crystalline with good strength and flexibility. The mechanical strength of PVDF is due to its crystalline phase, and flexibility is due to its disordered phase [84]. It can dissolve in organic solvents like N, N-dimethylformamide (DMF), N, N-dimethylacetamide (DMAc) and N-methyl-2-pyrrolidone (NMP), and membrane can be prepared by well-known industrially scalable phase inversion method [85]. However, the hydrophilic nature of PVDF makes it more susceptible to fouling with interaction with the foulant present in wastewater [86]. Different modification techniques were applied to improve the performance and antifouling properties of the PVDF membrane. The surface roughness and contact angle of the PVDF membrane increased by adding $CaCO_3$ nanoparticles in the dope solution, and the membrane exhibited lower thermal loss when $CaCO_3$ was added to it, resulting in a more thermally stable membrane [87–90]. Méricq et al. [91] entrapped TiO_2 nanoparticles in

PVDF membrane in order to improve the fouling properties by the NIPS process. The membrane shows hydrophilic properties with improved permeability and limited fouling, thus reducing the frequency of cleaning. With the addition of 25 wt.% TiO_2 permeability of more than 150 L/m^2h due to the improvement of finger-like macro voids. The permeate flux of the modified membrane increases with exposure to UV radiation compared to a neat PVDF membrane. With a 10% TiO_2 (contact angle ~59.7°), the hydrophilicity is improved as compared to a neat PVDF membrane (contact angle ~82.8°) [92]. Nowadays, the use of these inorganic nanoparticles is limited. More importance is given to the use of bioderived materials like lignin, cellulose nanofiber, CNC, and chitosan [93] in membrane preparation. A small percentage of CNC loading can improve the mechanical properties, and it is reported that with the addition of 1% CNC to PVDF, the tensile strength is improved by 118% and 114% improvement in the tensile modulus [94]. Various properties of PVDF, like surface wettability, mechanical and thermal properties, can also be altered by incorporating an oxidized form of CNF (TEMPO-mediated Oxidized) and sodium hydroxide and cationization functionalized CNC with PVDF [95–97]. Recent literature reported the fabrication of an electrospinning PVDF membrane incorporated with CNC and its application in oil-water separation and power sensing. The membrane shows a 16% improvement in flux and is a promising material for the removal of oil from water [98]. Thus, PVDF, along with bio-based nanoparticles such as CNC, can be a potential material for fabricating composite membranes for water purification applications. Huang et al. [99] treated oily wastewater with a PVDF membrane which was grafted with polyvinylpyrrolidone (PVP). PVDF is inherently hydrophobic, which increases the chance of fouling; therefore, grafting of PVP imparts hydrophilicity to the membrane surface, showing a smaller contact angle than a neat PVDF membrane. It was also found that the average permeation water flux through the PVDF–PVP membranes was more than that

through the PVDF membranes. But fouling was still a challenging issue which was overcome by washing the membrane with 3 wt% NaOH aqueous solution.

Obaid et al. [100] treated PVDF electrospun membrane with triethylamine (TEA) under reflux. The treatment alters the physiochemical properties of the membrane, which can be used for the treatment of oily wastewater and emulsions. Moreover, this membrane treats oily wastewater under gravitational force where no energy is required. It shows an outstanding flux of 20664 L/m^2h with a separation efficiency of 99%. The average pore diameters for the treated membrane decreased by 28% compared to the pristine membrane, while the total pore area increased from 4.2 to 4.6 m^2/g. PVDF membrane is hydrophobic with a WCA of 130°, and the modified membrane shows a WCA of 83°, which shows improvement in the hydrophilicity of the membrane.

Li et al. [101] developed a PVDF membrane with opposite wettability on both surfaces. The difference between the contact angle of the opposite side is more than 150°. The WCA difference between the two sides is up to 150°, and this was achieved via one single-step unidirectional segregation strategy. They introduced a glycerol sacrificial coating on the nonwoven fabric support to control the one-way migration of the hydrophilic copolymer poly (vinylpyrrolidone-vinyltriethoxysilane) (PVP-VTES) during phase inversion. PVP-VTES was solely migrated onto the top from the inside polymeric solution to form a superhydrophilic surface. The developed membrane exhibits excellent separation performances for both oil-in-water and water-in-oil emulsions with its switchable oil-water separation performance. A summary of PVDF membranes with different additives used for the separation of oil-water is presented in **Table 1.2.**

Table 1.2: Comparison of the properties of PVDF membranes with different additives used for oil-water separation

Material	Permeation flux (L/m^2h)	Pressure (kg/cm^2)	Separation efficiency (%)	Reference
PVDF/Al_2O_3/PVP/sodium hexaphosphate	138.5	1	93.55	[102]
PVDF	0.0051- 0.012	0.5 - 2.3	77	[103]
Ag-epigallocatechin gallate-PVDF	735	0.5	95.4	[104]
Cellulose/electrospun PVDF-HFP	124	0.6	90.1	[105]
PVDF/TiO_2/PVP	72.2	vacuum pump	> 90%	[106]
PVDF–b–P(PEGMA–co–BVIm–Br)	428 ± 2.6	5	96.1 ± 1.3	[107]
PVDF/SNTs/PVP	220	1	94.2	[108]
PVDF/SiO_2/PVP	198	1	94.5	[108]
PA@PEI/PVDF	12203.6	1	98.5	[109]
ZVT/PVDF	180	1	93.82	[110]
SYFZr-Tis/PVDF	300	1.5	90.63	[111]
FePc/PVDF	125.9	1	96.7	[112]
ZnO@PVDF Janus membranes	1210	gravity	97.24	[113]
PVDF/ZnO	N/A	N/A	96	[114]
PMAPS-g-PVDF	~5000	1	99.3	[115]
PVDF-NiNPs@Ag/C-CNTs	97	gravity	98.8	[116]
PVDF-PDA-PEI	4.4	1	98	[117]

1.3.2 Different Techniques for Fabrication of Polymeric Membranes

This section discusses about the available techniques for the fabrication of polymeric membranes. For the preparation of polymeric membranes, a variety of fabrication methods are available, such as phase inversion, electrospinning, stretching, interfacial polymerization, track-etching, etc. However, the choice of techniques for membrane preparation depends on the materials that will be used and the desired structure that will be needed for the particular application. Such as factors like membrane material (polymer type), pore size requirement, and surface properties. Therefore, it is also essential to select the appropriate method and material to achieve the desired membrane for the specific application to which it is targeted.

1. **Phase inversion**

Phase inversion is a regulated transition from the liquid to the solid state of an initially homogenous polymer solution caused by the demixing of one or more solvents. This procedure involves either utilizing a non-solvent (such as water) or evaporating the solvent(s) in which the polymer is dissolved. This process is less expensive than other fabrication methods, and it is also a desirable and industrially practicable method. This method can be divided into various categories [118], including:

a. Immersion precipitation/ Non-solvent induced phase separation (NIPS)
b. Thermally-induced phase separation (TIPS)
c. Evaporation-induced phase separation (EIPS)
d. Vapour-induced phase separation

a. Immersion precipitation/ Non-solvent induced phase separation

Initially, a polymer solution is prepared, and this solution is cast on a suitable support and then submerged in a coagulation bath containing a non-solvent; an exchange of the solvent

and non-solvent occurs, resulting in the transfer of solvent to the non-solvent and the membrane is formed [119]. This process is known as NIPS, as shown in **Figure 1.4**. DMF, NMP and DMA are examples of regularly used solvents with a non-solvent, often water, as an affordable non-solvent during the process.

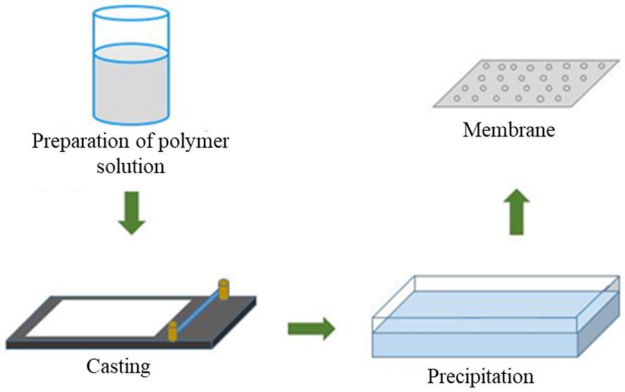

Figure 1.4: Schematic of non-solvent-induced phase separation

b. Thermally-induced phase separation (TIPS)

This technique is based on heat transfer phenomena. It is one of the important methods for creating membrane and microcellular foam. Evaporation, extraction, or freeze-drying are used in this method to remove the solvent from the polymer solution [120]. In order to create a homogenous polymer solution, a solvent and polymer are combined at a high temperature, and then the phase separation is caused by cooling the solution. By using the right cooling procedures, a microporous membrane with regulated pore size, low defect tendency, and both isotropic and anisotropic topologies can be produced. TIPS method is used to prepare polymeric membranes from various polymers like polyethylene, poly (ethylene-co-vinyl alcohol), polymethylmethacrylate, PP, and many other materials [121,122].

c. Evaporation-induced phase separation (EIPS)

This method involves dissolving the polymer in a solvent (or in a binary or ternary mixture of solvents), and a less volatile non-solvent, a viscous polymer solution, is first created.

The produced polymer solution is subsequently cast using a doctor blade process on a flat porous substrate [123]. The solvent from the cast solution on the porous substrate evaporates, leaving behind a thin film. With solvent evaporation, the non-solvent enriched droplets enlarge and coalesce, and the polymer solution separates into a polymer-rich phase, and a polymer-lean phase and the non-solvent enriched droplets are finally removed in order to create the porous membrane [124].

2. Stretching

This is a mechanical method for membrane preparation, where stretching is applied either uniaxially or biaxially (**Figure 1.5)**. This technique involves stretching a thin sheet of extruded polymer sheet to generate the pores. For the manufacturing of membranes, the stretching process does not require any solvent. This method is suitable for preparing membranes from high-crystalline polymers. The polymers are stretched to produce membranes, with the crystalline portion responsible for the membrane's strength and the amorphous region responsible for the porous structure. Stretching causes the molecular chains of the polymer to reorganize and break. Stretching is done in two steps: (a) cold stretching and (b) hot stretching. The extruded film forms a micropore nucleating site during cold stretching, while hot stretching controls the ultimate pore size and membrane structure [125]. This fabrication method is mainly useful for chemically resistant polymers, where it is difficult to dissolve in a solvent. Membranes from semicrystalline polymers like PP, polytetrafluoroethylene (PTFE), and PE are frequently fabricated by using this technique. Several factors like temperature, ratio and rate of stretching, and molecular weight of polymer decided the pore structure of the membrane [126].

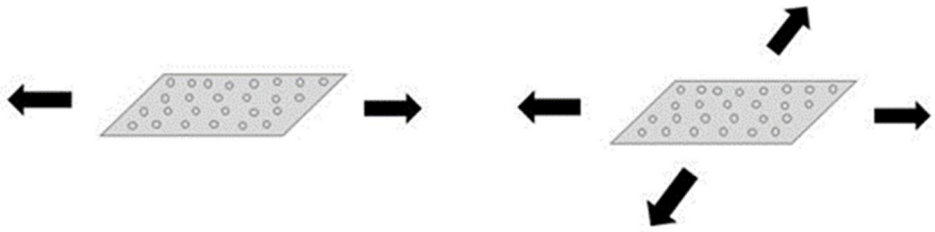

Figure 1.5: Preparation of membrane by uniaxially or biaxially stretching

3. Sintering

This method is useful for preparing membranes from polymer with excellent chemical and thermal resistance. This method is mostly used for the preparation of MF membranes. The powdered material is suitable for this technique; initially, the powder is compressed, followed by sintering at the required temperature. Due to the effect of compression, the powdered particles coalesce, and the interface present between them goes off [127,128]. In this method, the pore size of the membrane is determined by the size distribution of the polymer particles used in sintering. This method of preparation of membrane is usually applicable for inorganic and some polymers like PP, PE and PTFE [129,130].

4. Track etching

In this method, a nonporous polymeric film is exposed to high-intensity radiation or charged particles from a source like linear accelerator facilities and cyclotrons [128]. As these charged particles or high-energy radiation pass through the film, they break the polymer chain, which causes the creation of tracks on the film; a schematic for the preparation method is shown in **Figure 1.6**. This approach allows for accurate control of pore size distribution and a wide range of pore sizes from 1 to 1010 cm^2. The pore size is governed by the etching temperature and time, while the membrane porosity is determined by the film exposure time [131].

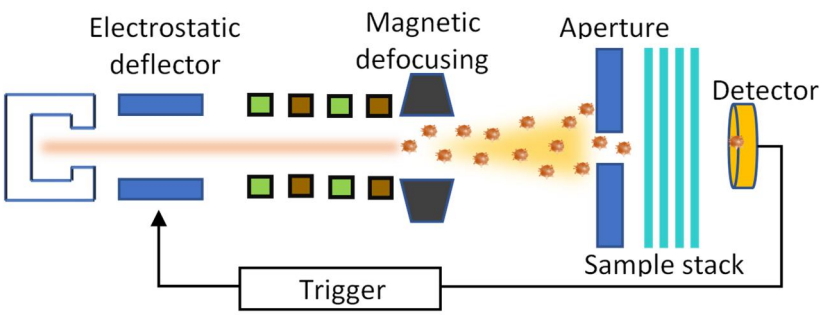

Figure 1.6: Schematic showing single ion-irradiation setup used to fabricate track etched membrane

5. Electrospinning

In this method, the electrostatic force is used to spin the fibers to form a membrane. Strong electric fields are applied to a polymer blend solution or melt during electrospinning, producing nanofibers that deposit on a grounded collector, as shown in **Figure 1.7**. In a strong electrical field, the surface tension of the polymer solution keeps it at the capillary nozzle's tip, and the electrical force develops a charge on the liquid's surface. The Taylor cone is forced to eject at a specific time when the applied electrical field reaches a critical value and is greater than the surface tension of the solution. A stable jet is formed when the required potential difference is reached. The force of the jet carries a charge, and hence, the direction of the jet can be controlled by the applied electrical field. Electrospun fibrous membranes have been utilized for filtration and membrane distillation processes because of the fine control of the fibre size, shape, and morphology [132].

Other procedures used for membrane production include coating, selective etching, layer-by-layer assembly (LBL), and graft polymerization. Polyelectrolytes are sequentially deposited over a substrate to create spray-coated membranes. In the LBL approach, the substrate was alternately coated with cations and anions, and after each deposition, the substrate was washed to remove any polymer that had been weakly deposited.

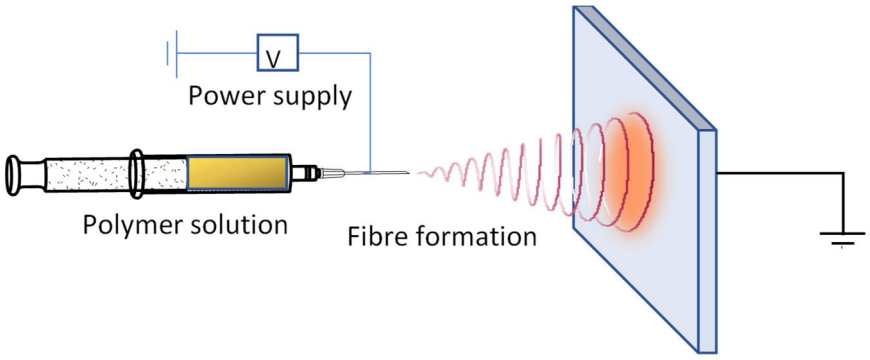

Figure 1.7: Schematic showing electrospinning of polymer solution

1.3.3 Major Problem Associated with Membrane in Oil-water Separation

During the separation process, oil and other associated contaminants accumulate over the membrane surface or inside the pores **(Figure 1.8)**, which is the basic cause of the decline of the membrane flux, effectiveness, lifespan and efficiency.

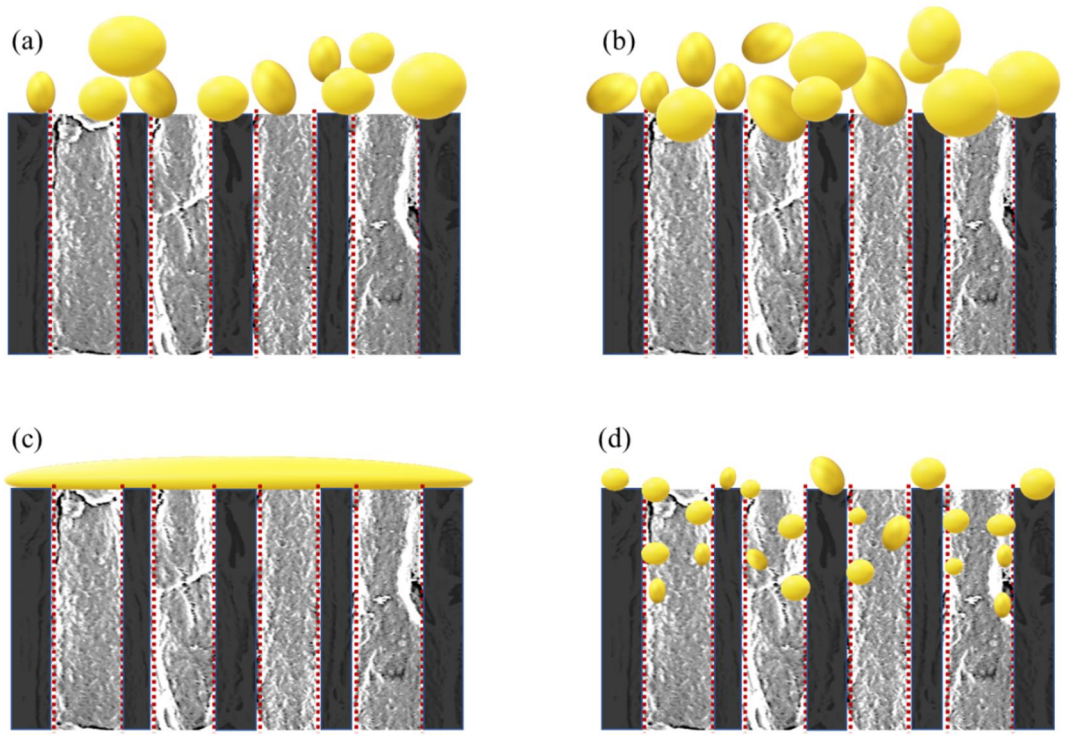

Figure 1.8: Schematic representation of the fouling of membrane by oil droplets (a) partial blockage (b) blockage by forming a cake layer on the surface of the membrane (c) complete blockage of the pores by forming a continuous layer of oil (d) oil droplets inside the pores of the membrane

For dead-end filtration, the concentration of the retentate increases over time. The resistance for the permeation of the liquid increases, membrane flux declines continuously, and the foulant layer thickness increases over the surface and inside the pores of the membrane, resulting in complete blockage of the pores [133]. This phenomenon can be reduced to some extent by using a tangential flow over the membrane surface using a cross-flow setup. But over time, the problem of fouling persists, and the membrane needs to be periodically cleaned to remove the fouling, which hampers the continuous operation of the membrane filtration process, which may result in uneconomical operation. Hence, the problem of membrane fouling needs to be given inevitable importance, which reduces the performance of membranes over time.

The performance and commercial viability and the long-term application of the membrane to efficiently separate oil and water depend mainly on the product throughput (permeation flux) and the oil rejection or rejection efficiency. These factors can be altered by changing the driving force involved (changing the pressure and the flow rate), changing the pore size, and changing the tendency fouling by the oil present in the water. Several factors were involved in the fouling of the membrane during oil-water separation, as shown in **Figure 1.9.**

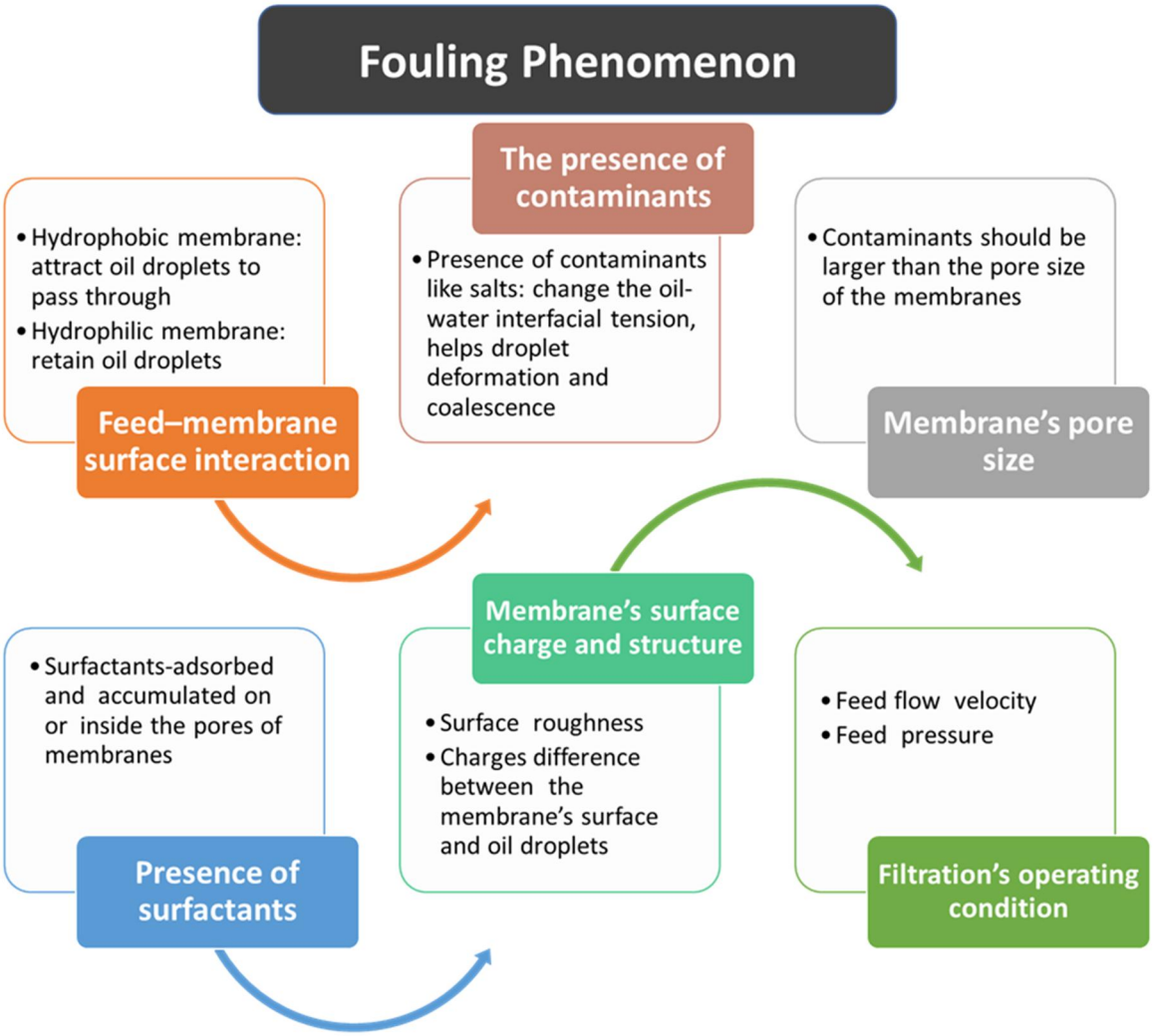

Figure 1.9: Factors affecting the fouling phenomenon

1.3.4 Oil-Water Separation Mechanisms and Fouling as Measurable Parameters

For the separation of oil from water using a porous polymeric membrane, molecular sieving is the primary mechanism involved, based on the size of the oil droplets (as discussed in section 1.2) present in the water. The pore size of the membrane is mainly involved in the efficient separation of oil droplets from water. The pores in the membrane should be typically smaller than the oil droplets but larger than the size of the water molecules; as a result, the membrane will act as a molecular sieve, selectively retaining the oil droplets and allowing the water molecules to pass through them. The separation performance of the membrane is also significantly impacted by the size and the type of oil present in water. As

mentioned before, the oil may be present as free oil, dissolved oil or emulsified oil, and the size of the free oil droplets is typically larger compared to emulsified or dissolved oil. Therefore, emulsified or dissolved oil may require a membrane with a smaller pore size, whereas free oil requires a larger pore size for efficient separation from water. In addition to pore size, other properties like wettability, governed by surface roughness, hydrophobicity or hydrophilicity and functional groups present on the surface of the membrane affect the efficiency and performance of the membrane in selectively separating oil from water. The applied pressure also controls the oil removal efficiency and the water permeation flux; the oil will pass through the membrane if the transmembrane pressure is higher than a critical pressure (P_c). If the transmembrane pressure is higher than the P_c, it will overcome the capillary pressure, and the oil droplet will be forced into the pores of the membrane. On the other hand, if the transmembrane pressure is lower than the P_c, the capillary pressure will stop the oil droplets from passing through the pores of the membrane. The critical pressure (P_c) is given by **Equation 1.1:**

$$P_c = 2\gamma_{o/w}\frac{\cos\theta}{r_o}\left[1-\left(\frac{2+3\cos\theta-\cos^3\theta}{4\left(r_o/r_p\right)^3\cos^3\theta-\left(2-\sin\theta+\sin^3\theta\right)}\right)^{1/3}\right] \quad (1.1)$$

where,

$\gamma_{o/w}$ is the interfacial tension between oil and water

θ is underwater oil contact angle (given by 180 – water contact angle)

r_o & r_p radius of oil droplet and radius of pores of the membrane, respectively

The oil droplet will pass through the pores of the membrane without applying any pressure if the value of P_c becomes negative; from **Equation 1.1**, it becomes possible when $\theta<90°$. So, to separate out the oil from water without passing through the pores of the membrane,

θ should be sufficiently greater than 90°, indicating that the membrane should be hydrophilic.

Flux Decline

The flux through a membrane is calculated by using Equation 1.2.

$$J_{w1} = \frac{V}{A \times \Delta T} \tag{1.2}$$

Where V is the volume of permeate (m^3), ΔT is the filtration time (h), A is the effective membrane area (m^2), and J_{w1} is the permeation flux (L/m^2h or LMH). As the filtration continues for a longer time, the flux declines and can be measured with flux decline ratio, which is the ratio of instantaneous flux (J_t) to the normalised permeate flux before fouling (J_o), given as J_t / J_o

Flux Recovery Ratio

A criterion for the antifouling capacity of the membrane is the flux recovery ratio (FRR); the antifouling property of the fabricated membrane was studied by filtering DI water followed by oil-water emulsion and again followed by DI water, and then FRR was calculated. Initial DI water flux (J_{w1}) is measured, then the membranes were used for oil-water separation and, washed with DI water and used again for PWF measurement (J_{w2}) by keeping the conditions the same as that of the previous procedure. Due to the adsorption of oil on the membrane surface, fouling occurs, and as a result, the water flux is decreased due to the deposition of the crude oil layer on the membrane. The expression is given as follows

$$FRR(\%) = \frac{J_{w2}}{J_{w1}} \times 100 \tag{1.3}$$

where J_{w1} and J_{w2} are the water flux before and after oil filtration, respectively.

Oil Rejection

Rejection is one of the important parameters to evaluate the performance of the membrane, which also indicates the permeate and retentate quality. For measuring the rejection ratio (R) in the case of oil-water separation, initially, the PWF is measured, and after measuring the PWF (J_{w1}), the feed was replaced with crude oil emulsion in water, and the permeate flux (J_p) was recorded. R was calculated with the following Equation:

$$R(\%) = \left(1 - \frac{C_f}{C_i}\right) \times 100 \tag{1.4}$$

$$\eta = 1 - \frac{C_f}{C_i} \tag{1.5}$$

Where, C_f and C_i (mg/L) are the oil concentrations in the permeate and initial feed water solutions, respectively and η is the oil rejection rate.

Reversible and Irreversible Fouling

The decline in flux is either due to reversible fouling or irreversible fouling. To further analyze the antifouling performance, the reversible flux decline ratio (DR_r) and irreversible flux decline ratio (DR_{ir}) are evaluated. The fouling that occurs at the surface of the membrane is somehow recoverable by cleaning; this is called reversible flux, and the irreversible fouling completely blocks the pores and cannot be recovered by cleaning. The following Equations are used to calculate DR_r and DR_{ir}

$$DR_r(\%) = \left(\frac{J_{w2} - J_p}{J_{w1}}\right) \times 100 \tag{1.6}$$

$$DR_{ir}(\%) = \left(\frac{J_{w1} - J_{w2}}{J_{w1}}\right) \times 100 \tag{1.7}$$

Where J_p is the oil permeate flux when the membrane is used for the removal of oil for the first time.

1.3.5 Methods for Modification and Incorporate Nanomaterials into Membranes

The commercial polymeric membranes available are mostly hydrophobic, making them prone to fouling during oil-water separation. In order to overcome the fouling problem and improve the performance, different strategies are followed, including plasma treatment, surface coating, grafting with functional groups, blending of hydrophilic polymers and incorporation of nanomaterials to the membrane matrix [134]. These methods are broadly classified as physical and chemical methods, represented as a schematic in **Figure 1.10**. For oil-water separation, nanomaterial incorporation in the membrane aims to improve the performance of the membrane by altering the wettability (making it hydrophilic to reduce the contact angle) and other physical and chemical properties. The addition of nanomaterials in the membrane matrix can also provide better control over pore size distribution and enhance the overall performance of the membrane due to their unique physical and chemical properties. Among the different techniques available to add nanomaterials to the membrane, surface coating/dip coating of the membrane [135], vacuum deposition [136], electrospinning [137] and blending of nanomaterials into the dope solution [138] are commonly followed.

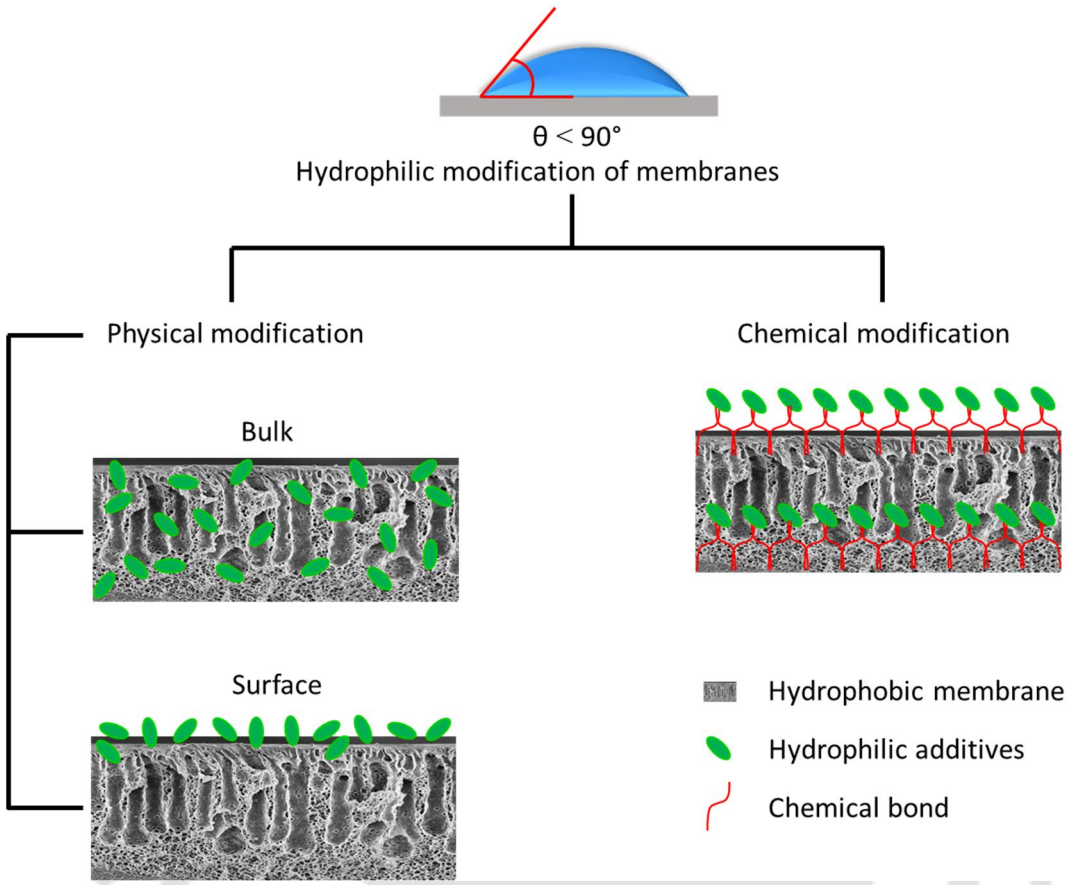

Figure 1.10: Methods for hydrophilic modification of membrane

Dip coating: It is an easy and reliable technique for adding nanoparticles to polymeric membranes. This method involves dipping the membrane into a solution containing the nanomaterials, allowing the particles to adhere to its surface, and then removing the membrane and allowing it to dry so the solvent can evaporate. Following coating, the nanoparticles make a thin layer over the membrane surface that improves the membrane's properties [139,140]. This technique makes it simple and efficient to coat a large membrane area cost-effectively and can be used to efficiently prepare membranes on a large scale. However, the effectiveness of the coating depends on several factors, such as the properties of the nanomaterial, the solvent used for coating, uniform dispersion of the nanomaterials in the solvent and the surface of the membrane [141]. The possibility of leaching of the nanoparticles during filtration is a major disadvantage associated with this method. It may

also be a challenge to control the thickness and uniformity of the coating on the membrane, and there is a risk of the nanoparticles forming aggregates or agglomerates. Moreover, the solvent used for the dispersion of nanoparticles should be compatible with the membrane material.

Vacuum deposition: This method involves the use of a vacuum chamber for the deposition of nanoparticles on the surface of polymeric membranes. The membrane is usually placed in the vacuum chamber, and the nanoparticles are heated or evaporated to form a vapour; subsequently, the vapour condenses onto the membrane surface, forming a thin film of the nanoparticles on the surface of the membrane [142]. This method is mostly beneficial for coating the membrane with a very thin layer of nanoparticles with controlled thickness and uniformity. The thickness and uniformity can be controlled by adjusting the temperature, pressure, and vapour deposition time. There are different types of vacuum deposition methods, like physical vapour deposition (PVD), chemical vapour deposition (CVD), and atomic layer deposition (ALD) [143]. The selection of the method for deposition depends on the properties of the nanomaterials and the desired properties of the membrane. The vacuum coating process requires specialized equipment, which can be expensive and time-consuming, making it less accessible for small-scale applications [144].

Direct blending with polymer solution: This method is one of the simplest methods for the addition of nanoparticles in the membrane. The nanoparticles are added directly during the dope solution preparation. This technique does not require any specialized equipment or time and can be easily scaled up for industrial production [145]. Desired amounts of nanoparticles are mixed with the polymer solution to form a composite solution, which is then cast to form a membrane using techniques such as phase inversion. The method is compatible with almost all types of nanomaterials and all polymer materials, and the properties of the composite membrane can be tailored by adjusting the nanomaterial

concentration [146]. Uniform distribution and dispersion of nanoparticles in the solvent are some of the major limitations of this method, which can affect the properties of the composite membrane. However, this limitation can be overcome by the application of proper dispersion techniques [147].

1.3.6 Different Nanomaterials Used in Membrane for Oil-Water Separation

Different nanoparticles are incorporated into the membrane structure to significantly improve antifouling and separation performance [148]. Different nanoparticles like SiO_2 [149], TiO_2 [150], carbon nanotubes [151], GO [152], silver-based nanoparticles [153], Fe_3O_4 [154], ZrO_2 [155], Al_2O_3 [156], CNC [157], etc. are being used. Detailed discussion regarding the addition of CNC will be carried out in the further section. GO coated in polyamide membrane creates fully recoverable UF membranes with a hierarchical surface roughness, which helps in minimizing the oil adhesion to the surface of the membrane, which in turn reduces the fouling and enhances the separation performance [158]. Guo Fanjin et al. [159] developed a PVDF aluminium oxide (Al_2O_3) nanowires and GO nanosheets membrane for oil-water separation. The addition of GO-Al_2O_3 nanowires improved the roughness of the PVDF membrane. The permeability of the membrane was 31 times that of the GO–PVDF membrane, which has an optimal mass ratio of Al_2O_3 to GO of 7.5. The GO–Al_2O_3–PVDF membrane also shows an improvement in hydrophilic and oleophobic properties. Both the GO–PVDF and GO–Al_2O_3–PVDF membranes had high oil-water separation rates of 97.9% and 99.4%, respectively. The oil concentration used was 200 mg/L. The study suggests that the GO–Al_2O_3–PVDF membrane has potential application in oil-water, and further research on its cleaning procedure is needed. Prince et al. [160] prepared a PES hollow fiber UF membrane using graphene-attached poly acrylonitrile-co-maleimide (G-PANCMI). The results showed that the G-PANCMI played an important role in enhancing the hydrophilicity, permeability, and selectivity of the PES

membrane. The water contact angle of the PES membrane was reduced by 64.5%, while the oil contact angle was increased by 158% compared to the unmodified PES membrane. The liquid entry pressure of oil was also increased by 350%, indicating improved anti-fouling properties of the modified membrane. Additionally, the water permeability increased by 43% with >99% selectivity. Researchers have developed a superhydrophilic and underwater superoleophobic CC@TiO_2@Ag membrane with a broccoli-like morphology using a hydrothermal and photo-deposition method. They found that the Ag content strongly affects the oil-water separation and self-cleaning performance of the membranes. The CC@TiO_2@Ag membrane demonstrated high separation efficiency of various oils, with efficiencies above 99% after 60 cycles. Additionally, the CC@TiO_2@Ag membrane showed superior self-cleaning, reusability, flexibility, and mechanical durability. The membrane has broad prospects in underwater oil recovery, self-cleaning, and wastewater purification [161]. Zioui D. et al. [162] reported the fabrication of TiO_2/P(VDF-TrFE) nanocomposite membrane using solvent casting, and its potential for oily wastewater treatment was evaluated. The results of the membrane characterization revealed that the TiO_2 nanoparticles were uniformly distributed throughout the pores with an interconnected structure. The photocatalytic tests showed complete removal of COD, total hydrocarbons, and phosphates, as well as significant reductions in suspended solids, turbidity, TOC, nitrates, and chloride in oily wastewater. The pH range of 4 to 5.5 was found to be the most effective for removal efficiency. After seven hours of sunlight exposure, the treated water became colourless. The TiO_2/PVDF-TrFE nanocomposite membrane, which combines an inexpensive nanocatalyst and a UV radiation source available in sunlight, proved to be effective for oily water remediation and has the potential for future applications. The PS-PAA/TiO_2 membrane prepared by Sumithraarachchi et al. [163] enhances the oil-water separation efficiency, reusability, and durability. Polystyrene

was cross-linked with acrylic acid either through ex-situ or in-situ polymerization on TiO_2 nanoparticles. The resulting membranes had enhanced oleophilic properties with oil contact angles close to 0° and hydrophobic properties with water contact angles varying from 141 to 155°. The PS-PAA/TiO_2 membranes exhibited exceptional oil-water separation efficiencies of about 99%, separating both highly viscous and light oils from water under gravity and antigravity-driven processes. Another study aims to produce melt-blown membranes from polypropylene (PP) and TiO_2 for oil-water separation and photocatalysis. PP and varying amounts of TiO_2 are melt-blended to create masterbatches that are fabricated into melt-blown membranes. The thermal stability and photocatalytic effect of the membranes increase with TiO_2 content. The PP/TiO_2 membranes have a good morphology, better hydrophobicity even after ultraviolet irradiation, and a high oil flux of around 15,000 L/m^2h. The membranes also exhibit stable oil-water separation efficiency after repeated use and are suitable for mass production to separate oil from water in industrial dyeing wastewater [163]. Xiong Zhu et al. [164] focus on developing a bio-based polylactic acid (PLA) membrane with a superhydrophilic surface for efficient oil-water separation. To achieve this, the researchers used TiO_2 particles coated on the surface of the membrane by the spin coating method to create a rigid and robust TiO_2 armour on the PLA membrane. This unique interface provided the PLA membrane with stable superhydrophilicity and underwater superoleophobicity, making it efficient for oil-water separation. The PLA membrane demonstrated a permeation flux higher than 930 L/m^2 h and a rejection higher than 99% under 0.1 MPa for four oil-water mixtures, with stable permeability over ten cycles. Additionally, the PLA membrane showed stable water flux, permeability recovery, and high rejection to BSA and ink over long-term operation. Similarly, SiO_2 was also incorporated in the PLA matrix to prepare a membrane by electrospinning technique for oil-water separation. Lu Zihan et al. [165] successfully

created porous PLLA/M-SiNP nanofibers using electrospinning and acetone post-processing. The modified SiNPs were uniformly distributed inside and on the surface of the fibers, and increasing amounts of M-SiNP led to increased fiber diameter. A two-step process was followed to incorporate hydrophobic silica nanoparticles (SiNPs) into highly porous PLA nanofibers. The SiNPs were first synthesized and then modified to be hydrophobic. The PLA/SiNPs composite fibrous membranes were electrospun and then re-crystallized with acetone at room temperature, resulting in the transformation of non-porous fibers into porous ones with a high surface area. The presence of SiNPs inside and outside the fibers enhanced the hydrophobicity of the PLA/SiNPs nano-fibrous membrane, with a water contact angle greater than 150°. The incorporation of SiNPs into porous PLA membranes reduced their modulus and tensile strength (280.66 and 5.92 MPa) but increased their strain to fracture (80.82%). The oil absorption capacity was highest when the weight ratio of PLA and SiNPs was 1:1, and the flux of the prepared membranes was significantly enhanced (5200 L/m^2h) due to the presence of SiNPs. The PSf membrane was modified by blending SiO_2 nanoparticles to enhance its hydrophobicity. The modified membrane had larger interconnected surface pores compared to the unmodified membrane, resulting in a permeate flux of 17.32 L/m^2h for the modified membrane and 1.08 L/m^2h for the unmodified membrane, indicating 16 times increase in permeability. The addition of SiO_2 nanoparticles also improved the antifouling properties of the membrane. These results suggest that blending SiO_2 nanoparticles into the membrane composition can enhance its permeability and antifouling properties [165]. Tjale L. et al. [138] studied the development of hydrophobic/oleophilic PS/PP-FOTS-SiO_2 NPs membranes using an in-situ phase separation process. Initially, the membranes were hydrophilic with contact angles ranging from 72 to 80°, while pore sizes ranged from 0.03 to 0.25 μm. The incorporation of FOTS-SiO_2 NPs resulted in slightly hydrophobic/oleophilic membranes with a contact angle of 89

± 6°. The prepared membranes can successfully remove oil from water with oil fluxes and separation efficiency of 84.9 L/m^2h and 83.4%, respectively. The iron base nanoparticle is widely used as an additive with polymeric membranes for different applications, including oil-water separation. Zeng et al. [166] proposed a method for the fabrication of a superhydrophobic and magnetic poly (lactic acid) (SMPLA) membrane with the addition of Fe_3O_4 nanoparticles. The SMPLA membrane was found to possess superhydrophobicity, with a water contact angle of 151.7°, and exhibited strong resistance to organic solvents, acids, alkalis, and boiling water, as well as abrasion. The membrane exhibits a good self-cleaning ability with an oil-water separation efficiency of up to 99.5%. The development of electrospun nanofibrous membranes by incorporating iron oxide (Fe_3O_4) nanoparticles (NPs) to treat oily wastewater effectively is an emerging technique. Iron nanoparticles in the form of iron acetate powder were used with PSF to develop a hydrophilic, high-flux, and mechanically stable PSF-iron-based nanofiber membrane by electrospinning a PSF solution containing iron acetate powder and depositing a polyamide (PA) layer using interfacial polymerization on both sides of the membrane. This treatment changed the membrane wettability to highly hydrophilic with a contact angle of 37 ± 5°. The membrane porosity also increased to 83 ± 7% after the deposition of the PA layer and, consequently, increased the water flux to 0.38 m^3/m^2h [167]. Al-Husaini I. S. et al. [168] developed a PES by electrospinning technique; this membrane was strengthened using a hot press technique and the addition of Fe_3O_4 NPs to improve hydrophilicity and anti-fouling resistance. The developed membrane exhibited excellent oil removal efficiency (94.01%) and water flux recovery (79.50%) with a water productivity of over 3200 L/m^2h and showed antifouling fouling character. Ouda M. et al. [169] reported the fabrication of PES-maghemite composite membranes for oil-water separation. The membranes with different wt.% of γ-Fe_2O_3 were characterized, and their performance was evaluated in terms of water flux, flux

recovery, and oil rejection was evaluated. A flux recovery ratio of 56% and PWF of 1323 ± 27 L/m^2h was obtained by the addition of 0.25 wt.% PES/γ-Fe_2O_3 in the membrane. The removal efficiency increased from 39.2% in the PES membrane to 81.7% in the 1.00 wt.% PES/γ-Fe_2O_3 composite membrane. Among the various nanomaterials, bio-based nanomaterials are gaining additional importance for their potential applications in membrane technology. These nanomaterials are derived from plants, trees, or agricultural waste and offer several advantages over inorganic nanomaterials. CNC is one such nanomaterial with the advantage of being biocompatible, having high mechanical strength, and availability of surface-active groups, making them ideal for different functionalizations.

1.3.7 CNC as an Additive in Membrane

The use of CNC in membrane fabrication technology is a green approach to water remediation technology. A summary of the different polymeric membranes using nanocellulose as an additive with the targeted pollutants and the removal rate is shown in **Table 1.3**. As mentioned in the previous section, CNC provides good mechanical stability and rigidity to the membrane. Because of the high crystallinity of CNC, it can be used for an extensive range of pH, and the membrane can be acid-washed for regeneration without a change in properties. CNCs have a high surface area containing numerous active sites that interact and immobilized pollutants present in wastewater. CNC contains a hydroxyl group on its surface, which makes it highly hydrophilic, and it does not swell in water [170]. CNC is suitable for different types of functionalization due to the abundant and free hydroxyl groups on the surface. The addition of different functional groups such as carboxyls, sulfonates, amines, thiol, carbonyls, and phosphates onto the surface of CNC makes it versatile to bind a specific pollutant present in wastewater [171]. Other important advantages of using CNCs in the membrane are it give higher permeability, can select

specific components, and have better resistance to biofouling as compared to the membrane without CNC [172]. Many researchers have reported the incorporation of CNCs into a large number of polymer matrices like polyimide [173], PAN [174], cellulose acetate (CA) [175,176], poly (vinylidene fluoride) (PVDF) [177], poly (ether sulfone) (PSf) [178], poly (vinyl alcohol) (PVA) [177]. Even with a small amount of CNC loading, it improves the membrane properties distinctively, and thus, the presence of all these special properties makes CNC a favourable candidate to be used with different polymers for the fabrication of high-performance membranes. Many patents and research papers have demonstrated that wood biomass/cellulose-based waste material is a sustainable and economically feasible raw material for the manufacture of CNCs [179]. The acid hydrolysis method is the most commonly used method for the fabrication of CNCs [180]. The use of sulfuric acid, hydrochloric acid, nitric, etc., in the preparation of CNC does raise significant environmental and safety concerns due to its hazardous nature. To address these concerns, researchers are actively exploring alternative methods for the fabrication of CNCs that are safer and more environmentally friendly. Some of these methods include enzymatic hydrolysis, mechanical treatment and deep eutectic solvents; however, these methods are expensive and do not produce high-purity CNCs. Therefore, the acid hydrolysis method is still a preferred method for the fabrication of CNCs, with a provision to recycle the acid solution in the process[179]. Rajendran N. et al. [181] carried out a detailed techno-economic analysis and life cycle assessment of CNC production from a wood-based source by acid hydrolysis method, and their results indicated that CNC fabricated using acid recovery process was economically more profitable than without the acid recovery process. **Figure 1.11.** shows the strengths, weaknesses, opportunities, threats analysis and prospects for research based on nanocellulose-based membranes.

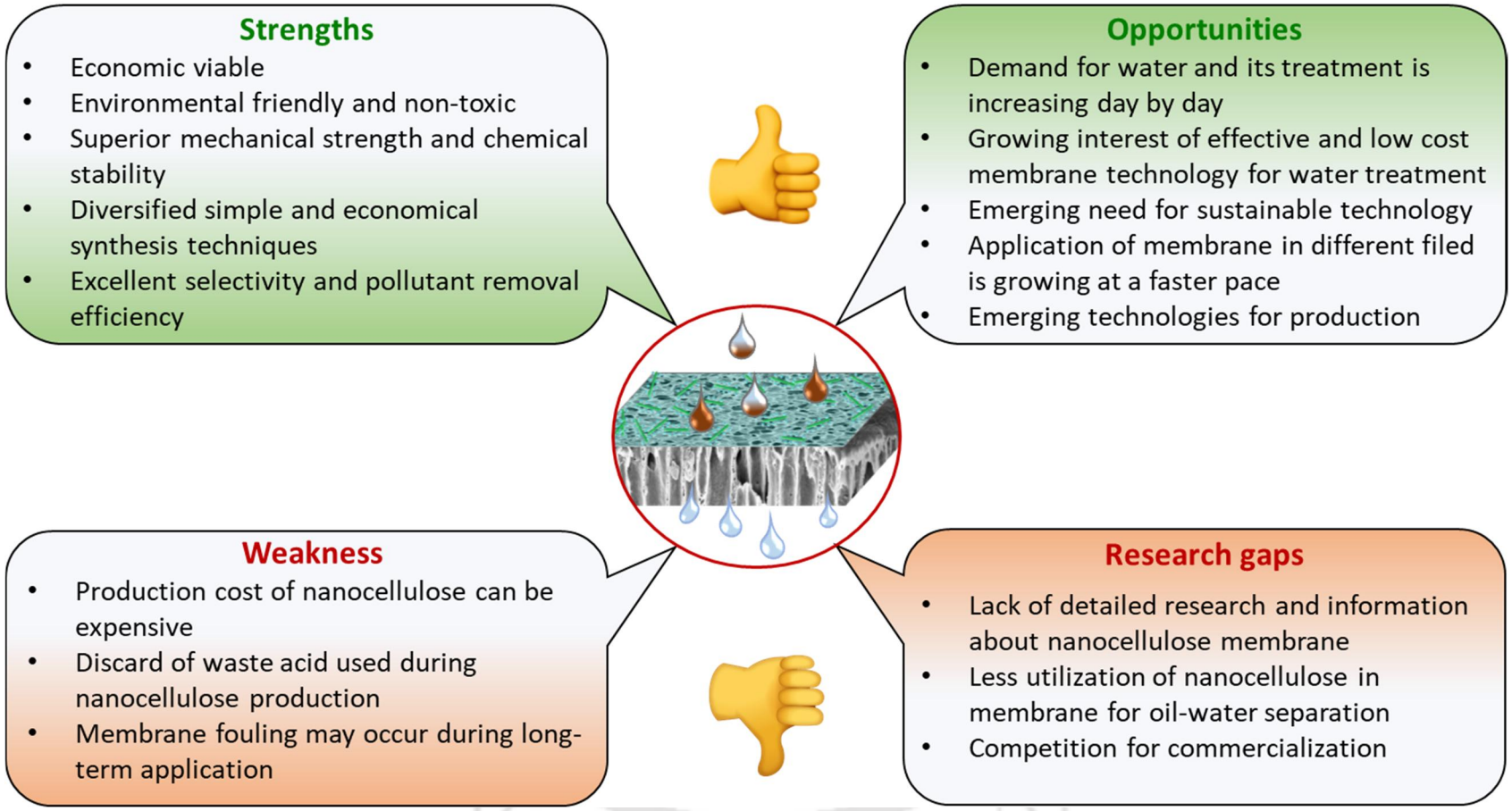

Figure 1.11: Overall strengths, weaknesses, opportunities prospects for research based on nanocellulose-based membrane

Table 1.3: Summary of composite membranes based on nanocellulose for water treatment with the targeted pollutants and the removal rate

Membrane material	Nanocellulose (%)	Pressure (kg/cm^2)	Pollutants	Flux (L/m^2h)	Removal rate	Reference
PVDF	0.1 wt %	1	BSA	230.8	92.5	[182]
Chitosan	90 wt%	2	Dyes	64	98 % (Victoria Blue) 84 % (Methyl Violet) 70 % (Rhodamine)	[183]
PA/PLS	0.05 wt%	6	Salt	106.9	98.3 % (Na_2SO_4) 96.1 % ($MgSO_4$)	[184]
Cu mesh	–	Gravity	Aqueous crude oil mixture	~35 000	–	[185]
PES	1 wt%	–	Color & COD	–	94 % (Color) 88 % (COD)	[186]
Polyamide (PA)	–	6	Na_2SO_4	204	96.7 %	[187]
Polysulfone	0.21	5	Nitrate	7.2 ± 1.8	94%	[188]
Cellulose ester	26.7 mg/ml	–	Antibiotic	~168	89 % Tetracycline hydrochloride	[189]
PA/PES	0.01 wt% CNC/Ag	4.8	Salt Bacteria	25.4	99.1 % (Na_2SO_4) 99.4 % (*E. Coli*)	[190]

PES	2 wt%	0.30	Humic acids (HAs), BSA	~60	71.9 % (HA) 82.7 % (BSA)	[191]
Polyamide	0.21 g	6 to 10	Sodium chloride calcium chloride	12.7 ± 1.9	98.3 ± 0.8% 97.1 ± 0.5%	[192]
Polyamide-amine-epichlorohydrin (PAE)	~2 g/m^2	1	BSA	~53	79.7%	[193]
Polyamide (PA)	–	–	Bacteria (*E. Coli*)	44.3 ± 0.7	~89 %	[194]
PES-Z-CNF@TFN	0.05	4	divalent salt	14.4	98.3 (Na_2SO_4)	[195]
PVDF (electrospun)	1 wt%	–	Soyabean oil-water	85.65	99%	[98]

Different properties of the membrane improved by the incorporation of CNCs are discussed in detail in the following sections.

1.3.7.1 *Improved Mechanical Property*

For application in industrial wastewater purification, a membrane should have excellent mechanical strength and rigidity so that it can offer resistance to the prevailing high-pressure conditions required for separation. CNC can impart high mechanical strength and porous structure to the membrane, and the hydroxyl group present on the surface of one CNC is available for bonding with other CNC and can form a high-order arrangement, due to which it gives favorable mechanical strength and rigidity [177]. A small percentage of CNC loading can improve the tensile strength of the polymeric membrane by 50%, and elongation is improved as compared to the nascent polymeric membrane [178,196]. However, the tensile strength does not increase linearly with an increase in CNC loading. Polyvinylidene fluoride-co-hexafluoropropylene (PVDF-HFP) membrane has 2 wt% CNC shows the highest tensile strength with an improvement of 75%, and it decreases with an increase in CNC loading [197–199]. The decrease in structural properties with an increase in CNC loading is due to the agglomeration of CNCs inside the polymer matrix, where the interaction of particle to particle dominates the polymer nanoparticle interactions. Higher loading also creates inhomogeneity, which becomes a site for stress concentration, resulting in a decrease in tensile strength [197]. CNCs tend to aggregate and affect both amorphous and semicrystalline polymers, making it difficult to obtain a homogeneous dispersion. The CNCs get aggregated when their surface come in contact with each other due to short-range thermodynamic interactions. The aggregation of two similar particles is called homoaggregation, so the homoaggregation of CNCs causes inhomogeneity in the membrane and affects the crystallinity of the polymer as it perturbs polymer chain

alignment. This is one of the reasons behind the nonlinearity in the increase of tensile strength of the membrane with the increase in CNC loading.

1.3.7.2 *Porosity, Permeability, Separation Capacity and Hydrophilicity*

In comparison to the pure polymeric membrane, the addition of CNC to all polymeric membranes causes some structural and morphological differences. It may become more porous, and the interconnection may increase. With CNC loading of 0.8% to the CA membrane, it shows an increase in porosity of 23.6% compared to pure CA membrane with a total membrane porosity of 66.4%. The water flux also reached a maximum value of 72% with 0.5% of CNC loading, which is 10.9% higher than the pure CA membrane [176]. CA-CNC membrane also has a higher flux of 13,500 L/m^{2}h bar than PAN-CNC membrane, having a flux of 5,900 L/m^{2}h bar. This is also due to the presence of larger pore size and hydrophilicity of CA-CNC-based membrane compared to PAN-CNC-based membrane [198]. Improvement in hydrophilicity of the membrane containing CNCs comes from the abundant availability of hydroxyl groups on its surface. However, with higher CNC loading, the mean pore size diameter decreases after reaching a certain maximum value, which will lead to a decrease in the overall permeability of the membrane at higher loading. The decrease in pore size diameter is because of an increase in solution viscosity with an increase in CNC loading, which reduces pore size during the phase inversion process [199]. Even in the case of the electrospun membrane, the pore size diameter becomes smaller with an increase in the amount of CNC. The higher amount of CNC increases the diameter of the electrospun polymer fibres, which results in smaller pore sizes. This was observed by Lalia et al. [197] in the preparation of PVDF-HFP electrospun membrane with CNC loading. The decrease in pore size with an increase in CNC loading will directly affect the flux of the membrane. It is noteworthy to mention that the amount of CNC affecting different properties of the membrane depends upon the type of polymer used for membrane

fabrication. Zhen et al. [177] also demonstrated that the addition of a small amount of CNC to PVDF/poly (methyl methacrylate) (PVDF/PMMA) membrane modifies the hydrophilicity. The inclusion of CNCs with proper concentration to the polymeric membrane will considerably improve porosity and hydrophobicity, leading to the use of less nonsustainable material to improve the same level of porosity and hydrophobicity.

1.3.7.3 *Antifouling Property*

In many separation processes, such as oily wastewater treatment, antifouling properties of the membrane are of vital importance to ensure high separation efficiency and regeneration. Many polymeric membranes cannot be used repeatedly for many cycles due to their fouling characteristics. Several methods have been attempted for different types of membranes to make them antifouling, such as making the membrane surface hydrophilic, surface coating or grafting, and blending with antifouling material [200,201]. The antifouling properties of different polymeric membranes were improved by loading them with CNC. When CNC (0.5 wt%) is incorporated into the CA membrane, a significant improvement in the antifouling property is shown with an increase in flux recovery ratio of 68% in comparison to pure CA membrane [176]. After repeated use for 10 cycles of filtration, the membrane shows excellent separation efficiency of 99% with almost the same flux, which indicates the antifouling property of the membrane [202]. This is due to the inherent hydrophilicity of the CNCs, which ensured their exceptional antifouling properties.

1.3.7.4 *Biocompatibility*

Membrane technology has been used in biomedical applications since 1943 when Kolff and Berk treated a uremic patient with a membrane dialyzer [203]. Since then, the membrane has been used in different biomedical applications, including hemodialysis [204], gas exchange during bypass heart surgery [205], tissue engineering [206], bioartificial organs [207], and biopharmaceutical purification [208]. A membrane for

biomedical applications can be used depending on its biocompatibility because bioincompatibility can give rise to serious health concerns. For example, the blood has to pass through an extracorporeal tubing loop during open-heart surgery, and repeated contact of blood with an artificial surface results in serious consequences to the patient's health [209]. Therefore, to avoid such serious side effects, proper biocompatible material should be used in membrane fabrication. CNCs are derived from a natural source; they are intrinsically biocompatible, which is also proved by several studies. Wang et al. [210] developed a membrane by doping CNCs into a high-molecular-weight polyethylene (HMWPE) used in artificial joints as bearing material, which shows improvement in biocompatibility after doping with CNCs compared to pure HMWPE membrane. Polypyrrole (PPy) membrane with nanocellulose material was developed for use in hemodialysis membranes, which can effectively remove small uremic toxins. This composite membrane is more biocompatible compared to the pure polymeric reference membrane [211]. Cationic CNCs (CCNC) combined with anionic alginate biocompatible double membrane is used for complexing drug codelivery, where both the layers of the membrane release drugs with different behaviours. CCNC is contained in the inner layer, which releases drugs in a sustained manner, and the outer layer is released rapidly [212].

1.3.8 Use of Magnetic Field in Membrane Fabrication Technique

With the advent of new technology and the requirement for more specific functions, new and novel techniques are being employed for the fabrication of membranes. One such technique is the application of magnetic nanoparticles such as FeO, Fe_2O_3, Fe_3O_4 and other metal oxides or nanohybrid materials like GO/iron oxide nanohybrids, metal oxide/SiO_2 are gaining considerable importance due to their superior chemical and mechanical properties, and good dispersal. Literature suggests that the addition of magnetic nanoparticles (mNPs) during membrane fabrication helps to move the particles in the

magnetic field direction and improves water flux and rejection. During the membrane preparation process, magnetic fields can be employed to regulate how mNPs are aligned. The surface properties of the membrane can be improved by providing a magnetic field, which causes mNPs to be directed to migrate to the surface of the membrane and lead to improvements in mechanical strength, water filtration efficiency, and fouling resistance. It can also result in an improvement of the magnetic properties of the membrane, like magnetic permeability and magnetic anisotropy. The applied magnetic field can increase the stability of the mNPs and stop them from aggregating or settling to the bottom of the solution, enhancing its homogeneity and uniformity in the prepared membrane. The magnetic field applied during membrane formation can further influence the formation of the polymeric membrane and affect the pore structure of the membrane, resulting in changes in its permeability and selectivity. During the membrane-formation process, the magnetic field is applied either with the help of a magnetic coil or with the aid of permanent magnets.

The use of a magnetic field during the membrane preparation process encourages the mNPs to migrate to the surface, thereby significantly improving the membrane surface properties. P. Jian et al. [154] prepared a PSF–Fe_3O_4 composite membrane by adding magnetic Fe_3O_4 nanoparticles by phase inversion method, and the performance was evaluated under a magnetic field and observed that rejection of lysozyme was reduced. Huang et al. [213] reported the use of a magnetic field during the fabrication of PVDF/Fe_3O_4 membrane during the phase inversion process. Their results indicated that when the concentration of Fe_3O_4 mNPs is more than 60%, the magnetic field forces the mNPs to arrange along the direction of the applied field and results in the formation of "lamellar microvoids". The membrane with 70% Fe_3O_4 showed the best performance in PWF and fouling resistance. Another study reports that the application of a magnetic field increases the performance of

Fe_3O_4/GO/PVDF membranes. A simple one-step chemical coprecipitation approach to create superparamagnetic and hydrophilic Fe_3O_4/GO (MGO) particles with Fe_3O_4 nanoparticles evenly dispersed on the surface of GO nanosheets. The synthesized MGO composite particles were dispersed in a PVDF solution. The functional layer containing MGO particles is then generated by applying a magnetic field to arrange the MGO particles on the surface of the PVDF membrane during the phase inversion procedure. Compared to membranes without magnetic field treatment, the results reveal that this technique improves the resultant membranes' pure water flow, hydrophilicity, and antifouling characteristics. The MGO/PVDF membranes have a high PWF (484 L/m^2h) and a high flux recovery ratio (up to 83.0%). Thus, the authors reported that magnetic field-induced ordered organization of MGO composite particles during membrane fabrication is a potential method for producing a high-performance membrane [214]. A similar study was conducted by Zinadini et al. [215] by using $ZnFe_2O_4/SiO_2$ as mNPs to fabricate PES nanocomposite membranes by phase inversion method under a magnetic field. The study aims to investigate the effect of coagulating in a magnetic field on the properties of $ZnFe_2O_4/SiO_2$/PES nanofiltration membranes fabricated using the phase inversion method. The results revealed that adding $ZnFe_2O_4/SiO_2$ nanoparticles to the casting solution enhanced the hydrophilicity of the membrane surface. The magnetic treatment of the casting solution resulted in an orientation of the nanofillers in the top layer of the membrane, which in turn influenced the PWF, hydrophilicity, and antifouling properties of the fabricated membranes. However, the high concentration of nanofillers caused pore blockage, resulting in a decrease in flux.

1.4 Research Gap

Although using a chemical dispersant is an efficient way for the treatment of an oil spill, there are several drawbacks and potential detrimental effects. Therefore, before choosing to utilise chemical dispersants in an oil spill response, it is crucial to weigh these

disadvantages against the advantages carefully. To address the drawbacks associated with conventional chemical dispersants, bio dispersants as potential substitutes need to be explored. On the other hand, although several polymeric membranes have been developed for oil-water separation, there is still a need for the development of new and more efficient membranes that can separate oil and water with high selectivity and permeability. The application of bio-based nanomaterial in membrane technology is limited. Despite the extensive use of different inorganic-based nanoparticles to 'tailor' membrane pore structure, surface properties and cross-section morphology by the selection of appropriate fabrication methods, there is still a challenge to produce reliable membranes with anti-fouling properties, chemical resistance, high mechanical strength with high flux and selectivity. This is due to the presence of diverse compounds in oily wastewater, including many molecules that stick to the membrane and promote fouling, thereby reducing membrane life, which is still a very challenging problem affecting the filtration process. A novel material having a high resistance for such compounds is required to be developed with different surface modifications of the existing membranes. Therefore, there is a possible scope for research to utilize bio-based nanomaterial in membrane technology. Moreover, improvement in membrane fabrication techniques and application of bio-nanoparticle coated with mNPs has a broad scope.

1.5 Objectives

The overall aim of the current research work is to fabricate membranes with emphasis on utilizing nanoparticles derived from bio-based source, as an additive in the membrane and application of magnetic field during membrane preparation to improve its properties. And also, to utilize it for removal of oil from oily wastewater with more than 95% rejection of oil and limiting the oil concentration in to 10 mg/L as per the Central Pollution Control Board's Environment (Protection) Rules of 1986.

The specific objectives are:

- *To understand the interaction of the oil-water system with modified biopolymer as an environment-friendly dispersant for oily wastewater treatment:* This objective aims to comprehensively analyze the dynamic interplay between the oil-water system and a specifically tailored biopolymer, engineered to function as an environmentally benign dispersant in the context of treating oily wastewater.
- *Fabrication of polymeric nanocomposite membrane with cellulose nanocrystal and its characterization and performance study:* Synthesis and characterization of a polymeric nanocomposite membrane incorporating cellulose nanocrystals, followed by an in-depth investigation into its performance and functionality like selectivity, antifouling ability.
- *Fabrication of polymeric nanocomposite membrane with magnetic cellulose nanocrystal and its characterization and performance study:* Preparation of a magnetic cellulose nanocrystal incorporated into polymeric nanocomposite membrane, followed by detailed analysis of its structural attributes, properties and performance characteristics. Furthermore, this objective also includes investigating the application of this membrane for oil-water separation applications and assessing its effectiveness in this context.
- *Effect of magnetic field-induced coagulation during phase inversion of PVDF/FeCNC membrane on its performance:* This objective includes the investigation of the influence of magnetic field-induced coagulation on the phase inversion process of cellulose nanocrystal incorporated PVDF membrane and its subsequent impact on the membrane's performance characteristics. Additionally, investigates the viability of the membrane for oil-water separation applications and evaluates its efficiency.

1.6 Organization of the Thesis

The current thesis is divided into seven chapters. **Chapter 1** is the current chapter, which includes the introduction and literature review. **Chapter 2** includes the sample preparation methods and methodologies for preparing different materials and membranes used in the research. It also includes different materials used for the experimental work and different characterization methods used. **Chapter 3** discusses the role of biopolymer as a bio-dispersant to stabilize crude oil droplets and its application for enhancing the degradation of oil by isolated bacteria. Biopolymers XG and Oligo lactic acid conjugate chitosan (OCH) are used as bio-dispersants. The stabilized oil droplets are allowed to be degraded by the isolated bacteria *Pseudomonas aeruginosa* CoE-SusPol3. **Chapter 4** explains the fabrication of CNC from waste paper sources and their characterization. It also discusses the incorporation of CNC in polyvinylidene fluoride (PVDF) membranes for enhanced performance mechanical and antifouling properties. The application of magnetic CNC (FeCNC) in PVDF membranes in place of neat CNCs was discussed in **Chapter 5**. It includes the characterization of the fabricated membrane in its potential application in oil-water separation. **Chapter 6** presents the study of the effect of a magnetic field on PVDF-FeCNC during membrane formation. It discusses the fabrication of PVDF nanocomposite membranes using self-synthesized FeCNC as an additive by applying a magnetic field during coagulation and applying it for the testing of oil-water separation performances. **Chapter 7** summarizes the research work that has been carried out and gives brief suggestions concerning future research in the field.

Chapter 2
Materials and Methods

In this chapter, detailed information about the major experimentation, various materials and methods used to carry out the research work is described. It provides information about sample preparation methods, different characterization techniques and the procedure involved. For ease of study, the material used, experimental procedures followed, and the characterization methods used are categorized into three sections. It gives information about the raw material used for the preparation of cellulose nanocrystal (CNC) and oligo lactic acid conjugate chitosan (OCH), and the method involves for its preparation and further functionalization of CNC with different iron nanoparticles to make it magnetic CNC (FeCNC). This chapter also provides information about the fabrication of polymeric membranes with CNC, FeCNC and by application of a magnetic field. Various characterization methods using instruments, such as FTIR, ATR-FTIR, FESEM, AFM, UV-VIS spectrophotometer, XPS, EDX, and XRD, are also discussed. It goes on to describe the characteristics of the prepared membranes through measurements of water contact angle (WCA), BSA flux and rejection, as well as pure water flux (PWF), equilibrium water content (EWC) and oil-water separation.

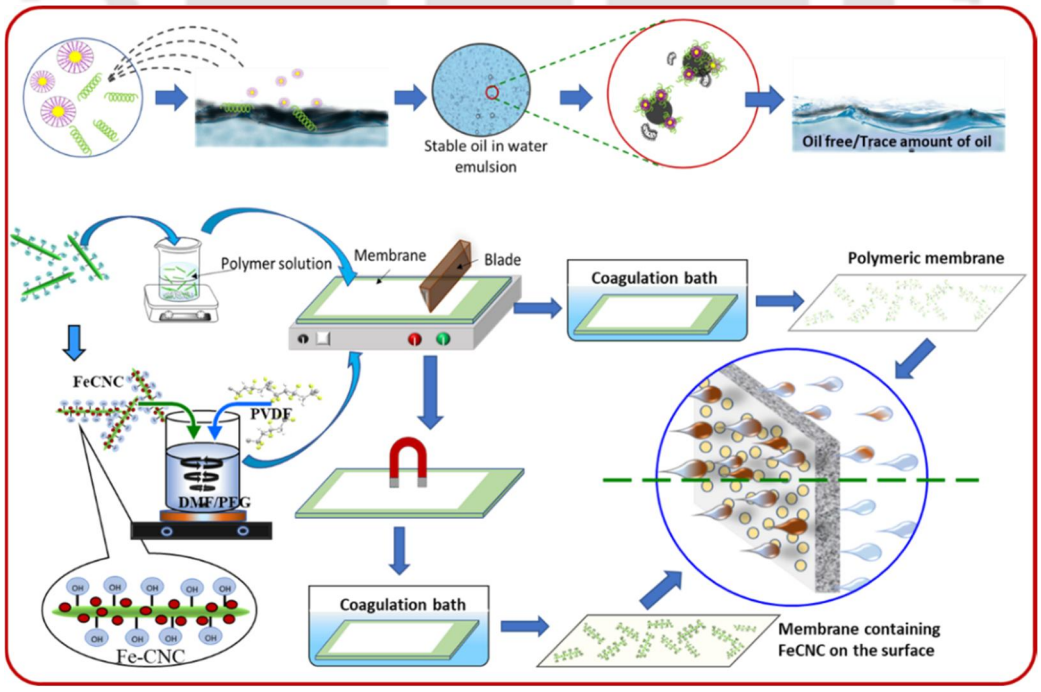

2.1 Materials

Poly(vinylidene fluoride) (PVDF) pellets with Mn=107 kDa were used for membrane fabrication, Poly(ethylene glycol) (PEG) average Mn=4000 Da was used as pore former, and N, N-Dimethylformamide (DMF) (purity > 99%) was used as a solvent were purchased from Sigma Aldrich Co. (USA). Sulphuric acid (>99%) and Bovine serum albumin (BSA) Mn=66 kDa were procured from HiMedia Laboratories Pvt. Ltd. India. Waste paper collected from office was cut into small pieces and used for cellulose nanocrystal (CNC) production. Ferrous Chloride (hydrate) ($FeCl_2$) and Ferric chloride anhydrous ($FeCl_3$) were used for magnetic cellulose nanocrystal (FeCNC) preparation. Ammonia Solution was used as a reducing agent, and methanol was used for washing FeCNC, supplied by Sigma-Aldrich (India). Millipore water (Metrohm, ELIX 3) was used as a non-solvent in a coagulation bath for the preparation of membranes, pure water flux (PWF) measurement, contact angle measurements and for the preparation of xanthan gum (XG) solution. A nickel-coated Neodymium Iron Boron magnet (NdFeB) with a magnetic field of 350-450 gauss was used during membrane casting. XG from *Xanthomonas campestris* (CAS Number: 11138-66-2, MDL: MFCD00131256) was used to increase the viscosity of the continuous phase. 20% assay L-lactic acid and medium molecular weight chitosan with a degree of deacetylation greater than 70% were used for the synthesis of oligo lactic acid conjugate chitosan (OCH) (procured from Sigma-Aldrich, India). Dichloromethane (DCM) of 99.9 % purity, was used as a solvent for GC analysis (purchased from Sisco Research Laboratories Pvt. Ltd. (SRL)-India). 2,5-dihydroxybenzoic acid (DHB) was used as a matrix for the matrix-assisted laser desorption ionization time-of-flight mass spectrometry (MALDI-TOF-MS) study. The crude oil used was collected from an oil field in the Upper Assam Basin, having a density of 0.93482 gm/cm^3. Meat extract, peptone, sodium chloride,

agar and Gram staining kit were procured from HiMedia (India). All the above chemicals were analytical grade and used without any further purification.

2.2 Methods

2.2.1 Pre-treatment of Waste Paper and Preparation of CNCs

The waste paper was cut into small pieces and soaked in water for one hour; after that, it was defibrized using a homogenizer (IKA T25 digital ultra Turrax®) at 10000 rpm for 15 min. Homogenized pulp was obtained by filtering using a fine mesh and pre-treated using 5 wt% H_2O_2 and 3 wt% NaOH solution in the ratio of 1:30 to degrade the chromophoric groups and change it to colorless groups [216,217]. Further, the homogenized pulp solution was kept at stirring (800 rpm, 60 °C) for 2 h at room temperature. It was washed several times with DI water to obtain a neutral pH. Finally, the obtained pulp was dried at 60 °C in a hot air oven for 24 h to remove the water present in it. The dried pulp was further ground with a high-speed mechanical grinder for disintegration. CNC was prepared from the pulp by sulphuric acid hydrolysis procedure discussed by Dhar et al. [218]. In brief, the finely grounded pulp (approx. 2 g) was used for hydrolysis using sulphuric acid (H_2SO_4). The concentration of H_2SO_4 used was 64 wt%. The finely grounded pulp was put in the acid solution, and it was kept under vigorous stirring continuously for 2 h using a magnetic stirrer at 500 rpm at 45 °C. In order to stop the hydrolysis reaction, chilled deionized water was used in excess amounts. After that, centrifugation was done, followed by dialysis. Dialysis was carried out using a cellulose acetate membrane until pH 7 was reached. Finally, the CNC was obtained by freeze-drying the neutralized pH suspension at -80 °C. A flow chart for the preparation of CNC is shown in **Figure. 2.1.**

Figure 2.1: Flow chart for pre-treatment of waste paper and preparation of CNCs

2.2.2 Fabrication of Magnetic Cellulose Nanocrystals (FeCNCs)

FeCNC was prepared using the co-precipitation method. Two iron salts were used ($FeCl_3$ and $FeCl_2$). 40 mg of CNC was uniformly dispersed in DI (20 ml) water using a benchtop ultrasonicator (amplitude 30%, for 10 min). Both $FeCl_3$ (80 mg) and $FeCl_2$ (20 mg) salts were dissolved in 30 ml of DI water and subsequently added to the dispersed CNC suspension. The solution was kept under vigorous stirring (~600 rpm) for 2 h at 55 °C, and

the temperature was raised to 85 °C after 2 h and the stirring speed to ~1000 rpm. For the adsorption of Fe_3O_4 nanoparticles onto the surface of CNCs, 2 ml of ammonia solution (25%) was used. Ammonia solution was used as a reducing agent; it was added very slowly in a dropwise manner into the CNC iron salt solution at 85 °C and stirred at ~1000 rpm for 4 h. During the addition of ammonia solution, the suspension turned brownish-black. After 4 h, the FeCNC suspension was washed three times with ethanol to remove the impurities and centrifuged to separate out the FeCNC. Finally, it was dried in an oven at 60 °C to obtain dried FeCNC, which was later ground into powder using mortar. Fe_3O_4 nanoparticles were also prepared following the same procedure. **Figure 2.2** shows the schematic for the preparation of FeCNC by the co-precipitation method.

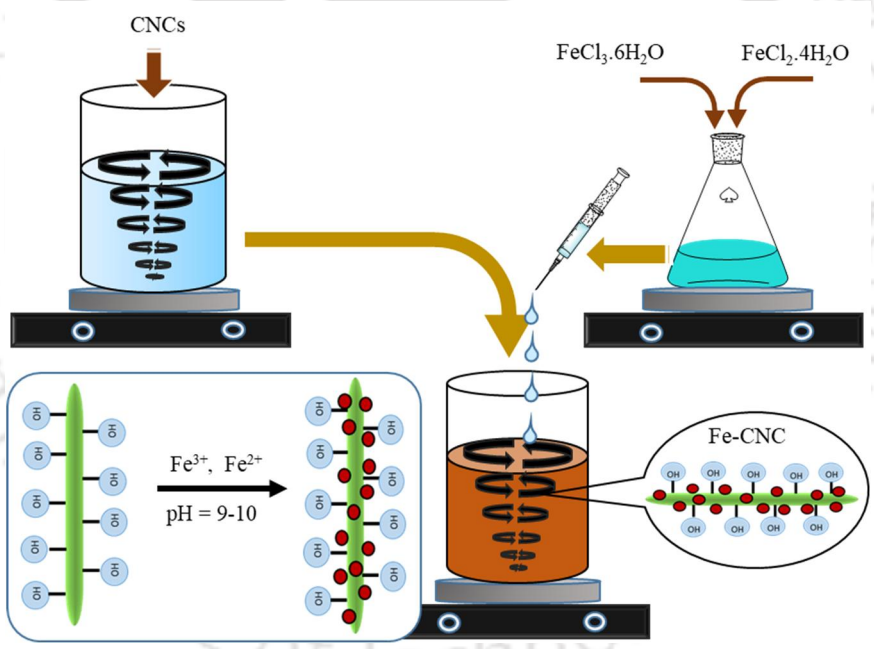

Figure 2.2: Schematic for the preparation of FeCNCs

2.2.3 Synthesis of Oligo Lactic Acid Conjugate Chitosan (OCH), Preparation of Xanthan Gum (XG) Polymer Solution

OCH was synthesized using lactic acid oligomer and chitosan, where chitosan was insitu grafted with lactic acid oligomer by polycondensation reaction according to the procedure reported in Pal and Katiyar 2016 [219]. In brief, a polycondensation reaction was carried

out by heating a mixture of lactic acid and chitosan (3.33:1 wt/wt%) in the microwave at 110 °C for 30 min. Before heating, the mixture was kept in ambient condition for 12 h to soak the lactic acid thoroughly into the chitosan, and then inert gas (nitrogen) was purged into the reaction vessel. The inert atmosphere was maintained with nitrogen gas till the completion of the reaction. A heating belt was used over the connection line to avoid the condensation of unbound water and by-products. During the condensation reaction, the lactic acid oligomers got attached to the chitosan backbone during the reaction, resulting in the formation of a dark brown-black product. Prior to use, the synthesized OCH was purified using vacuum filtration by dissolving it in acetone.

XG powder was added to Millipore water at various concentrations (0.01 to 0.08 g/50 ml) to prepare the polymer solution. The desired amount of xanthan gum powder was added slowly to the Millipore water, with continuous stirring at 800 rpm. After adding the polymer powder, the stirring speed was reduced to 100 rpm, and it was maintained for 12 h to ensure total hydration and complete dissolution of the XG powder. Finally, the prepared polymer solutions were kept in a closed glass container with parafilm sealing to minimize oxygen uptake until used. Crude oil was added to the XG solution in a 1:10 ratio of oil to water and immediately homogenized at 10000 rpm for 5 min (IKA T25 digital ULTRA TURRAX) to prepare the emulsion.

2.2.4 Preparation of Membranes

Membrane fabrication was carried out using the non-solvent induced phase separation (NIPS) method (Schematic for preparation of polymeric membrane is shown in **Figure 2.3**). DI water and DMF were used as non-solvent and solvent, respectively. Initially, CNCs FeCNC and Fe_3O_4 nanoparticles were uniformly dispersed in a certain amount of DMF (25% of total DMF used) by sonication. After obtaining a homogeneous suspension of CNCs, PVDF was added and kept at stirring (500 rpm) at 60 °C for 12 h to get the casting

solution. Degassing was done to remove the air bubbles completely by keeping the solution ideal for 24 h. Thin cast films were obtained after casting the degassed homogeneous solutions over a glass plate at room temperature. The glass plate was put in the coagulation bath immediately after casting containing DI water (28 ± 2 °C), where demixing takes place, which promotes phase separation of the casted films **(Figure 2.3a)**. Finally, the obtained membranes were washed and kept in fresh DI water. Different compositions used for membrane preparation are listed in **Table 2.1**. Solvent (DMF) and pore-forming agent (PEG) wt% were kept constant throughout all the combinations, with 83% and 2%, respectively. To prepare the membrane with the influence of a magnetic field, the casting glass plate was kept over a magnetic field (350-450 gauss), the direction of which was horizontal to the glass plate at a distance of 2-2.5 cm. After a delay of 15-20 s, the glass plate was immersed in the coagulation bath, and in order to complete the coagulation process, the membrane was transferred to fresh DI water and kept for 24 h **(Figure 2.3b).**

Table 2.1: Different compositions used for the preparation of PVDF/CNC membrane

Nomenclature for membranes with		**Weight %**	
CNC	**FeCNC**	**CNC/FeCNC**	**PVDF**
M0	M0	0	15
M0.5	FeCNCM1	0.5	14.5
M1	FeCNCM2	1	14
M1.5	FeCNCM3	1.5	13.5
M2	FeCNCM4	2	13
M3	FeCNCM5	3	12

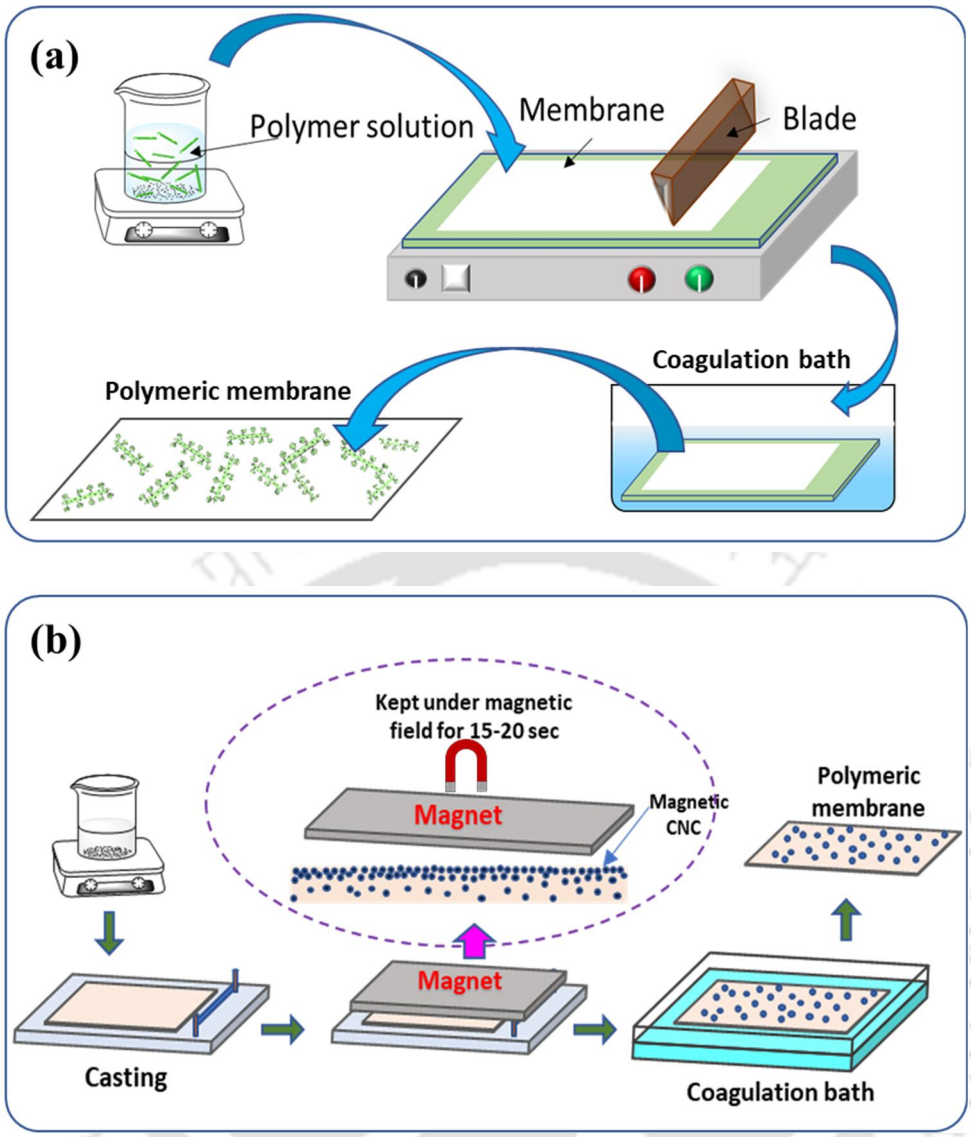

Figure 2.3: Schematic for preparation of polymeric membrane by NIPS (a) without magnetic field and (b) with magnetic field

2.2.5 Oil-in-Water Emulsion Preparation

Crude oil was used to prepare oil in water emulsion. The concentration of crude oil used is 1000 mg/l of water. The oil in water emulsion was prepared using a benchtop ultrasonicator and sonicated for 30 min (amplitude 30%), and further, this emulsion was used for membrane filtration. A UV calibration curve was prepared by diluting the stock solution to 18 mg/l, 12 mg/l, 9 mg/l, 4 mg/l, 1 mg/l and 0.5 mg/l times. The UV calibration curve was used to determine the concentration of crude oil in the solution after filtration.

2.2.6 Isolation of Oil-Degrading Bacteria and Molecular Characterization

The bacteria used in the current study was isolated from the crude oil collected from an oil field of the upper Assam Basin. The collected crude oil was stored for 30 days at room temperature to eliminate the non-oil-utilizing bacteria. Further, this oil was spread onto the surface of the nutrient agar and incubated for 3 days at 30 °C. After a series of three subcultures, the bacteria were characterized using Gram staining. The procedure for the isolation of oil-degrading bacteria by the streak plate method is represented in **Figure 2.4**. Further, molecular identification was performed using 16S rRNA sequencing, and phylogenetic analysis was performed to identify the bacterial strain. The isolated bacteria are named *Pseudomonas aeruginosa* CoE-SusPol3.

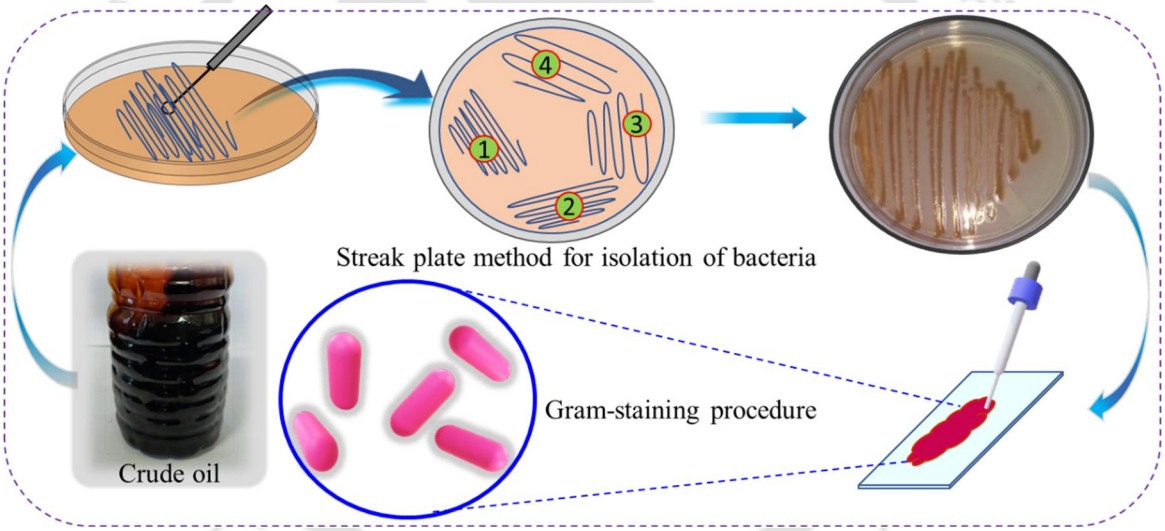

Figure 2.4: Schematic showing isolation of oil-degrading bacteria by streak plate method

A detailed explanation of genome extraction and phylogenetic analysis is presented below.

- **Genome extraction**

Chromosomal DNA was extracted by using a spin column kit (HiMedia, India or similar manufacturers). The bacterial 16S rRNA gene (1500 bp) [220] was amplified using a polymerase chain reaction in a thermal cycler and was purified using Exonuclease I-Shrimp Alkaline Phosphatase (Exo-SAP) [221]. Purified amplicons were sequenced by the Sanger

method in ABI 3500xL genetic analyzer (Life Technologies, USA). Sequencing files are edited using CHROMASLITE (version 1.5) and further analyzed by the Basic Local Alignment Search Tool (BLAST) with the closest culture sequence retrieved from the National Centre for Biotechnology Information (NCBI) database that finds regions of local similarity between sequences [222]. The program compares nucleotide or protein sequences to sequence databases and calculates the statistical significance of matches. The BLAST algorithms are used to infer functional and evolutionary relationships between sequences as well as help identify members of gene families. (i) Initial search to find potentially closely related type strain sequences using the BLASTN program (ii) Pairwise alignment to calculate the sequence similarity values between the query sequence and the sequences identified in step (i) [223]. Therefore, each isolate is reported with the first five-ten hits observed in the said database.

- **Phylogenetic analysis**

The evolutionary history was inferred using the Neighbor-Joining method [224]. The optimal tree with the sum of branch length = 0.25511190 is shown. The percentage of replicate trees in which the associated taxa clustered together in the bootstrap test (1000 replicates) are shown next to the branches. The tree is drawn to scale, with branch lengths in the same units as those of the evolutionary distances used to infer the phylogenetic tree. The evolutionary distances were computed using the Kimura 2-parameter method and are in the units of the number of base substitutions per site. The analysis involved 17 nucleotide sequences. All positions containing gaps and missing data were eliminated. There were a total of 1322 positions in the final dataset. Evolutionary analyses were conducted in MEGA6 [225].

2.2.7 Crude Oil Degradation by *Pseudomonas aeruginosa* CoE-SusPol3

The isolate was used to prepare the inoculum by transferring a single colony of bacteria into a fresh nutrient broth, followed by incubation at 30 °C and 120 rpm until the exponential phase. Further, this actively growing culture with an optical density of 0.5 at 600 nm was inoculated into a nutrient broth containing different crude oil ratios. The mixture of crude oil, XG and OCH was the only carbon source. Then, these samples were observed for oil degradation for up to three weeks. The samples were collected after 7 days from all the flasks in triplicates and analyzed for the degradation of hydrocarbons. Biodegradation of crude oil by the *Pseudomonas aeruginosa* CoE-SusPol3 was measured by calculating the peak area of different components present in crude oil obtained from GC analysis and comparing it with the controlled one. Percentage degradation was calculated using the equation given below:

$$Percentage\ degradation = \left[1 - \frac{Peak\ area\ of\ sample}{Peak\ area\ of\ the\ controlled\ sample}\right] \times 100 \qquad (2.1)$$

2.3 Analytical Instrumentation and Characterization

2.3.1 Characterization of Membrane and Synthesized Additives (CNC & FeCNC)

2.3.1.1 *Field Emission Scanning Electron Microscopy (FESEM), Energy Dispersive X-ray Spectroscopy (EDX) and Field Emission Transmission Electron Microscopy (FETEM) analysis*

For the prepared CNCs, the surface and cross-sectional morphology of the fabricated membrane were observed under a Field emission Electron Microscope (FESEM) (Zeiss, Sigma 300). Prior to observation, CNCs were dispersed in DI water using sonication and drop cast over aluminum foil. Drop cast CNCs were sputter-coated with gold for ~180 s and observed using FESEM. The membrane surface and the cross-section were also observed in FESEM. For taking cross-sectional images of the PVDF and composite

membranes, it was fractured under liquid nitrogen and kept in a hot air oven at 45 °C for 24 h to remove the moisture. The membranes were then mounted to the stub using carbon tapes. The membrane samples were also sputter-coated under a vacuum with a thin layer of gold. FESEM was also used to observe the shape and size of isolated bacteria. The bacteria sample was prepared by drop-casting the bacterial culture onto the filter paper and oven-dried at 60 °C until completely dried. Prior to observation, all the bacteria samples were also sputter-coated under a vacuum with a thin layer of gold for ~180 s to improve the conductivity. CNC suspension was dropped over a copper TEM grid and observed under FETEM (JEOL, Model: 2100F).

To investigate the presence of FeCNC in the membrane and to analyze the elemental distribution, Energy Dispersive X-ray spectroscopy (EDX) analysis was carried out. Initially, EDX of the membrane surface was carried out for the membrane with FeCNC fabricated with and without a magnetic field. Further, to find out the dispersion of FeCNC in the membrane matrix, EDX of the cross-section was carried out. The elemental mapping of iron (Fe) in the EDX analysis of the membrane cross-section was used to evaluate the migration behaviour of FeCNC in the membrane matrix with the application of the magnetic field during membrane casting.

2.3.1.2 *Fourier Transform Infrared (FTIR) of the Composite Membranes*

FTIR spectroscopic analysis was carried out to determine the chemical composition of the membranes, CNC, FeCNC, crude oil, chitosan, XG and OCH. Fourier transform infrared spectrometer with attenuated total reflectance (ATR) attachment at room temperature (Frontier, PerkinElmer) was used to collect the IR spectra. All the samples were positioned over the ATR crystal surface made of zinc selenide, and the analysis was executed in the range of 4000 to 600 cm^{-1} for 16 consecutive scans at a 4.0 cm^{-1} resolution. To compensate for the influence of humidity, an air background spectrum was collected before the analysis.

All the measurements were taken in transmittance mode, and IR solution software was used for analysis.

2.3.1.3 *Thermal Gravimetric Analysis (TGA)*

The thermal behaviour of the prepared CNCs from waste paper and the polymeric composite membrane was studied with the help of TGA (4000 PerkinElmer). The temperature programme followed to study the thermal behaviour was an initial temperature of 30 °C and a final temperature of 700 °C, and the heating rate used was 10 °C/min. Heating was accomplished in an inert atmosphere using nitrogen gas.

2.3.1.4 *Contact Angle Measurements*

Drop Shape Analyzer (Kruss® DSA 25, Germany) equipped with a CCD camera was used to measure the contact angle. The membrane was initially dried overnight at 45 °C in a hot air oven to completely remove the moisture. Then, a membrane dimension of ~2 cm × 2 cm was attached to a glass slide for analysis. DI water was used to measure the contact angle of the polymeric composite membranes at 23 ± 1 °C. Measurement was done at three separate locations on the membrane surface, and the average value was taken.

2.3.1.5 *Water Content and Porosity*

The water content of the membrane samples was determined to find out the water absorption capacity of the membrane. The uniform size of membrane samples is soaked in distilled water for 24 h and then blotted to remove free surface water, and the weight is recorded immediately after that it is allowed to dry for the removal of the water, and the dry weights were measured. The water content from dry and wet weights obtained by using 2.2 [226]:

$$Water\ content\ (\%) = \frac{W_w - W_d}{W_w} \times 100 \qquad (2.2)$$

Where W_w and W_d are the weights of dry and wet membranes, respectively. The average value of three measurements is taken to reduce experiment error.

To calculate the porosity (P), gravimetric method was adopted, and equation 2.3 was used [227]:

$$P(\%) = \frac{W_w - W_d}{ADρ} \times 100 \quad (2.3)$$

Where W_w, W_d, A, and D are the wet weight (g), the dry weight (g), the area (cm^2) and the thickness (cm) of the membrane, respectively, and ρ is the density of water (0.998 g/cm^3).

2.3.1.6 *Pore Size Measurement*

TECHPoro Capillary flow porometer (Make: M/s Tech Inc, Chennai, India) was used to measure the pore size of the fabricated membrane. Initially, the wetting liquid is allowed to spontaneously fill the pores of the membrane by soaking it for 12 h in the wetting liquid. Then, an inert gas (nitrogen) is pumped at an increasing pressure, which displaces the liquid from the pores of the membrane. The size of displaced pores decreases from large to small with increasing pressure. The pore size distribution is obtained by measuring both the pressure and flow rate of the gas. The pore size is measured using the Washburn equation [228]:

$$D = \frac{4\gamma \cos\theta}{p} \quad (2.4)$$

Where, D: pore diameter, γ: surface tension of liquid (dynes/cm), θ: contact angle of liquid p : differential gas pressure

2.3.1.7 *X-Ray Diffraction (XRD) Analysis*

XRD measurements of CNCs were carried out at room temperature using an X-ray diffractometer (SmartLab, Rigaku, Japan) with Ni-filtered Cu K-α radiation at a wavelength of 1.541 Å. The voltage and current were set as 45 kV and 112 mA, respectively, as the operating conditions for receiving and diverging slits with a scan speed of 20 degree/min and 0.02 sec/step for 2θ range of 5° to 50° [229]. OriginPro 8.5 software was used for calculating the peaks area, which was subsequently used to calculate the crystallinity index (I_{CR}) of the polymer blend films using equation 2.5 [230]:

$$I_{CR} = \frac{CP_A}{CP_A + AR_A} \times 100 \tag{2.5}$$

where, CP_A and AR_A are the area of the crystalline peaks and the area of the amorphous regions, respectively.

2.3.1.8 *X-ray Photoelectron Spectroscopy (XPS)*

XPS analysis of the CNCs and membrane surface was performed in (PHI-5000, VersaProbe III, X-ray photoelectron spectrometer, Japan) using an Al K-α X-ray source, with a pass energy of 55 eV. XPS spectra were collected over the binding energy range of 0-1200 eV and dwell time of 20 μS. All measurements were carried out at a takeoff angle of 45°.

2.3.1.9 *Mechanical Testing*

Mechanical testing was carried out to test the mechanical behavior and pressure-bearing capacity of the membrane samples in a 5 kN universal testing machine (UTM) (Z005TN, Zwick Rowell). The electromechanical UTM is attached with a mobile top head and fixed bottom, controlled by a motorized screw mechanism. The membrane samples were cut into a standard size of 10 mm in width and 100 mm in length, and the thickness was noted. The

membrane was attached in between the top arm and fixed bottom arm of the UTM, maintaining a gauge length of 50 mm. Samples were stretched with 1 KN pressure at 2 mm/min. All measurements were carried out in three samples, and the average values were taken to avoid error.

2.3.1.10 *Pure Water Flux (PWF), Rejection ratio and Fouling Evaluation (in dead-end membrane testing setup)*

PWF, water flux recovery ratio (FRR) and BSA/oil rejection were measured by a solvent-resistant stirred cell (Amicon stirred cell, Millipore). The dead-end membrane testing setup is shown in **Figure 2.5**. Dead-end filtration is the most fundamental type of membrane filtration, where the water flows perpendicularly to the membrane, and the water is pushed through the membrane by applying pressure. The entire feed flow is driven across the membrane, where the filtered material collects on its surface.

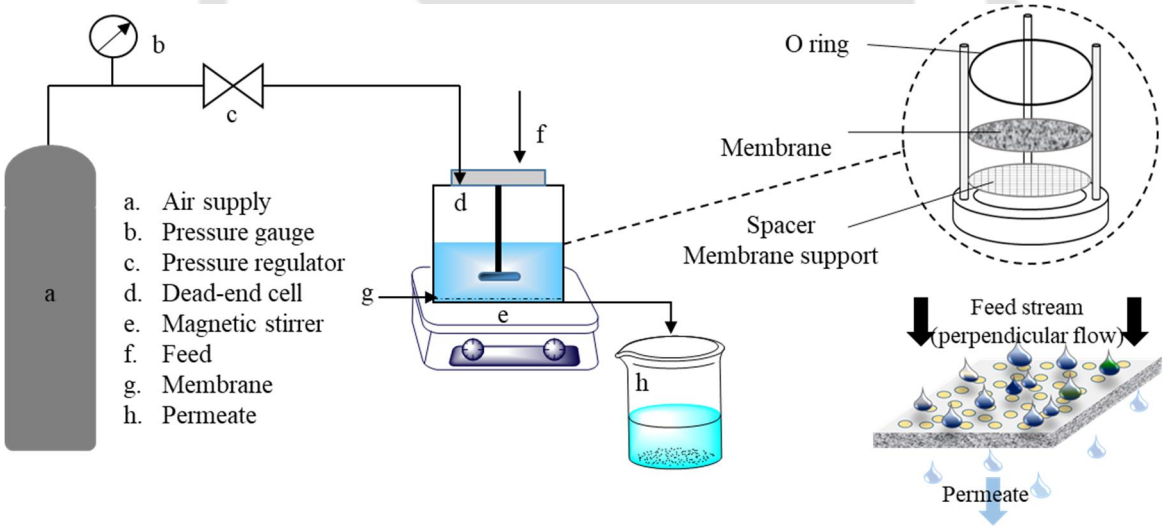

Figure 2.5: Schematic for dead-end membrane filtration setup

Each of the membranes was pre-compacted at 1.5 kg/cm^2 to get stable flux for 30 min before carrying out all the measurements. All the measurements were carried out at the stirring speed of 200 rpm at 1 kg/cm^2 over an effective filtration area of 3.422 × 10^{-3} m^{2,} and pressure was applied using nitrogen gas. Flux is calculated by using equation 2.6 [231].

$$J_{w1} = \frac{V}{A \times T} \tag{2.6}$$

where V is the volume of filtered water (m^3), T is the filtration time (h), A is the effective membrane area (m^2), and J_{w1} is the pure water permeation flux (L/m^2h or LMH).

Subsequently, after measuring the PWF (J_{w1}), the feed was replaced with 0.2 mg ml^{-1}/1000 mg l^{-1} of BSA/crude oil emulsion in DI water, and the permeate flux (J_p) was recorded. The concentration of the filtered solution was measured with a UV–visible spectrophotometer (PerkinElmer, Lambda 25); the concentration of the filtered BSA solution was measured at 280 nm. The rejection ratio (R) was calculated using equation 2.7 [232]:

$$R(\%) = \left(1 - \frac{C_f}{C_i}\right) \times 100 \tag{2.7}$$

Where, C_f and C_i (mg/L) are the filtered BSA/crude oil concentrations in the permeate and initial feed water solutions, respectively.

The membranes were washed with DI water and used again for PWF measurement (J_{w2}) by keeping the conditions the same as those of the previous procedure. Due to the adsorption of BSA/crude oil on the membrane surface, fouling occurs, and as a result, the water flux is decreased due to the deposition of the BSA/crude oil layer on the membrane. Calculation of FRR is done to determine the antifouling capacity. The expression [233] is given as follows

$$FRR(\%) = \frac{J_{w2}}{J_{w1}} \times 100 \tag{2.8}$$

where J_{w1} and J_{w2} are the water flux before and after BSA/crude oil filtration, respectively.

To further analyze the antifouling performance, the total flux decline ratio (DR_t), reversible flux decline ratio (DR_r) and irreversible flux decline ratio (DR_{ir}) are evaluated for all the membranes. The following equations [234] are given below:

$$DR_t(\%) = \left(1 - \frac{J_p}{J_{w1}}\right) \times 100 \tag{2.9}$$

$$DR_r(\%) = \left(\frac{J_{w2} - J_p}{J_{w1}}\right) \times 100 \tag{2.10}$$

$$DR_{ir}(\%) = \left(\frac{J_{w1} - J_{w2}}{J_{w1}}\right) \times 100 \tag{2.11}$$

2.3.1.11 *Pure Water Flux (PWF), Rejection ratio and Fouling Evaluation (in cross-flow membrane testing setup)*

The membranes were also tested in a cross-flow membrane test set, where the fluxes were measured for 48 h. The schematic for the setup is shown in **Figure 2.6**.

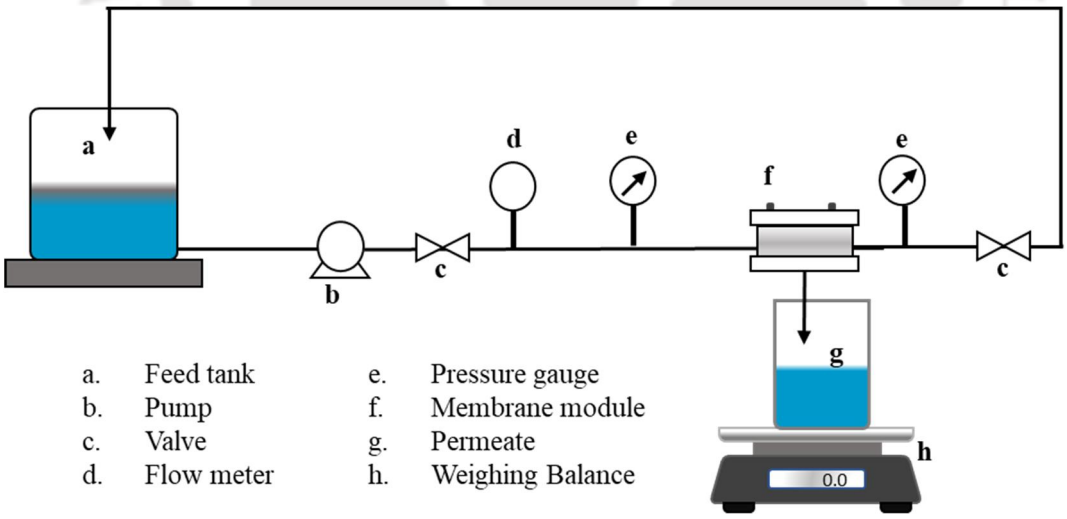

Figure 2.6: Schematic for Cross-flow membrane filtration setup

The effective filtration area of the membrane is 4.536×10^{-3} m^2. Before measurement, the membrane was pre-compressed at 1.5 kg/cm^2 for 12 h and then tested for water flux and

oil-water separation. A pressure of 1 kg/cm^2 was maintained during the measurement, with a flow rate maintained at 1 L/min.

2.3.2 Characterization of Crude Oil Emulsion and Bio-Dispersant

2.3.2.1 *Optical Microscopy and Particle Size Analysis*

The optical image of crude oil emulsions and emulsion stabilized by OCH and XG-OCH were taken by using a polarised optical microscope (POM) (Eclipse LV100N POL, Nikon Co., Japan). A small drop was placed in the middle of a clean glass slide, and a coverslip was placed gently over the drop without applying any pressure, allowing it to spread out in between and observed under POM. Images were taken after the emulsion droplet reached a steady shape. The size of the droplets was measured with the help of ImageJ software [235]. An average of 60 to 100 droplets was measured, and the average value was reported. Further, the crude oil emulsion droplet size stabilized by XG-OCH was determined with DelsaTM Nano C (Beckman Coulter, USA) for 0 and 3 weeks.

2.3.2.2 *Measurement of Rheological Properties*

The rheological properties measurement of each sample was carried out using an interfacial rheometer (Anton-Paar, MCR 301) with a cone and plate geometry of diameter 49.981 mm diameter and cone angle of 1.992°. Viscosity measurements for all the samples were carried out in the shear stress range from 0 to 100 s^{-1}.

2.3.2.3 *Gas chromatography (GC)*

The degradation of stabilized crude oil emulsion by the isolated bacteria was evaluated with gas chromatography (GC). Crude oil was extracted using 10 ml DCM, and one microlitre of the extracted sample was used for GC analysis. The GC system (Varian, USA) was equipped with an HP-5MS capillary column, and nitrogen gas was used as a carrier for the analysis. The following method for GC analysis was developed, taking reference from

Kondyli A. and Schrader W. [236]. The equipment was set at a temperature of 40 °C for 3 min; after that, the temperature was raised to 280 °C at 10 °C min^{-1} to and held for 5 min.

2.3.2.4 *API Gravity*

API Gravity of the crude oil sample was determined using a specific gravity bottle and a weighing balance. An empty specific gravity bottle was weighed on the weighing balance, and then 10 ml of crude oil sample was loaded to the same specific gravity bottle and weighed to determine the weight of the crude oil sample. The density of crude oil was calculated from the weight and volume of crude oil. Specific gravity was calculated using the formula [237]:

$$Specific\ gravity(SG) = \frac{Density\ of\ sample}{Density\ of\ water} \tag{2.12}$$

API Gravity was calculated using the following relation [238]

$$API = \frac{141.5}{SG} - 131.5 \tag{2.13}$$

2.3.2.5 *Extraction of Biosurfactant and Characterization by MALDI-TOF-MS*

Biosurfactant-mediated hydrocarbon degradation was evaluated by determining the presence of biosurfactants in the broth. Biosurfactant was extracted using the existing protocol. Briefly, the culture broth was centrifuged at 5000 rpm for 15 min to separate the cells. The obtained cell-free supernatant was extracted using an equal volume of chloroform and methanol (2:1 v/v) [14]. Further, the organic phase was collected and evaporated to obtain the biosurfactant. The obtained biosurfactant was dissolved in DHB matrix (10 mg/ml) prepared in methanol. The prepared sample-matrix mixture was loaded on a stainless-steel target plate and dried at room temperature. Further, the analysis was carried out using the MALDI-TOF-MS (Make: Bruker, Model: AUTOFLEX SPEED) with an accelerating voltage of 19 kV.

2.3.2.6 *Surface Tension Measurement*

Surface tension was measured using Drop Shape Analyzer (Kruss® DSA 25, Germany) equipped with a CCD camera. To compute the surface tension, the pendant drop method was used. The sample from the syringe was allowed to make a drop of 10 µl using a needle size of 1.8 mm. Then the image of this drop was captured with the CCD camera to measure the surface tension at 28 °C. Measurement was done for three different drops, and the average value was taken.

Chapter 3
Interaction of Oil-Water System with Bio-Dispersant to Understand the Separation and Biodegradation Process

This chapter discusses the application of naturally available biopolymers as bio-dispersants to stabilize crude oil droplets instead of harmful synthetic chemical dispersants and enhance its degradation. Biopolymers xanthan gum (XG) and oligo lactic acid conjugate chitosan (OCH) were used as a bio-dispersant, which forms a stable crude oil-in-water emulsion. The stabilized emulsion droplets were allowed to be degraded by the isolated bacteria Pseudomonas aeruginosa CoE-SusPol3, and the degradation percentage obtained for the stabilized emulsion is 74.31%, whereas for the unstabilized emulsion is 34.06%. The in-situ production of biosurfactants from the isolated bacteria also assisted the degradation of hydrocarbons present in crude oil by decreasing the surface tension of the crude oil to 28.53 (± 0.05) from 32.44 (± 0.22). Hence, using such bio-based materials could be a potential and sustainable solution for the treatment of oil spills.

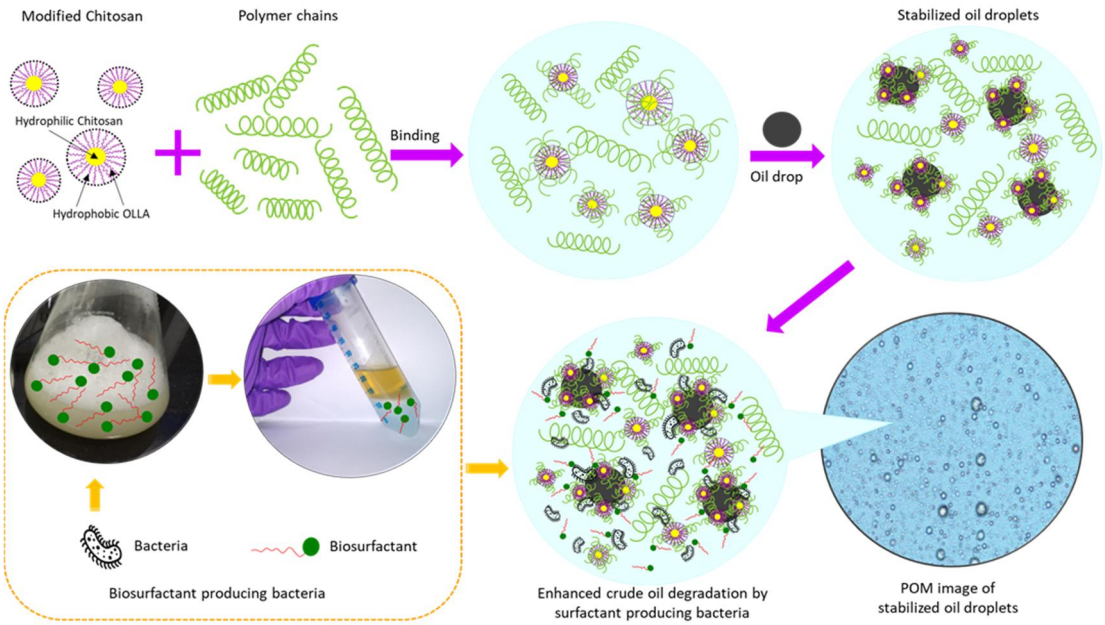

Research outputs of this chapter: *"Oligo lactic acid conjugate chitosan as a bio-dispersant for enhanced biodegradation of crude oil in oil-spill remediation",* ***Manuscript submitted to Water Science and Engineering.***

3.1 Introduction

Many industries like food oil refineries, restaurants, dairy and poultry processing plants and petrochemicals are just a few of the industries that produce wastewater that is contaminated with oil. As this wastewater has a serious effect on the environment mentioned in Chapter 1, the treatment of this oily water is indispensable. Since the source of oily wastewater is very broad, the scope for applying different treatment methods is also wide. In the case of large-scale oil spillage, the most widely used method is the use of chemical dispersants. However, the harmful effect of chemical dispersant use is also questionable, and the application of biobased materials as bio-dispersants is gaining more and more importance. The employment of biodispersants and bioremediation techniques is proven to be the most environmentally benign solution for ensuring the ecosystem's sustainability. Thus, the current chapter aims to utilize natural additives, like polysaccharides and attach them to oil droplets to increase their stability and understand the interaction of oily with it to understand the effectiveness and lower the use of chemical dispersants needed for the treatment of oily wastewater. The application of such natural biomaterials has the advantage of being biodegradable and readily compostable, causing a negligible negative effect on the environment [239,240]. Polymers, including xanthan gum (XG) and chitosan, are targeted in this work to use as bio-dispersant to stabilize the crude oil emulsion in water. Chitosan is a linear chain polysaccharide obtained by deacetylation of chitin, a biopolymer found mainly in the shells of crabs and shrimps. The chitosan used was modified to become a nanoamphiphilic material with hydrophobic and hydrophilic parts called oligo lactic acid conjugate chitosan (OCH) according to the procedure mentioned in section 2.2.3. The structure of OCH is represented in **Figure 3.1a**. XG is an anionic polysaccharide composed of a β-(1→4)-D-glucopyranose glucan backbone with

side chains of (1→3)-α-D-mannopyranose-(2→1)-β-D-glucuronic acid-(4→1)-β-D-mannopyranose on alternating residues, and the structure is represented in **Figure 3.1b**.

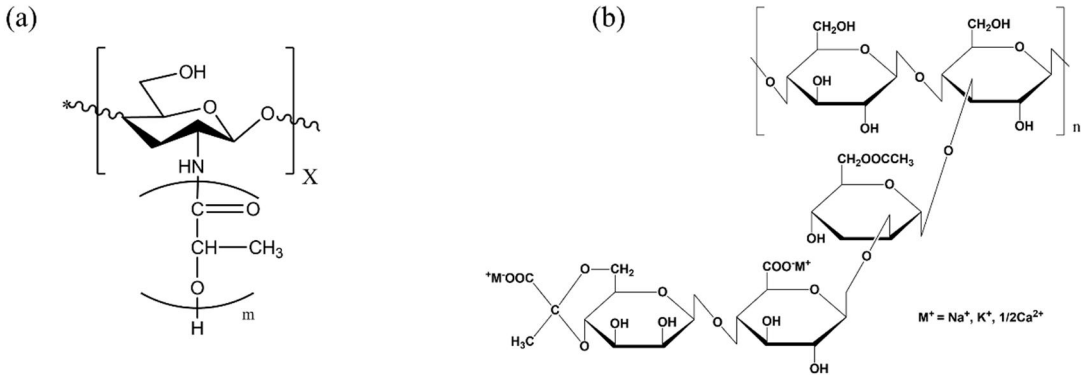

Figure 3.1: Chemical structure of (a) oligo lactic acid conjugate chitosan (OCH) (b) xanthan gum (XG)

A highly stable crude oil-in-water emulsion is formed with a minimal concentration of this newly developed material. Applying this environmentally friendly bio-dispersant can possibly minimize the use of synthetic chemical dispersants required for the treatment of oil spills. It is further speculated that the emulsion stabilized by OCH has more surface area for microbes to assimilate the crude oil. Hence, this study also investigates the degradation of OCH-stabilized crude oil emulsion with the isolated bacteria and the effect of biosurfactant produced by these microbes for the degradation.

3.2 Results and Discussion

3.2.1 Identification of Different Functional Groups Present in Oligo Lactic Acid Conjugate Chitosan (OCH), Chitosan, Xanthan Gum (XG) and Crude Oil by Fourier Transform Infrared Spectroscopy (FTIR)

FTIR analysis was conducted to confirm the presence of different functional groups in XG and crude oil. FTIR spectra of XG indicate the available functional groups, including acetal, hydroxyl, carbonyl and carboxyl, shown in **Figure 3.2a**. The peaks observed around 3100

to 3600 cm^{-1} indicate the axial deformation of –OH bonds. Axial deformation of the C–H bonds because of the symmetrical and asymmetrical stretching of C–H bonds are represented by the peak at 2910 cm^{-1}. The small hump at 1730 cm^{-1} represents the axial deformation of C=O ester due to carbonyl groups. The two peaks at 1602 and 1665.6 cm^{-1} linked to axial deformation of C=O of enols because of the asymmetric stretching of carbonyl groups. Symmetrical stretching of C–O bonds in the carboxylate anion present in XG is represented by the peak at 1412 cm^{-1} [241]. The peaks at 1022, 1057 and 1162 cm^{-1} were an indication of the axial deformation of C–O. The characteristic peak of chitosan (**Figure 3.2c**) attributed to N–H and O–H stretching are represented by peaks at 360 and 3292 $cm^{-1,}$ respectively; the bands at 2922 and 2877 cm^{-1} correspond to symmetric and asymmetric stretching of C–H bond present in chitosan. C=O and C=N stretching of the amide group is represented by the peaks at around 1647 and 1326 $cm^{-1,}$ respectively, and the bands at 1063 and 1026 cm^{-1} correspond to C–O stretching.

FTIR spectra of OCH are shown in **Figure 3.2d**, and the peaks developed due to intermolecular hydrogen bonding are seen at 1745, 1382, 1130, and 1092 cm^{-1}. The peak at 1540 cm^{-1} is detected, which represents the (–OCONH–) of chitosan with repeated units of lactic acid, as discussed by Pal and Katiyar [219]. Crude oil is a complex mixture of different hydrocarbons with a small amount of sulfur, nitrogen and oxygen. **Figure 3.2b** shows the FTIR spectra plot of crude oil. A number of bands representing different types of C–H vibrations were seen in the FTIR spectra. Two strong peaks were observed at 2921 cm^{-1} and 2854 cm^{-1}, representing the vibration for aliphatic $–CH_2$ groups [242]. The sharp peak at 1459 cm^{-1} is associated with the C–H bending vibrations in methylene groups. The peak observed at 1605 cm^{-1} is attributed to stretching vibrations of the C–C bond of the aromatic rings, indicating the presence of aromatic compounds in the crude oil. Peaks at 1305 cm^{-1} represent the esters and ether groups present in the crude oil, and the peak at

1377 cm^{-1} represents the C–H bending vibration of the methyl group [243]. The bands at 1170 cm^{-1} and between 900 and 700 cm^{-1} represent different aromatic C–H bending vibrations in-plane and out of the plane, respectively [244]. Peaks in the range between 1000 to 1310 cm^{-1} represent the stretching and bending vibrations of N– and S– related functional groups [245].

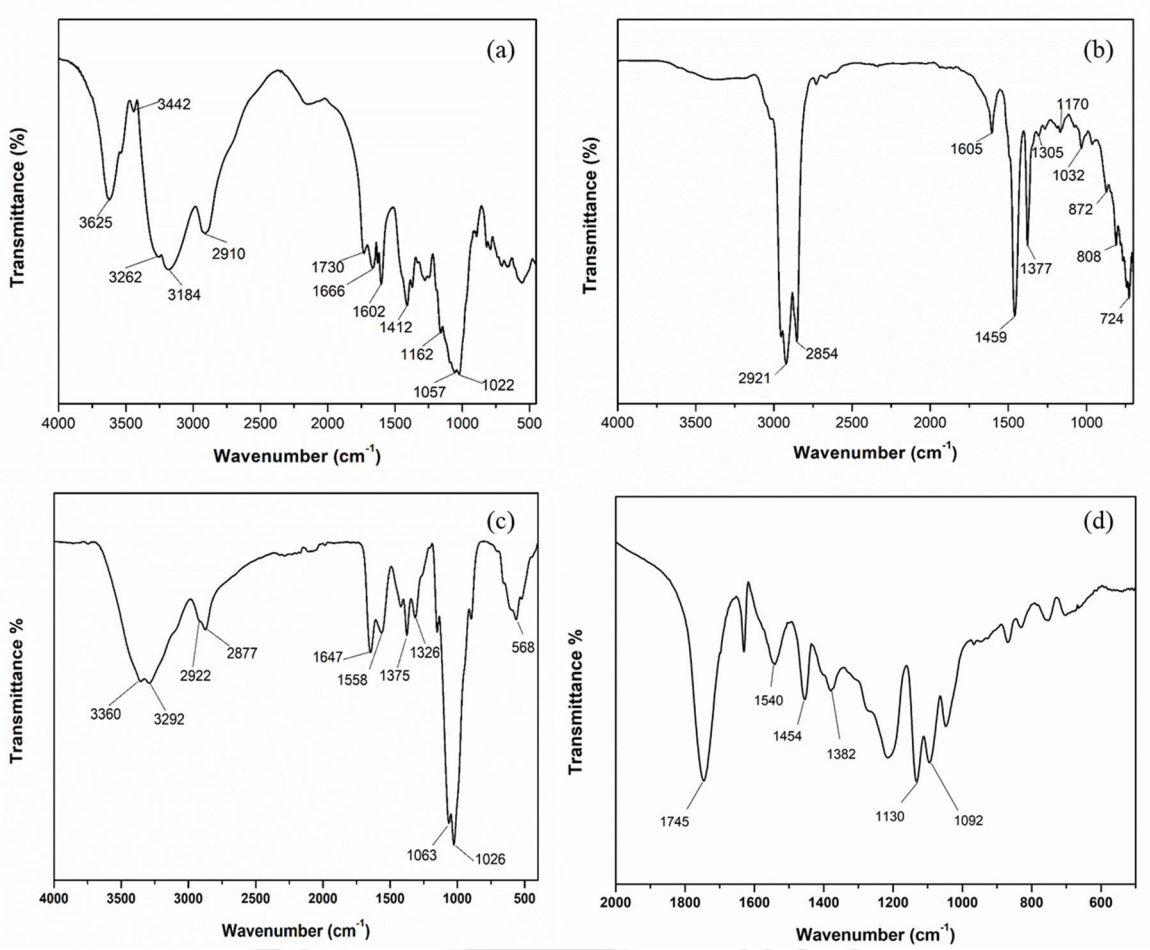

Figure 3.2: FTIR spectra of (a) XG and (b) crude oil (c) chitosan (d) OCH

3.2.2 Droplet Size Analysis of Emulsion from the POM Image

Chitosan is a biodegradable, non-toxic, edible and hydrophilic polymer. Chitosan was modified to OCH, which converts from hydrophilic to amphiphilic [246]. It gets attached to the oil droplets and improves their stability. Based on literature survey, it was found that chitosan ranging from 0.5 wt% to 1 wt% is used along with other materials like silica

nanoparticles, phytosterol particles or food-grade chitosan alone [5–7]. Current works conducted experiments using various concentrations of OCH, ranging from 0.5 wt%, 0.6 wt%, 0.8 wt% and 1 wt%, with the aim of determining the optimal concentration for achieving emulsion stability. It was identified that the OCH concentration of 0.8 wt% and 1 wt% reflects a good optical image of emulsion, which remains stable for more than 3 weeks. Therefore, the concentration 0.8 wt% was chosen as the optimum level for our specific emulsion system.

Further studies can be carried out to confirm the consistency of these findings and to assess long-term emulsion stability under various conditions. Different crude oil emulsions with water, XG and OCH were observed under an optical microscope. The size of the droplets (an average of 60 to 100 droplets was used for the measurement) from the image obtained was measured using ImageJ software. When the emulsion of crude oil was only with water, the droplet size was larger compared to the emulsion stabilized by XG and OCH. The initial droplet size obtained was 5294 ± 2096 nm, which increased to 9799 ± 3369 nm after 3 weeks, as represented in **Figure 3.3(a & b)**. The size of the emulsion droplets was nonuniform, as can be observed in the images, and increased with time because of the coalescence of droplets. The coalescence of the droplets can also be observed under the microscope. When XG was added to the emulsion, it dissolved with water, increased the viscosity of the continuous phase, and restricted the movement of the droplets, hence preventing the coalescence of the droplets. The initial droplet size obtained was 3237 ± 921 nm and changed to 4775 ± 1727 nm after 3 weeks, as shown in **Figure 3.3(c & d)**. Thus, the presence of XG improved the stability of the emulsion as compared to the emulsion without XG. However, when OCH was added to the emulsion stabilized by XG, it further enhanced the stability. The presence of nonamphiphilic OCH, together with the XG improves the colloidal stability by enhancing the continuous phase viscosity and delaying

the coalescence and creaming of oil droplets. OCH is a nonamphiphilic material having both hydrophobic and hydrophilic parts; the hydrophobic part gets adsorbed to the oil surface, thus creating a barrier that prevents the coalescence of the crude oil droplets. The emulsion remained more stable compared to the crude oil emulsion containing only XG and water. This improvement in the stability of the emulsion droplets arises due to the presence of a polymer layer over the droplets, which increases the electrostatic and repulsive force between the droplets and thus prevents the coalescence of the droplets [14]. The initial droplet size was 1457 ± 288 nm, which increased to 1894 ± 748 nm after 3 weeks (**Figure 3.3(e & f)**). The increase in droplet size after 3 weeks was not significant compared to the other two cases; hence, these crude oil droplets are stable against coalescence.

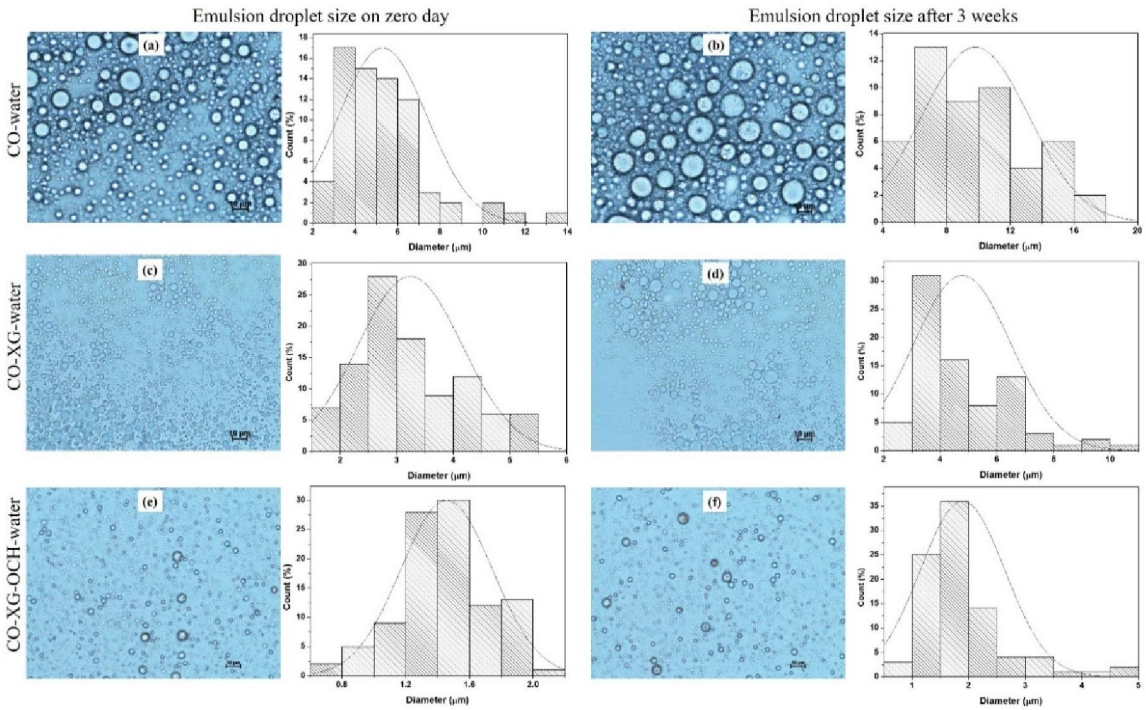

Figure 3.3: Microscopic image of crude oil emulsion initially at 0-days and after 3 weeks (a & b) without any stabilizing agent, (c & d) stabilized by XG, and (e & f) stabilized by OCH and XG, respectively

Droplet size analysis results of crude oil emulsion stabilized by XG and OCH are shown in **Figure 3.4**. **Figure 3.4a** represented the droplet size at 0 days, and **Figure 3.4b** illustrated the droplet size after 3 weeks. The result obtained indicates that the emulsion stabilized by OCH remains nearly equal for 3 weeks. Initially, the droplet size obtained was 1544 nm, which changes to 1989 nm after 3 weeks, indicating that the presence of OCH in the emulsion prevents the droplet from coalescence. The particle size results obtained are comparable with the results obtained from droplet size measurement using ImageJ software shown in **Figure 3.3(e & f)**. Thus, using modified chitosan significantly enhanced the stabilization of oil droplets and provided more surface area for bacteria to adhere to and degrade the crude oil droplets.

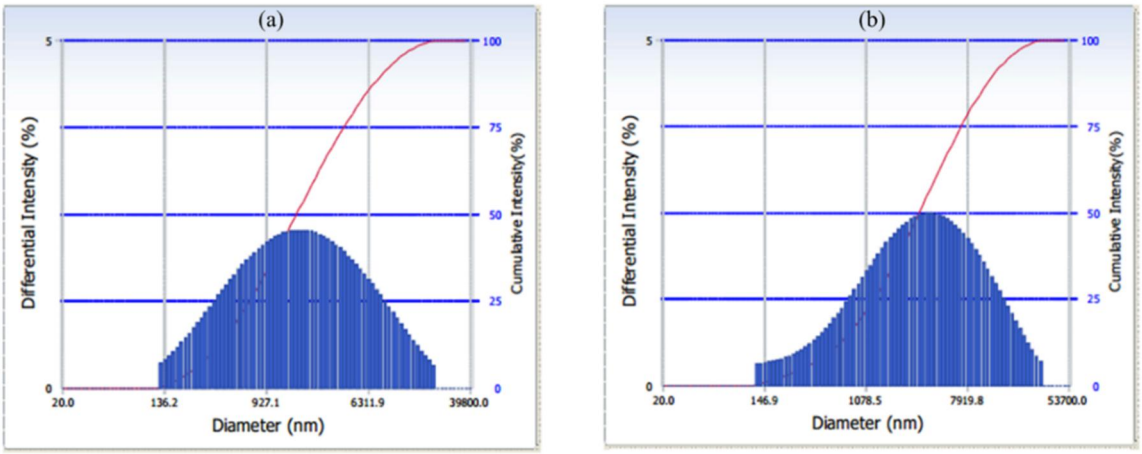

Figure 3.4: Delsa nano results of emulsion droplet size (a) in 0 days (b) after 3 weeks

3.2.3 Rheological Properties of the Solutions

The flow curve for the XG solution and XG with OCH at different shear rates (0-100 s^{-1}) at room temperature is shown in **Figure 3.5**. With the increase in XG concentration, an increase in shear viscosity is observed in **Figure 3.4a**. Initially, the viscosity of XG solution with all concentrations (0.01 to 0.08 g/50 ml) decreased with an increase in shear rate, exhibiting shear thinning property at a low shear rate; comparable results were obtained when OCH was added to the XG solution (**Figure 3.5(a & c)**).

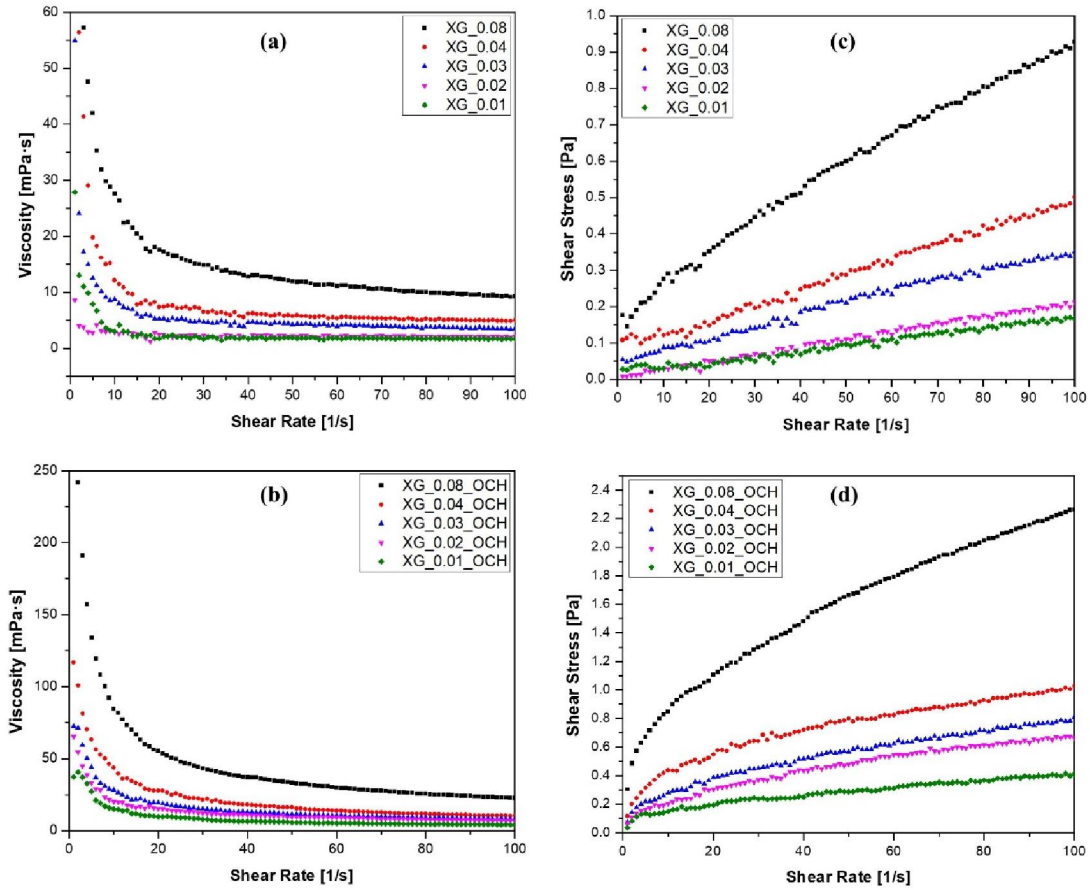

Figure 3.5: Plot for the viscosity of (a) XG solution and (c) XG-OCH solution for different concentrations as a function of shear rate; shear stress versus shear rate for different (b) XG concentrations and (d) XG-OCH solution

It behaved like a Newtonian fluid after reaching a specific shear rate, and the viscosity remained constant. In other words, it is evident that the viscosity was enhanced with an increase in the concentration of XG; thus, the droplets remained stable for a longer time. There is a significant improvement in the viscosity of the continuous phase with the addition of XG, which restricts the movement of oil droplets. However, the addition of OCH further enhanced the continuous phase's viscosity compared to the solution containing only XG. The hydrophobic part of the OCH was preferentially attached to the oil droplets, thereby forming a polymer layer around the droplets to form a micelle-like structure. The improved viscoelasticity of the continuous phase resulted from the addition of XG and OCH and was responsible for the improvement of the stability of the emulsion. Shear stress

vs shear rate curves are presented in **Figure 3.5(b & d)**; it indicates that shear stress increased with an increase in shear rate, and the relationship is almost linear. However, the addition of OCH to the XG solution increases shear stress, and this behaviour was observed in all concentrations of XG solutions.

3.2.4 Characterization of *Pseudomonas aeruginosa* CoE-SusPol3 and its Role in Crude Oil Degradation

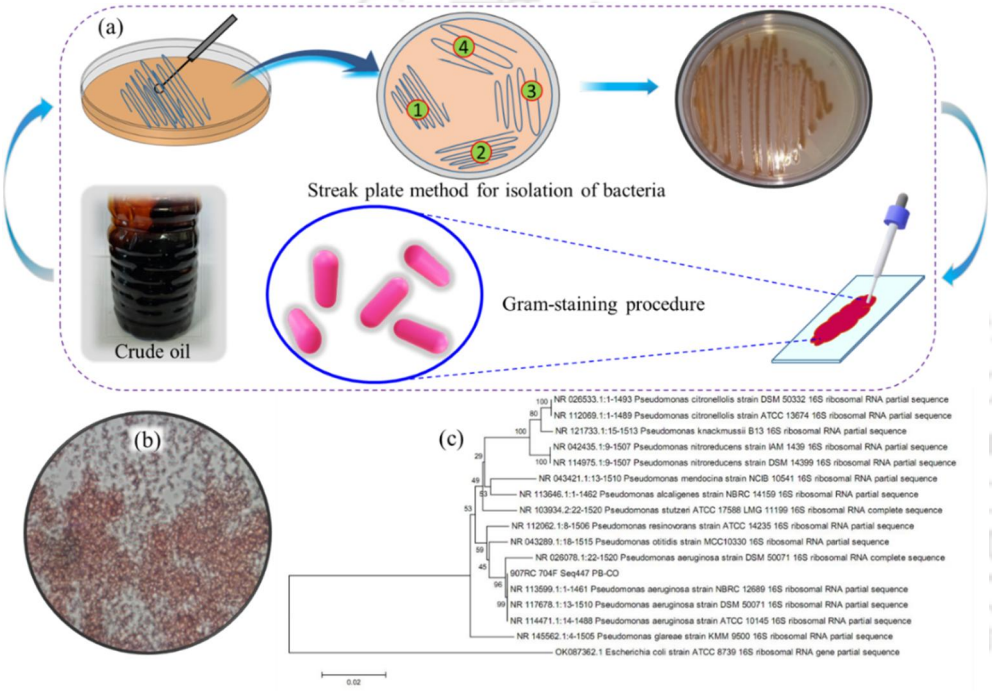

Figure 3.6: (a) Schematic representation of isolation procedure and identification of bacteria by Gram-staining (b) POM image of isolated bacteria, identified as gram-negative (c) phylogenetic tree of isolated bacteria based on 16S rRNA gene sequence. The tree was obtained using the Neighbor-Joining method.

The isolation process of crude oil-degrading bacteria and phylogenetic analysis are shown in **Figure 3.6(a & c)**, respectively. After Gram staining, the characteristic pink colour indicates that the isolated bacteria are Gram-negative, represented in **Figure 3.6b**. The molecular identification by 16S rRNA suggests that the isolate is *Pseudomonas aeruginosa* CoE-SusPol3, exhibiting 100% closer homology with *Pseudomonas aeruginosa.* The partial genome sequence is submitted to GenBank, available from the National Centre for

Biotechnology Information (NCBI), with an accession number of OK355350. **Figure 3.7a** showed the culture broth containing initial crude oil samples before degradation with three different components, and flasks were incubated at 30 °C for 7 days. **Figure 3.7b** shows the crude oil sample after degradation with the isolated microbe. It was observed that there was an enhancement in the crude oil degradation after 7 days of incubation with the bacteria, with the media consisting of the modified chitosan and XG. The samples without OCH and XG show lower crude oil degradation, which was also confirmed by GC results. FESEM analysis of the culture after 24 h of cultivation in media was carried out to ensure the presence of bacteria and identify its shape and size. The image in **Figure 3.7c** clearly shows the presence of normal rod-shaped bacteria with dimensions of 1.180 ± 0.174 µm, and **Figure 3.7d** represents the histogram showing the length distribution of bacteria.

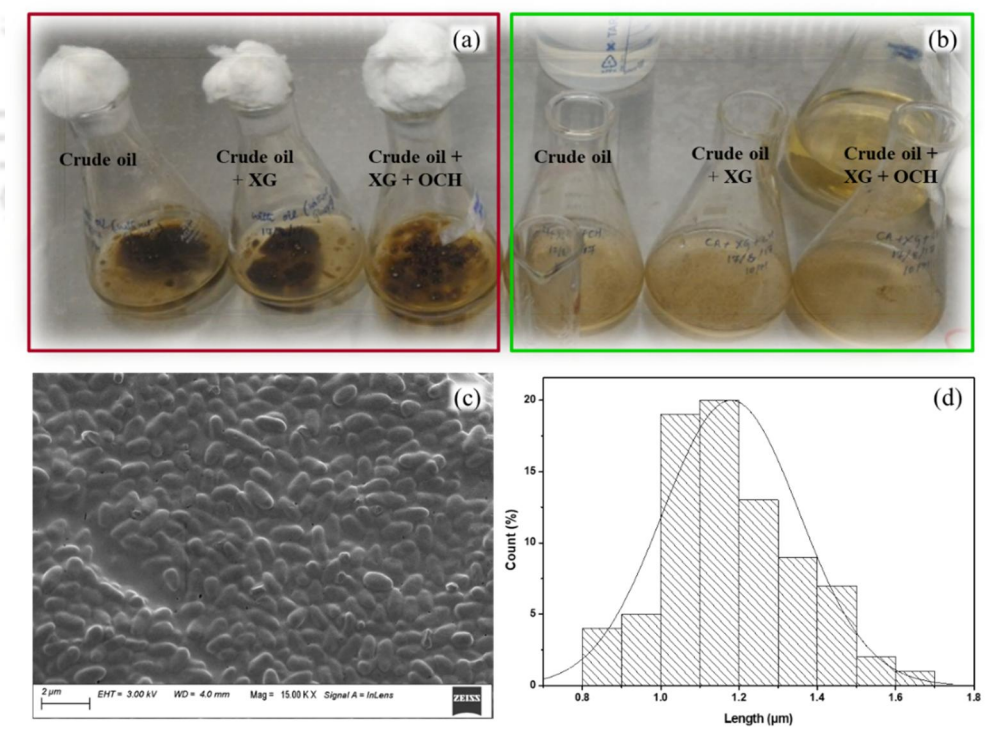

Figure 3.7:(a) Initial crude oil samples before degradation (b) crude oil samples after 7 days of degradation (c) FESEM image of the oil-degrading bacterial consortium (d) histogram showing length distribution of individual isolated bacteria calculated from the FESEM image using ImageJ

3.2.5 Role of Biosurfactant Produced by *Pseudomonas aeruginosa* CoE-SusPol3 on Oil Degradation

Biosurfactants are composed of hydrophobic and hydrophilic moieties with various phospholipids, polysaccharides and proteins with several functional groups. Most of them consist of carboxyl, phosphate and amino groups [247]. These have unique properties such as emulsification, dispersion and foaming. Microorganisms produce a number of surfactants, such as low molecular weight polymers that help reduce surface tension. Another class consists of high molecular weight molecules that help in the emulsification of the hydrocarbons present in crude oil and enhance the oil degradation [248,249].

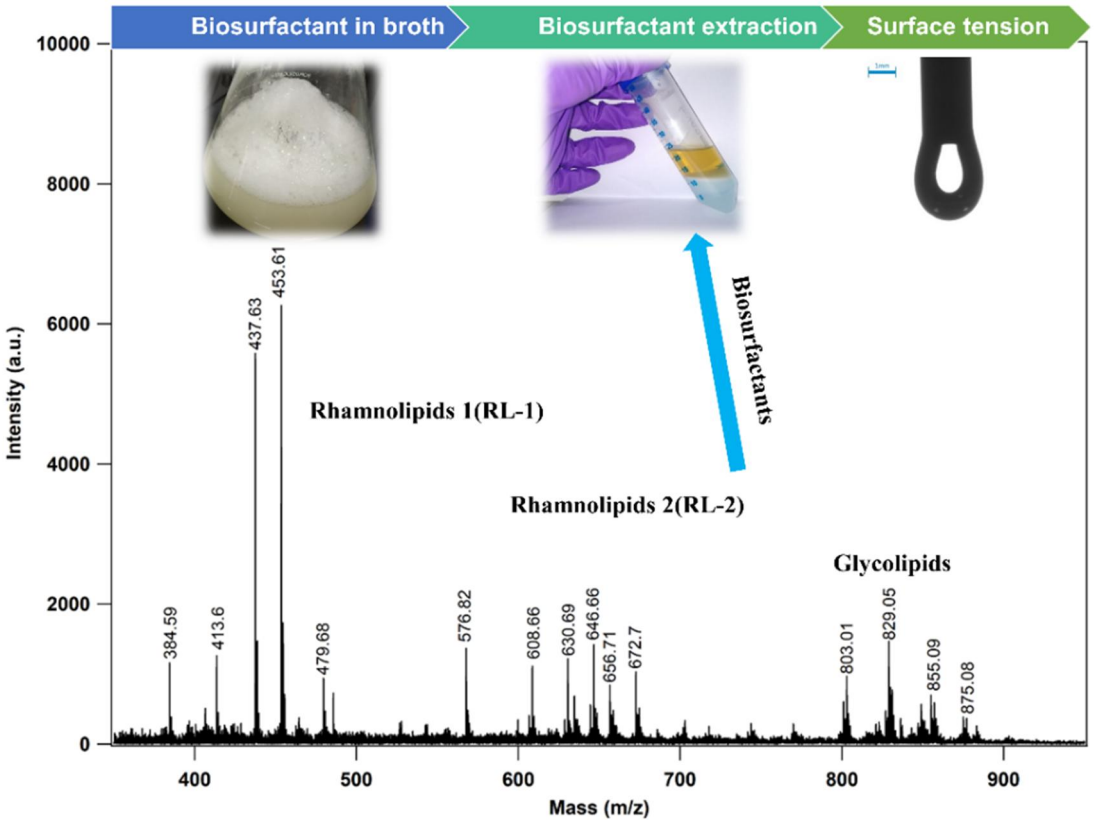

Figure 3.8: MALDI-TOF-MS spectrum of biosurfactant produced by isolated bacteria

Biosurfactants help to reduce the surface tension of the oil to make it easy for bacterial attachment on its surface and utilization of the oil for its metabolism. From **Figure 3.8** in the MALDI-TOF-MS spectrum, it is observed that the peaks m/z 400-500 indicate the

rhamnolipids 1 (RL-1), m/z 600-700 indicated the presence of rhamnolipids 2 (RL-2), and the m/z 800-900 represent the presence of other types of glycolipids [250,251]. These are the main surface-active compounds present in biosurfactants with low surface tension, and these are also non-toxic in nature [251,252].

The surface tension of the media used for the bacterial study, biosurfactant, crude oil and mixture of crude oil and biosurfactant used in the degradation study was evaluated to understand the mechanism of action of the bacteria in the utilization of the hydrocarbons as carbon source. The surface tension of crude oil was reduced to 28.53 (± 0.05) mN/m from 32.44 (± 0.22) mN/m when biosurfactant was present in the system. The surface tension of different components is shown in **Table 3.1**. The adherence of microorganisms to hydrocarbons is arduous due to their hydrophobicity and low solubility. In the current study, the isolated bacteria can degrade the hydrocarbons of crude oil emulsion stabilized by OCH and assisted by the action of surfactants produced by them. The biosurfactant helps in the reduction of the surface tension of the emulsion, which assists the bacteria in adhering to the surface oil droplets and accelerates the degradation.

Table 3.1: Surface tension values obtained from pendant drop method

Sl. No.	Samples	Surface Tension (mN/m)
1	Water	71.57 (± 0.12)
2	Lab media	55.66 (± 0.17)
3	Crude oil	32.44 (± 0.22)
4	Biosurfactant	25.81 (± 0.07)
5	Crude oil + biosurfactant	28.53 (± 0.05)

3.2.6 Analysis of Oil Degradation by Gas Chromatography

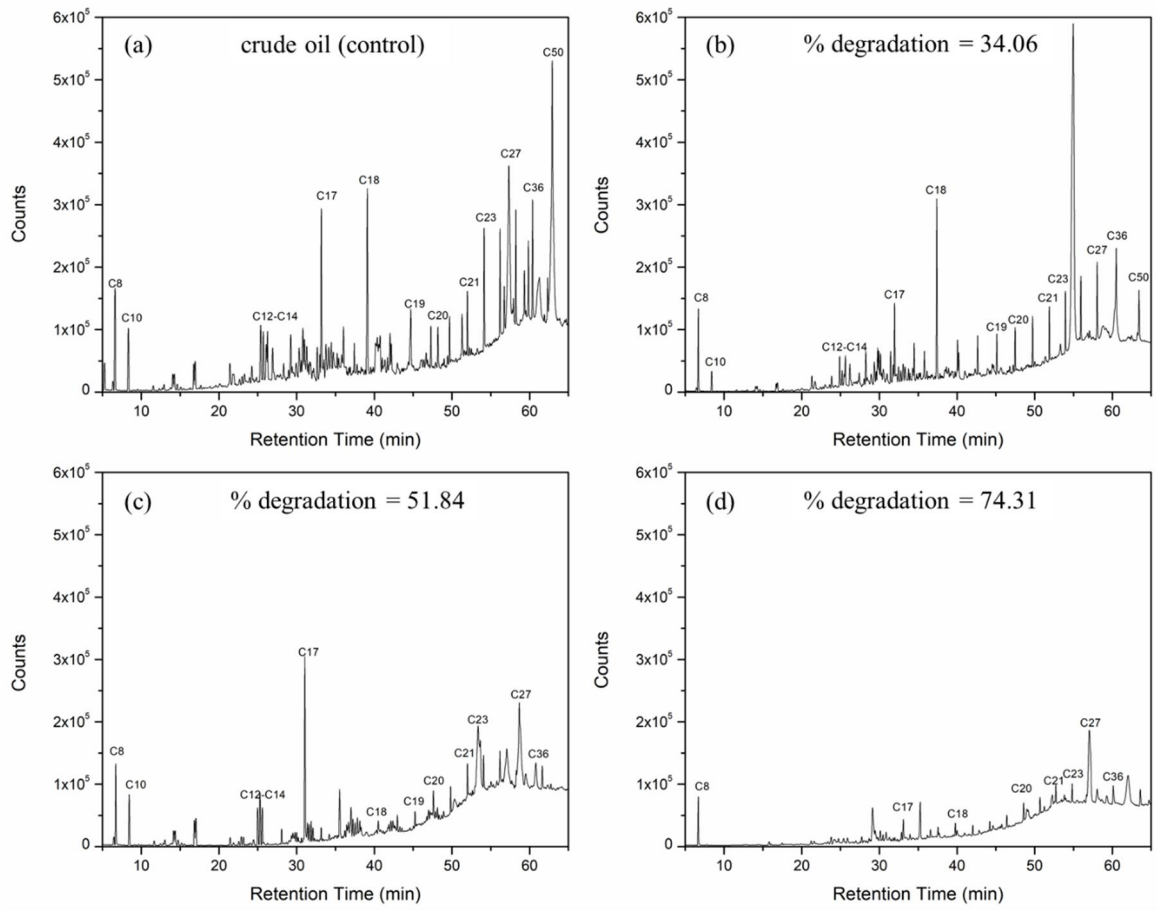

Figure 3.9: Comparison of GC spectra of (a) controlled crude oil (b) crude oil with *Pseudomonas aeruginosa* alone (c) crude oil with the *Pseudomonas aeruginosa* and XG (d) crude oil with *Pseudomonas aeruginosa*, XG and OCH

The isolated bacteria, *Pseudomonas aeruginosa* CoE-SusPol3, can utilize and degrade most of the hydrocarbons present in crude oil. The bacterial growth and degradation of crude oil are dependent on the medium and growth conditions. When the bacterial strain was grown on the crude oil supplemented with XG and OCH, maximum degradation was observed due to the reduction of surface tension of the crude oil, which assisted the bacteria in attaching to the oil droplets and enhanced its degradation. The crude oil degradation was evaluated using GC, wherein the crude oil was extracted using DCM from the broth and subsequently injected into the GC column. The spectra of crude oil without OCH and XG show different peaks corresponding to the various components (ranging from lower chain

alkanes C8–C21 and longer chain alkanes C22–C50) present in the crude oil. **Figure 3.9a** shows GC spectra of the controlled crude oil sample, which shows higher peak intensity of all the components of the crude oil, ranging from C8–C50, than the other three systems. **Figure 3.9b** shows the GC spectra of crude oil containing *Pseudomonas aeruginosa* CoE-SusPol3 without any other components (XG and OCH). It reflects that the intensity of the peaks of longer chain alkanes C22–C50 was reduced. However, when XG and OCH were added to crude oil with *Pseudomonas aeruginosa* CoE-SusPol3, the peak intensity decreased further, as seen in **Figure 3.9(c & d)**. A significant decrease in the peak intensity of alkanes C8–C50 indicates higher degradation of stabilized crude oil with OCH and XG compared to the unstabilized system. The percentage degradation by *Pseudomonas aeruginosa* CoE-SusPol3 alone (without the addition of XG and OCH) was 34.06%. The biodegradation of crude oil hydrocarbons increased to 51.84% when XG was added to the system, which further increased to 74.31% due to the combined effect of XG and OCH (results are summarized in **Table 3.2**). Thus, it indicates that the application of OCH aided the biodegradation of hydrocarbons present in the system by *Pseudomonas aeruginosa* CoE-SusPol3. Such synergistic effects of biopolymers as bio-dispersants and microbial degradation could result in a novel environment-friendly oil spill remediation technology for treating accidental oil spills.

Table 3.2: Droplet size and % degradation of CO in different systems

	CO-water		**CO-XG-water**		**CO-XG-OCH-water**	
	0 days	3 weeks	0 days	3 weeks	0 days	3 weeks
Droplet size (nm)	5294 ± 2096	9799 ± 3369	3237 ± 921	4775 ± 1727	1457 ± 288	1894 ± 748
% degradation (from GC analysis)	34.06%		51.84%		74.31%	

3.3 Summary

The addition of nanoamphiphilically OCH as a bio-dispersant for oil spills can be a potential substitute for synthetic chemical dispersants. The addition of OCH results in a more stable emulsion compared to the emulsion stabilized by only XG. The droplet size measurement for droplets stabilized by XG-OCH indicated that there was no significant increase in the size of the droplets; the initial size was 1457 ± 288 nm, which changed to 1894 ± 748 nm after 3 weeks. It indicated that the crude oil droplets are stable against coalescence compared to the crude oil emulsion in water, where the droplet size was 5294 ± 2096 nm, which increased to 9799 ± 3369 nm. The isolated bacteria (characterized as gram-negative and identified as *Pseudomonas aeruginosa* by 16S rRNA gene sequencing) has the capability to degrade crude oil and also produce surfactant, which assists in the degradation process. The percentage degradation of hydrocarbon present in crude oil by *Pseudomonas aeruginosa* was due to the synergistic effects of XG and OCH, which increased significantly to 74.31% compared to the system with XG (51.84%) and crude oil alone (34.06%). Such synergistic effects of biopolymers as bio-dispersants and microbial degradation could result in a novel environment-friendly oil spill remediation technology for treating accidental oil spills.

Although the bacterial degradation of crude oil in water can be an effective strategy, there are several challenges and potential problems with this process. The effectiveness of bacterial degradation depends on the type or species of bacteria that is present or introduced. Other factors like environmental variables, including temperature, pH, salinity, oxygen levels, and nutrition availability, also influence the activity of the bacteria, which determines its effectiveness. Because of these difficulties, it is unlikely that bacterial action alone will completely degrade crude oil. In many instances, a combination of bioremediation methods, physical containment, mechanical recovery, and other procedures

is required to efficiently reduce the effects of crude oil on water and promote the natural breakdown of hydrocarbons over time. After bacterial breakdown has occurred, leftover traces of crude oil can be removed from water using membrane separation techniques. Membrane separation is a technique that divides elements of a fluid mixture according to their sizes, molecular weights, and other characteristics using a barrier (membrane). This is particularly useful for getting rid of smaller oil droplets or dissolved hydrocarbons that bacteria might not have completely broken down.

Chapter 4

Fabrication of Cellulose Nanocrystal (CNC) Incorporated Polyvinylidene Fluoride (PVDF) Membrane for Enhanced Performance, Mechanical and Antifouling Properties

Polyvinylidene fluoride (PVDF)/Cellulose nanocrystal (CNC) thin composite membrane was developed by incorporating CNCs into the PVDF matrix in different amounts. Structural morphology obtained from FESEM images revealed that the occurrence of the porous finger-like structures increased with an increase in CNC content in the dope solution. This was also corroborated by an increase in pure water flux (PWF) with the addition of CNC content. 48% high PWF was obtained for PVDF/CNC as compared to pristine PVDF membrane with the addition of 3% CNC at a pressure of 1 kg/cm^2. Water contact angle (WCA) also decreased from 85° to 69° with increasing the wt% of CNC in the dope solution, which signifies improved hydrophilicity. Further, the PVDF/CNCs showed a high Bovine serum albumin (BSA) rejection of 93% and flux recovery ratio (FRR) of 76.76%, whereas the pristine PVDF membrane showed a BSA rejection of 70.86% and a FRR of 40.82%. Thus, the presence of CNC in the PVDF membrane prevented BSA fouling and showed improvement in BSA rejection.

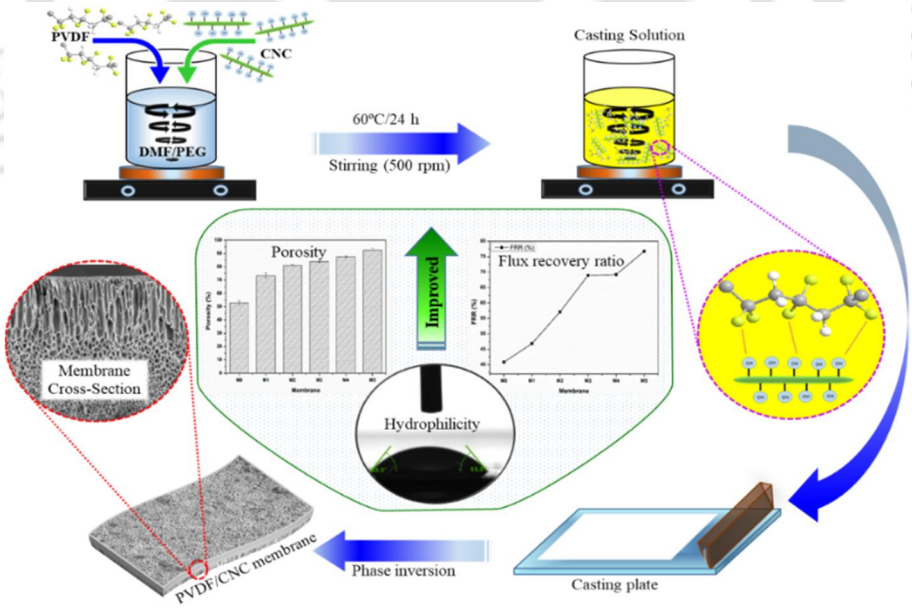

Research outputs of this chapter: *"Fabrication of Cellulose nanocrystal (CNC) from waste paper for developing antifouling and high-performance Polyvinylidene fluoride (PVDF) membrane for water purification". Published in* ***Carbohydrate Polymer Technologies and Applications,*** *Volume 5, 2023, pp. 100309*

4.1 Introduction

Polymeric membrane-based separation is becoming a promising method for treating wastewater and gaining additional importance due to its low cost and easy removal of harmful products associated with wastewater. The use of non-sustainable materials and synthetic nanoparticles in membrane fabrication poses significant environmental concerns. Environmental problems are now a major concern for both humans and other living things. Many synthetic goods and materials have been developed over time to meet human requirements. The environment and life could be negatively impacted by these synthetic materials. To overcome these threats and due to the depletion of non-renewable resources, there is a growing interest in renewable resources and the use of bio-based materials as raw materials for the creation of value-added products for a variety of purposes. Cellulose is one such sustainable material that is abundantly available, the structure represented in **Figure 4.1a**. It contains both a disordered region and an orderly-arranged region called the crystalline region. The acid hydrolysis method is used to eliminate the disordered region of cellulose to produce highly crystalline cellulose nanocrystals (CNCs) [218,253]. CNCs are rod-like structures having a length of a few hundred nanometers and a diameter of up to 100 nm [254,255], and high-performance membranes have recently been created by adding CNC as an additive. Apart from being a bioderived material, it also has many advantages, like it has good tensile strength and imparts rigidity to the membrane [256–259]. Its high crystalline nature allows it to be used in different pH ranges since the paracrystalline region, which is more reactive with acid than the crystalline region, was removed during hydrolysis [260]. CNCs are used in pollutant remediation technologies and also as a catalyst for dye degradation from wastewater [261,262]. CNCs have abundant –OH groups on their surface that act as active sites, which can be used for different types of functionalization, such as adding amine groups, carboxyl and succinic anhydride [263]. These active sites also help

in immobilizing the pollutants in wastewater by forming strong hydrogen bonds. Different types of functionalization allow CNCs to bind with specific pollutants present in wastewater. CNCs formed via sulfuric acid hydrolysis possess sulfate half-ester, sulphate ($–SO_4^{2–}$) and sulfonic groups ($–SHO_3$) on their surface, which are more effective binding sites for heavy metals [253,264]. On the other hand, carboxylate CNC produced using dicarboxylic acids containing –ve charge on its surface is more effective in adsorbing UO_2^{2+} [263,265]. CNC–COOH formed by functionalization with sodium periodate/chlorite effectively removes Cu^{2+} ions from water [266]. CNC contains a high surface area and is hydrophilic due to the presence of these numerous –OH groups on its surface [171].

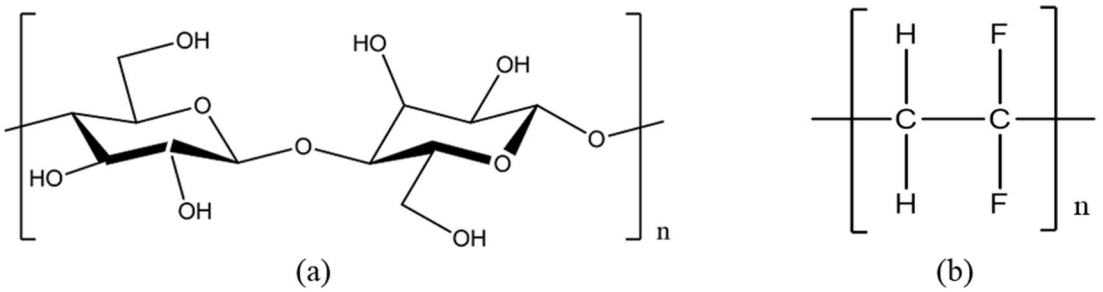

Figure 4.1: Structure of (a) cellulose and (b) PVDF

In the membrane separation process, the flux decline is a severe problem in most of the pristine membranes, resulting in declining membrane lifetime, increased operational cost and energy, and reduced membrane selectivity [267]. One of the best ways to improve membrane technology is through membrane modification. Different methods have been adopted to reduce fouling and improve performance, including chemical modification [268], plasma treatment [269], surface coating [135], grafting with functional groups [270], blending of hydrophilic polymers [271] and incorporation of nanomaterials into the membrane matrix [134]. Among these methods, nanoparticles incorporated into the membrane structure significantly improved antifouling and separation performance [272]. Different nanoparticles like SiO_2 [273], TiO_2 [274], carbon nanotubes [275], graphene

oxide [276], silver-based nanoparticles [277], Fe_3O_4 [154], ZrO_2 [155], Al_2O_3 [156], etc. are being used with different polymers to improve performance and antifouling property. Many previous studies suggested that the improvement in membrane hydrophilicity helps in reducing the fouling of the membrane [278,279]. Therefore, hydrophilic CNCs, along with other additives such as graphene oxide (GO), are used with different polymers to enhance the hydrophilicity, mechanical and antifouling properties of the membrane [280]. A negative electric layer is produced by the sulphate lipid molecules on the surface of CNCs, and this layer can be widely distributed in polar solvents like water. When a very small quantity (less than 2%) of CNCs are added, a stable dispersed system can be formed. The CNC particles also form a crosslinked three-dimensional network structure due to hydrogen bonding between them [281,282]. With such favourable properties in CNC, it becomes a suitable replacement for inorganic nanoparticles in membranes.

Among the different types of membrane materials available, Polyvinylidene fluoride (PVDF) is considered as an ideal material due to its outstanding chemical resistance, thermal stability, mechanical durability and good membrane-forming ability structure shown in **Figure 4.1b**. PVDF is semi-crystalline; hence, it has both strength and flexibility and mechanical strength is due to its crystalline phase, and flexibility is due to its disordered phase [84]. It can dissolve in organic solvents like N, N-dimethylformamide (DMF), N, N-dimethylacetamide (DMAc) and N-methyl-2-pyrrolidone (NMP), and membrane can be prepared by well-known industrially scalable phase inversion method [85]. However, because of the hydrophilic nature of PVDF, it is more susceptible to fouling with interaction with the foulant present in wastewater [86]. Different modification techniques were applied to improve the performance and antifouling properties of the PVDF membrane. The surface roughness and contact angle of the PVDF membrane increased by adding $CaCO_3$ nanoparticles in the dope solution, and the membrane exhibited lower thermal loss when

$CaCO_3$ was added to it, resulting in a more thermally stable membrane [87–90]. PVDF membrane with more than 25% TiO_2 improves the membrane permeability significantly and hence increases the flux and prevents the decline of flux over time [75], and with only 10% TiO_2 (contact angle ~59.7°), the hydrophilicity is improved as compared to neat PVDF membrane (contact angle ~82.8°) [92]. Nowadays, the use of these inorganic nanoparticles is limited; more and more importance is given to the use of bioderived materials like lignin, cellulose nanofiber, CNC, and chitosan [93] in membrane preparation. A small percentage of CNC loading can improve the mechanical properties, and it is reported that with the addition of 1% CNC to PVDF, the tensile is improved by 118% and 114% improvement in the tensile modulus [94]. Various properties of PVDF, like surface wettability, mechanical and thermal properties, can also be altered by incorporating an oxidized form of CNF (TEMPO-mediated Oxidized) and sodium hydroxide and cationization functionalized CNC with PVDF [95–97]. Recent literature reported the fabrication of an electrospinning PVDF membrane incorporated with CNC and its application in oil-water separation and power sensing; the membrane shows a 16% improvement in flux and is a promising material for the removal of oil from water [98]. Thus, PVDF, along with bio-based nanoparticles such as CNC, can be a potential material for fabricating composite membranes for water purification applications.

In this work, CNCs were prepared, and its potential application in membrane fabrication to improve the antifouling property, mechanical property and filtration performance was explored. The novelty lies in using CNCs derived from waste paper in membrane application, where waste material is converted to a value-added product. Moreover, the advantage of being environmental friendly and the nontoxic nature of CNC overcomes the limitation of potential contamination of filtrate by the leached inorganic and other additives from the membrane. CNCs were prepared from waste paper by acid hydrolysis technique,

and a detailed characterization of it was carried out. The properties of pristine PVDF and PVDF/CNC composite membranes were compared to ascertain their suitability and applicability for wastewater treatment. Details characterization, including membrane structure, surface hydrophilicity, thermal and mechanical characteristics of the membranes, were thoroughly investigated to understand the effect of CNCs in the composite membrane. Bovine serum albumin (BSA) was used as a model pollutant to check the antifouling properties of the membrane, and its characteristics were discussed in detail based on the amount of CNC added to the dope solution.

4.2 Results and Discussion

4.2.1 Characterization of CNC

ATR-FTIR analysis of the prepared CNCs was carried out to characterize the chemical composition and define the functional groups present in it. FTIR spectrum of CNCs is shown in **Figure 4.2a**, showing the prominent peak at 2890 cm^{-1} representing C–H stretching vibration and 1371 cm^{-1} showing $–CH_2$ wagging. Two peaks were observed at 1061 cm^{-1} and 892 cm^{-1}, corresponding to –C–O–C– pyranose ring stretching vibration and –CH vibration of β-glucosides of CNCs, respectively [283]. The peak at 1161 cm^{-1} corresponds to asymmetric –C–O–C– stretching of glucosidic linkages, in-plane C–OH stretching at C–6, which is evident for CNC. Free hydroxyl groups for stretching vibration are represented by the wide-ranging hump from 3500-3200 cm^{-1}. Free –OH bending present in the CNC is represented by the peak at ~1632 cm^{-1} [218].

The XRD plot for fabricated CNC from waste paper is shown in **Figure 4.2b**. The XRD plot shows peaks at 14.62°, 16.35°, 22.63°, and 34.40° representing the lattice planes (1 $\bar{1}$ 0), (1 1 0), (2 0 0) and (0 0 4), which indicates the typical cellulose-I structure. The peak at 20.40° representing lattice planes (0 2 1) is a typical characteristic for crystals in cellulose type I polymorph [284]. The sharp peak at 22.63° represents the separation distance

between the hydrogen bonds in cellulose-I. Comparing with the XRD data of waste paper, it clearly indicates that the peak intensity was higher for CNCs, and the common peaks for cellulose were also observed in the XRD plot of waste paper. The presence of filler minerals in the waste paper is indicated by the diffraction peaks at 12.10° [285]. The crystallinity index (I_{CR}) calculated using equation 1 was found to be 78% for CNCs compared to the I_{CR} of 38% for waste paper, which represents that the CNCs obtained from waste papers are highly crystalline in nature. The acid hydrolysis process removes the disordered portion of the cellulose, and the crystalline part is left behind, thus forming highly crystalline CNC. This result also matches the d-spacing calculated from the SAED pattern of the FETEM image. Thus, FTIR spectra, together with the XRD data, confirm the formation of CNCs and have the Cellulose I crystalline structure after acid hydrolysis and freeze-drying.

Figure 4.2c shows the FESEM image of the fabricated CNC from waste paper. The image showed uniformly dispersed rod-shaped CNC; however, agglomeration of CNC was also observed because of the strong intermolecular hydrogen bonding of CNCs. It was evident from **Figure 4.2c** that the CNC is a rod-shaped structure with an average diameter of 49 ± 5 nm and an average length of 286 ± 31 nm. The FETEM micrograph in **Figure 4.2d** also shows that the fabricated CNC has rod-shaped morphology, and the SAED pattern also implies the crystalline nature of the fabricated CNC (**Figure 4.2e**).

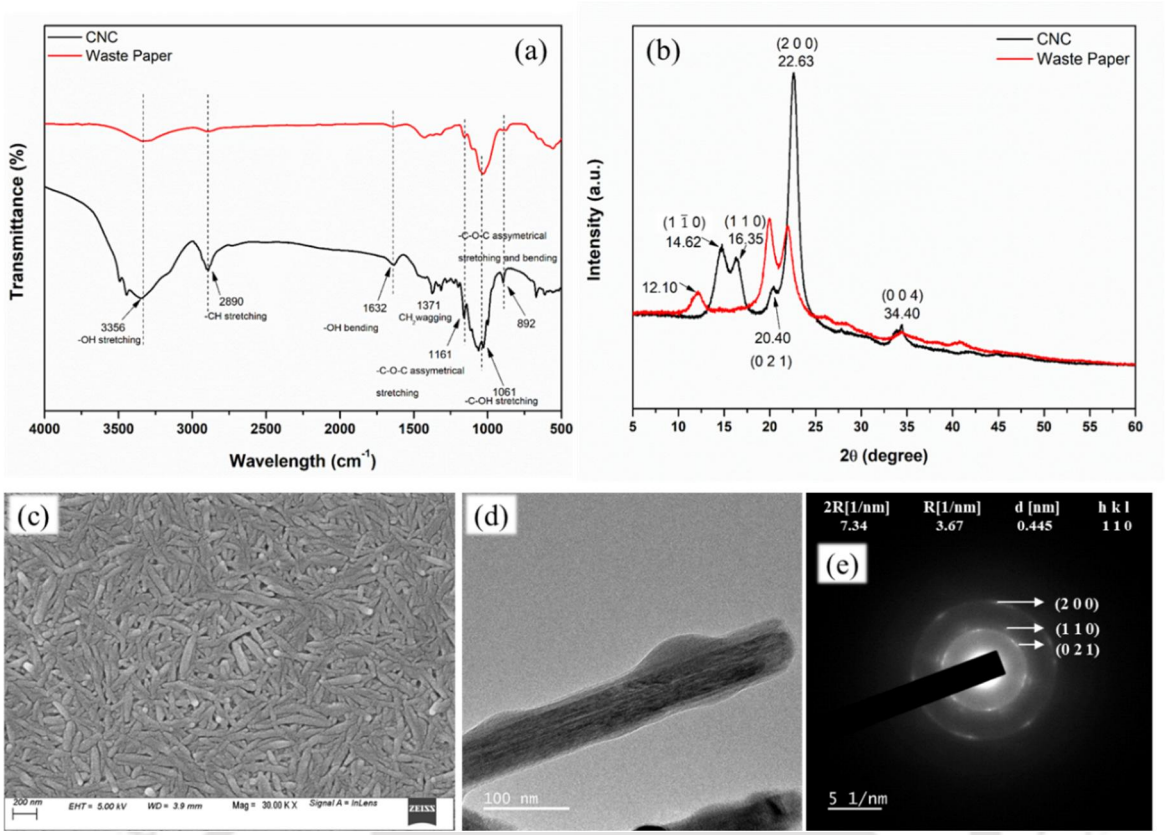

Figure 4.2: Different characterization of CNC using (a) FTIR spectroscopic analysis of CNC and waste paper (b) XRD spectra of CNC and waste paper (c) FESEM image of CNC (d) FETEM image of CNC showing rod-like structure (e) SAED pattern of CNC

4.2.2 Characterization of PVDF and PVDF/CNC Composite Membrane

4.2.2.1 *FTIR Spectroscopic Analysis of the Membranes*

ATR-FTIR scan was carried out in the wavenumber range 4000−600 cm^{-1} to investigate the chemical composition and surface functional groups present on PVDF and PVDF/CNC membranes. As seen from **Figure 4.3a**, the pristine PVDF membrane shows characteristics peak at around 1405 cm^{-1}, which represents the CH_2 wagging vibrations, 1182 cm^{-1} shows the C–C band vibration, the peak at 875 and 840 cm^{-1} represents the asymmetric stretching vibration of C–C–C and C–F stretching vibration of PVDF respectively [286].

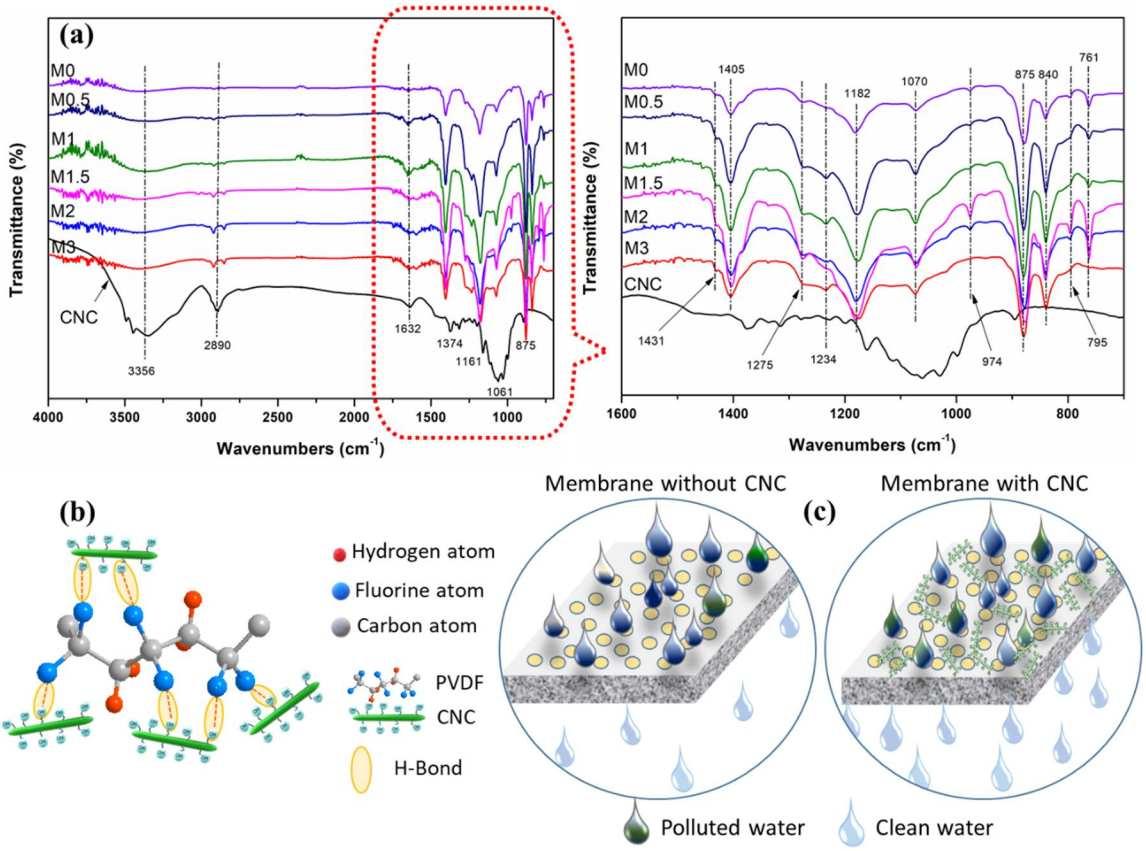

Figure 4.3: (a) FTIR spectra of PVDF, PVDF/CNC membrane, and CNC (b) schematic showing the interaction of CNCs with PVDF and possible formation of hydrogen bonding between them (c) schematic representing the PVDF membrane without CNC with less water flux and PVDF membrane with CNCs having more water flux

In the FTIR spectra of PVDF/CNC composite membrane, the characteristics peak of both PVDF and CNC was observed. A peak at 3356 cm^{-1} is observed, representing the –OH stretching vibration of cellulose, which is also a characteristic of CNC. Peak 1061 cm^{-1} representing –C–O–C– pyranose ring stretching vibration CNC shows a slight shift in composite membrane and is observed at 1070 cm^{-1}. The FTIR spectra also give an idea about the crystalline phase of the prepared PVDF-based membrane. α-phase and β-phase crystals are the two most important crystal phases of PVDF [287]. The small distinctive band at 761, 795, and 975 cm^{-1} corresponds to the α-phase crystals, which appear in almost all PVDF-based membranes. The exclusive characteristic peak for β-phase crystals is

detected in wavelengths of 1275 and 1431 cm^{-1} for all the membranes [288]. When CNCs are added to the PVDF membranes, γ-phase crystals seem to appear, which is absent in the PVDF membrane without CNC. The γ-phase crystal is represented by the exclusive band at 1234 cm^{-1} [289]. The broad peak at 3356 cm^{-1} indicates the hydrogen bond formed with the hydroxyl group of CNC and PVDF in the composite membrane, also represented in **Figure 4.3b**, which is absent in the pristine PVDF membrane [96,290,291]. From these results, it can be concluded that characteristics of CNCs were present in the composite membrane, indicating the presence of CNCs.

4.2.2.2 *Morphological Analysis of the Membrane*

The PVDF and PVDF/CNC membrane surface and fractured cross-sectional surface were observed under a field emission scanning microscope, and the effect of CNCs on PVDF membranes was studied. All membrane surfaces show a porous structure; however, the PVDF membrane without CNC shows a less porous surface as compared to the PVDF/CNC membrane. The pores are also well distributed over the surface, as shown in **Figure 4.4(a-f)**. While observing the cross-sectional structure, a typical asymmetrical structure was observed for all membranes; a dense sponge-like structure, a thin skin layer and finger-like porous channels. **Figure 4.4(b1-f1)** shows that the finger-like channels are more prominent in the PVDF/CNC composite membrane than in the PVDF membrane without CNC, as in **Figure 4.4a1**. The reason behind such a structure is that these hydrophilic CNCs enhance the spreading of water at a faster rate into the casting solution. The presence of CNCs also accelerates the process of phase separation and, thus, the generation of pores. The length of the finger-like pores also increases in the PVDF/CNC composite membrane in comparison to the membrane without CNC. The finger-like channels even extended to the bottom in the case of **Figure 4.4(e1 & f1)**, resulting in more interconnectivity and high porosity.

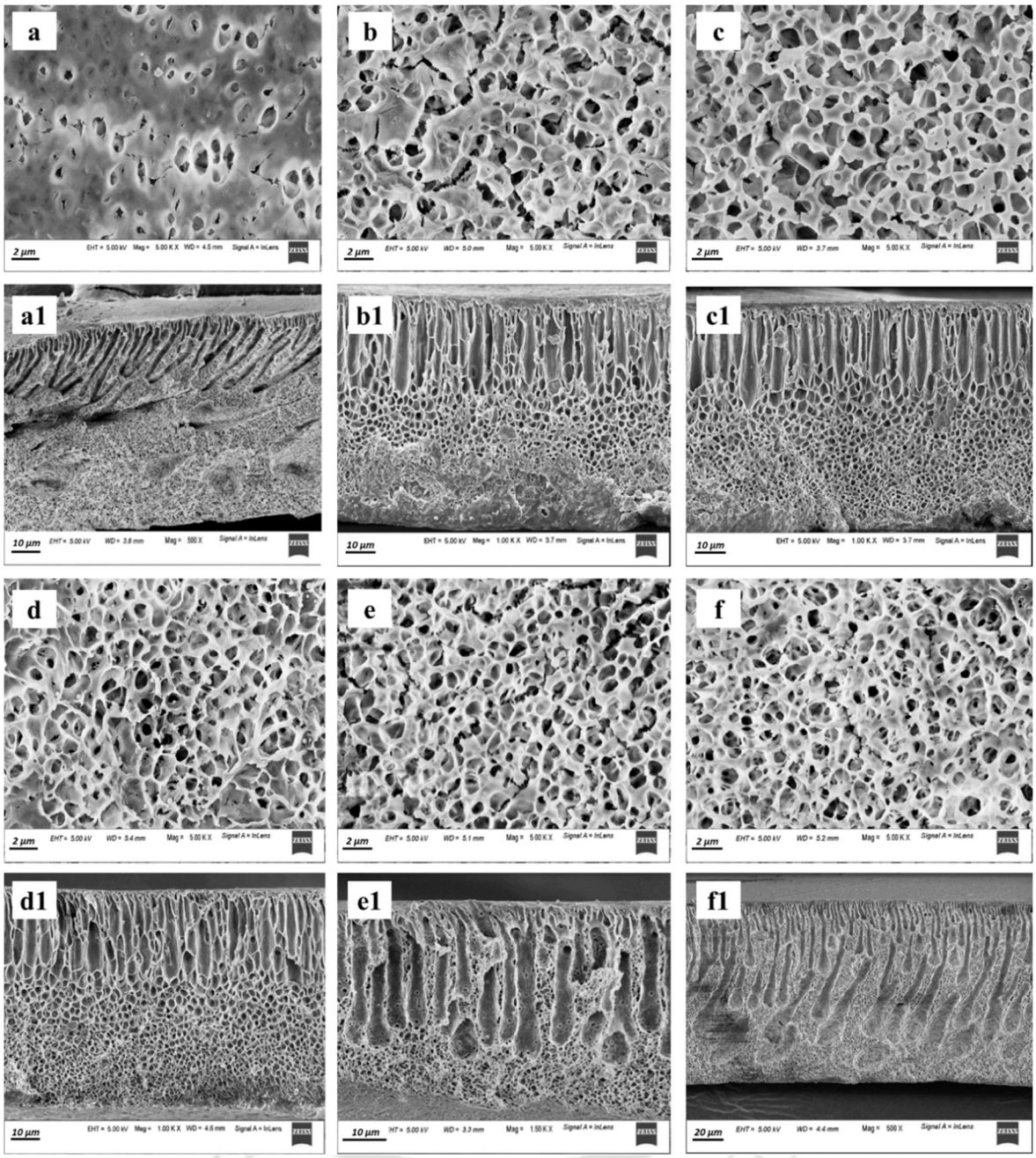

Figure 4.4: FESEM images of PVDF and PVDF/CNC membrane (a-f) surface morphology showing the increase in pore at the surface with an increase in the amount of CNC from 0 to 3% (a1-f1) cross-sectional structure also shows the finger-like structure are more prominent and even extended to the bottom of the membrane with an increase in the CNC

The incorporation of CNCs into the membrane initiated thermodynamic instability of the polymer solution and improved gelation, resulting in the formation of a more prominent finger-like structure that improves the membrane's performance [292]. The presence of hydrophilic CNCs also enhances the solvent and non-solvent exchange process during phase inversion because of the affinity of CNCs towards the water that accelerates the solvent exchange in the casting solution. The distribution of CNCs in the PVDF membrane can be observed in **Figure 4.5.** A high magnification (50 kX) FESEM image clearly indicates the presence of rod-shaped CNCs in the membrane matrix and is distributed over the surface of the membrane.

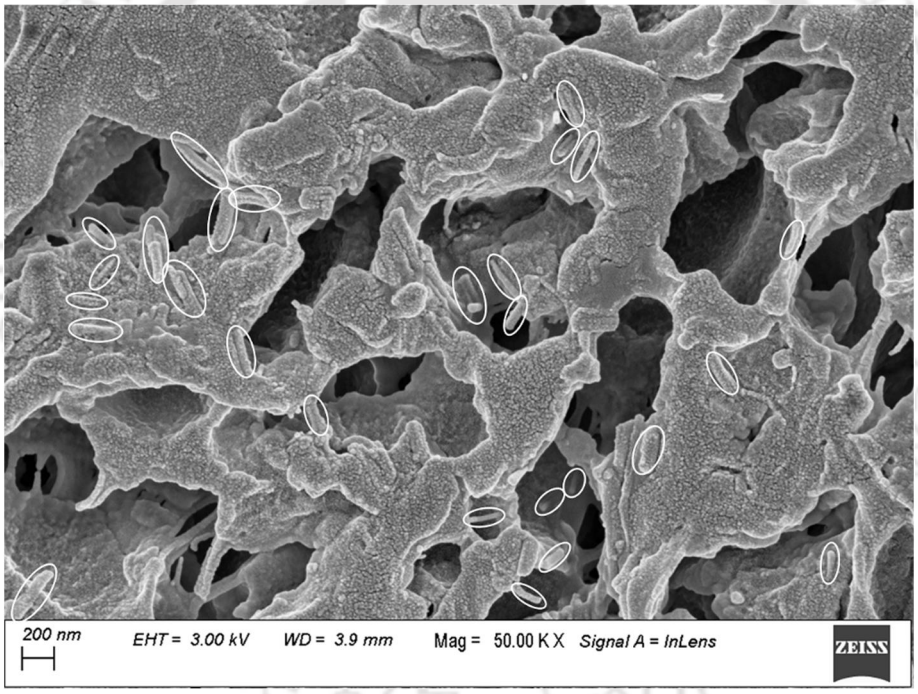

Figure 4.5: High magnification FESEM image of PVDF membrane showing the presence of rod-shaped CNCs

4.2.2.3 *XPS Analysis of CNC and the Membranes*

To further understand the surface properties and composition of the membrane and CNC, XPS analysis was carried out, and the results are shown in **Figure 4.6**. Wide survey XPS spectra of CNC, pristine PVDF membrane (M0) and PVDF/CNC membrane (M4) were

shown in **Figure 4.6a**. Only C and O elements are observed in the survey spectrum of CNC, corresponding to C1s binding energy of 284.8 eV and O1s binding energy of 530.9 eV [293]. Similarly, C and F elements are observed in pristine PVDF membrane corresponding to C1s binding energy of 284.8eV and F1s binding energy of 686.52 eV [153]. A prominent peak for the F element was observed in the survey spectrum of pristine PVDF membrane, whose intensity was reduced significantly for PVDF membrane containing CNC (which is shown in the insert zoomed image of **Figure 4.6b** at binding energy 686.33 eV). This reduction in the intensity of the F element present in PVDF is due to the presence of CNCs over the membrane surface, which was also confirmed by the magnified FESEM image in **Figure 4.5**. **Figure 4.6b** also represents a high-resolution XPS spectrum of PVDF membrane containing 2 wt% of CNC. Intense F1s peak was observed for pristine PVDF membrane at a binding energy of 686.52 eV, which was shifted to 686.33 eV due to the addition of CNC, indicating the presence of dipole interaction. **Figure 4.6c** depicted C1s spectra of CNCs showing three peaks at 286.20 eV, 284.83 eV and 283.16 eV representing O–C–O/C=O, C–O and C–C/C–H species, respectively [294]. PVDF represents four peaks at 289.33 eV, 286.38 eV, 284.85 eV and 283.40 assigned to the CF_2, C–O (adventitious carbon), CH_2 and C–C/C–H species, respectively [295]. However, the CF_2 species was not prominent in the PVDF/CNC membrane due to the availability of CNCs on the surface of the membrane, which also corroborates with the FTIR results. A binding energy difference of 0.24 eV C–C species and 0.43 eV in O1s spectra (**Figure 4.6d**) in PVDF and PVDF/CNC membrane was also observed, indicating a different chemical environment in the surface of membrane containing CNCs compared to pristine PVDF membrane.

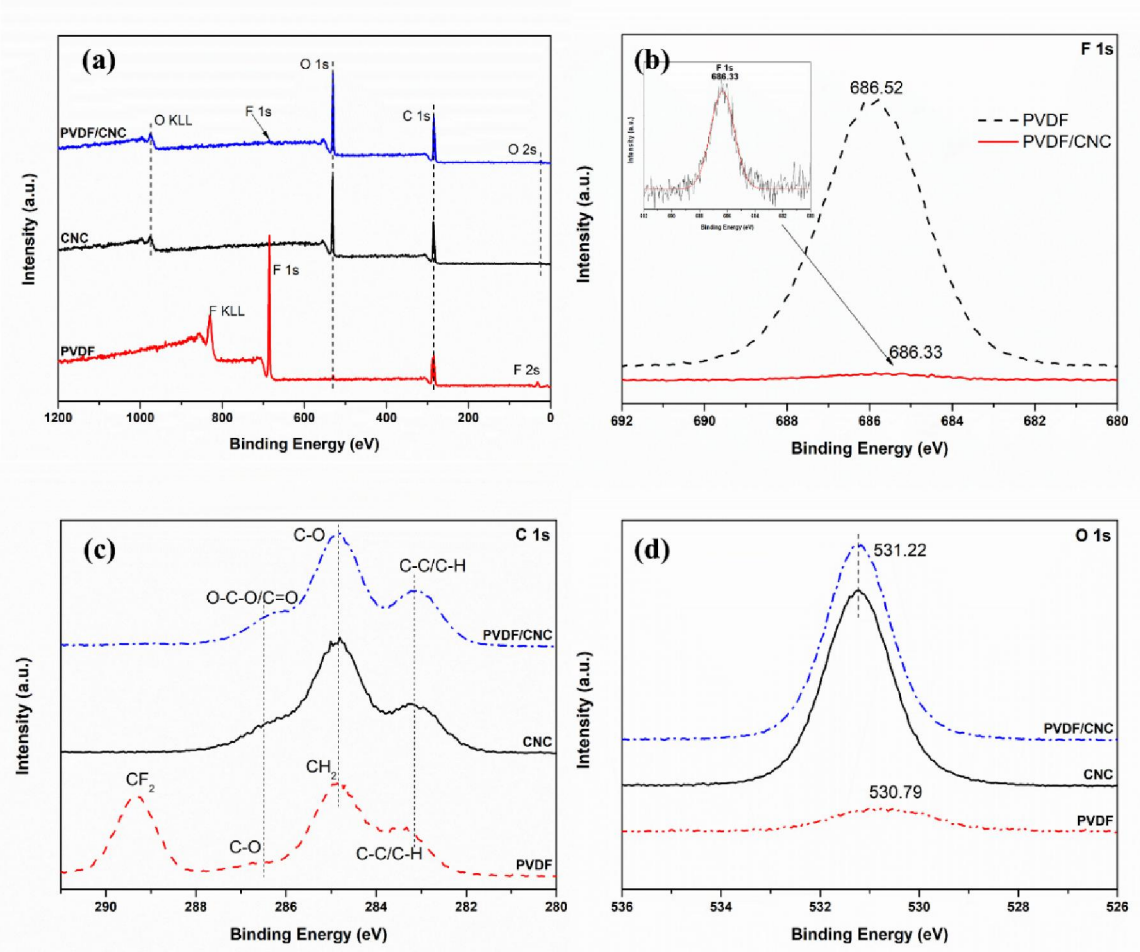

Figure 4.6: XPS spectra of CNC added PVDF membrane surface compared to CNC and pristine PVDF membrane (a) XPS spectra of PVDF, CNC and PVDF/CNC membrane surface (b) F1s spectra of PVDF and PVDF/CNC membrane surface (c) O1s spectra of PVDF, CNC and PVDF/CNC membrane surface.

4.2.2.4 *Thermal Analysis of the Membranes*

The effect of CNCs on the thermal degradation of the PVDF membrane was characterized using TGA. TG and DTG curves of pure PVDF, PVDF/CNC membrane and CNCs are shown in **Figure 4.7**. PVDF and PVDF/CNC decompose at different temperatures due to their differences in chemical compositions. Glycosyl units of cellulose decompose during the thermal degradation of CNCs, and on the other hand, PVDF decomposition corresponds to the fragment formation of vinylidene oligomers, dimers and monomers [296]. The

decomposition temperature of the PVDF/CNC composite membrane decreases when the concentration of CNCs in the polymer solution is increased. The decomposition temperature decreases from 482 °C to 465 °C from M0 to M3 when CNC content increases to 2 wt%. The reason behind the decrease in the decomposition temperature of the membranes with an increase in CNC concentration is evident because CNC has a lower decomposition temperature than PVDF [291]. The decomposition temperature may decrease slightly with the addition of CNCs; still, all the membranes were stable up to a temperature of more than 350 °C, which signifies that the PVDF/CNC membrane can be used at high temperatures.

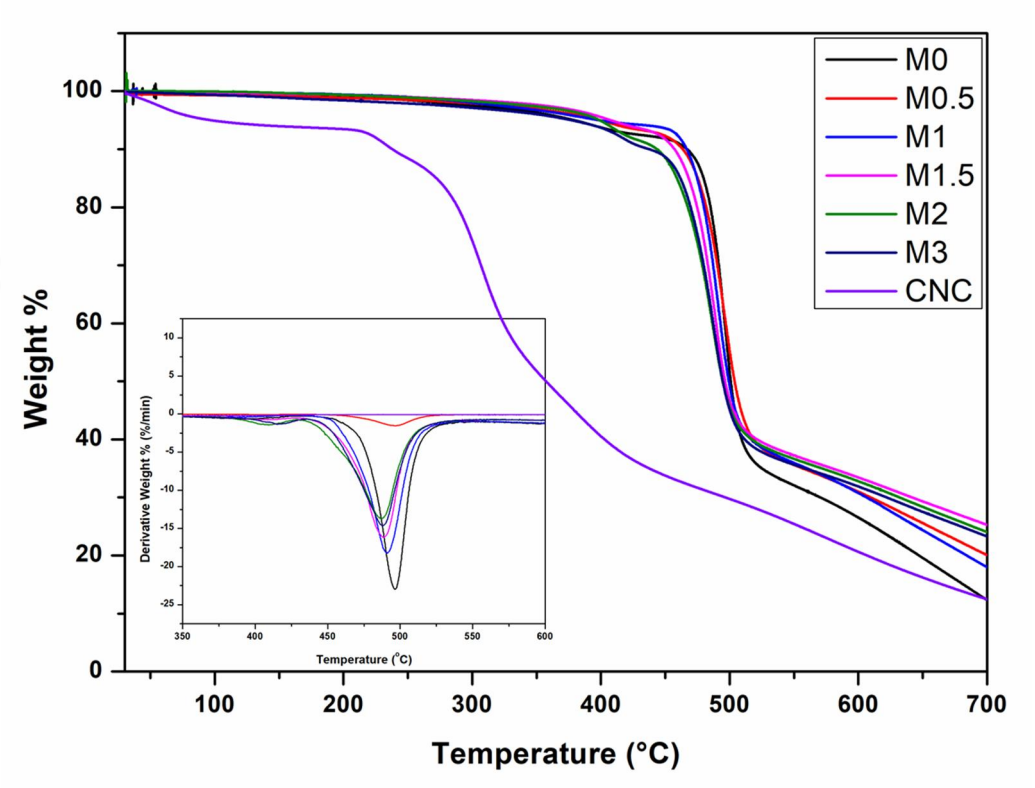

Figure 4.7: Comparison of TGA and DTG curves of PVDF, PVDF/CNC membrane and CNC

4.2.2.5 *Mechanical Property Analysis of the Membranes*

The stiffness of the membrane is determined by Young's modulus. It was calculated by determining the slope of the linear portion of the stress-strain curve. The stress-strain curve

and Young's modulus of PVDF/CNC membrane are represented in **Figure 4.8(a & b)**, respectively. Young's modulus of the pristine PVDF membrane is about 0.95 ± 0.06 MPa, which increases to 1.85 ± 0.17 in the case of M1. It indicates enhancement of the stiffness of the PVDF/CNC composite membrane with the addition of more CNCs in the dope solution. The Young's modulus of the membrane with 3% CNCs was the lowest, which is attributed to the fact that with the increase in CNC concentration beyond a threshold value, the dispersion becomes challenging (which can also be seen in **Figure 4.9c & d**), results in low stiffness [296]. Another parameter to determine the membrane's resistance to deformation is the tensile strength, which represents the maximum stress that the samples can withstand just before breaking. **Figure 4.8c** shows the tensile strength curve, and **Figure 4.8d** represents the elongation-at-break of the PVDF/CNC composite membranes. The tensile strength of the membrane increases to 5.4 ± 0.27 MPa with an increase in CNC concentration up to 1.5%, but at a higher loading of 3%, the tensile strength decreases to the lowest value of 2.11 ± 0.03 MPa. The decrease in tensile strength is due to the lack of proper dispersion and agglomeration at higher concentrations [297]. The percentage elongation for PVDF/CNC membrane at low concentration (till 1.5% of FeCNC) is more than 50%. Then, increasing the concentration of CNCs to 3% reduced the percentage elongation to 26.1 ± 4.5 %, indicating the increase in brittleness of the membrane as compared to the pristine PVDF membrane [291]. The tensile strength and the percentage elongation of the prepared membranes were compared with the available literature and presented in **Table 4.1**. It is evident from the literature comparison that the incorporation of CNCs into the PVDF membrane shows better tensile strength and percentage elongation than many of the available literature which contains additives other than CNC.

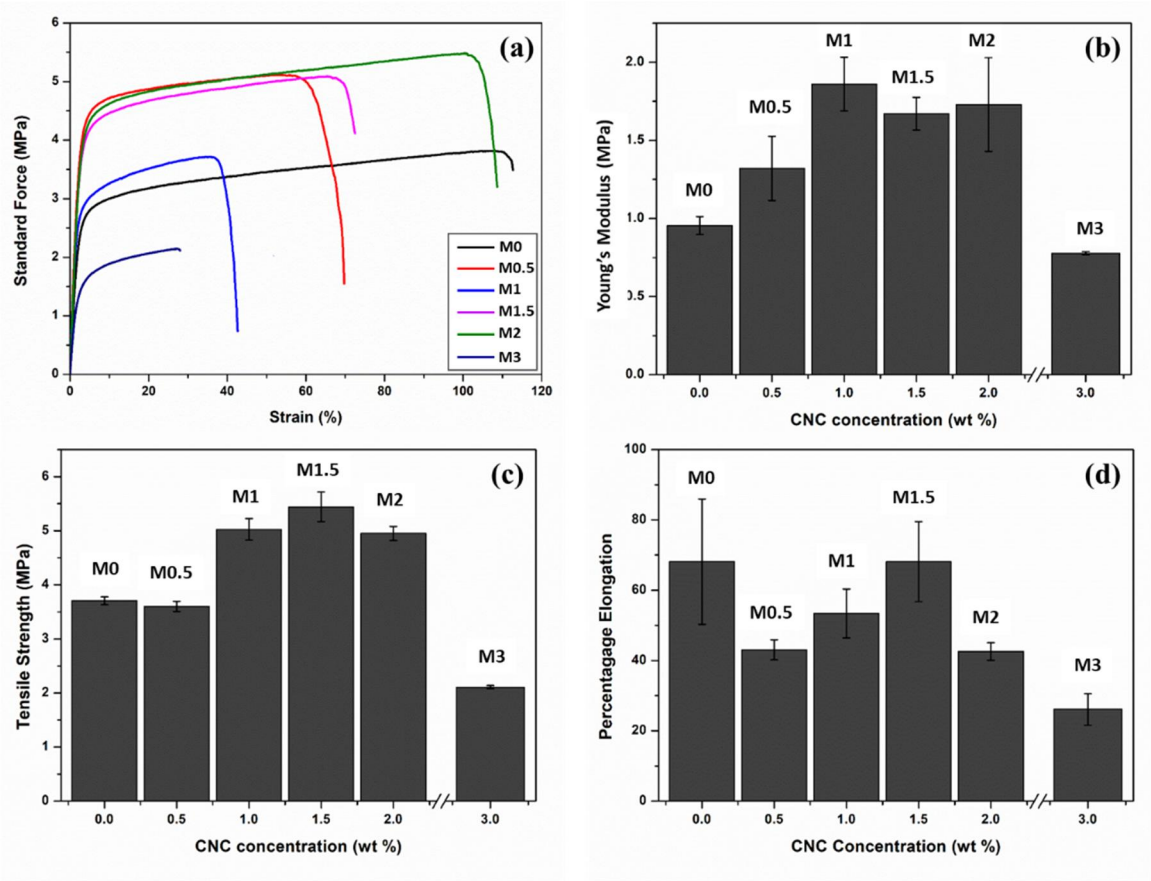

Figure 4.8: Effect of CNC on (a) stress-strain curve (b) Young's modulus (c) tensile strength (d) percentage elongation of PVDF membrane

Table 4.1: Comparison of tensile strength and percentage elongation of the membrane reported in this work with the available literature

Compositions	Tensile strength (MPa)	% Elongation	Reference
PVDF/NMP 15/85	2.78	65.30	[298]
PVDF/PSNT (silica nanotubes)	2.76	22.40	[299]
PVDF/SiO_2/PVP	1.52	12.00	[300]
PVDF/DBM (30%)	6.18	25.68	[301]
PVDF/CNF nanocomposite (5 wt%)	1.05	11.70	[96]

PVDF/MWCNTs-OH	2.81	62.43	[302]
PVDF-SiO_2(3)-HDTMS	3.80	37.00	[303]
PVDF/SiO_2 (1.6%)	2.10	50.00	[304]
PVDF/1% Tin dioxide	0.74	3.75	[305]
PVDF/CNC (1.5%)	**5.4 0**	**>50.00**	**This work**

4.2.2.6 *Hydrophilicity/Hydrophobicity, Porosity and Equilibrium Water Content (EWC) of the Membranes*

Water contact angle (WCA) was measured mainly to assess the surface hydrophilicity of the membrane, which primarily depends on surface roughness, membrane porosity and composition [292]. Hence, it plays an important role in membrane permeation and antifouling properties. WCA at 0, 5 and 10 min were measured for the different membranes to evaluate the change in membrane hydrophilicity time. WCA measurement was carried out to determine the membrane hydrophilicity and the effect of CNCs on it. A smaller WCA indicates that the membrane surface is more hydrophilic. **Figure 4.9a** denotes the effect of CNCs on the WCA of the membrane. At time t = 0 min, the PVDF membrane without CNC shows the maximum contact angle of 85°, indicating the least hydrophilicity at that angle. With an increase in the concentration of CNCs in the polymer solution, the contact angle gradually decreased to 69° for M1.5, resulting in an increase in the surface hydrophilicity of the composite membranes. A similar decreasing trend of WCA was seen for time t = 5, 10 min; however, the lowest WCA was seen for M1.5 at t = 5 min is 58.8 and t = 10 min is 42.2. The decrease in WCA can be explained by the fact that the addition of CNC imparts more hydrophilicity to the membrane surface because of the presence of hydroxyl groups on CNC, which was also confirmed by XPS and FTIR results.

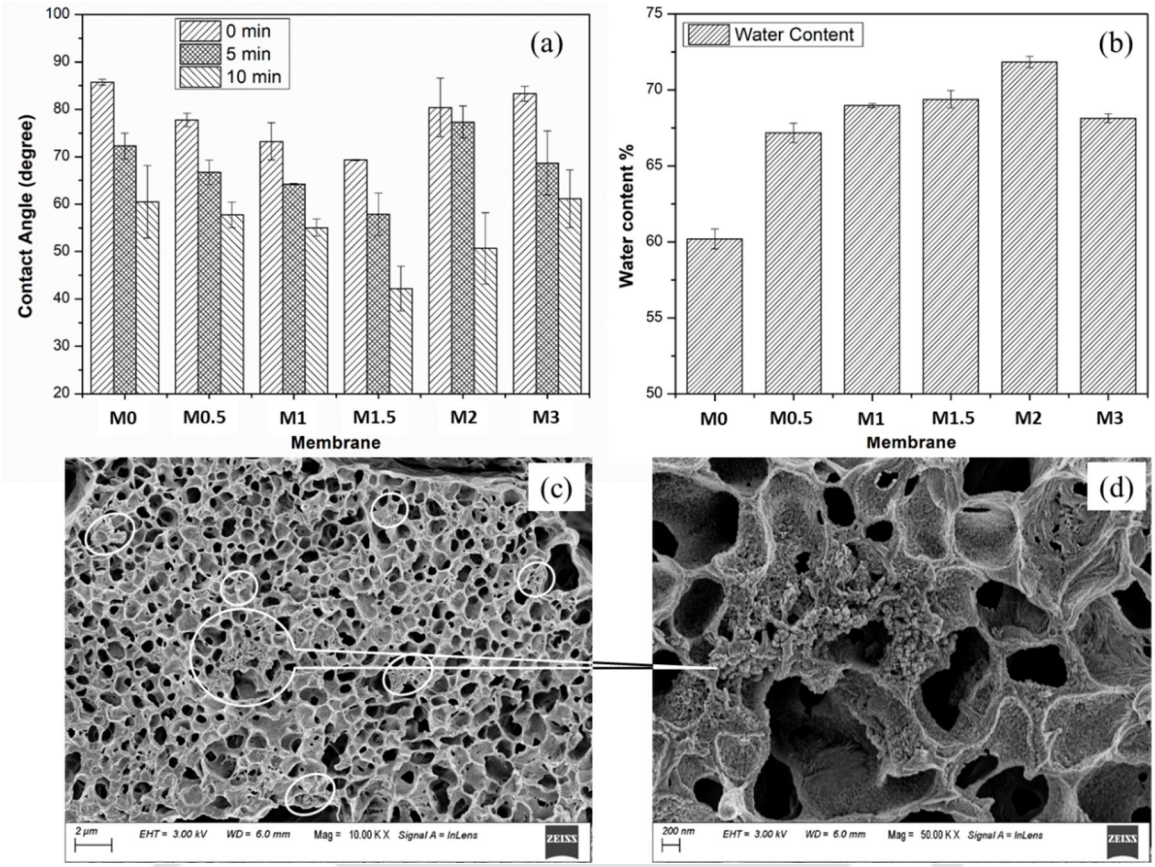

Figure 4.9: (a) Contact angle of PVDF and PVDF/CNC membranes at 0, 5 and 10 min intervals (b) EWC of PVDF and PVDF/CNC membranes (c) agglomerated CNCs present over the surface of the membrane (d) magnified image of agglomerated CNCs

These hydroxyl groups present on the surface of CNCs form hydrogen bonds with water molecules, making the CNCs attracted to water. When CNCs are incorporated into the PVDF membrane, the introduction of these hydrophilic functional groups to the surface of the membrane increases its affinity for water. These hydrogen bonds of CNC with water molecules result in a stable water layer on the membrane's surface, which reduces the contact angle of the membrane, indicating an increase in wettability and hydrophilicity. CNCs also have a high surface area; when CNCs are dispersed onto a PVDF membrane, they effectively increase the overall surface area of the membrane. This increased surface area provides more sites for water molecules to interact, resulting in enhancing the

hydrophilicity of the membrane. However, the increase in contact angle after increasing CNC concentration beyond 1.5 wt% shows an increase in contact angle (in the case of M2 and M3). The increase in contact angle is due to the agglomeration of CNC, which results in an increase in surface roughness. The agglomeration of CNCs on the surface of the membrane can be clearly seen in the FESEM image in **Figure 4.9(c & d)**. The hydrophilic/hydrophobic properties and permeability of membranes are also indirectly linked to the water content [306]. As noted in the previous section, the availability of free –OH groups on the surface of CNC imparts hydrophilic characteristics to CNC. Hence, the water content is also increased in the membrane with a higher concentration of CNC, as shown in **Figure 4.9b**. The water content increased from 60 to 71.83% when CNC content increased from 0.5 to 2 wt% in the dope solution. This leads to the development of a more hydrophilic membrane.

The results of porosity for the PVDF and PVDF/CNC membrane are shown in **Figure 4.10.** The effect of CNC on porosity can be seen in **Figure 4.10,** that the porosity of the membrane increases with the addition of CNC. The porosity increases to 40% in the case of M3 when compared to the pristine PVDF membrane. This increase in porosity can be explained by the fact that CNC is a hydrophilic material containing abundant –OH on the surface, which improves the diffusion rate of solvent and non-solvent (water), resulting in high porosity formation [307]. This result also reached an agreement with the FESEM image of the membranes.

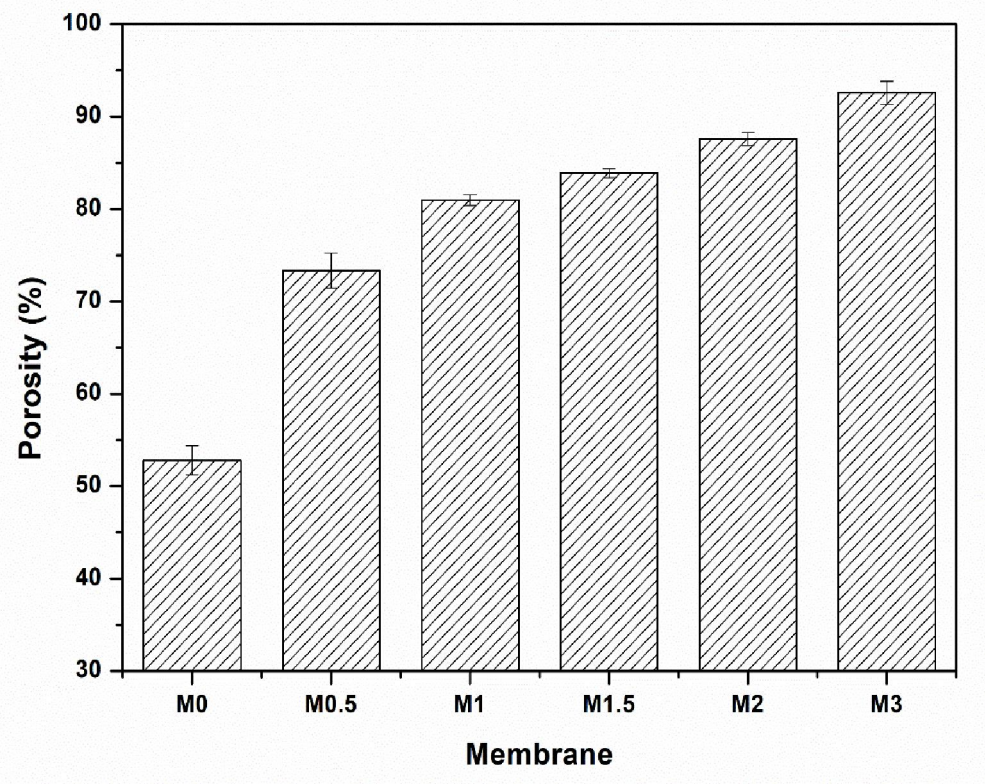

Figure 4.10: The porosity of PVDF and PVDF/CNC membranes

4.2.3 Performance Evaluation of the Membranes

The data for pure water flux (PWF) before BSA filtration, after BSA filtration and BSA solution filtration were shown in **Figure 4.11.** The PWF increases by ~48% in PVDF/CNC membrane with 3% CNC as compared to the pristine PVDF membrane. The PWF increases when CNC content increases because of the increase in porous structure and more finger-like structure formation in the membrane, thus decreasing membrane resistivity. As discussed above, the increase in CNC concentration imparts hydrophilicity, which causes a change in the membrane morphology, as seen in the FESEM images (**Figure 4.4**). Since CNC contains a large specific surface area containing a sufficient amount of –OH groups that also facilitate the hydrogen bonding, this results in more attraction of water molecules towards the membrane surface to pass through it and thus results in higher water flux. Hence, hydrophilic membranes are less prone to fouling because they resist the adhesion of hydrophobic substances, which leads to improvement in filtration efficiency and longer

membrane lifespan. However, the PWF decreased after the BSA solution was filtered through the membrane, resulting from membrane fouling by the BSA protein.

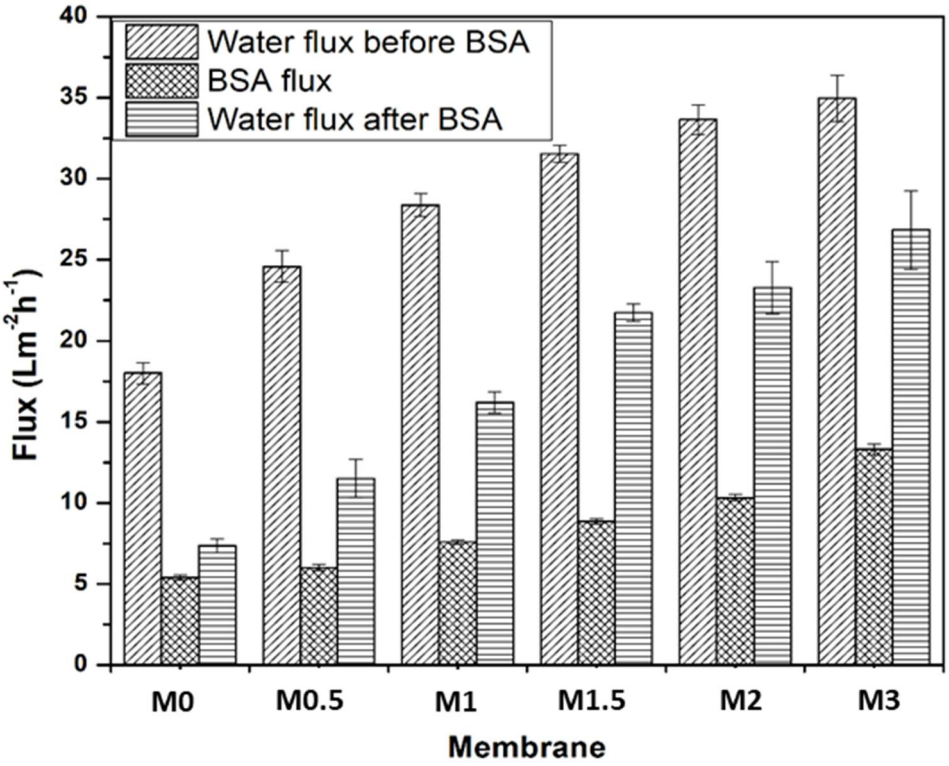

Figure 4.11: Comparison of pure water permeation flux before BSA solution filtration, after BSA filtration and BSA filtration

BSA rejection was studied for all the prepared membranes, and a comparison plot was shown in **Figure 4.12a**, which is mainly determined by the average pore and the skin layer. It showed that the BSA rejection of the M0 membrane was 70.86% and increased with the increase in the addition of CNC content to the membrane. The rejection increased to 83.14% after the addition of 1.5 wt% CNC, and it further increased significantly to 93% when CNC concentration increased to 2 wt% in the case of M2. As mentioned earlier, the increase in CNC content improves hydrophilicity and results in more affinity of water molecules towards the membrane and selectively allows the water molecules to pass through the pores of the membrane and retain the BSA molecules. Subsequently, a decrease in BSA rejection was observed when CNC concentration was 3% in the case of M3. This

decrease in BSA rejection was observed due to the larger and more pores in the membrane, which contribute to more penetration of BSA molecules through it, as seen in the FESEM images (**Figure 4.4**).

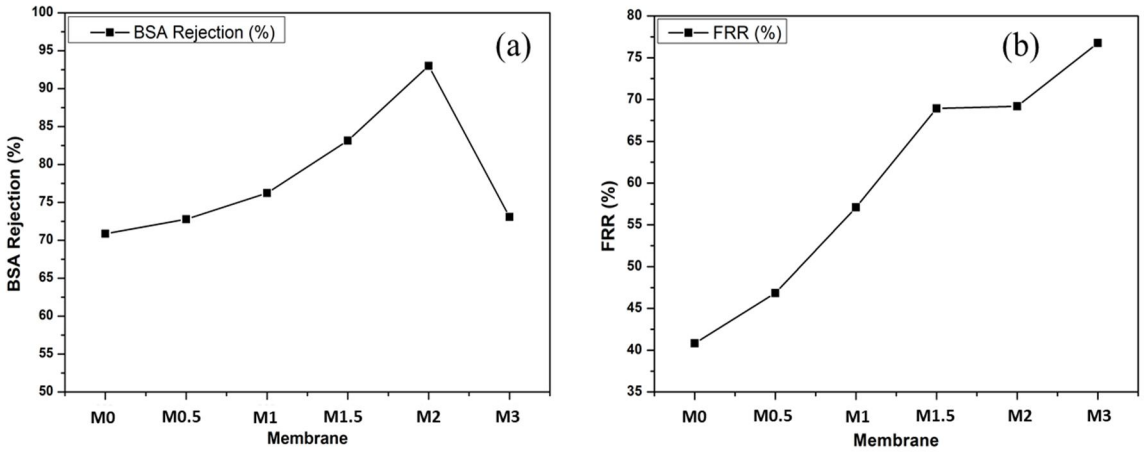

Figure 4.12: (a) BSA rejection rate (b) flux recovery ratio (FRR) values of PVDF and PVDF/CNC membranes

The determination of flux recovery ratio (FRR) is a criterion to measure the antifouling property of the membrane. Initially, DI water was filtered through the membrane, followed by BSA solution and again followed by DI water, and then FRR was calculated. **Figure 4.12b** showed that when CNC content in the dope solution was increased from 0 to 3 wt%, the FRR increased from 40 to 76%. This indicated that there was a significant enhancement in the antifouling property of the PVDF/CNC composite membrane. These results can be corroborated by the increase in water flux and hydrophilicity of the membrane. **Figure 4.13** showed that pristine PVDF membrane (M0), total flux decline ratio (DR_t) and irreversible flux decline ratio (DR_{ir}) value attained was 70% and 59.2%, respectively; however, a decrease in DR_t and DR_{ir} was observed for the PVDF/CNC membranes. Additionally, the reversible flux decline ratio (DR_r) increases sharply for M0-M1.5 and becomes almost stable for M1.5-M3. The decrease in DR_t and DR_{ir} with the increase in CNC wt% indicates

that fouling caused by BSA protein on the composite membranes was minor because of the hydrophilic groups present on the surface of the membranes imparted by CNCs.

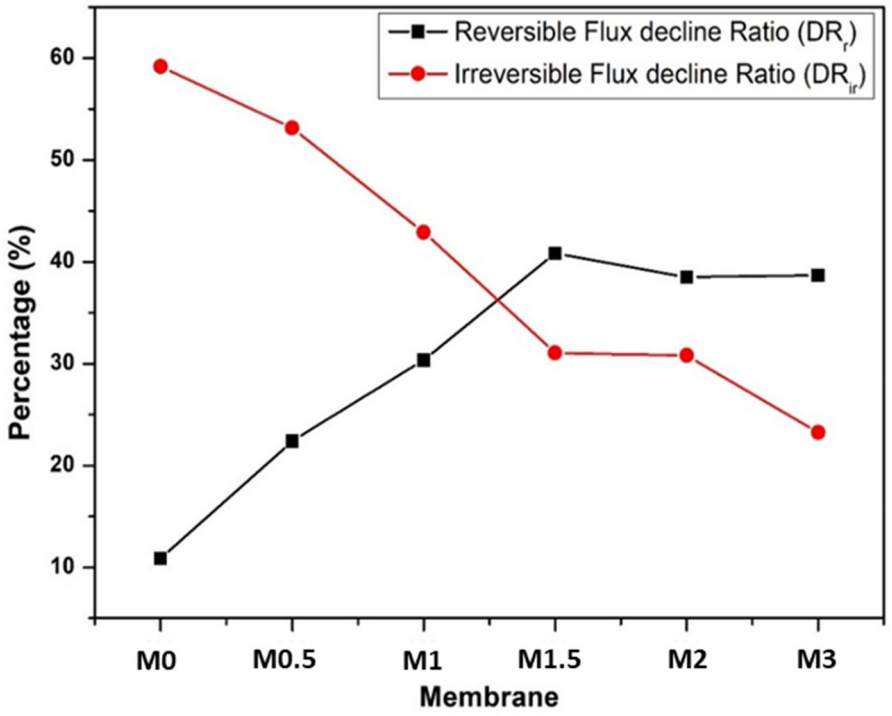

Figure 4.13: Reversible and irreversible fouling resistance ratio of PVDF and PVDF/CNC membranes

4.2.4 Relaxation Model or Membrane Filtration in Nonstationary Process for PVDF/CNC Membrane

It was observed that the flux calculated from filtration experiments data decreases over time. In order to confirm the dependencies of flux over time, a mathematical model and correlation of this model with the experimental data were determined. A relaxation model or membrane filtration in a nonstationary process was applied to validate the experimental data. The change in permeate flux (J) with time was explained using a kinetic equation, where the reduction of flux is proportional to its value.

$$\frac{d}{dt}(J - J_\infty) + \frac{1}{t_o}(J - J_\infty) = 0 \qquad (4.1)$$

$$\ln\left(\frac{J-J_\infty}{J_o-J_\infty}\right) = -\frac{t}{t_o} \quad (4.2)$$

Where, J , J_∞, J_o and t_o are volumetric permeate flux in time t, equilibrium permeate flux, initial permeate flux and time constant, respectively.

Time constant t_o was determined using equation (4.2), which represents the decline rate of the flux. **Figure 4.14** was used to determine t_o from the above equation for PWF of the composite membranes.

From equation (4.2), we obtained

$$J_t(t) = (J_o - J_\infty)e^{-\frac{t}{t_o}} + J_\infty \quad (4.3)$$

The flux over time, determined using the mathematical model, was compared with the experimental data represented in **Figure 4.15**. Before carrying out all the measurements, the membrane is compacted at 1.5 kg/cm^2 for sufficient time. During this period, the flux may fluctuate initially due to the presence of air pockets or gaps in the membrane, and channelling may occur, leading to the development of uneven flow paths, and it gets stabilized over time. The theoretical results are based on the assumption that to obtain an optimum result from the membrane, the measurements and calculations are carried out in this phase, where the permeate flux goes down and becomes stable with time. Therefore, in the initial phase, there is a variation in the theoretical flux and experimental flux. After compaction (30 min), the flux obtained from the experimental data and the results obtained from the relaxation model showed a good correlation. Thus, the stable flux obtained from the membrane over time can be predicted using this model, and the optimum time required to achieve the stable flux can be determined.

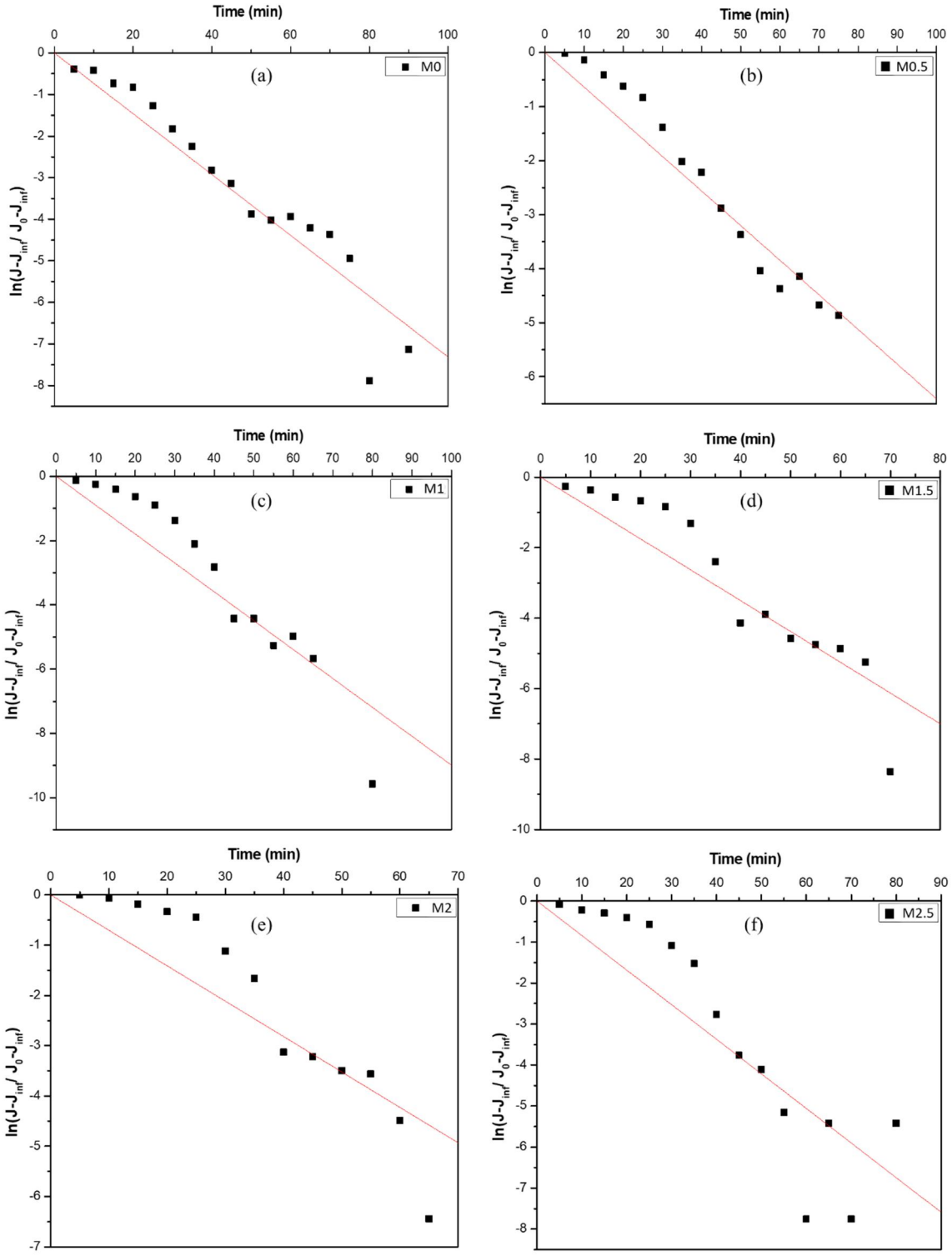

Figure 4.14: Curve for determination of characteristic decline time (t_o) of membrane filtration for (a) M0 (b) M0.5 (c) M1 (d) M1.5 (e) M2 (f) M3

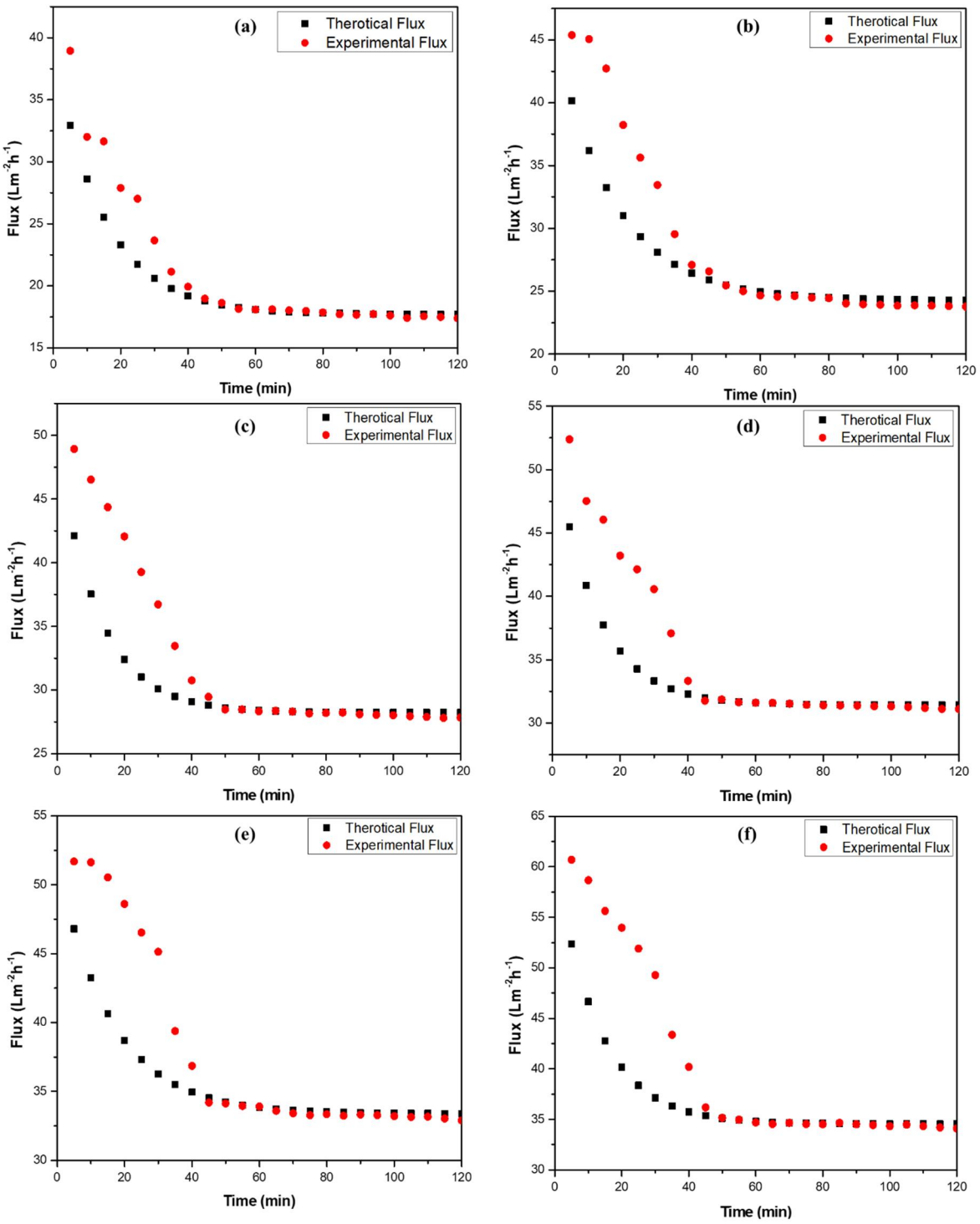

Figure 4.14: Comparison of experimental value and theoretical values of the volumetric flux of membrane filtration for (a) M0 (b) M0.5 (c) M1 (d) M1.5 (e) M2 (f) M3

4.3 Summary

CNCs were fabricated from waste paper with a high degree of crystallinity of 78% by acid hydrolysis method. The fabricated CNCs were characterized for their shape and size by FESEM and FETEM, which indicate the rod-shaped morphology of CNCs. CNCs are used as an additive in different wt% to PVDF during membrane preparation, and its effect on membrane morphology and performance was investigated. The results showed that the addition of CNCs to the membrane greatly influences the membrane structure and antifouling properties. Investigation of the antifouling property was done using BSA solution, and it was found that in comparison with the pristine PVDF membrane, the PVDF/CNC membrane showed remarkable improvement in the antifouling properties, signified by an increase in FRR to 76.76% and decreases in DR_{ir} values to 23.24% from 40.82% and 59.18%, respectively. The WCA for the pristine PVDF membrane is 85°, and it decreases to 69° when the CNC concentration is increased to 1.5 wt%. This signifies that the hydrophilic property of the membrane was improved by adding CNCs to the casting solution. Pristine PVDF membrane has a porosity of 52.7%, which increased to 92.5% in PVDF/CNC composite membrane when CNC content increased to 3%. It also showed an increase in permeation flux of ~48% compared to the neat PVDF membrane. Tensile strength increases to 5.4 ± 0.27 MPa at 1.5% CNC loading in the dope solution, and Young's modulus also increases with an increase in CNC concentration up to 2%. Fabrication of CNCs from waste paper opens an effective way to utilize the waste paper. Adding such cost-effective nanoparticles derived from waste paper to the polymeric membrane at a lower concentration and proper dispersion in the dope solution can become a promising candidate for developing antifouling and high-performance membranes.

Chapter 5

Fabrication of Polyvinylidene Fluoride (PVDF) Nanocomposite Membrane for Oil-Water Separation Based on Surface-Modified Magnetic Cellulose Nanocrystal

This chapter discusses the use of magnetic CNC (FeCNC) based membrane for the removal of oil from water. In Chapter 4, it was observed that by the addition of CNCs to the membrane, the pure water flux (PWF) was improved by 48%, and the BSA rejection was improved by ~20%. In order to further investigate and attempt to improve the flux, modified CNCs, called FeCNC, were used in the membrane in place of neat CNCs. A thin film membrane was prepared by adding FeCNC into the PVDF matrix. The presence of FeCNCs also accelerates the process of phase separation and, thus, the generation of pores. Compared with the pristine PVDF, PVDF/CNC membranes, the PVDF/FeCNC membrane showed significant improvement in the permeation flux and oil removal capacity. Contact angle also decreases initially with increasing the wt% of FeCNC in the casting solution, which signifies the improvement in hydrophilicity. PWF obtained for PVDF/FeCNC membrane was 77.75 L/m^{2}h (2% FeCNC) and 188.11 L/m^{2}h (3% FeCNC), which is significantly higher than the pristine PVDF membrane (18 L/m^{2}h) at a pressure of 1 kg/cm^2.

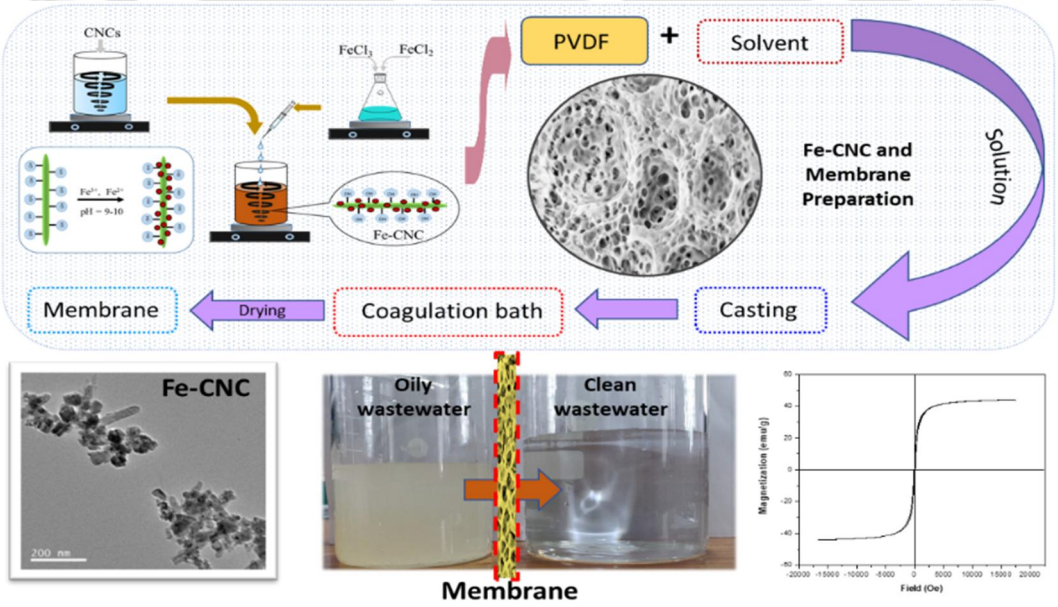

Research outputs of this chapter: *"Magnetic cellulose nanocrystal embedded PVDF membrane for oil-water separation",* ***Manuscript under preparation.***

Patent: *"Magnetic nanocomposite polymeric membrane for purification of water and process of preparation thereof". (Application No.: 202131014583)*

5.1 Introduction

The magnetic particles can be incorporated into the polymeric matrix to form magnetic polymeric membranes. The magnetic nanoparticles can be made of iron oxide (FeO, Fe_2O_3, Fe_3O_4) and other metal oxides or iron oxide coated with a protective layer to prevent them from aggregating and losing their magnetic properties [308]. The iron nanoparticles can be incorporated into the polymeric matrix through different methods, including solvent casting, phase inversion, and layer-by-layer assembly [309,310]. Iron nanoparticles have been used in polymeric membranes for various applications, including oil-water separation. The presence of iron nanoparticles in the polymeric membrane matrix can improve the separation efficiency and performance of the membrane [311,312]. In addition, iron nanoparticles can enhance the mechanical stability, thermal stability, and hydrophilicity of the polymeric membrane. This makes them suitable for use in various separation processes, including NF, UF, and RO. The high surface area of iron nanoparticles also allows for improved separation performance in water flux, rejection of contaminants, and fouling resistance, making it a promising candidate for water treatment applications [313]. Polymeric membranes with iron nanoparticles also show promising results in removing heavy metal ions [314,315] and organic pollutants [316,317] from water, making them useful in environmental remediation applications.

The use of magnetic nanoparticles in polymeric membranes for oil-water separation has gained attention due to their unique properties. Polymeric membranes with magnetic nanoparticles have high permeability, selectivity, and stability, making them a promising alternative for oil-water separation. When incorporated into a polymeric membrane matrix, the magnetic nanoparticles can improve the separation efficiency by attracting the oil droplets and retaining them within the membrane [318]. The size, shape, and surface properties of the magnetic nanoparticles play a crucial role in their performance for oil-

water separation. For example, smaller magnetic nanoparticles with a high specific surface area and hydrophobic surface properties can effectively attract oil droplets and retain them within the membrane. Thus, the use of magnetic nanoparticles in polymeric membranes for oil-water separation has shown promising results and has the potential to be a cost-effective and environmentally friendly solution for the separation of oil and water [319].

However, the use of iron nanoparticles in polymeric membranes can also pose certain challenges, such as clogging, corrosion, and aggregation of the nanoparticles. Agglomeration of nanomaterials is a common issue in the preparation of mixed-matrix membranes (MMMs), as it can lead to non-uniform distribution of the nanomaterials in the polymer matrix. This can negatively impact the performance of the membrane, including reduced water flux, decreased rejection of contaminants, and increased fouling [320,321]. Therefore, careful consideration and optimization are required for the use of iron nanoparticles in polymeric membranes. The nanohybrid concept aims to overcome this issue by combining two or more nanomaterials to form a hybrid material with improved performance. The idea is that the combination of different nanomaterials with complementary properties can lead to synergistic effects, resulting in improved membrane performance. Considering this idea, cellulose nanocrystal (CNC) was combined with iron nanoparticles to form a nanohybrid material called magnetic CNC (FeCNC) by co-precipitation method. This prepared FeCNC to have potential as a new class of nanohybrid material for application in the fabrication of MMMs with the added advantage of being environmentally friendly as it is derived from biosource. FeCNCs have a high specific surface area, making them effective at improving the separation efficiency of membranes. Furthermore, FeCNCs can be easily manipulated and controlled using magnetic fields, which makes them useful for various applications in membrane filtration that will be discussed in the next chapter. In addition, the FeCNCs exhibit good thermal stability and

mechanical strength, which are essential factors in developing high-performance membranes. FeCNCs in membrane technology provide a new avenue for developing more efficient and effective membranes. So, this chapter examines the use of FeCNC as a nanohybrid material to be used as an additive in PVDF-based membranes and to understand the change in properties and its potential application for oil removal from water.

5.2 Results and Discussion

The results and observations obtained from various analytical methods are discussed in this section of the chapter, along with probable scientific explanations.

5.2.1 Characterization of FeCNC and Fe_3O_4 Nanoparticle

5.2.1.1 *Morphology Study of CNC, Fe_3O_4 and FeCNC*

FeCNC was prepared by the co-precipitation method. Drop-casted CNC and FeCNC were observed under FESEM. It was observed that the Fe_3O_4 nanoparticles were dispersed over the surface of CNCs uniformly to form FeCNCs through the simple-one-step co-precipitation method. CNCs fabricated via hydrolysis show rod-like morphology with an average length of 286 ± 31 nm and diameter of 49 ± 5 nm (aspect ratio ~6) **Figure 5.1a**.

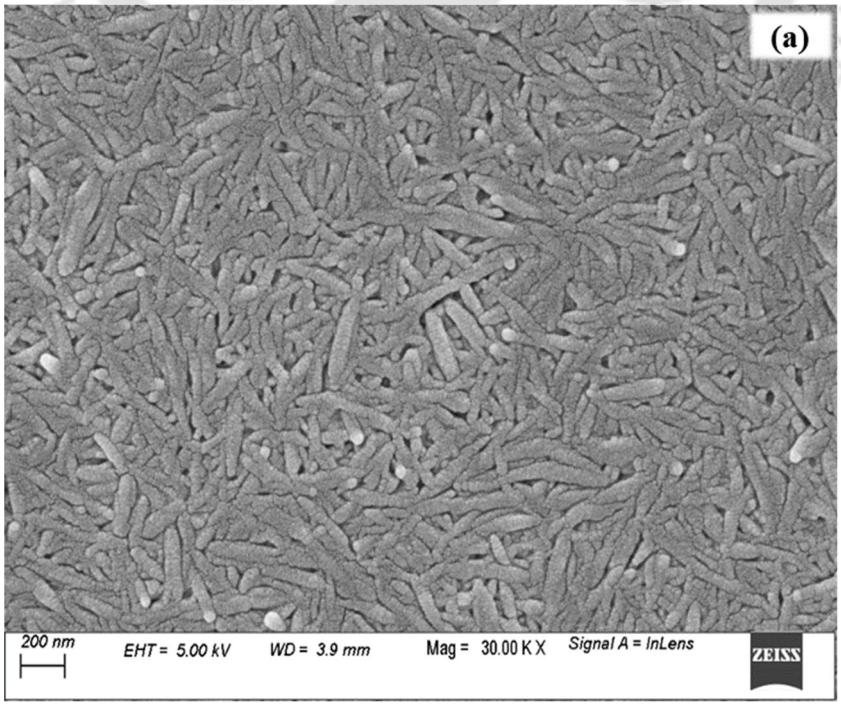

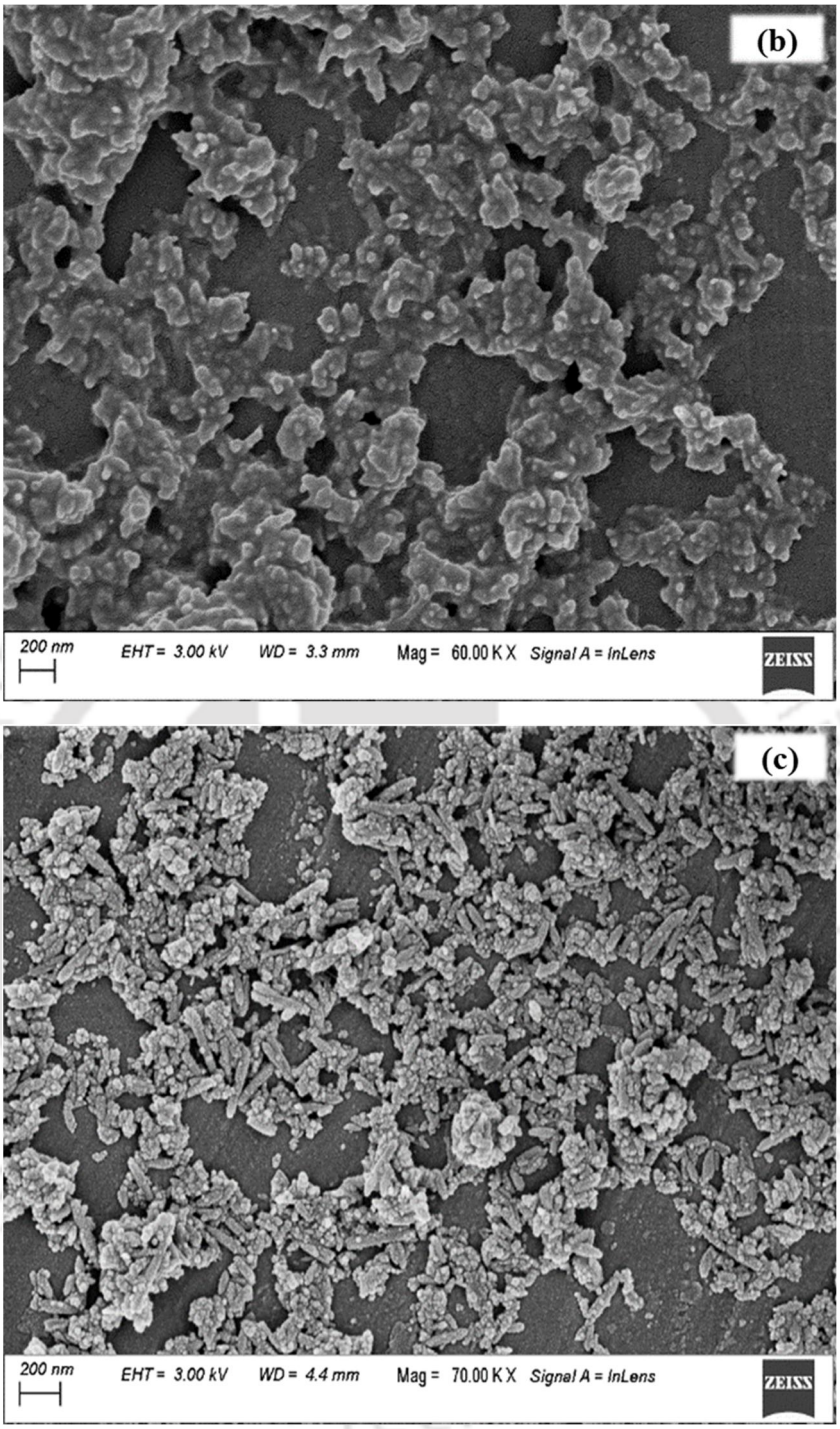

Figure 5.1: FESEM image of (a) CNC (b) Fe_3O_4 nanoparticles (c) FeCNC

Similarly, **Figure 5.1b** shows the spherical iron nanoparticles prepared by the co-precipitation method. These spherical iron nanoparticles decorated over the surface of rod-shaped CNC, which gives a rough rod-shaped morphology (**Figure 5.1c**). The size distribution of Fe_3O_4 particles is ~15−30 nm, which precipitated over the surface of CNC.

The prepared FeCNCs have a new dimension with an average length of 336 ± 60 nm and diameter of 61 ± 6 nm compared to those of CNCs. The precipitation of Fe_3O_4 nanoparticles over the surface of CNC to form FeCNCs results in a change in the dimensions of FeCNCs, which results in a change in the aspect ratio (~5). The interaction of Fe_3O_4 deposited over the surface of CNC is very strong and remains attached even after intense sonication during dispersion during sample preparation for FESEM.

5.2.1.2 *XRD Analysis of CNC and FeCNC*

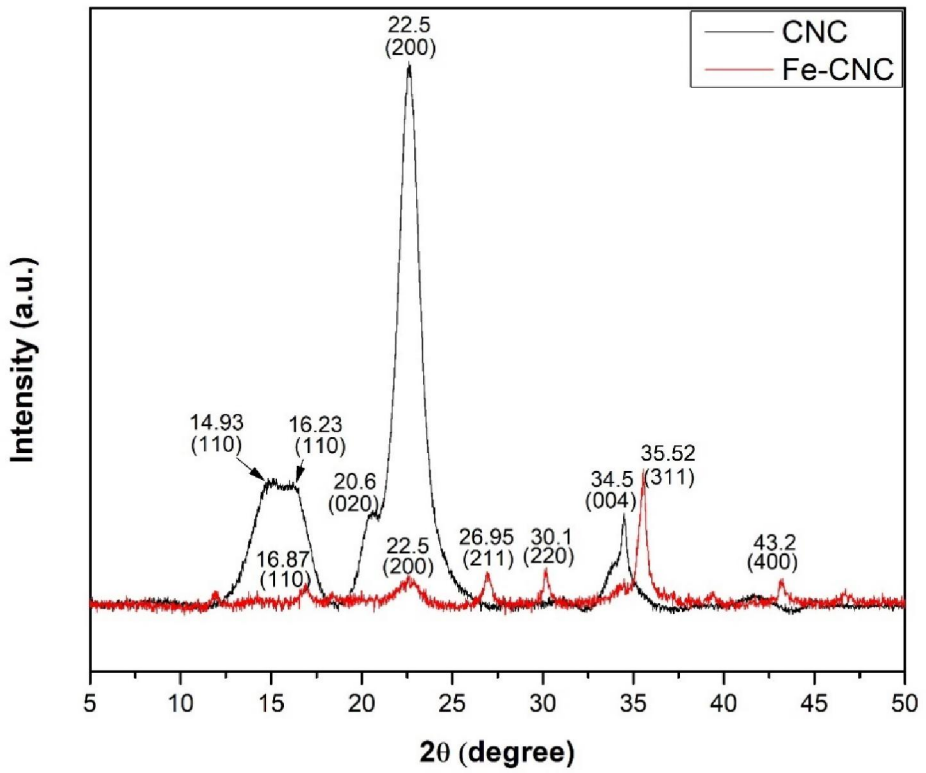

Figure 5.2: XRD diffractogram for CNCs and FeCNC

As seen in **Figure 5.2**, the XRD diffractogram for the CNCs plot shows a peak at 2θ = 14.62°, 16.35°, 22.5°, 34.7° representing the crystallographic planes $(1\bar{1}0)$, (110), (002) and (004), which represent the typical cellulose-I structure. The peak at 20.40° is a characteristic of crystals with a miller index (021) in cellulose type I polymorph [322]. In the XRD diffractogram of FeCNC, new peaks were seen at 2θ = 26.95°, 30.1°, 35.52°, 43.2°, which corresponds to the crystallographic plane (211), (220), (311), (400)

respectively of Fe_3O_4 nanoparticles. The peak at 2θ = 22.5° corresponds to the (002) lattice plane of cellulose I, which confirms the presence of the crystalline CNCs in the system. The peak at 2θ = 16.23° shows a slight shift to the new position of 2θ = 16.87° also corresponds to crystallographic planes (110) of CNCs.

5.2.1.3 *XPS Analysis of CNC and FeCNC*

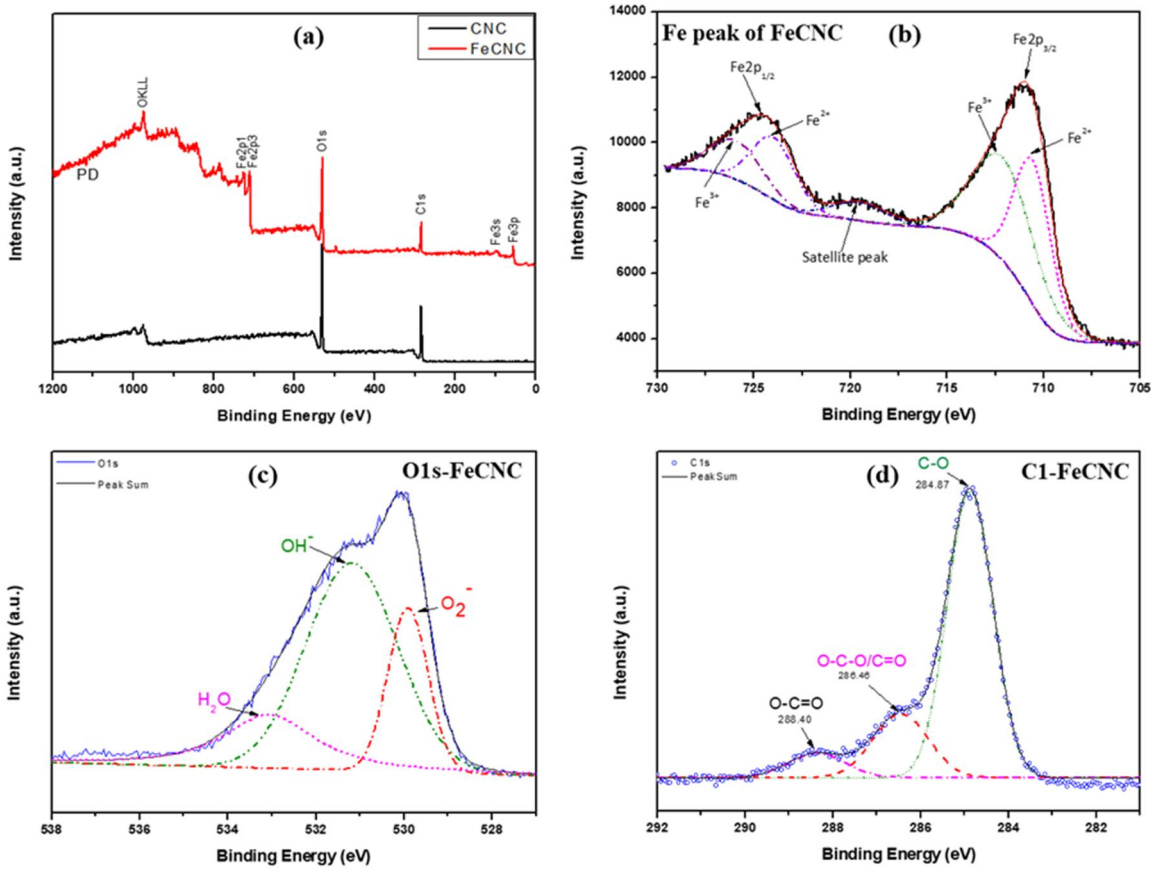

Figure 5.3: (a) Broad XPS spectra of CNC and FeCNC (b) Fe 2p spectra of FeCNC (c) O1s spectra of FeCNC and (d) C1s spectra of FeCNC

CNC and FeCNC were characterized by XPS, and the results are displayed in **Figure 5.3.** Broad spectra of CNC and FeCNC are presented in **Figure 5.3a,** which proves the presence of three elements C, O and Fe, where Fe is exclusively present in the spectra of FeCNC. The Fe 2p peak of the FeCNC was split into five peaks, as shown in **Figure 5.3b.** The two peaks positioned at 710.7 eV and 723.9 eV correspond to the peaks of Fe^{2+} species of $2p_{3/2}$

and $2p_{1/2,}$ respectively. Whereas 712.5 eV and 726.1 eV correspond to the peaks of Fe^{3+} species representing $2p_{3/2}$ and $2p_{1/2}$. Peak 719.4 eV is attributed to a satellite peak, which indicates the formation of Fe_3O_4 nanoparticles over the surface of CNCs. The O1s spectrum of FeCNC is represented in **Figure 5.3c,** which was also deconvoluted into three peaks, 530.2 eV, 531.3 eV and 533.3 eV. 530.2 eV represents the oxygen anion (O^{2-}) present in Fe_3O_4, and 531.3 eV corresponds to hydroxide (OH^-) over the surface of FeCNC due to the presence of metal oxides. Whereas the peak 533.3 eV corresponds to the physically adsorbed H_2O [323–328]. **Figure 5.3d** depicted C1s spectra of FeCNCs showing three peaks at 288.40 eV, 286.46 eV and 284.87 eV representing O–C=O, O–C–O/C=O and C–O species, respectively [294].

5.2.1.4 *TGA Analysis of CNC and FeCNC*

The thermal behaviour of CNCs and FeCNCs was determined using TGA, TG and derivative thermo gravimetric (DTG) curves are shown in **Figure 5.3**. The thermogram shows that there is a slight degradation of CNCs till 100 °C, which is due to the removal of moisture and volatile components initially present in the CNCs. After that, another degradation profile is observed till 300 °C, also representing the removal of moisture and sulphate groups present over the surface of CNCs imparted during sulphuric acid hydrolysis, and ~10% weight loss occurs in this range. The next stage of degradation is ~300−400 °C, which is due to the degradation of cellulose, where the cellulose polymer chains start to break down. This results in a significant drop in weight, and ~90% of weight loss occurs in this region. And finally, the CNCs get completely decomposed at 650 °C, leaving behind no residue. The onset degradation temperature and the temperature at the maximum weight loss of CNC occurred at ~358.66 °C and ~383.5 °C, respectively.

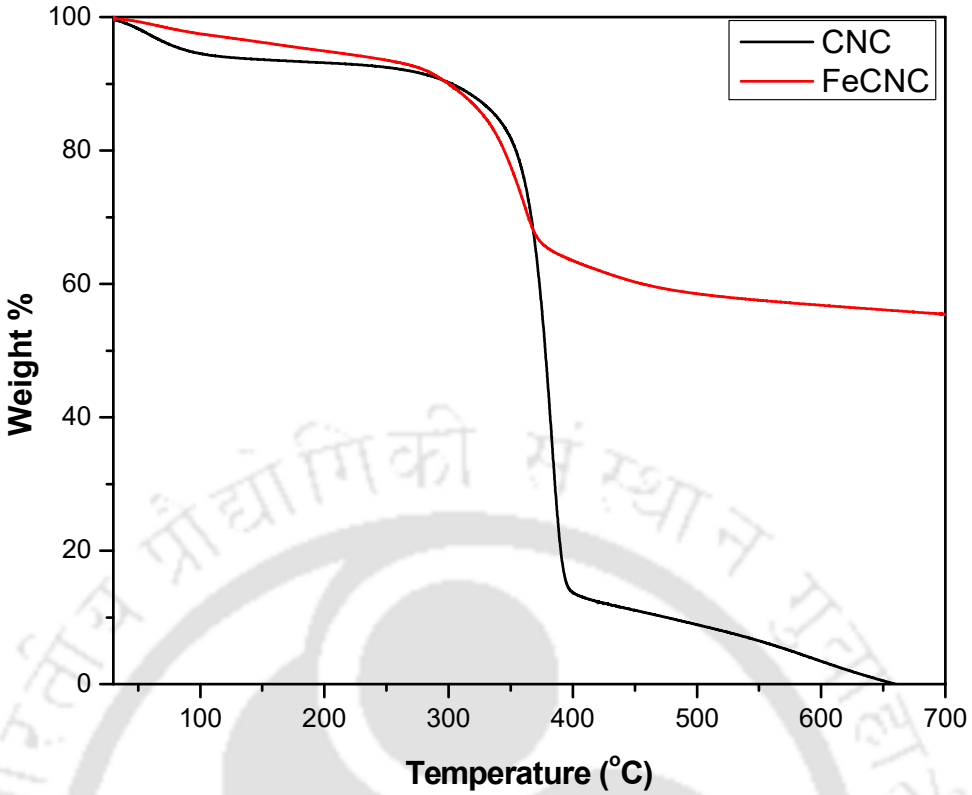

Figure 5.4: TGA profiles for the FeCNCs (red colour) and CNCs (black colour), respectively

On the contrary, FeCNCs contain both CNC and Fe_3O_4 nanoparticles. The presence of these iron nanoparticles can influence the thermal behaviour of the CNC. The initial weight loss trend is similar due to the removal of moisture and volatile components, as seen in CNCs. Iron nanoparticles are known for its high thermal stability, and the presence of iron nanoparticles over the surface of CNC can enhance the overall thermal stability. FeCNCs showed high thermal stability as compared to pristine CNCs, with ~10 % weight loss up to 300 °C and 25 % weight loss in the temperature range of 300−500 °C. The onset degradation temperature was found to be ~325 °C, and maximum weight loss occurs at ~362 °C. FeCNCs showed higher thermal stability as compared to the incorporation of Fe_3O_4 nanoparticles with the hydroxyl groups of CNCs. The difference in the weight percentage at ~500 °C was used to calculate the amount of Fe_3O_4 nanoparticles deposited

over the surface of CNC, and it was found that ~50 wt % of the Fe_3O_4 nanoparticles were on the CNC surface.

5.2.1.5 *Energy dispersive X-ray spectroscopy (EDX) Analysis of FeCNC*

For confirmation of the elemental composition and the compositional analysis of the fabricated FeCNC, EDX technique was used. **Figure 5.4** shows the elemental mapping of FeCNC. It also provides a quantitative assessment of the elements present in FeCNC, and it confirms the presence of iron (Fe), oxygen (O), and carbon (C) in the FeCNCs.

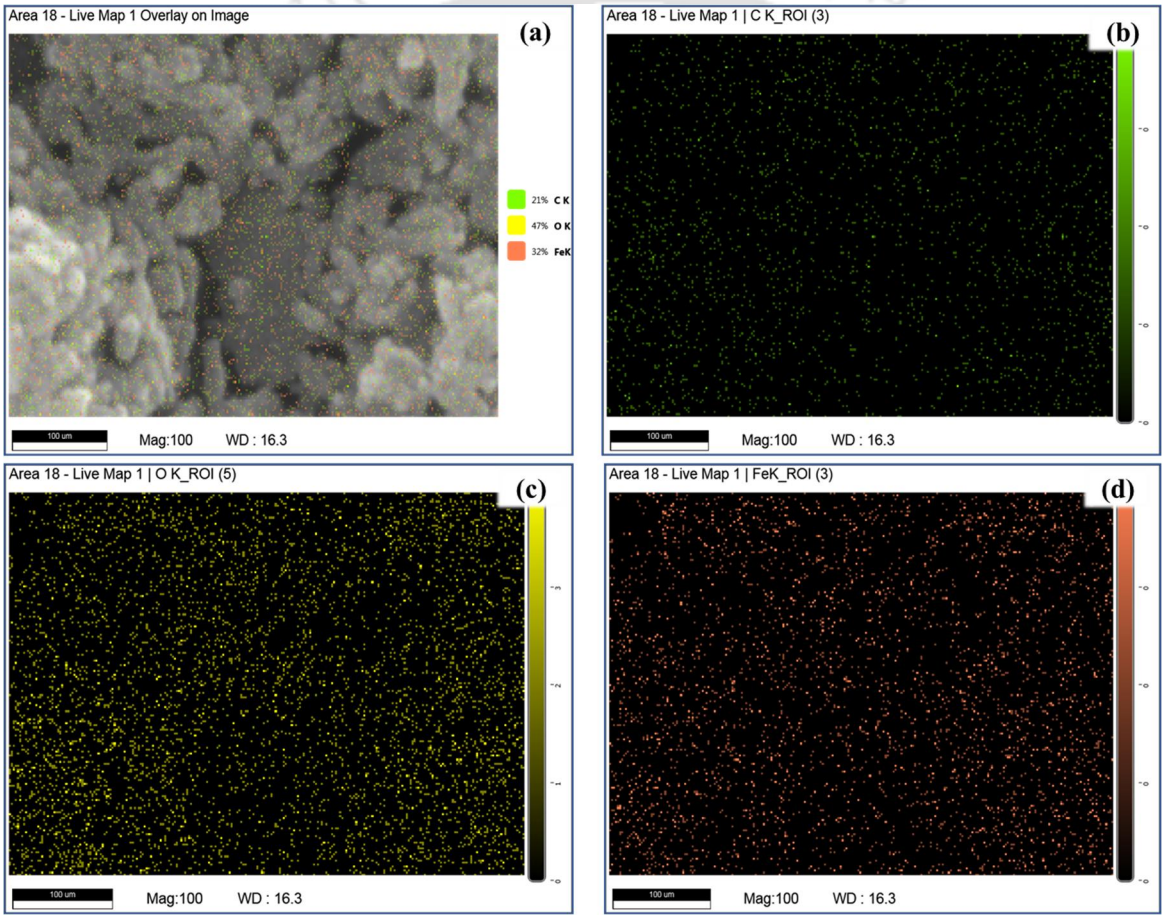

Figure 5.5: Elemental mapping of FeCNC (a) overlay on the image where elemental mapping was carried out (b) C (c) O and (d) Fe

It is noteworthy to mention that EDX confirmed the presence of both iron & oxygen in nanoparticles. The average weight percentages obtained from EDX were 47.2 ± 1.4 % of Fe, 34.2 ± 0.7 % of O and 18.6 ± 0.7 % of C, which reflect the mass of each element in

FeCNC relative to the total mass. The atomic percentages obtained from EDX quantification were 18.7 ± 0.9 %. 47.1 ± 0.2%, 34.2 ± 0.7 % of Fe, O and C indicate the number of atoms of each element relative to the total number of atoms. This information helped in understanding the overall composition of the FeCNCs. The wt% of Fe content (47.2 ± 1.4 %) is consistent with the TGA studies (~50%), which corresponds to the Fe_3O_4 nanoparticles that are adsorbed onto the surface of CNCs. Thus, the presence of iron nanoparticles on the surface of CNCs opens up possibilities for applications where magnetic properties are advantageous.

5.2.1.6 *VSM of FeCNCs*

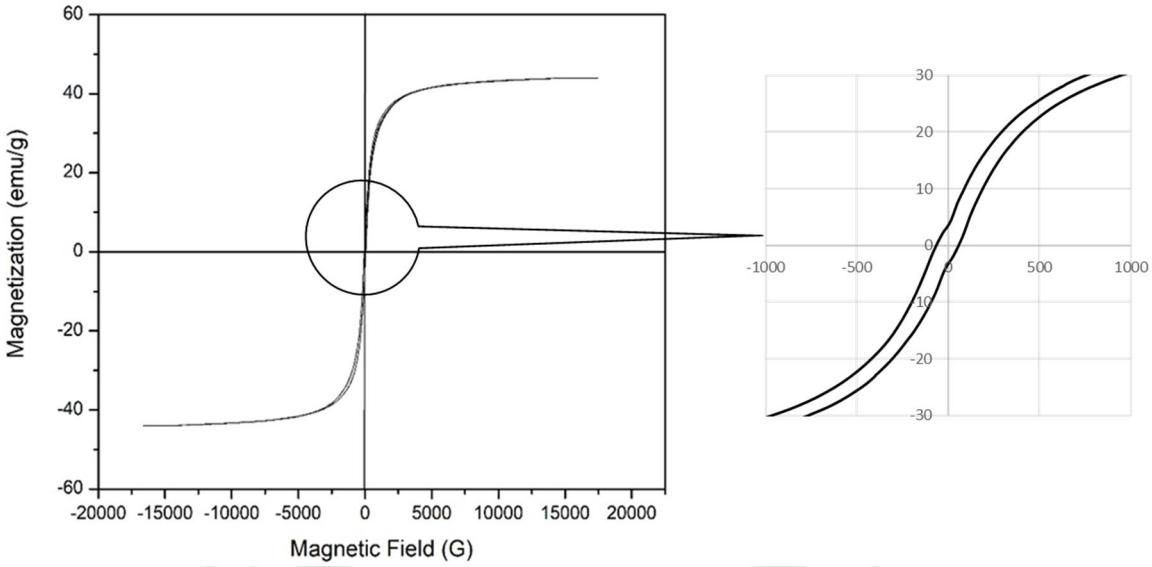

Figure 5.6: Magnetic hysteresis loop for fabricated FeCNCs obtained from VSM (at 298 K)

Deposition of Fe_3O_4 nanoparticles over the surface led to the modification of the CNC surface. The presence of these Fe_3O_4 nanoparticles over the CNC surface results in magneto-responsive behaviour. The magnetic properties of these prepared FeCNCs were evaluated using a vibrating sample magnetometer (VSM) at 298 K. In the hysteresis loops of the FeCNCs shown in **Figure 5.6**, the magnetization reduces from a plateau state to zero

on the removal of the magnetic field. The curve also showed low coercivity, having a hysteresis loop. This behaviour signifies that the prepared FeCNC particles are ferromagnetic due to these Fe_3O_4 nanoparticles. The saturation magnetization of FeCNC obtained is ~44.01 emu/g, which is almost similar to the previously reported value [329], and Fe_3O_4 have a magnetization saturation value of 91.57 emu/g [330]. The formation of ferromagnetic FeCNCs due to the deposition of Fe_3O_4 particles on bioderived material can have a potential application in magneto-responsive membranes for the removal of different impurities from wastewater.

5.2.2 Characterization of Membrane

5.2.2.1 *Morphology of Composite Membrane*

The PVDF and PVDF/CNC membrane surface and fractured cross-sectional surface were observed under a FESEM, and the effect of FeCNC on PVDF membranes was observed. All membrane surface shows a porous structure; however, pristane PVDF membrane shows a less porous surface as compared to the membrane with PVDF/FeCNC membrane. The pores are also well distributed over the surface, as shown in **Figure 5.7 (a)** and **(b)**.

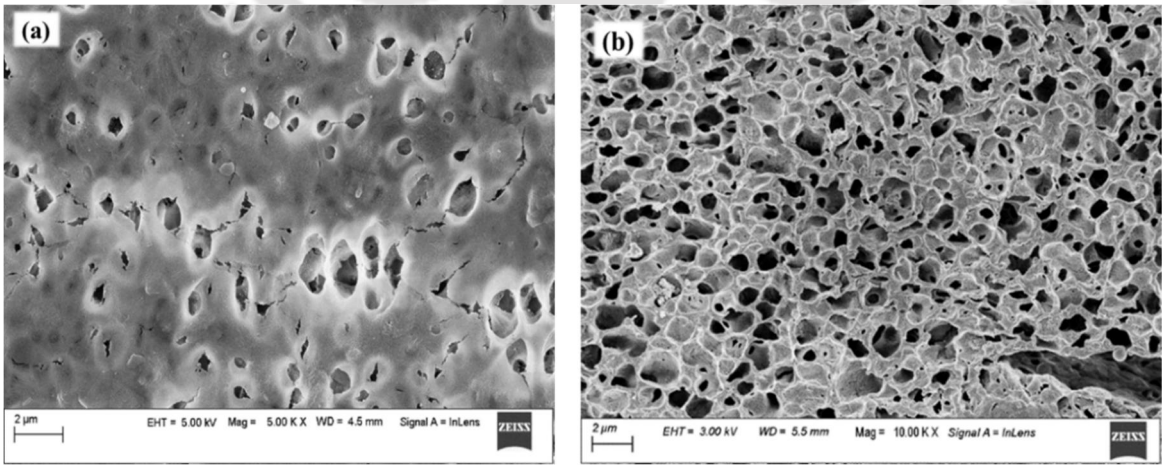

Figure 5.7: Surface morphology of (a) PVDF and (b) PVDF/FeCNC membrane

While observing the cross-sectional structure, a typical asymmetrical structure was observed for all membranes; a very thin skin layer, finger-like channels, and support

sponge-like dense layer. The finger-like pores are larger in the PVDF/FeCNC composite membrane (**Figure 5.8b)** as compared to that of the pristine PVDF membrane (**Figure 5.8a)**, which is due to the spreading of water at a faster rate into the casting solution due to the presence of hydrophilic FeCNCs. The presence of FeCNCs also accelerates the process of phase separation and, thus, the generation of pores. The length of the finger-like also increased in the PVDF/FeCNC composite membrane in comparison to the neat PVDF membrane and even extended to the bottom, resulting in more interconnectivity and high porosity. The addition of FeCNCs initiated thermodynamic instability of the polymer solution and improved gelation and thus formed a more prominent finger-like structure, which improves the performance of the membrane [331]. The presence of hydrophilic FeCNCs enhances the exchange of solvent and non-solvent during phase inversion; the affinity of FeCNCs towards water accelerates the solvent exchange in the casting solution.

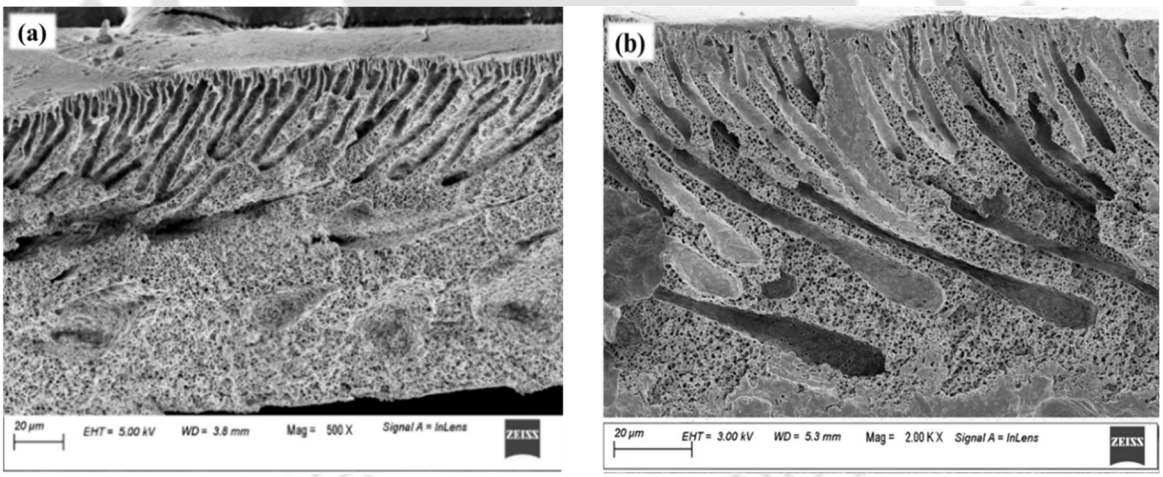

Figure 5.8: Cross-sectional image of (a) PVDF and (b) PVDF/FeCNC membrane

5.2.2.2 *Hydrophilicity of the Membranes: Contact Angle Measurements*

Contact angle measurement was carried out in order to evaluate the hydrophilicity of the PVDF/FeCNC membrane, which mainly depends on surface roughness, membrane porosity and composition. The measurement was done immediately after placing the DI water drop on the surface of the membrane. A higher contact angle indicates the membrane

is hydrophilic, and a lower contact angle indicates the membrane is hydrophilic. **Figure 5.9** depicts the contact angle measurement results of pristine PVDF (M0) membrane and PVDF/FeCNC membrane; it is observed that the M0 membrane showed the highest contact angle of 85.7° indicating that it is more hydrophobic as compared to the PVDF/FeCNC membrane.

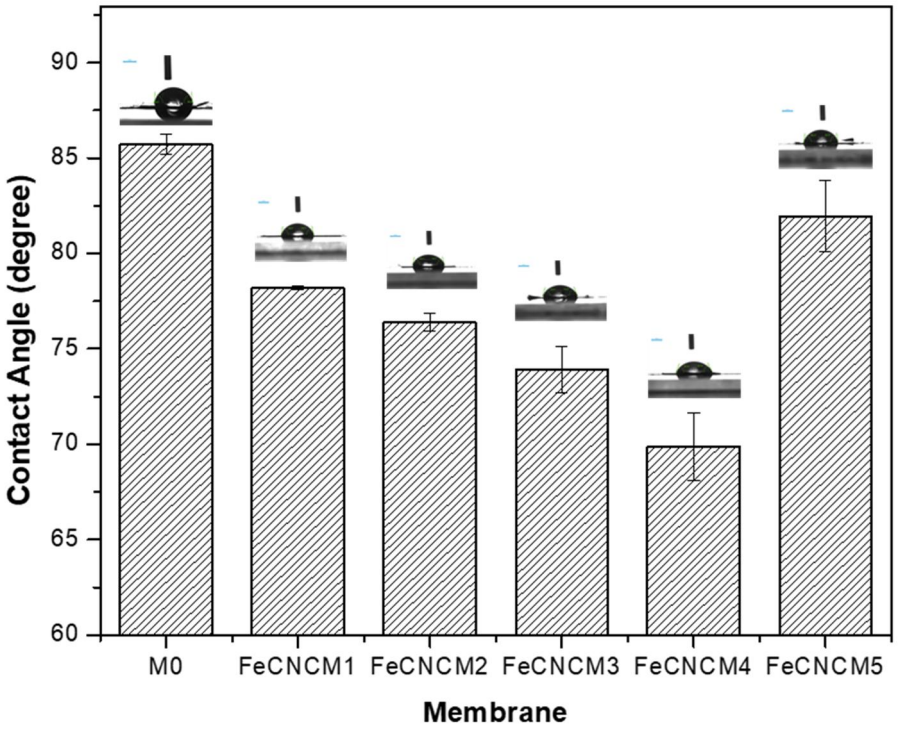

Figure 5.9: Water contact angle of PVDF and PVDF/FeCNC membranes

The WCA decreases with increases in the concentration of FeCNC in the PVDF membrane, indicating the increase of the surface hydrophilicity of membranes after blending FeCNC in the casting solution. The contact angle decreases from 85.7° to 69.9° with an increase in FeCNC concentration from 0.5% to 2%. PVDF is inherently hydrophobic due to its fluorinated polymer structure. Incorporating CNCs into the PVDF alters its intrinsic hydrophobic surface, as CNCs have a hydrophilic character. When FeCNCs are incorporated into the PVDF membrane, they bring these hydrophilic functional groups with them. This modification makes the membrane surface more hydrophilic compared to pristine PVDF. The decrease in water contact in the composite membrane results from the

addition of FeCNCs, imparting more hydrophilicity to the membrane surface due to the presence of hydrophilic −OH groups on the surface of FeCNCs and the attachment of Fe_3O_4 nanoparticles on the surface of CNCs. Thus, the presence of FeCNCs reduces the contact angle of the membrane, indicating that water will spread more readily on the membrane's surface. However, the addition of 3% FeCNC to the casting solution increases the contact angle to ~82°; the reason behind this is that higher concentrations of FeCNCs do not disperse uniformly in the solution and tend to agglomerate. The presence of these agglomeration nanoparticles imparts more roughness to the membrane surface, and in turn, the contact angle increases. FESEM image of FeCNC is shown in **Figure 5.10b,** which forms agglomeration on the surface of the membrane represented in **Figure 5.10a**. A high-resolution (zoomed) FESEM image (**Figure 5.10c**) of the membrane surface more clearly shows the agglomerated FeCNC on the surface of the membrane.

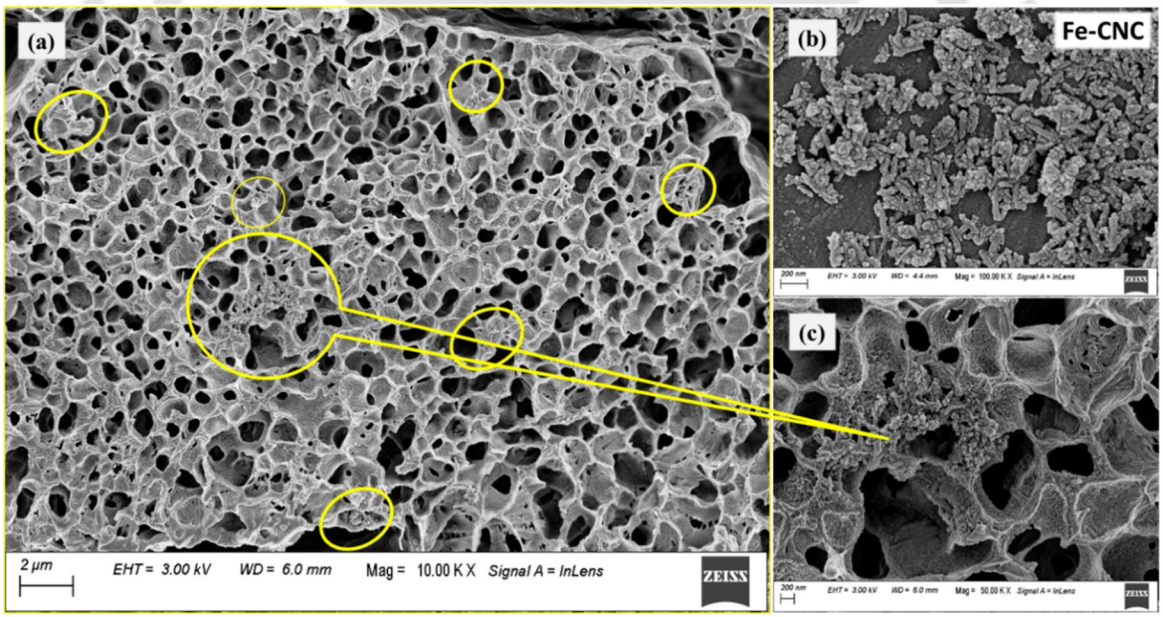

Figure 5.10: Surface morphology of a membrane containing FeCNC at higher concentration, (b) rod-shaped image of FeCNC and (c) high-resolution FESEM surface image of membrane showing the agglomeration of FeCNC on the membrane

5.2.2.3 *Equilibrium Water Content (EWC), Porosity and Pore Size*

The hydrophilic/hydrophobic properties and permeability of membranes are also indirectly linked to the determined by the water content. As compared to pristine PVDF membrane, the water content is increased due to the hydrophilic character of FeCNC with abundant free hydroxyl groups. The water content increased from 60 to ~71% when FeCNC concentration increased from 0.5 to 2 wt% in the casting solution, as seen in **Figure 5.11a**. This indicates the membrane formed with FeCNCs is more hydrophilic. The pore size was calculated from the surface FESEM image using ImageJ software, and it was found that surface pore size for the PVDF/FeCNC membranes ranges from 0.78 to .23 µm, which lies in the range of microfiltration. The porosity of the membranes was calculated by gravimetric method and shown in **Figure 5.11b**. It was observed that the porosity for PVDF and PVDF/FeCNC membrane was ~53 to 83%.

The highest porosity was observed in the case of FeCNCM5, which corroborates with the improvement of pure water flux (PWF). However, FeCNCM5 is less hydrophilic due to the agglomeration of FeCNCs in the casting solution. This increase in porosity can be explained by the fact that FeCNC is a hydrophilic material containing abundant −OH on the surface, which enhances the diffusion rate of solvent and nonsolvent (water) and results in the formation of high porosity. A comparison of contact angle and porosity obtained in this work with other available literature is shown in **Table 5.1**.

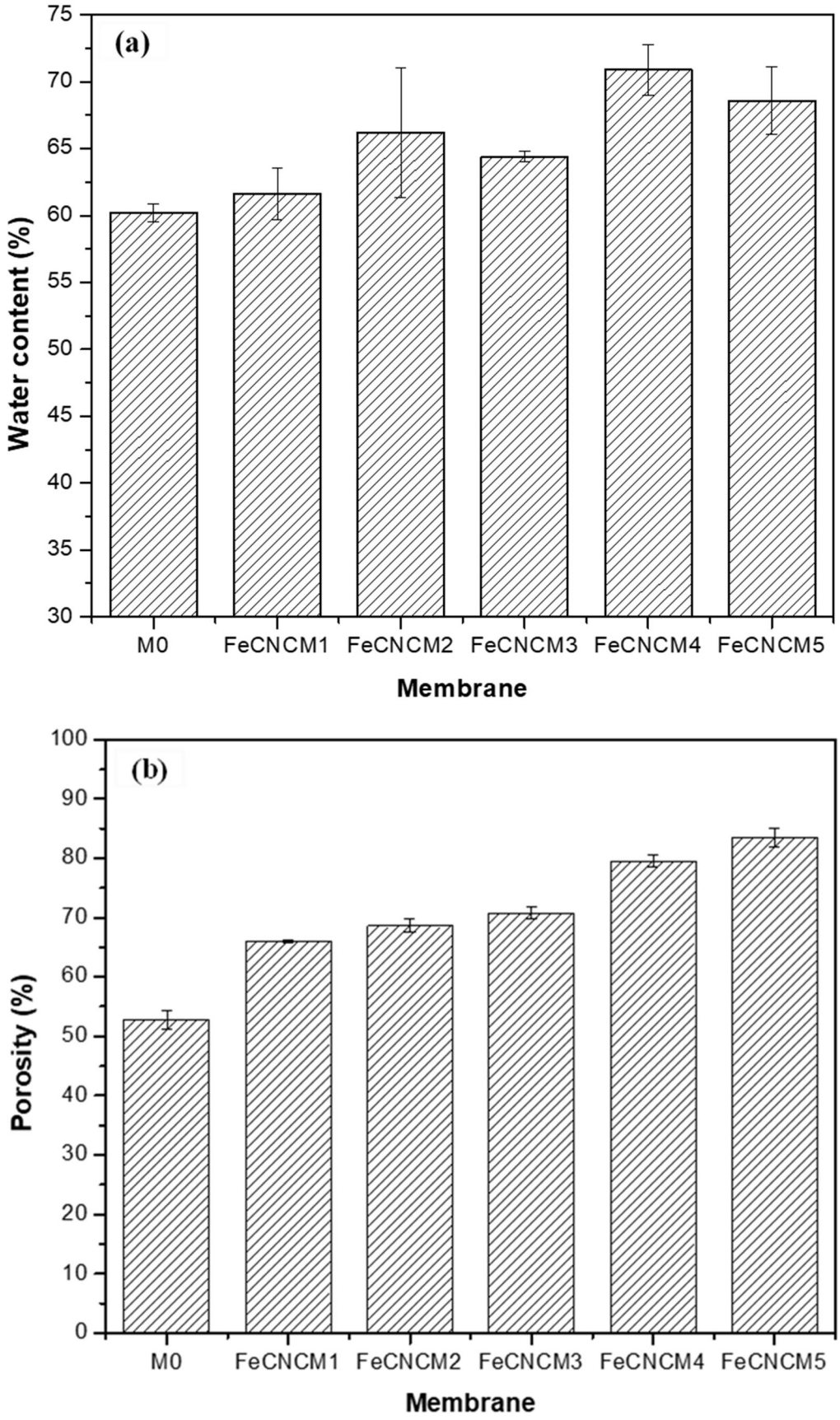

Figure 5.11: (a) Water content and (b) porosity of the composite membranes

Table 5.1: Comparison of contact angle and porosity with other reported works for PVDF membranes used for oily-wastewater separation

Composition	Contact Angle (°)	Porosity (%)	References
PVDF/CNC/CNT (2 wt%)	46	79	[332]
PVDF/CNF nanocomposite (5 wt%)	--	78	[96]
PVDF/MWCNT (1%)	38	89.36	[333]
PVDF/PSNT (silica nanotubes)	43.2	48	[334]
PVDF (different solvent)	70-75	60-80	[335]
PVDF/PC (20%)	71	35	[336]
PVDF/FeCNC (2 wt%)	**~70**	**~83**	**This work**

5.2.3 Performance Evaluation of the Fabricated Membrane

5.2.3.1 *Pure Water Flux (PWF) of PVDF/CNC Membrane and PVDF/FeCNC Membrane*

The prepared membranes were tested to find the PWF in order to evaluate its filtration performance. Initially, the testing was carried out in a dead-end filtration setup, for 2 h followed by testing the membrane in a cross-flow continuous membrane testing setup. It is evident from the dead-end filtration test results that an increase in the concentration of nanoparticles in the membrane results in an improvement of flux. It was observed that the highest PWF, ~34 L/m^{2}h was obtained for M3 with CNC content of 3 wt%. Comparing the performance of PVDF/FeCNC membranes with that of PVDF/CNC membranes, the flux obtained is significantly higher. The introduction of iron modified CNC into the membrane matrix results in high flux values. The highest average flux was obtained in the case of FeCNCM5 ~188 L/m^{2}h, which is significantly higher than M0, having a flux of ~18 L/m^{2}h (**Figure 5.12a & b**). Several factors that contributed to the improvement in flux of

PVDF/FeCNC membrane includes the increase in membrane porosity and hydrophilicity. The addition of FeCNC not only increase the pores within the membrane, it also imparts hydrophilicity to the membrane due to the inherent hydrophilic nature of CNCs. This facilitates better water flow through the pores of the membrane resulting in improved flux which is prominent in case of FeCNCM5. Thus, these results also signify the importance of incorporating FeCNC in the PVDF matrix for improvement in membrane properties. It is also noteworthy to mention that the flux of all the PVDF/FeCNC membranes are significantly higher than the corresponding PVDF/CNC membrane containing equal wt% of CNC. Thus, modified CNC with iron nanoparticles can be a better additive than unmodified CNC, for improving the performance of the membrane. A comparison of PWF for different membranes is shown in **Figure 5.13**. The same amount of added nanomaterials shows that the PWF of a PVDF/FeCNC membrane was greater than that of a PVDF/CNC membrane. Thus, a PVDF membrane incorporated with FeCNCs exhibits improved filtration performance, as it can resist the adhesion of hydrophobic contaminants, leading to longer filtration runs and more efficient separation.

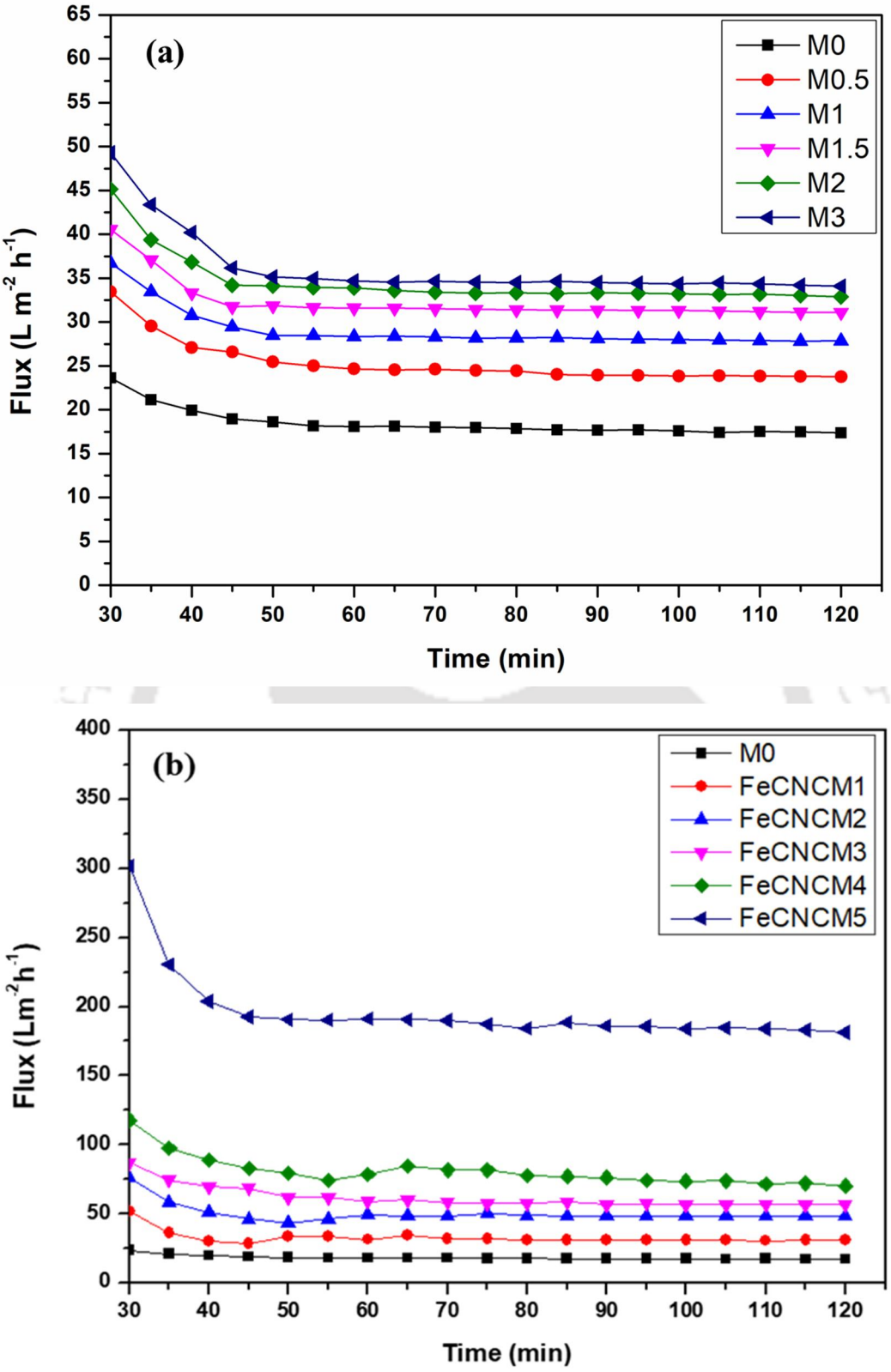

Figure 5.12: Comparison of PWF through (a) PVDF/CNC membranes and (b) PVDF/FeCNC membranes

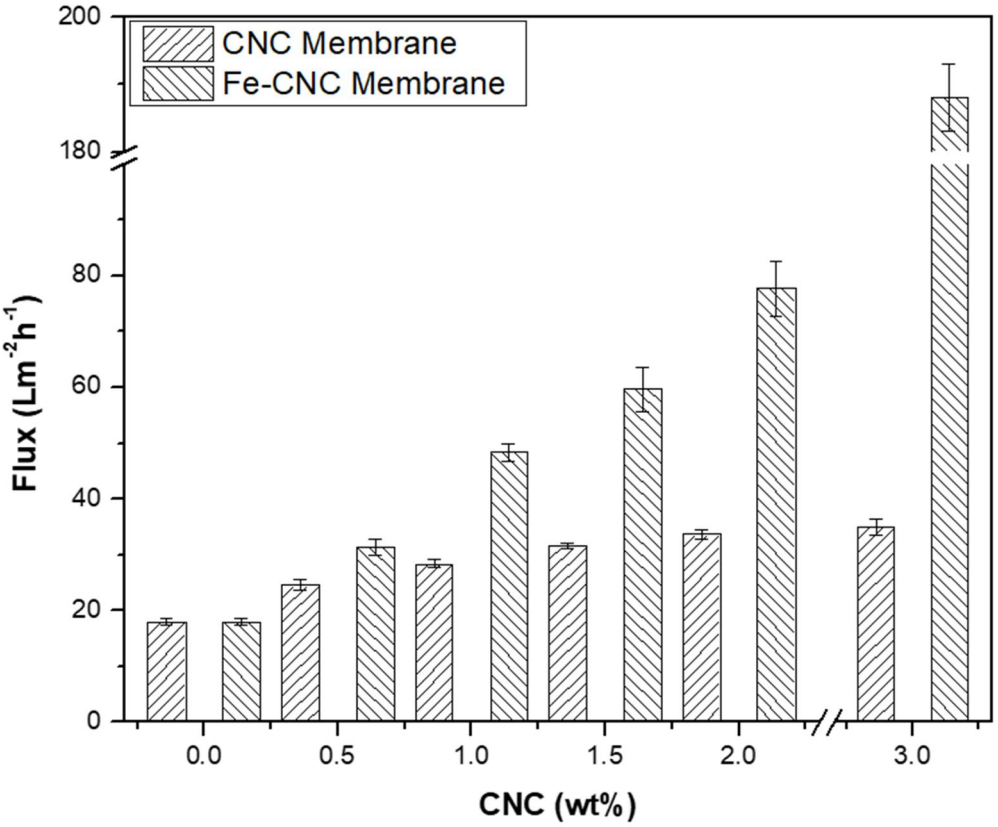

Figure 5.13: Comparison of PWF for PVDF/CNC and PVDF/FeCNC membranes

5.2.3.2 *Crude Oil-Water Emulsion Separation by PVDF/FeCNC Membrane*

After carrying out the different characterization and PWF of all the membranes, it was found that PVDF/FeCNC membranes have better performance than PVDF/CNC membranes. Hence, PVDF/FeCNC was used for crude oil-water emulsion separation in a dead-end filtration test setup. A similar trend of increasing flux has been observed with an increase in FeCNC concentration (**Figure 5.14)**. The highest flux obtained during oil-water separation is ~70 L/m^{2}h for FeCNCM4.

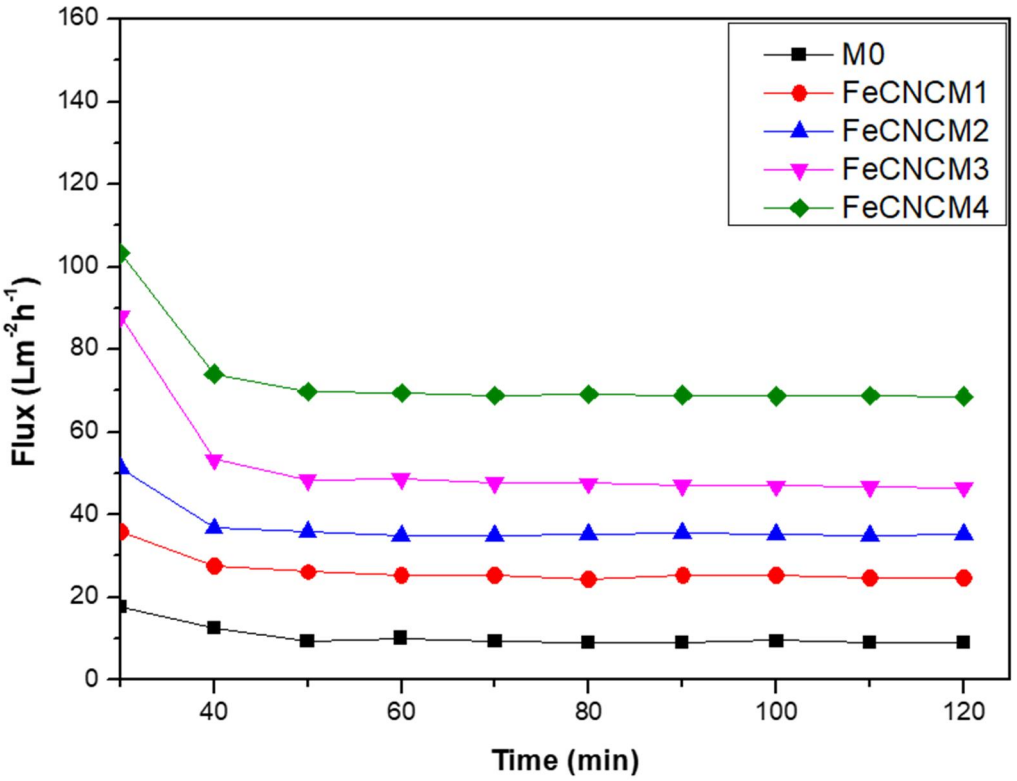

Figure 5.14: Water flux for PVDF/FeCNC membranes during crude oil-water emulsion separation in dead-end membrane test setup

A similar oil-water separation experiment was carried out for PVDF/FeCNC membranes in a cross-flow membrane test setup continuously for 48 h. Initially, the flux measurements were taken every 10 min, represented in **Figure 5.15a**, followed by measurements after every 2 h for the initial 12 h, and then it was measured after every 6 h for 48 h, shown in **Figure 5.15b** & **Figure 5.15c** respectively. A stable flux was obtained for an initial 12 h (the highest flux obtained is 80 to 70 L/m^{2}h for 12 h), and a slight decrease in flux was observed when measured for 48 h. A comparison of average water flux for dead-end and cross-flow filtration is shown in **Figure 5.15d**.

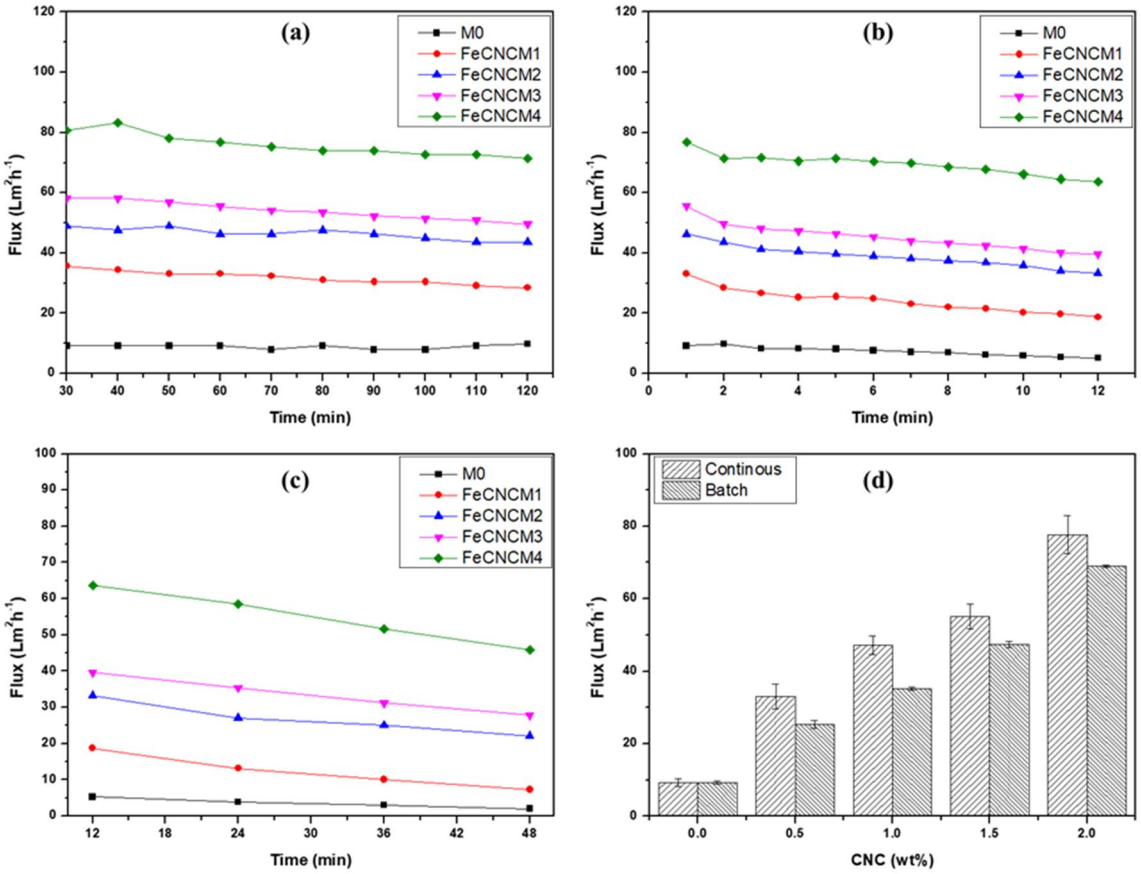

Figure 5.15: Water flux during oil-water separation for PVDF/FeCNC membrane measured in cross-flow membrane testing setup (a) for initial 2 h reading taken at 30 min interval (b) for next 12 h reading taken at 1 h interval (c) from 12 h to 48 h reading taken at 12 h interval (d) comparison of average water flux for dead-end and cross-flow filtration

5.2.3.3 *Crude Oil Rejection, Flux Recovery Ratio (FRR) and Flux Decline Ratio*

The efficacy of the membrane for crude oil rejection was evaluated by filtering crude oil in water emulsion with an initial crude oil concentration of 1000 mg/L. A UV-visible spectrophotometer was used to measure the crude oil concentration in the feed and permeate, which relied on a calibration curve (shown in **Figure 5.16b**) prepared by diluting the stock solution to 18 mg/l, 12 mg/l, 9 mg/l, 4 mg/l, 1 mg/l and 0.5 mg/l times (absorption spectra represented in **Figure 5.16a**. Finally, equations 2.7 and 2.8,

respectively, were used to obtain the crude oil rejection and flux recovery ratio, respectively.

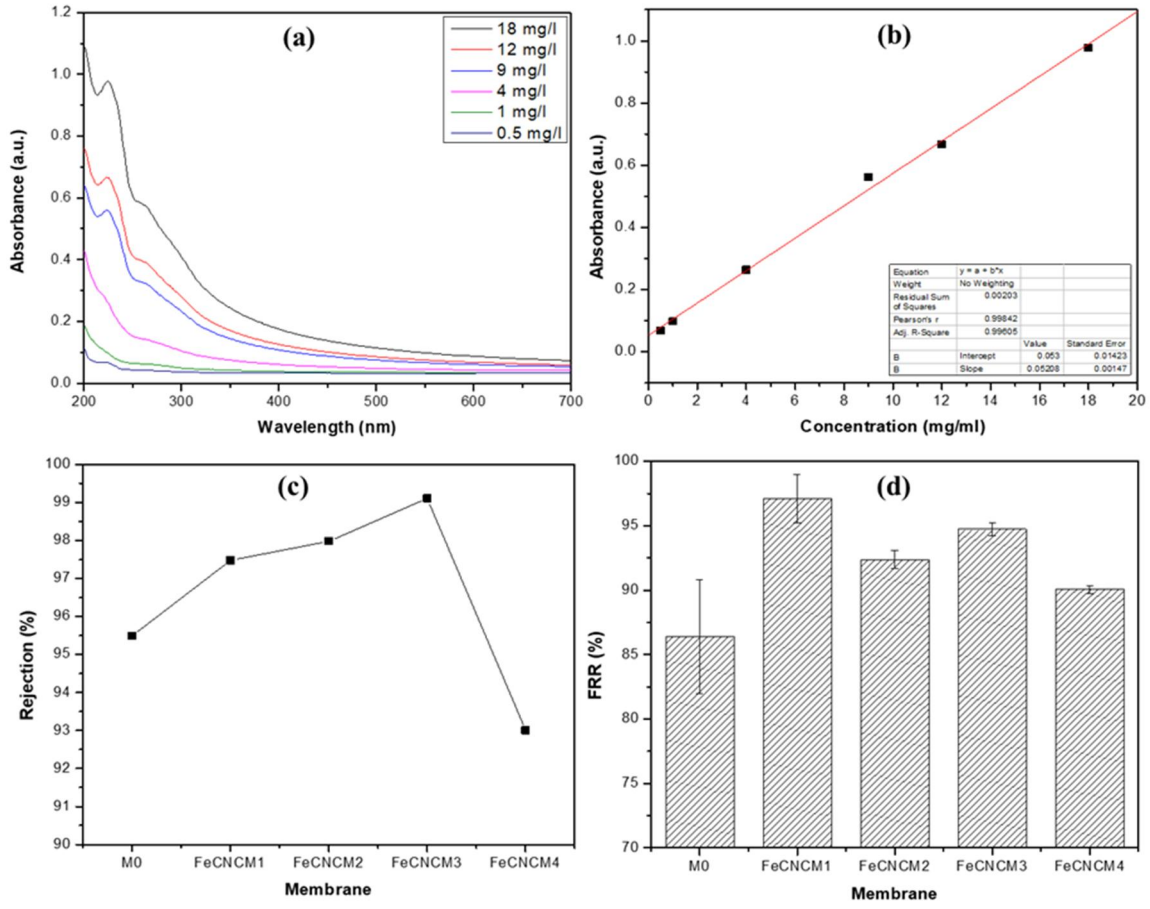

Figure 5.16: (a) UV-vis absorption spectra of crude oil emulsion with 18 mg/l, 12 mg/l, 9 mg/l, 4 mg/l, 1 mg/l and 0.5 mg/l (b) UV calibration curve for crude oil-water emulsion (c) crude oil rejection for different PVDF/FeCNC membrane (d) flux recovery ratio

As seen from **Figure 5.16c,** the crude oil rejection of the M0 membrane is ~95%, and it increases to ~99% for FeCNCM3. The rejection gradually increases with an increase in FeCNC concentration in the membrane from 0.5% to 1.5% and decreases to 93% in the case of FeCNCM4. Initially, the increase in rejection is due to the increase in hydrophilicity of the membrane. However, at higher concentrations of FeCNC, the decrease in rejection is mainly due to increases in the size of the pores, which allow more oil droplets to pass through the membrane. However, all the membrane shows oil rejection of more than 90%,

and all PVDF/ FeCNC membrane shows a higher FRR of ~90% (**Figure 5.17b**). A comparison of flux and oil rejection for PVDF membrane with other additives with the work is presented in **Table 5.2**.

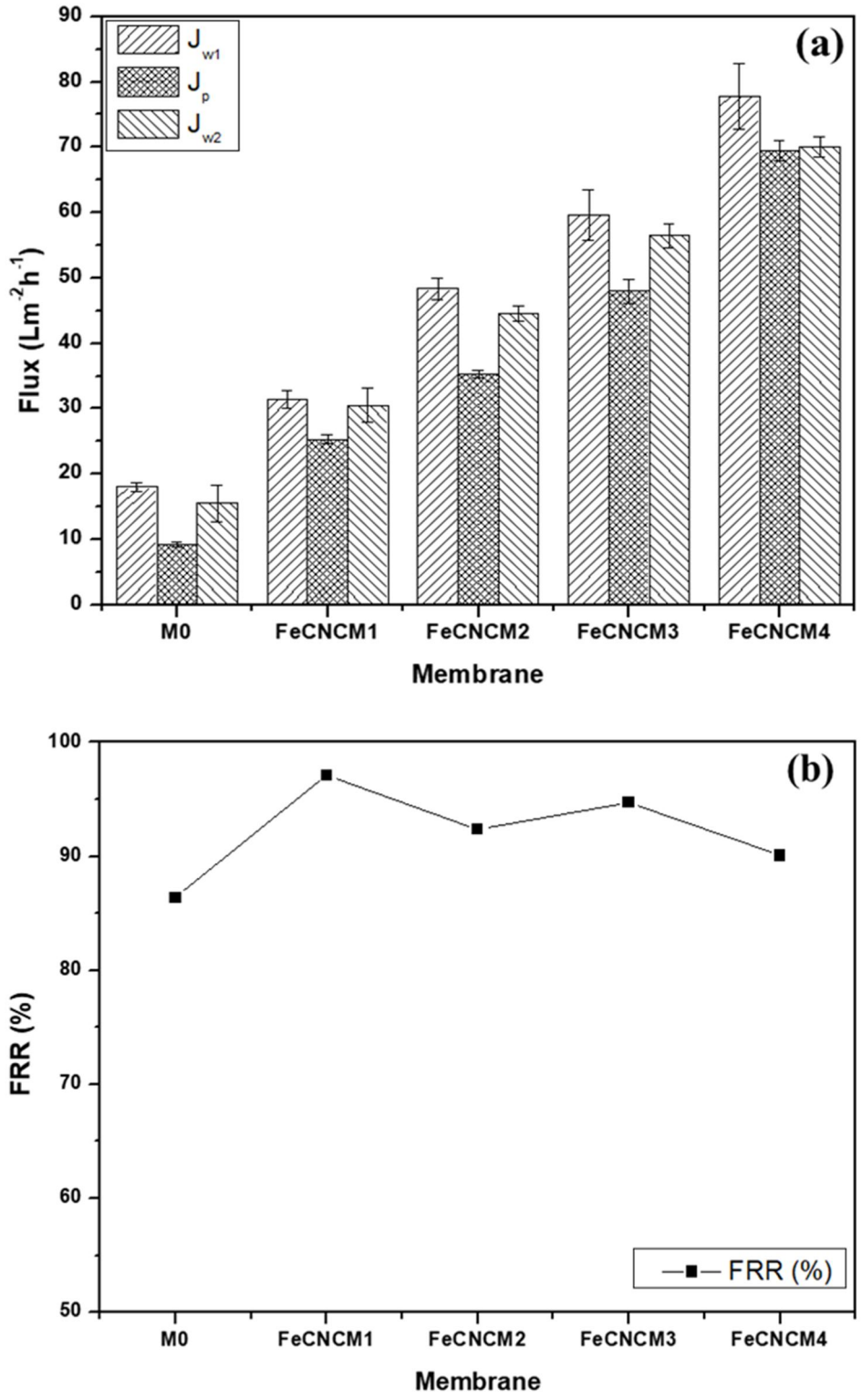

Figure 5.17: (a) Comparison of PWF and crude oil emulsion flux (b) water FRR

Table 5.2: Comparison with other reported works for PVDF membranes used for oily wastewater separation

Membrane	Pressure (kg/cm^2)	Flux (L/m^2h)	Rejection (%)	References
PVDF/CNC/CNT (2 wt%)	1	230.8	92	[332]
PVDF/MWCNT	1	683.17	99.89	[333]
PVDF/PSNT (silica nanotubes)	1	407	95.5	[334]
PVDF (different solvent)	1.5	92	97.4	[335]
PVDF/PC (20 wt%)	0.07	22.11	97.8	[336]
PVDF/TBC (3%)	2	60.5	99.5	[337]
PVDF	2	~60.5	94	[338]
PVDF-TiO_2/Al_2O_3	0.5-1.0	260	--	[339]
PVDF/FeCNC	**1**	**(2 wt%) 78 (3 wt%) 188**	**98.5**	**This work**

5.3 Summary

The chapter describes the advantages of incorporating FeCNCs into PVDF membranes and emphasizing their role in enhancing the performance of the PVDF membranes for water treatment and oil-water separation applications. The presence of FeCNCs accelerates the phase separation process during the formation of PVDF/FeCNC membrane, leading to the generation of well-defined pores in the membrane which leads to the improvement in performance of the membrane. The presence of FeCNCs within the PVDF matrix results in substantial enhancement in the membrane's permeation flux. Compared to pristane PVDF membrane, the oil removal capacity of, PVDF/CNC, and PVDF/FeCNC membranes is significantly higher. Furthermore, it was observed that the increase in concentration of

FeCNC concentration in the casting solution results in decrease in contact angle of the membranes. This reduction in the contact angle of the membrane, indicating an improvement in its hydrophilicity of the membrane, which plays a crucial role in oil-water separation. This improved hydrophilicity is likely due to the interaction between FeCNCs and water molecules, leading to a more open membrane structure and better water permeation. The results show that the PVDF/FeCNC membrane has a significantly higher PWF (77.75 L/m^2h with 2% FeCNC and 188.11 L/m^2h with 3% FeCNC) than the pristine PVDF membrane (18 L/m^2h) at a pressure of 1 kg/cm^2. This significant improvement in permeation flux makes the PVDF/FeCNC membrane a promising material for water treatment applications.

Chapter 6

Effect of Magnetic Field on PVDF-FeCNC during Membrane Formation and its Oil-Water Separation Performance

This chapter discusses about the fabrication of polyvinylidene fluoride (PVDF) nanocomposite membrane using self-synthesized magnetic cellulose nanocrystal (FeCNC) as an additive. The main motive is to study the effect of a magnetic field (350-450 gauss) applied during the coagulation process on the characteristics and performance of the membrane. The application of a magnetic field helps in the movement of these magnetic nanoparticles towards the direction of the applied magnetic field (to the surface). Thus improving the hydrophilic property of the membrane. The performance of the FeCNC-incorporated membrane was examined by measuring the pure water flux (PWF) and oil rejection capacity. EDX mapping results of the membrane indicate that FeCNCs migrate to the surface of the membrane when coagulated under a magnetic field. This migration of FeCNCs to the surface improves the hydrophilic property of the membrane and thus results in superior antifouling properties.

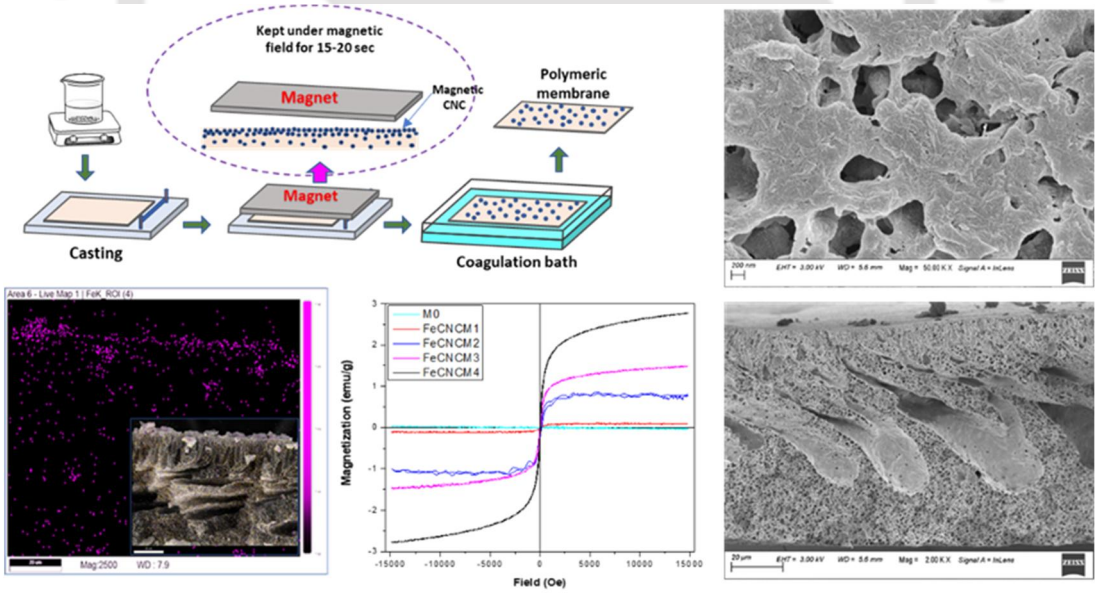

Research outputs of this chapter: "*Magnetic field assisted coagulation bath for preparation of PVDF/FeCNC membrane and its performance for oil-water separation*", ***Manuscript under preparation***

Patent: "*Aligned magnetic cellulose nanocrystal-based polymeric membrane for oil-water separation and purification of water*". *(Application No.: 202231052371).*

6.1 Introduction

To further improve the properties of the membrane, new and novel techniques are being employed for the fabrication of membranes. As discussed in Chapter 5, magnetic nanoparticles (mNPs) are being widely used in membrane fabrication due to their unique properties and good dispersal. mNPs such as FeO, Fe_2O_3, Fe_3O_4, and other metal oxides or nanohybrid materials like GO/iron oxide nanohybrids and metal oxide/SiO_2 are gaining considerable importance in membrane fabrication due to their superior chemical and mechanical properties. The addition of mNPs during membrane preparation can improve water flux, rejection, mechanical strength, water filtration efficiency, and fouling resistance. These properties can be further improved by tailoring the surface properties of the membrane by following a strategy to manipulate the distribution of mNPs on the surface. This can be achieved by applying a magnetic field during the membrane fabrication process. The applied magnetic field can help in increasing the stability of the mNPs and settling to the bottom of the solution during membrane casing. Further, it enhances the homogeneity and uniformity in the prepared membrane and forces the mNPs to migrate to the surface of the membrane. Moreover, the magnetic field applied during the process can affect the pore structure of the membrane, which results in changes in the permeability and selectivity of the membrane. Thus, using magnetic fields during membrane fabrication can improve the properties and enhance the performance of membranes. For instance, the addition of magnetic Fe_3O_4 nanoparticles by phase inversion method led to the preparation of a PSF–Fe_3O_4 composite membrane whose performance was evaluated under a magnetic field [154]. Also, the application of a magnetic field during the formation of Fe_3O_4/GO/PVDF membranes resulted in improved pure water flow, hydrophilicity, and antifouling characteristics [214]. Similarly, the use of $ZnFe_2O_4$/SiO_2 as mNPs during the fabrication of the polyethersulfone (PES) nanocomposite membrane by phase inversion

method under a magnetic field led to the enhancement of the hydrophilicity of the membrane surface. The magnetic treatment of the casting solution resulted in the orientation of the nano-fillers in the top layer of the membrane, which influenced the pure water flux, hydrophilicity, and antifouling properties of the fabricated membranes [215]. Hence, inspired by the use of Fe_3O_4 nanoparticles for the preparation of nanocomposite membrane herein, we discussed the use of Fe_3O_4/CNC nanohybrid material (designated as FeCNC) as an additive with polyvinylidene fluoride (PVDF) for membrane fabrication. PVDF/FeCNC were fabricated by phase inversion method under a magnetic field and thus able to migrate FeCNC to the top surface of the PVDF membrane. FeCNC has been added in different weight percentages in PVDF dope solution in the current study. The effect of the addition of different weight percentages of FeCNCs and its effect on the magnetic field-induced phase inversion was investigated. So far, there are no studies on the use of FeCNC mNPs in PVDF membrane fabrication and examining the influence of magnetic field-induced casting on the membrane structure, performance and antifouling behaviour. The prepared membranes were evaluated for different properties, including morphology, porosity, hydrophilicity, water flux, oil rejection and antifouling properties. The addition of FeCNCs has attracted more attention due to its excellent hydrophilicity; the hydrophilic nature facilitates the movement of water molecules through the membrane, enhancing the water flux and filtration efficiency. Additionally, it also provides a high surface area, offering more area for interactions with target substances during the filtration process, low toxicity, thermal stability and biocompatibility, with the added advantage of having magnetic properties by incorporation of Fe_3O_4 nanoparticles to the CNC surface. These characteristics make the membrane well-suited for a wide range of applications, including those involving sensitive biological or biomedical processes, where safety and stability are important.

6.2 Results and Discussion

The results and observations obtained from various analytical methods are discussed in this section of the chapter, along with probable scientific explanations.

6.2.1 Effect of the Magnetic Field-Induced Coagulation During Phase Inversion on the Performance of PVDF/FeCNC Membrane

6.2.1.1 *Morphology and Elemental Composition Analysis of Membrane Surface Obtained from EDX Analysis*

As reported before, FeCNC was prepared by the co-precipitation method. FESEM image shows the deposition of iron nanoparticles over the surface of CNCs uniformly to form FeCNCs. These spherical iron nanoparticles decorated over the surface of rod-shaped CNC give rise to a rough rod-shaped morphology (**Figure 6.1**). The prepared FeCNCs have a dimension with an average length of 336.32 ± 60.17 nm and a diameter of 61.14 ± 5.79.

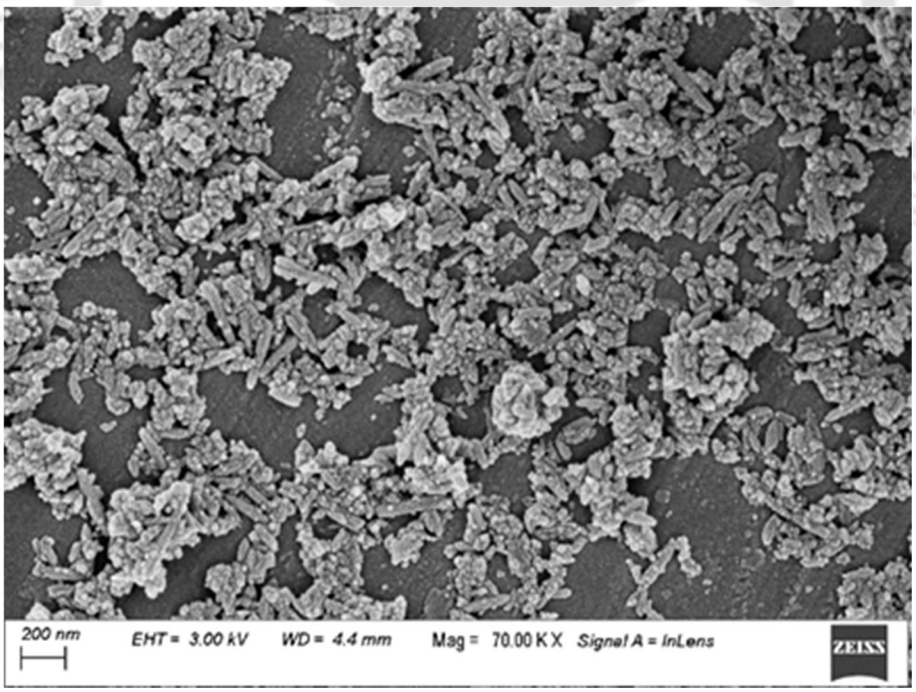

Figure 6.1: FESEM image of FeCNC, showing Fe nanoparticles decorated on the surface of CNC

The surface and the cross-sectional morphology of the membrane prepared with FeCNC without magnetic field and with magnetic field are depicted in SEM images in **Figure 6.2b & b1** and **Figure 6.2 c & c1**, respectively and compared with the membrane prepared without FeCNC. All membrane shows pores on their surface; however, the pores increase in the addition of FeCNC to the membrane. Neat PVDF membrane shows lesser pores as compared to the membrane with FeCNC (**Figure 6.2a & a1**). The membrane containing FeCNC, fabricated with and without the influence of the magnetic field, has no significant difference in pores at the surface. Similar to other membranes reported in previous chapters, the cross-sectional image of all membranes shows a typical asymmetrical structure with a very thin skin layer, finger-like channels and support sponge-like dense layer. The finger-like structure is more prominent in the membrane containing FeCNC, which is due to the spreading of water faster into the casting solution due to the presence of hydrophilic FeCNCs. The presence of FeCNCs also accelerates the process of phase separation and promotes the exchange between solvent and nonsolvent and, thus, the generation of more pores. But when compared with the membrane fabricated with a magnetic field, larger microvoids have been observed, and it is seen that the microvoids improve with an increase in the amount of mNPs [340]. These microvoids promote water passage through the nanocomposite membrane. Therefore, it can be inferred that the application of a magnetic field in the coagulation process significantly influences the formation of microvoids in the membrane cross-section. The migration of mNPs towards the direction of the field enhances the pore formation process. The application of an external magnetic field affects the trajectory of the FeCNC particles during the phase inversion process, thus changing the finger-like structure of the membrane [341]. It is also speculated that the improvements or formation of enlarged microvoid structures results in improving the permeability and antifouling ability of the membrane.

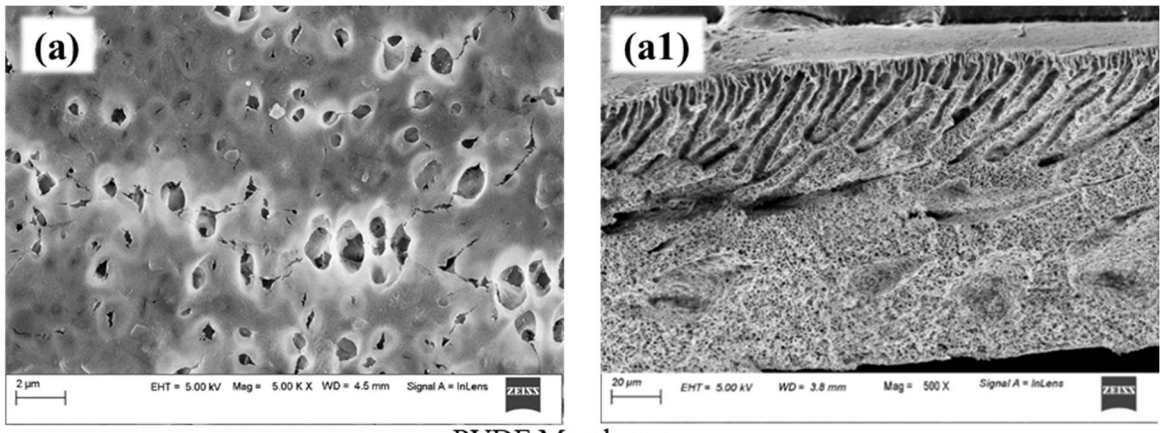

PVDF Membrane

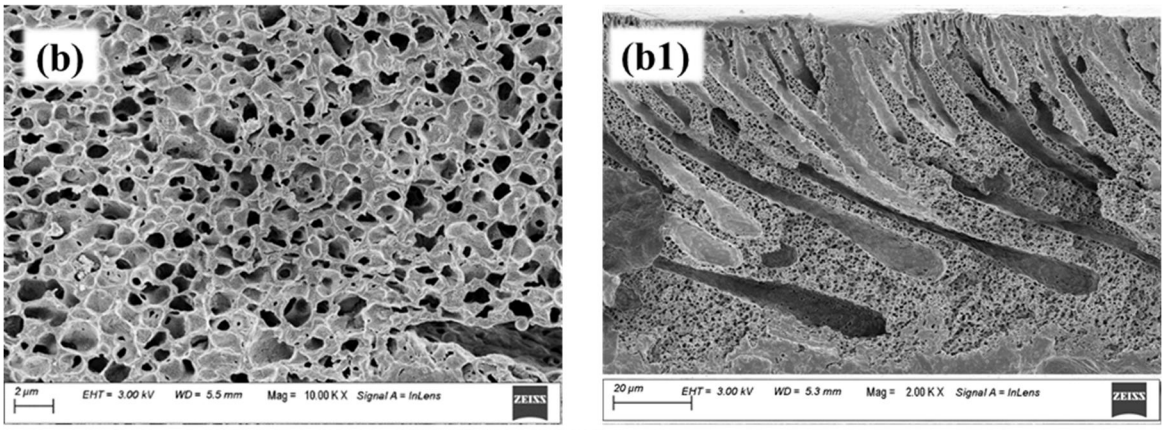

PVDF/ FeCNC Membrane

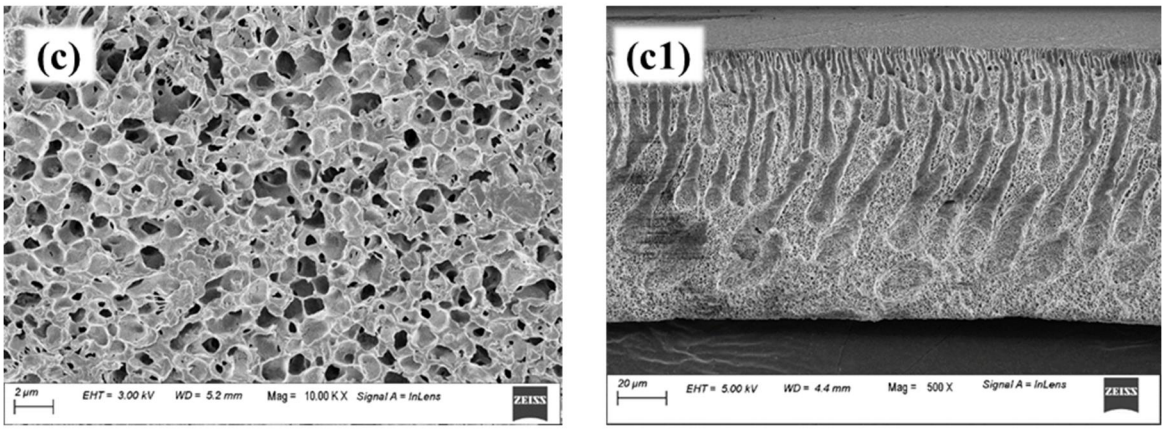

PVDF/ FeCNC Membrane (magnetic field)

Figure 6.2: FESEM images of (a) top surface (a1) cross-sectional image of neat PVDF (b & b1) top surface & cross-sectional image of PVDF/FeCNC membrane fabricated without magnetic field (c & c1) top surface & cross-sectional image of PVDF/FeCNC membrane fabricated with magnetic field

6.2.1.2 *Migration of FeCNC by the Influence of Magnetic Field*

Figure 6.3 shows the EDX spectrum of PVDF and PVDF/FeCNC composite membranes. The EDX spectrum of the neat PVDF membrane does not show any peak of Fe (**Figure 6.3a**), whereas the membrane containing FeCNC shows a prominent peak of Fe (**Figure 6.3b**). The number of peaks is higher in PVDF/FeCNC membrane fabricated under the influence of a magnetic field and becomes more prominent (**Figure 6.3c**).

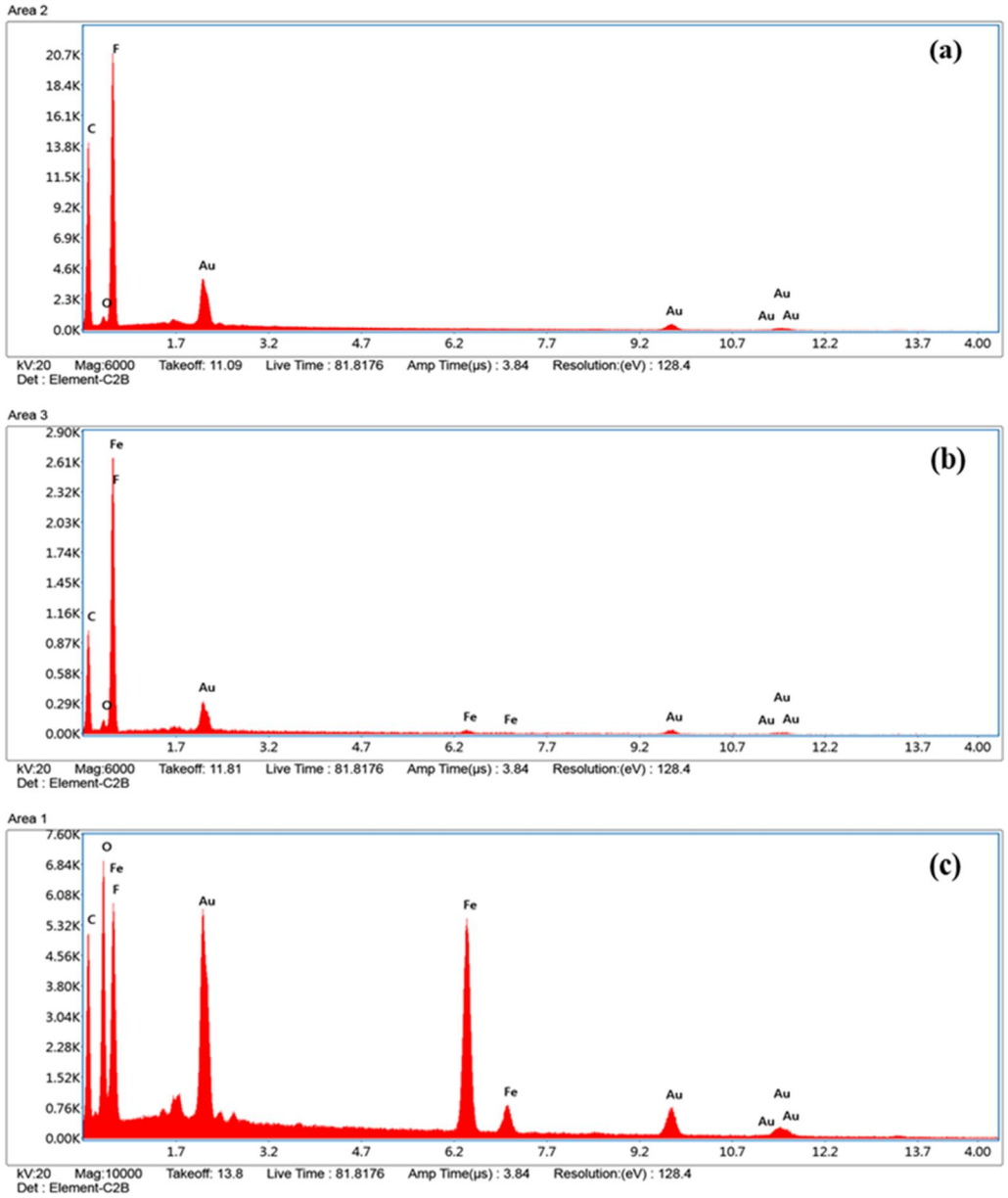

Figure 6.3: EDX spectrum of (a) PVDF membrane, (b) PVDF/FeCNC membrane, and (c) PVDF/FeCNC membrane prepared under the influence of magnetic field

Figure 6.4a shows a 50 kX magnified FeSEM image of the PVDF/FeCNC membrane without magnetic files, and **Figure 6.4b** shows an image of the PVDF//FeCNC membrane fabricated by the influence of the magnetic field. The migration of rod-shaped FeCNC to the surface of the membrane by the application of a magnetic field can be clearly seen in **Figure 6.4d**. EDX analysis of the surface of the membrane gives the elemental content of the surface represented in **Table 6.1**. It is observed that there is no iron content in the neat PVDF membrane and 0.58% iron on the surface of the membrane with FeCNC prepared without a magnetic field. However, the case of PVDF/FeCNC membrane prepared with the influence of a magnetic field shows 11.08% of Fe on the surface. This increase in Fe content is due to the migration of FeCNC particles to the surface of the membrane during the coagulation process under the influence of a magnetic field. The added magnetic field forces the FeCNC particles to migrate and enrich the surface.

Table 6.1: Elemental composition of each membrane surface obtained from EDX analysis

Elements	**Weight %**		
	PVDF membrane	**PVDF/FeCNC**	**PVDF/FeCNC (magnetic field)**
C	45.38	36.30	27.55
O	2.78	3.80	26.11
Fe	--	**0.58**	**11.08**
F	45.33	53.12	22.06
Au	6.51	6.21	13.20

To emphasize more on the migration of FeCNC to the surface of the membrane, EDX mapping of the Fe element was performed on the cross-section of the membranes. As seen in **Figure 6.4c**, the concentration of Fe is uniformly distributed in the PVDF/FeCNC membrane cast without a magnetic field. But in the case of PVDF/FeCNC (**Figure 6.3d**)

membrane cast under the influence of the magnetic field, the concentration of Fe (number of dots) on the surface of the membrane is higher than the inner layer of the membrane; this also indicates the migration of hydrophilic FeCNC towards the top layer of the membrane. Therefore, the fabrication of a PVDF/FeCNC membrane with magnetic field-induced coagulation and phase inversion can successfully enhance the accumulation of FeCNC on the surface of the membrane.

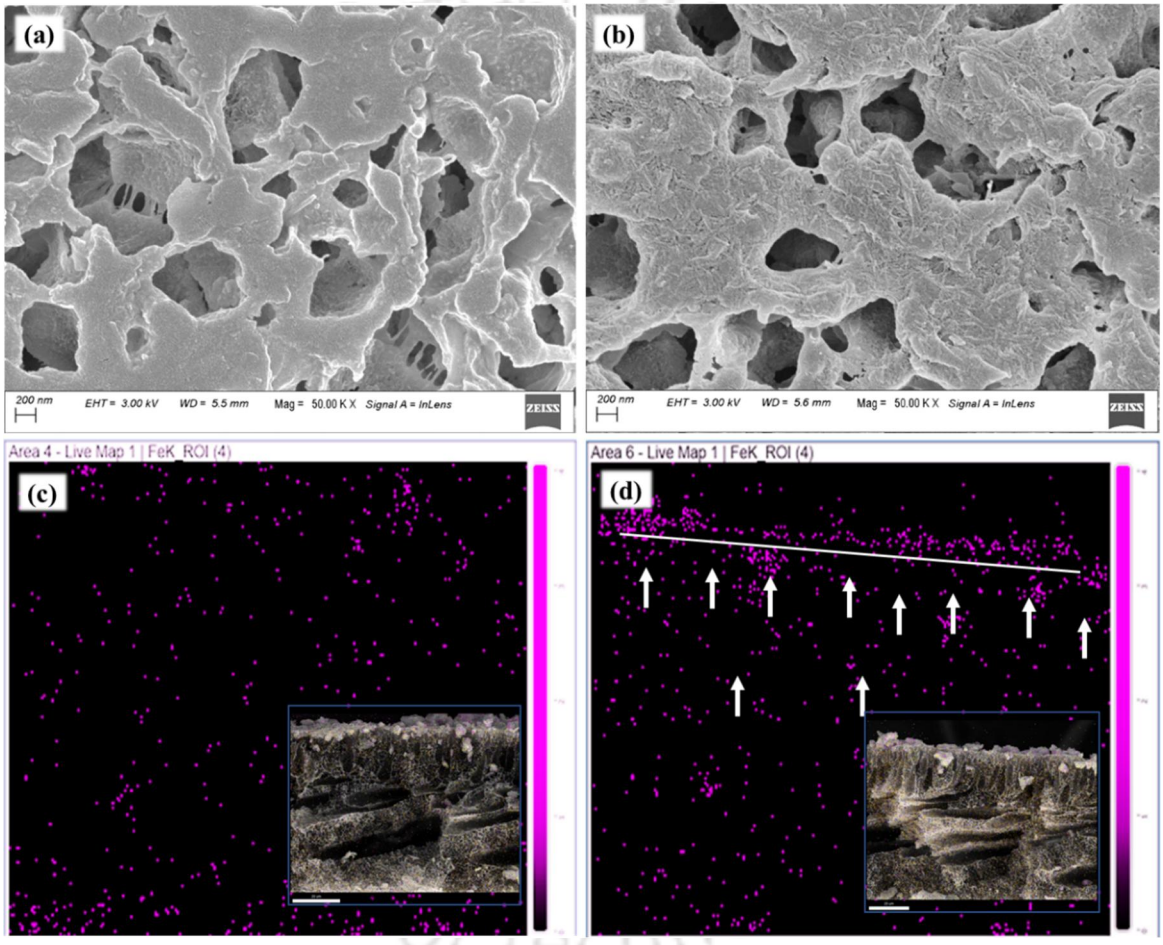

Figure 6.4: FESEM image of the top surface of the PVDF/FeCNC membrane (a) coagulated without magnetic field (b) coagulated under magnetic field. EDX mapping of Fe element in PVDF/FeCNC membrane (c) coagulated without magnetic field and (d) coagulated under magnetic field

6.2.1.3 *Vibrating Sample Magnetometer (VSM) Analysis of PVDF/FeCNC Membranes*

The presence of these Fe_3O_4 nanoparticles over the CNC surface results in magneto-responsive behaviour. The magnetic properties of these prepared FeCNCs were evaluated using a vibrating sample magnetometer (VSM) at 298 K. The hysteresis loops of the FeCNCs are shown in **Figure 6.5a**; the magnetization reduces from a plateau state to zero on the removal of the magnetic field. It is evident from the VSM curves that FeCNCs showed very low coercivity without any distinct hysteresis loop and absence of remanence, confirming the presence of the superparamagnetic Fe_3O_4 nanoparticles in the system. This behaviour signifies that the prepared FeCNC particles are superparamagnetic due to these Fe_3O_4 nanoparticles. The saturation magnetization of FeCNC obtained is ~44.01 emu/g, which is almost similar to the previously reported value [329]. The formation of superparamagnetic FeCNCs due to the deposition of Fe_3O_4 nanoparticles on bioderived material can potentially be applied in magneto-responsive membranes to remove different impurities from wastewater. The magnetic property of the membrane was also evaluated for all the membrane incorporation of FeCNC into it. The plot for M–H curves from VSM for all the fabricated membranes are plotted and represented in **Figure 6.5b**. These curves also represent without any distinct hysteresis loop, the value of magnetization for the membrane is lower as compared to the value of FeCNC ~44.01 emu/g. PVDF is a nonmagnetic material, but the incorporation of mNPs increases the magnetization value of the membrane (**Figure 6.5c**). The magnetization value of the membrane increases from 0.13 to 2.79 emu/g with an increase in the amount of FeCNC from 0.5 wt% to 2 wt%.

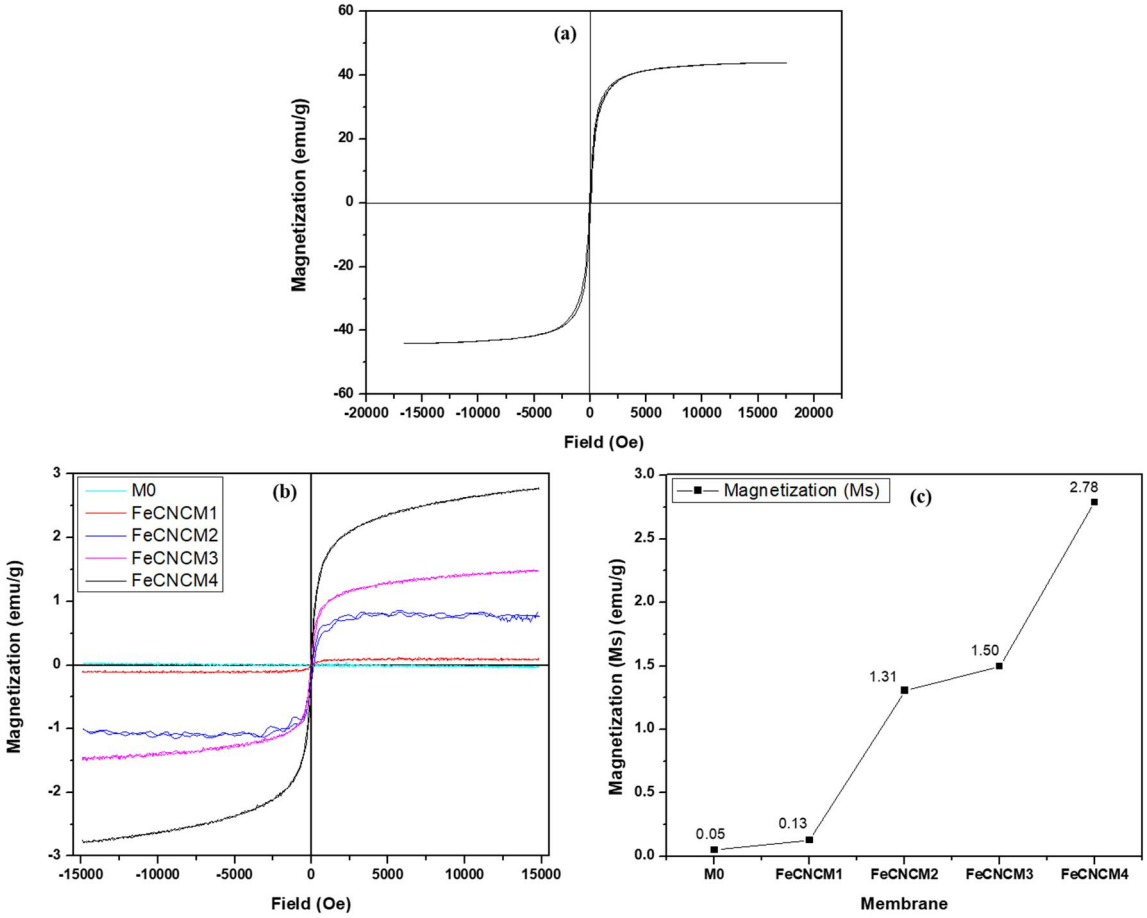

Figure 6.5: (a) Magnetic hysteresis loop for the fabricated FeCNCs (b) for membrane with different concentrations of FeCNCs (0, 0.5, 1, 1.5 and 2%) (c) magnetization vs different membranes containing different % of FeCNCs

6.2.1.4 *Hydrophilicity of the Membranes: Contact Angle Measurements*

Contact angle measurement was carried out to evaluate the hydrophilicity of the PVDF/FeCNC membrane, which mainly depends on surface roughness, membrane porosity and composition. The measurement was done immediately after placing the DI water drop on the surface of the membrane. A higher contact angle indicates the membrane is hydrophobic, and a lower contact angle indicates the membrane is hydrophilic.

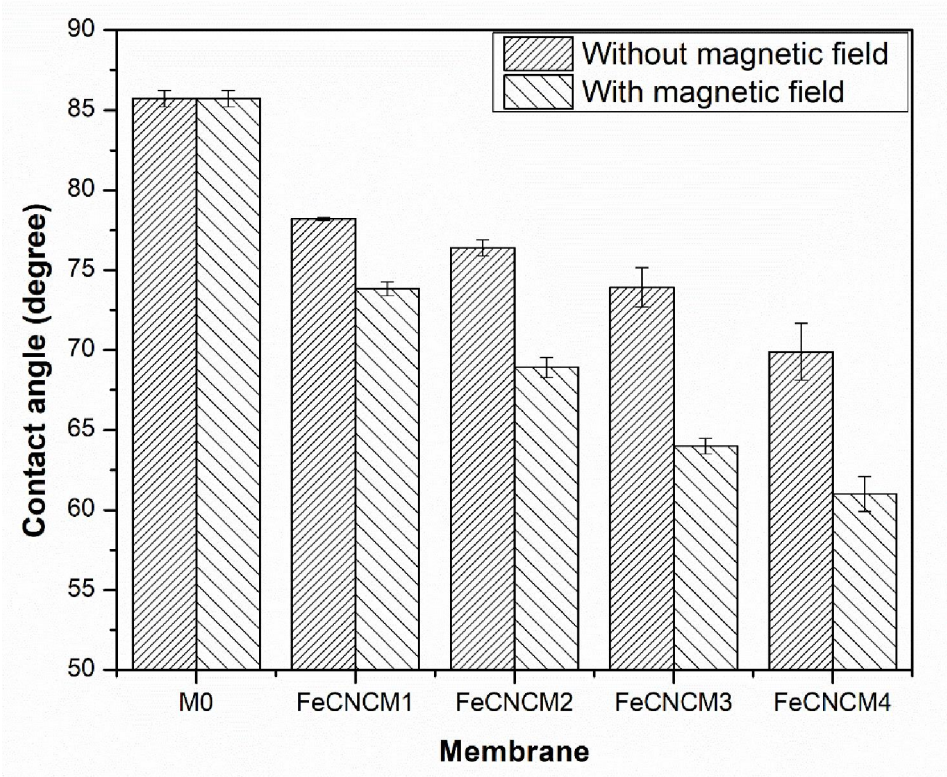

Figure 6.6: Contact angle for PVDF/FeCNC membrane fabricated under the influence of magnetic field

Figure 6.6 depicts a comparative contact angle results of PVDF/FeCNC membrane fabricated with magnetic field and without magnetic field. The pristine PVDF (M0) membrane showed the highest contact angle of 85.7°, indicating that it is more hydrophobic as compared to the PVDF/FeCNC membrane. The water contact angle decreases with increases in the concentration of FeCNC in the PVDF membrane, indicating the increase of the surface hydrophilicity of membranes after blending FeCNC in the casting solution. However, the PVDF/FeCNC membrane prepared with the influence of a magnetic field shows a lower contact angle than the membrane prepared without a magnet field. The contact angle decreases from 85.7° to 69.9° with an increase in FeCNC concentration from 0.5% to 2% for PVDF/FeCNC membrane without magnetic field, but for the same composition with the magnetic field, the contact angle reduced from 85.67° to 61°. The decrease in water contact angle in the composite membrane results from the addition of

FeCNCs imparts more hydrophilicity to the membrane surface due to the presence of hydrophilic −OH groups on the surface of FeCNCs and the attachment of Fe_3O_4 nanoparticles on the surface of CNCs. Due to the migration of FeCNC to the surface, it imparts more hydrophilicity to the membrane.

6.2.1.5 *Porosity and Pore Size Measurements of PVDF/FeCNC Membrane Fabricated with and without Magnetic Field*

It was observed that the porosity for PVDF and PVDF/FeCNC (2%) membrane was ~53 and 80.21%, respectively. The highest porosity was observed in the case of FeCNCM4, which corroborates with the results of improvement in pure water flux. This increase in porosity can be explained by the fact that FeCNC is a hydrophilic material containing abundant −OH on the surface, which enhances the diffusion rate of solvent and nonsolvent (water), resulting in the formation of high porosity [342]. As measured from the porometer, the pore size increases from 0.036 ± 0.003 μm to 0.082 ± 0.003 μm when FeCNC concentration increased from 0% to 2%. The increase in pore size is also related to the increase in the porosity of the membrane with an increase in the concentration of FeCNC. Further, the porosity and pore size of the PVDF/FeCNC membranes were fabricated with the influence of the magnetic field. **Figure 6.7a** represents the comparative plot of porosity vs increase in FeCNC concentration. There is a nominal increase in the porosity for membranes containing 0.5 and 1% FeCNC, but a significant change in porosity was observed for membranes containing 1.5 and 2% FeCNC when it is fabricated under the influence of the magnetic field. The porosity improved approximately from 71.13 to 82.24% and 80.21 to 88.79% in the case of 1.5% and 2% FeCNC respectively. At a lower concentration of FeCNC, there is no significant change in the pore size, but when concentration increases to 1.5 and 2%, a noticeable improvement in the pore size is observed, as seen in **Figure 6.7b**. The pore size increased from 0.063 to 0.076 microns and

0.082 to 0.095 microns for the membrane containing 1.5 and 2% FeCNC. It is also clearly noticed from the FESEM image that the membrane fabricated under the influence of magnetic field results in the formation of larger macro voids in the membrane cross-section, promoting water passage through the nanocomposite membrane.

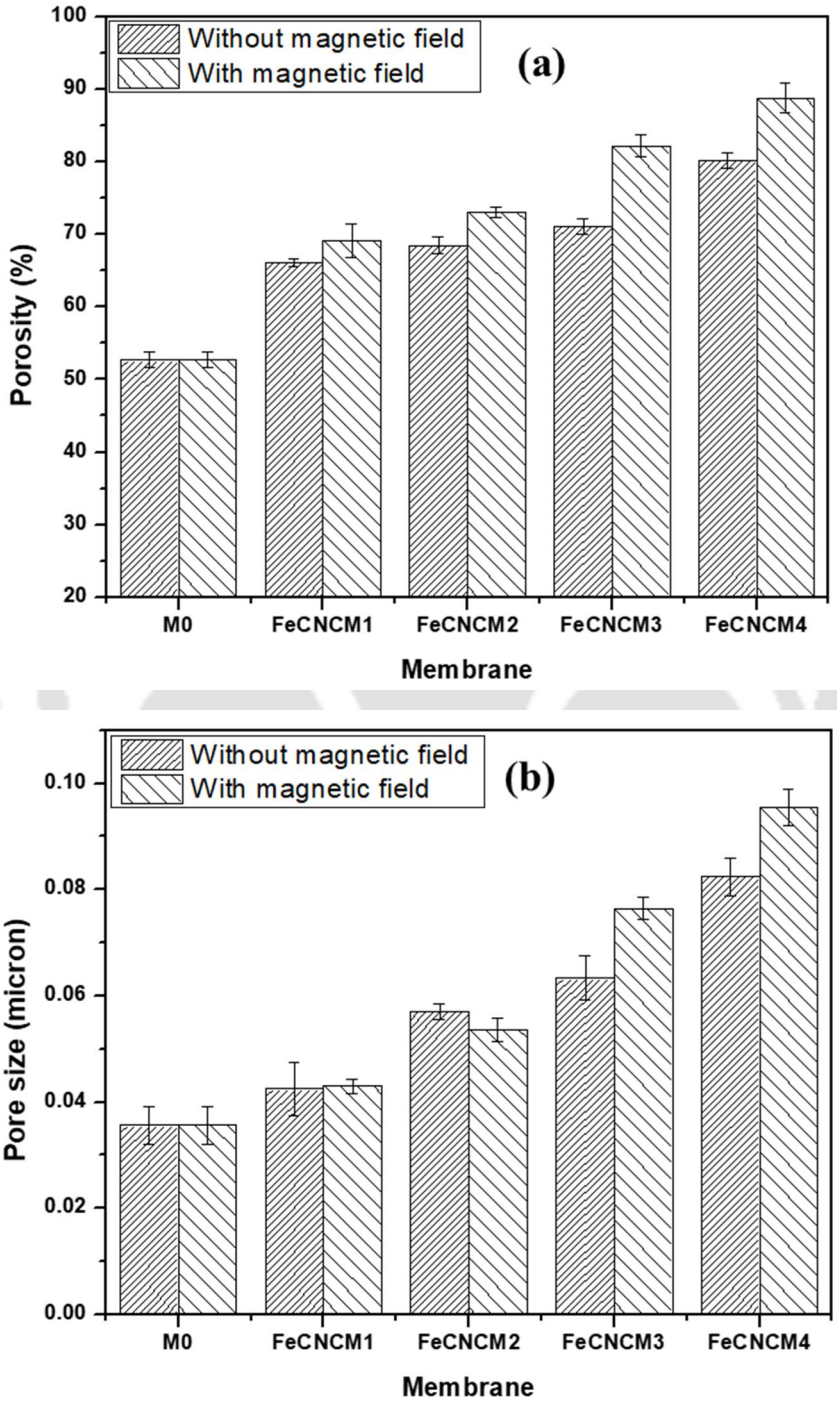

Figure 6.7: (a) Porosity and (b) pore size measurements of PVDF/FeCNC membrane fabricated with and without magnetic field

6.2.1.6 *Comparison of Pure Water Flux (PWF) of PVDF/FeCNC Membrane Fabricated with and without Magnetic field*

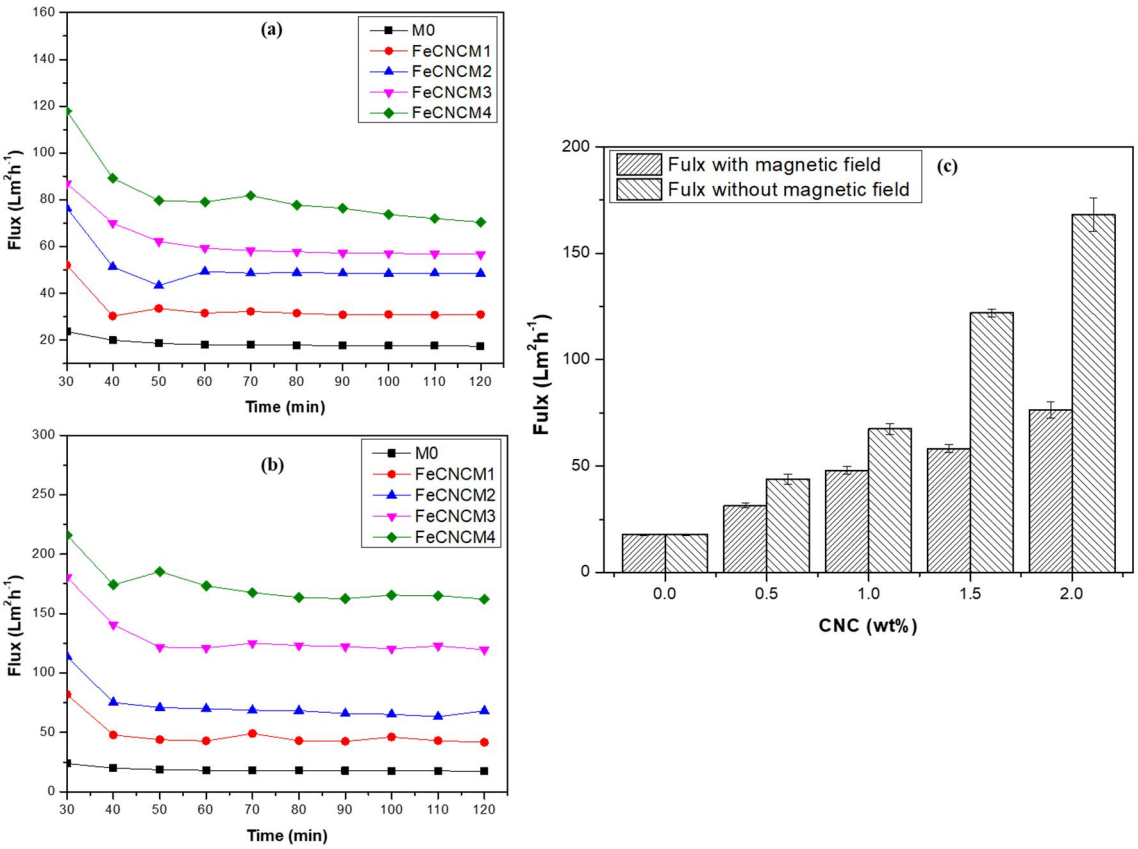

Figure 6.8: PWF for PVDF/FeCNC membrane (a) prepared without magnetic field, (b) with the magnetic field, and (c) comparison of PWF for both types of membranes

The prepared membranes were initially tested for pure water flux, and the stable water flux after 30 min of filtration was reported. It was observed that an increase in the concentration of nanoparticles in the membrane results in an improvement of flux, which may be due to the increase in porosity and hydrophilicity. Flux for PVDF/FeCNC membrane prepared with the magnetic field is significantly higher than PVDF/FeCNC prepared without magnetic field at a higher concentration of FeCNC. The percentage improvement in flux for FeCNCM1 and FeCNCM2 is ~39 and 40.50%, respectively. The improvement is more significant when the concentration of FeCNC is increased further to 1.5 and 2%. The PWF

increased by 109.68% and 120.22% for 1.5 and 2% FeCNC, respectively. The highest flux obtained was 168.11 L/m^{2}h and 214.65 L/m^{2}h for the PVDF/FeCNC membrane with 2% and 3% FeCNC, respectively, prepared with the influence of the magnetic field. The increase in flux is also due to the increase in the size of the pore, and the improvements or formation of enlarged macro void structures results in improving the permeability of water. A comparison of PWF for different membranes is shown in **Figure 6.8**. The same number of added nanomaterials shows that the PWF of a PVDF/FeCNC membrane fabricated under the influence of a magnetic field was greater than that of a PVDF/FeCNC prepared without the influence of the magnetic field.

6.2.2 Performance Evaluation of the Fabricated Membrane

6.2.2.1 *Crude Oil-Water Emulsion Separation by PVDF/FeCNC Membrane*

After conducting all the characterization, the membranes were tested for oil-water emulsion separation with an oil concentration of 1000 mg/l of crude oil in the feed. Similarly, the crude oil-water separation flux is also reported after 30 min of filtration of oil-water emulsion. It was observed before that PVDF/FeCNC membranes have better performance than PVDF/CNC membranes. But the oil-water separation performance is further enhanced for the membrane prepared under the influence of the magnetic field; the highest flux obtained was ~117 L/m^{2}h for FeCNCM4, which was only ~70 L/m^{2}h from the same FeCNCM4 prepared without magnetic field. A ~67% improvement in water flux for oil-water separation was obtained for membranes fabricated under the influence of a magnetic field. Stable water flux after compaction of the membrane for 30 min is shown in **Figures 6.9 (a & b)**. The flux increases with an increase in the concentration of FeCNC in the membrane, but the increment is more in the case of the membrane prepared with the magnetic field. A comparative plot for stable flux obtained for both types of membrane is also represented in **Figure 6.9c**. The PVDF/FeCNC membrane fabricated with the

influence of a magnetic field was also tested for its recyclability. The membrane was used for three different cycles; it was observed that there was no significant decrease in water flux for the membranes represented in **Figure 6.9d**. Thus, it also signifies that the membrane can be reused after a simple cleaning by washing with clean water, and there will be no loss in the water flux.

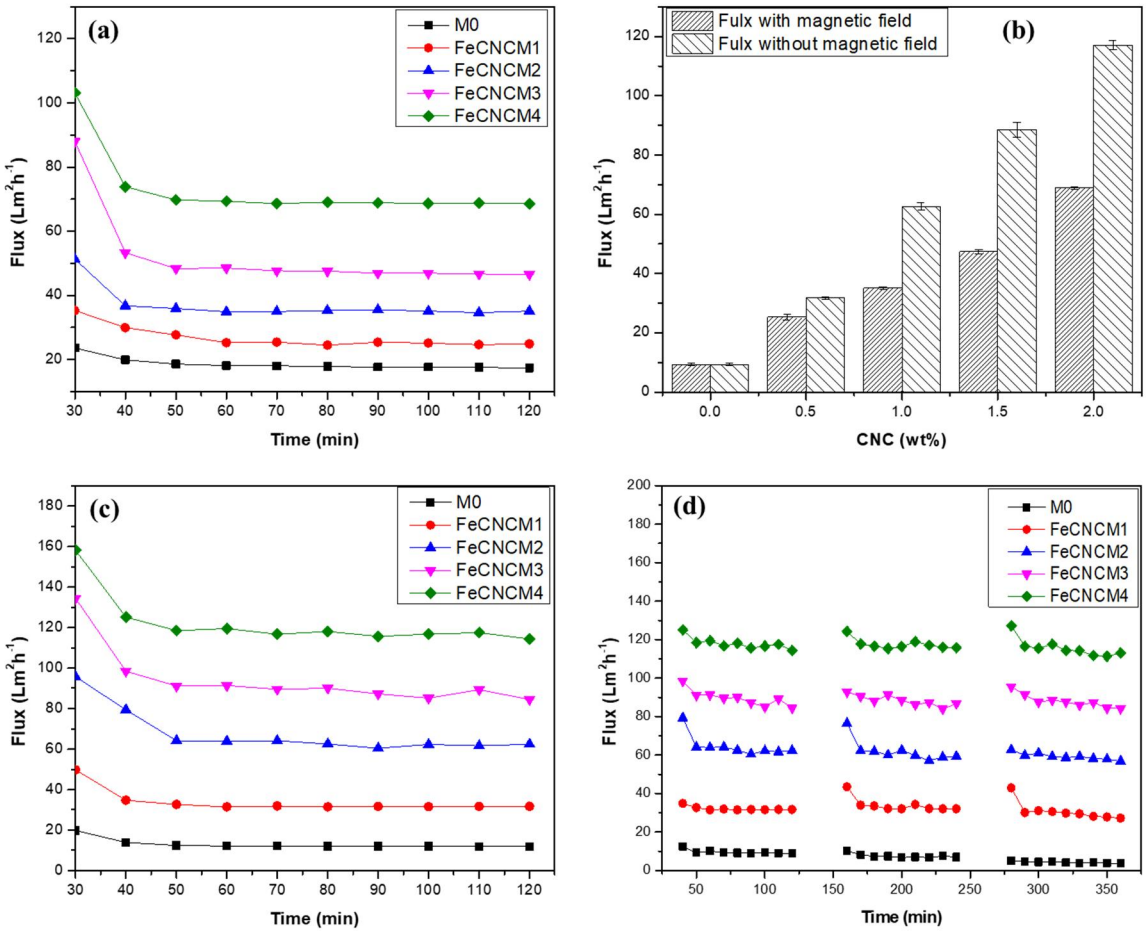

Figure 6.9: Water flux during oil-water separation for PVDF/FeCNC membrane (a) prepared without magnetic field (b) with the magnetic field (c) a comparison of water fluxes for both types of membranes (d) water flux for three different cycles (measurements taken in dead-end filtration setup)

To further check the long-term stability and performance of the membrane, the membranes were used for filtration of oil in water emulsion in a cross-flow membrane test setup for 48 h. The flux increases with an increase in the concentration of FeCNC in the membrane

(**Figure 6.10**). The decrease in flux with time in the cross-flow test is comparatively low for each membrane compared to the dead-end test setup. Due to the deposition of the cake layer over the membrane, there is a reduction in the cross-flow setup as compared to the dead-end test setup. **Figure 6.10** (**a, b & c**) shows the water flux during oil-water separation for PVDF/FeCNC membrane fabricated by using a magnetic field for initial 2 h, 12 h and 48 h, respectively, and a comparison batch and continuous filtration flux during oil-water separation is shown in **Figure 6.10d**.

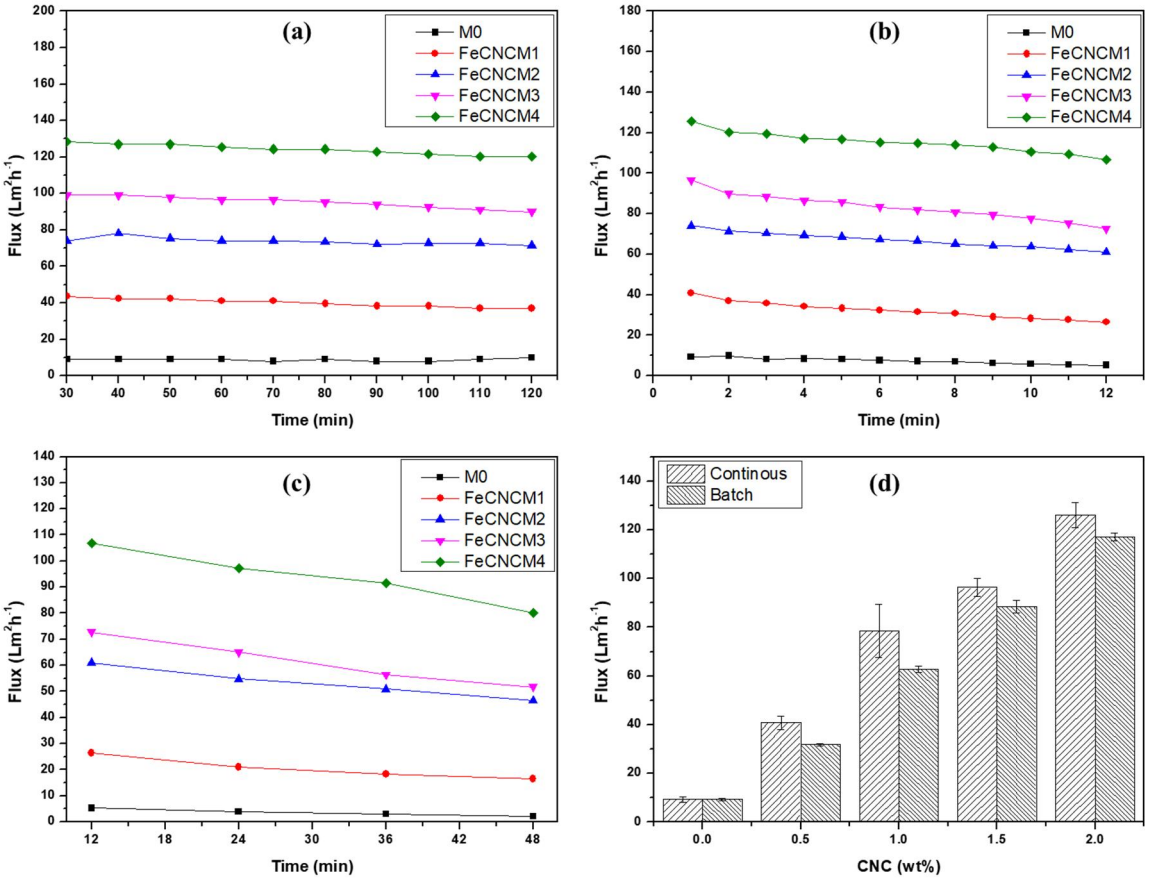

Figure 6.10: Water flux during oil-water separation for PVDF/FeCNC membrane prepared with the magnetic field (a) for initial 2 h readings are taken at 30 min interval (b) for next 12 h readings are taken at 1 h interval (c) from 12 h to 48 h readings are taken at 12 h interval (d) comparison of average water flux for dead-end and cross-flow filtration

6.2.2.2 *Crude Oil Rejection, Flux Recovery Ratio (FRR) and Flux Decline Ratio*

The crude oil rejection performance of the membranes was observed by filtering crude oil in water emulsion at an initial crude oil concentration of 1000 mg/L. The concentration of crude oil in feed and permeate was determined with UV–visible spectrophotometer. UV calibration curve was prepared by diluting the stock solution to 18 mg/l, 12 mg/l, 9 mg/l, 4 mg/l, 1 mg/l and 0.5 mg/l times. The UV calibration curve shown in **Figure 6.11a** was used to find out the concentration of crude oil in the solution after filtration. The crude oil rejection and flux recovery ratios were calculated using equations 8.6 and 8.7, respectively.

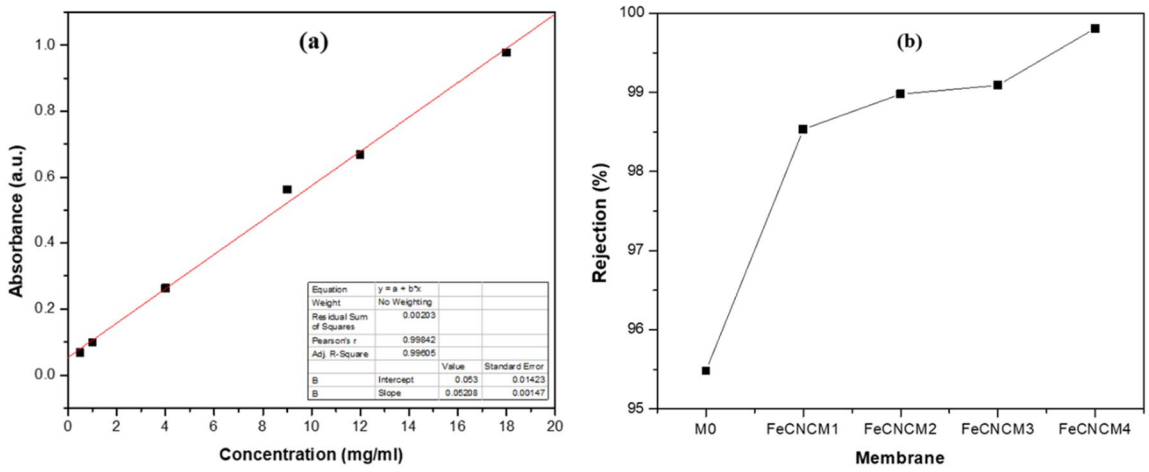

Figure 6.11: (a) UV calibration curve for crude oil-water emulsion (b) crude oil rejection for different PVDF/FeCNC membranes fabricated using magnetic field

The rejection percentage of crude oil for each membrane is shown in **Figure 6.11b**. The crude oil rejection of the membrane with FeCNC cast under the magnetic field increases with an increase in the concentration of FeCNC and rejects more than ~99% of oil when FeCNC concentration is 2%. The rejection increases due to the migration of hydrophilic FeCNCs to the surface of the membrane and makes the membrane more hydrophilic, which allows easy access to the water to pass through. This is also indicated by the reduction in the contact angle and increase in the size of the macro voids in the membrane cross-section,

as seen in the FESEM images. Hence, all the PVDF/FeCNC membrane fabricated with the influence of magnetic field shows a higher flux recovery ratio of ~98%.

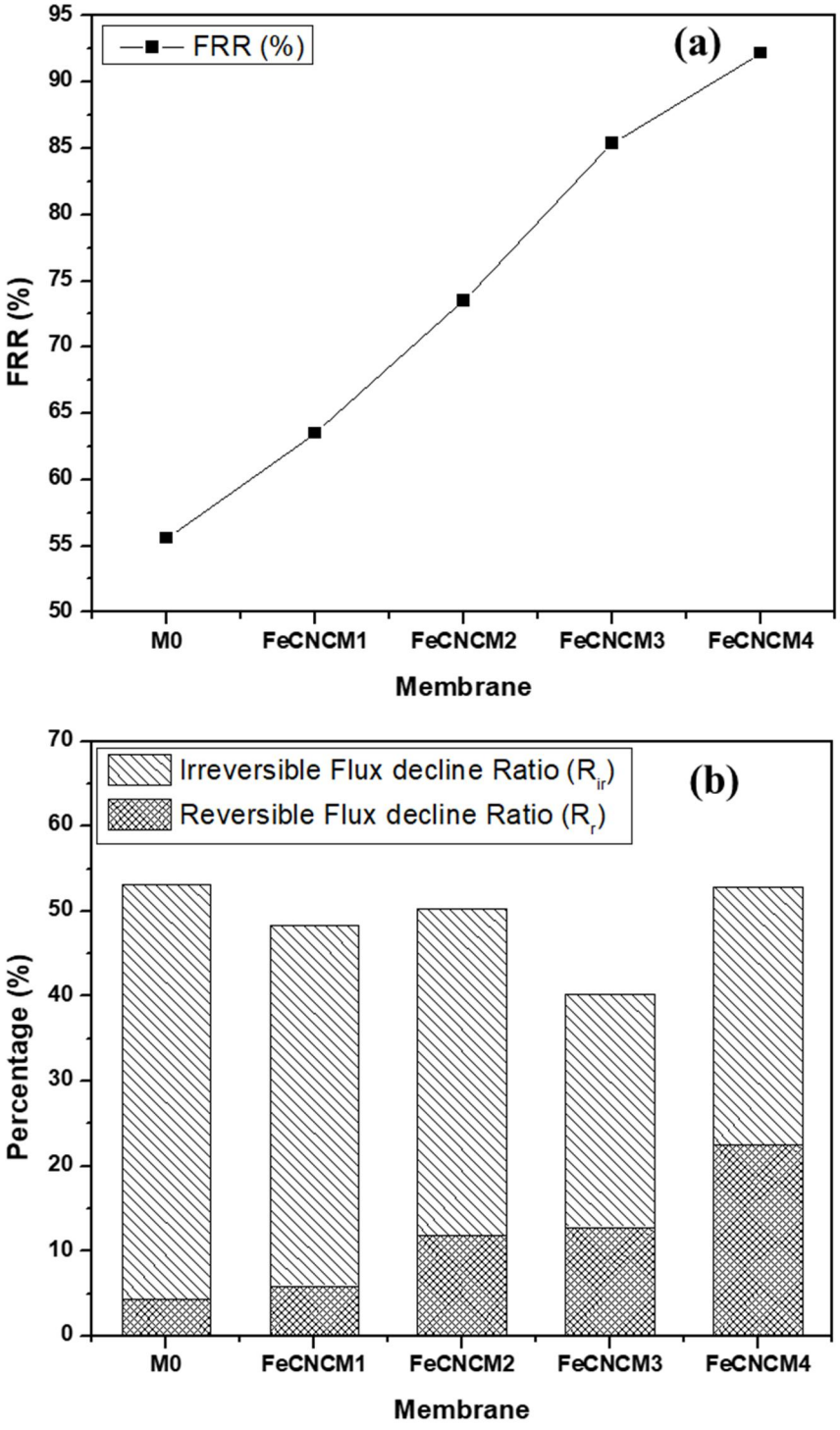

Figure 6.12: (a) Flux recovery ratio (FRR) values (b) reversible and irreversible fouling resistance ratio of PVDF and PVDF/CNC membranes

The flux recovery ratio (FRR) was determined for all the membranes to determine the antifouling capacity. The antifouling property of the fabricated membrane was studied by filtering DI water followed by oil-water emulsion and again followed by DI water, and then FRR was calculated. From **Figure 6.12a**, it is seen that the FRR increases from ~55 to 92.2% when FeCNC content increases from 0 to 2 wt% in the polymer solution. This indicated a significant improvement in the antifouling property of the PVDF/FeCNC composite membrane when fabricated with the influence of a magnetic field. To further analyze the antifouling performance, the total flux decline ratio (DR_t), reversible flux decline ratio (DR_r) and irreversible flux decline ratio (DR_{ir}) are evaluated for all the membranes represented in **Figure 6.12b**. The DR_t and DR_r value decreases, and DR_{ir} increases with increasing the FeCNC content. This indicates that fouling caused by the oil on the composite membranes is minor and can be recovered with a simple cleaning by backwashing.

To find out the formation of the cake layer and elemental composition of the deposited layer over the membrane after oil-water separation, FESEM image and EDX analysis were carried out. FESEM image of the top surface (**Figure 6.13a**) indicated the blockage of pores due to the deposition of foulants over it, but when the cross-section image (**Figure 6.13b**) of the fouled membrane was observed, no deposition was found inside the pore channels of the membrane. It can be concluded that the fouling occurs only on the surface and not inside the pores of the PVDF/FeCNC membrane, and hence, it shows better flux recovery and almost equal flux when tested for different cycles. The EDX analysis indicates the presence of a higher percentage of carbon, oxygen and fluorine, which is obviously contributed by the hydrocarbons present in the crude oil and the composition of the membrane. Apart from these elements, different heavy elements are also deposited over the membrane surface, which is presented in **Figure 6.13c**.

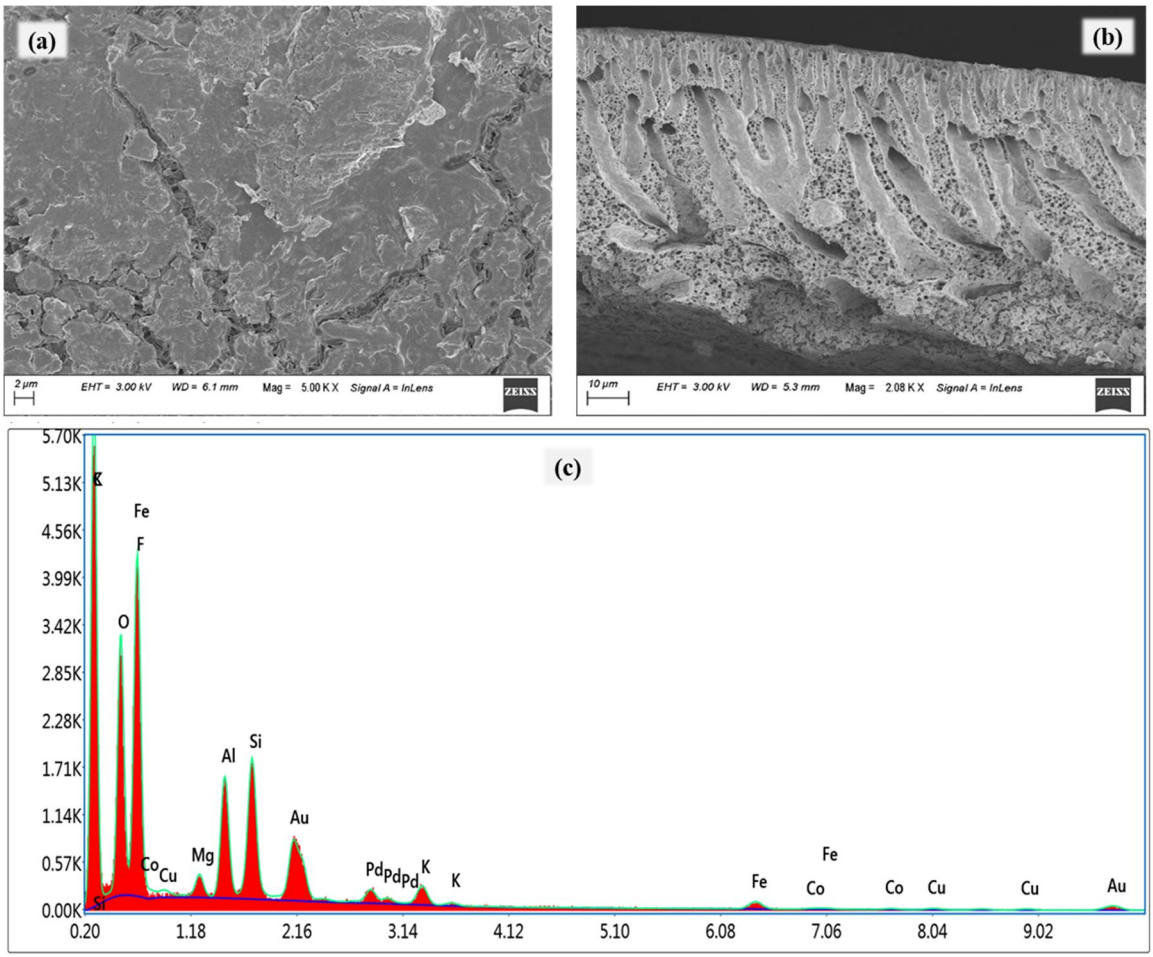

Figure 6.13: FESEM image of the fouled membrane of (a) top surface, (b) cross-sectional and (c) elemental composition of the top surface of the membrane containing cake layer over the membrane after oil-water separation

6.3 Summary

The findings from this chapter give an insight into the benefits of incorporating FeCNC into the membrane casting solution and applying a magnetic field during the membrane fabrication process. These modifications in method for membrane fabrication results in remarkable enhancements in the membrane's properties, specifically its hydrophilicity, porosity, PWF, and oil rejection capacity. The improvements in the membrane characteristics can be attributed to the deliberate application of a magnetic field during the fabrication process. These FeCNCs migrate towards the surface of the membrane, leading

to a surface enrichment of FeCNC and a corresponding improvement in membrane properties. It is notable that there is a significant increase in the water flux during oil-water separation for PVDF/FeCNC membranes prepared under the influence of magnetic field. The is a 67% improvement in water flux for oil-water separation, indicating a significant performance advantages conferred by this novel approach. This increase is flux is directly attributed to the magnetic field-driven surface enrichment of membrane by FeCNC, which enhances the membrane's permeability and thus its water transport capabilities. Furthermore, the application of a magnetic field increases the FeCNC content on the surface of the membrane and thus improves the oil rejection rate of the membrane. When the FeCNC concentration is 2%, a remarkable level of more than 99% oil rejection is achieved, which highlights the potential of using FeCNC combined with the application of a magnetic field during membrane fabrication. Therefore, application of FeCNC as a cost-effective, bio-derived filler in polymeric membranes and applying a magnetic field during fabrication can be a promising alternative for developing high-performance, antifouling membranes tailored for oil-water separation.

Chapter 7
Conclusions and Future Prospects

This is the final chapter that summarizes the findings of the research work, and also, the chapter will provide suggestions for the future scope of the work.

The first part of the research found that the addition of oligo lactic acid conjugate chitosan (OCH) as a bio-dispersant for oil spills can be a potential substitute for synthetic chemical dispersants. The addition of OCH results in a more stable emulsion compared to the emulsion stabilized by only xanthan gum (XG). The droplet size measurement indicated no significant increase in the size of the droplets; the initial size was 1457 ± 288 nm, which changed to 1894 ± 748 nm after 3 weeks. It indicated that the crude oil droplets are stable against coalescence compared to the crude oil emulsion in water, where the droplet size was 5294 ± 2096 nm, which increased to 9799 ± 3369 nm. The isolated bacteria were characterized as gram-negative and identified as *Pseudomonas aeruginosa* by 16S rRNA gene sequencing. These bacteria have the capability to degrade crude oil and also to produce surfactant, which assists in the degradation process. The percentage degradation of hydrocarbon present in crude oil by *Pseudomonas aeruginosa* CoE-SusPol3 was due to the synergistic effects of XG and OCH, which increased significantly to 74.31% compared to the system with XG (51.84%) and crude oil alone (34.06%). Such synergistic effects of biopolymers as bio-dispersants and microbial degradation could result in a novel environment-friendly oil spill remediation technology for treating accidental oil spills. The second part of the research discusses the use of cellulose nanocrystal (CNC) for membrane application. CNC has enormous potential, which makes it ideally suitable for membrane applications, and the production cost is also reduced with the advent of new and efficient methods. A new class of hybrid material, magnetic cellulose nanocrystal (FeCNC), was prepared by co-precipitation techniques and used along with polyvinylidene fluoride

(PVDF) for membrane fabrication, which improved the performance of the membrane. The effects of coagulation under a magnetic field on the characteristics of the PVDF/FeCNC membranes were evaluated. The results indicated that adding FeCNC nanoparticles to the casting solution improved the hydrophilicity of the membrane surface due to the migration of FeCNCs towards the direction of the applied field. The water contact angle was reduced from 85.67° to 61°. The porosity improved approximately from 71.13 to 82.24% and 80.21 to 88.79% in the case of 1.5% and 2% FeCNC, respectively. The pure water flux (PWF) increased by 109.68% and 120.22% for 1.5 and 2% FeCNC, respectively. A ~67% improvement in water flux for oil-water separation was obtained for membranes fabricated under the influence of a magnetic field. FRR increases from ~55 to 92.2% when FeCNC content increases from 0 to 2 wt% in the polymer solution. The crude oil rejection of the membrane with FeCNC cast under the magnetic field increases with an increase in the concentration of FeCNC and rejects more than ~99% of oil when FeCNC concentration is 2%. Thus, adding a magnetic field during coagulation caused the migration of the FeCNCs, especially to the top layer of the membranes, resulting in a change in the membrane morphology with larger microvoids. Hence, adding such cost-effective bioderived filler to the polymeric membrane and preparing the membrane with the magnetic field application can become a promising alternative for developing antifouling and high-performance membranes for the oil-water separation process. A summary of all the major research findings is presented in **Tables 7.1 & 7.2**.

Table 7.1: Summary of major research findings of all the chapters

Chapters	Research Findings
Interaction of oil-water system with bio-dispersant	✓ XG and OCH can be used as a bio-dispersant for oil spillage treatment ✓ Stabilize oil droplets for more than 3 weeks ✓ Crude oil degradation % of stabilized emulsion is 74.31%, whereas for the unstabilized emulsion, it is 34.06% ✓ Surface tension of the crude oil reduced to 28.53 (± 0.05) from 32.44 (± 0.22) ✓ Such synergistic effects of biopolymers as bio-dispersants and microbial degradation could be a possible solution for treating water with a larger amount of oil
Cellulose nanocrystal (CNC)-Polyvinylidene fluoride (PVDF) membrane	✓ CNC prepared from waste paper having rod-shaped morphology with an aspect ratio of ~6 and Crystallinity index (I_{CR}) of 78% ✓ PVDF/CNC composite membrane showed higher porosity, and it increases with an increase in CNC wt% (M0 = 52.8% to M3 = 92.6%)

	✓ Pure water flux increases by ~48% in PVDF/CNC membrane with 3 wt% CNC as compared to neat PVDF membrane ✓ Contact angle decreases from 85° to 67° with the addition of CNC ✓ Improve the mechanical stability (increased from M0 ~3.7 to ~5.4 MPa in M3)
Magnetic cellulose nanocrystal (FeCNC)-Polyvinylidene fluoride (PVDF) membrane	✓ CNC has an average length of 286.09 ± 31.21 nm, and a diameter of 49.02 ± 5.54 nm FeCNC has a new dimension with an average length of 336.32 ± 60.17 nm and diameter of 61.14 ± 5.79 nm ✓ Flux significantly improved: M0 ~18 L/m^2h to FeCNCM4 ~78 L/m^2h and FeCNCM5 ~188 L/m^2h ✓ 80-70 L/m^2h for FeCNC membrane during oil-water separation ✓ Porosity improved (M0 ~53 to FeCNCM5 ~83%) ✓ Oil rejection of ~95 % is obtained ✓ WCA decrease with the addition of FeCNC concentration ✓ Flux recovery ratio of PVDF/Fe-CNC membrane is >90%, whereas for neat PVDF membrane is <85%

	✓ Flux decline after to 68 L/m^{2}h after 12 h and 48 L/m^{2}h after 48 h
Magnetic cellulose nanocrystal (FeCNC)-Polyvinylidene fluoride (PVDF) membrane: under magnetic field	✓ Water contact angle was reduced from 85.67° to 61° ✓ Porosity improved approx. from 71.13% to 82.24% and 80.21% to 88.79% in the case of 1.5% and 2% FeCNC, respectively ✓ Pure water flux increased by 109.68% and 120.22% for 1.5 and 2% FeCNC, respectively ✓ Higher flux of 130-120 L/m^{2}h is obtained for membrane with 2 wt% FeCNC during oil-water separation ✓ Oil rejection >99% for (2 wt.% FeCNC) ✓ FRR increases from ~55 to 92.2% when FeCNC content increase from 0 to 2 wt% in the polymer solution

Table 7.2: Properties comparison for different membranes at 2 wt% of CNC and FeCNC

Pure water flux	Oil filtration flux	Oil Rejection	FRR	Contact angle	Tensile Strength
neat PVDF	neat PVDF	neat PVDF	neat PVDF	neat PVDF	neat PVDF
~18 L/m^{2}h	~10 L/m^{2}h	~95%	~41%	85°	3.7 MPa
PVDF/CNC	PVDF/CNC	PVDF/CNC	PVDF/CNC	PVDF/CNC	PVDF/CNC
~34 L/m^{2}h	~23 L/m^{2}h BSA	93% BSA	~69%	77°	5.4 MPa
PVDF/FeCNC	PVDF/FeCNC	PVDF/FeCNC	PVDF/FeCNC	PVDF/FeCNC	PVDF/FeCNC
~78 L/m^{2}h	~80-70 L/m^{2}h	~95%	>90% for all	~69°	4.35 MPa
PVDF/FeCNC	PVDF/FeCNC	PVDF/FeCNC	PVDF/FeCNC	PVDF/FeCNC	PVDF/FeCNC
(with magnetic field)	(with magnetic field)	(with magnetic field)	(with magnetic field)	(with magnetic field)	(with magnetic field)
~165 L/m^{2}h	~130-120 L/m^{2}h	~99%	92%	61°	4.57 MPa

Future Directives of the Research

Given our observed results from our research, we recommend the following future research:

- Application of the developed membrane in other areas like reverse osmosis, dye separation and desalination can be explored to widen its applicability.
- Study the effect of the surface coating of the membrane by CNC and FeCNC and its comparative study with the present research.
- Developing CNC-based stimuli-responsive and smart hybrid membranes and investigating the degradation of organic contaminants.
- Application of other surface functionalized CNCs in membrane fabrication can be explored.
- CFD modelling of the oil-water filtration to study the oil droplet behaviour in the pore of the membrane.

Research outputs

Patents Filed:

1. Magnetic nanocomposite polymeric membrane for purification of water and process of preparation thereof. (**Patent Application No.: 202131014583**)
2. Aligned magnetic cellulose nanocrystal-based polymeric membrane for oil-water separation and purification of water. (**Patent Application No.: 202231052371**)
3. New high efficiency polishing medium. (**Patent Application No.: 202231072748**)

Journal Publications:

1. **Pankaj Boruah**, Raghvendra Gupta and Vimal Katiyar, Fabrication of cellulose nanocrystal (CNC) from waste paper for developing antifouling and high-performance polyvinylidene fluoride (PVDF) membrane for water purification. Carbohydrate Polymer Technologies and Applications, 5 (2023) 100309, https://doi.org/10.1016/j.carpta.2023.100309.
2. **Pankaj Boruah**, Chethana Mudenur, Raghvendra Gupta and Vimal Katiyar, Oligo lactic acid conjugate chitosan as a bio-dispersant for enhanced biodegradation of crude oil in oil-spill remediation. **Manuscript submitted to Water Science and Engineering.**
3. **Pankaj Boruah**, Raghvendra Gupta and Vimal Katiyar, Magnetic cellulose nanocrystal embedded PVDF membrane for oil-water separation. **Manuscript under preparation.**
4. **Pankaj Boruah**, Raghvendra Gupta and Vimal Katiyar, Magnetic field assisted coagulation bath for preparation of PVDF/FeCNC membrane and its performance for oil-water separation. **Manuscript under preparation.**

5. Chethana Mudenur, **Pankaj Boruah,** Amit Kumar and Vimal Katiyar, Prodigiosin-Loaded Poly(lactic acid) to Combat the Biofilm-Associated Infections, ACS Applied Bio Materials, 5 (2022) 2143–2151, https://doi.org/10.1021/acsabm.1c01187.
6. Ishani Chakrabartty, Naba Kumar Kalita, **Pankaj Boruah**, Vimal Katiyar, Khalid Rehman Hakeem, Latha Rangan, Physico-rheological characterization of organically derived seed samples from Alpinia nigra (Gaertn.) B.L. Burtt, an ethnic medicinal plant of Northeast India, 152 (2020), 112560, https://doi.org/10.1016/j.indcrop.2020.112560.

Book Chapter:

1. **Pankaj Boruah**, Pradyut Dhar and Vimal Katiyar, Nanocellulose-based composites for applications as catalysts and pollutant remediation. Book: Cellulose Nanocrystals, (2020) 229–278, https://doi.org/10.1515/9783110648010-008.

Conferences/Seminars/Symposia/Workshops/Training:

1. **Pankaj Boruah**, Chethana Mudenur, Akhilesh Kumar Pal, Raghvendra Gupta and Vimal Katiyar, "Enhanced Degradation of Oil droplets using Biopolymer as Dispersant for Oil Spill Treatment" in 4th International Conference Kathmandu Symposia on Advanced Materials-2018, KaSAM-2018, October 26-29th, 2018, Kathmandu, Nepal.
2. **Pankaj Boruah**, Chethana Mudenur, Akhilesh Kumar Pal, Vimal Katiyar, "Modified Biopolymer as an Environmental Friendly Dispersant for Treatment of Oil Spills," International Symposium on Advances in Sustainable Polymers, ASP-17, January 8-11th, 2018.
3. **Pankaj Boruah**, Shinichi Sakurai, Raghvendra Gupta and Vimal Katiyar, "Blending poly(butylene succinate) with poly(lactic acid) and the effect of modified chitosan as Studied by Synchrotron X-Ray Scattering and DSC" in 15th International Conference

on Polymer Science and Technology, SPSI-MACRO-2018, December 19-22th, 2018, Pune, India.

4. **Pankaj Boruah**, S Sakurai, Raghvendra Gupta and Vimal Katiyar, "Morphology and Crystallinity of Biodegradable Poly (lactic acid)/Poly (butylene succinate) Blends and Effect of Modified Chitosan studied via Synchrotron X-Ray Scattering and DSC" in International Conference on Advances in Polymer Science & Technology, APA- 2018, November 1-3th 2018, Kathmandu, Nepal.
5. AICTE Training and Learning (ATAL) Academy Online FDP on "Mining & Mineral Processing", 23-27th November 2020.
6. Web conference on polymer processing and emerging technologies, 4-7th November 2020.
7. TEQIP Sponsored online national symposium on Nanomaterials for Engineering and Biomedical Applications (NEBA 2020), 27-29th July 2020.
8. TEQIP Sponsored online FDP on Technological Advancement in Environment friendly materials and Process (TAEFMP 2020), 20-25th July 2020.

Awards/Achievements/Research Internships:

1. Awarded MACRO Best Poster presentation at 15th International Conference on Polymer Science and Technology, SPSI MACRO-2018.
2. Awarded APA Best Poster for presentation in International Conference on Advances in Polymer Science & Technology, APA- 2018.
3. Awarded Onyx Group Nutriset Best Poster Presentation in 4th International Conference Kathmandu Symposia on Advanced Materials-2018.
4. Short-Term Student Exchange Program: 2018 KIT Global Human Resource Development Program at Kyoto Institute of Technology, Japan from April to September, 2018.

References

[1] L. Yu, M. Han, F. He, A review of treating oily wastewater, Arabian Journal of Chemistry. 10 (2017) S1913–S1922. https://doi.org/10.1016/j.arabjc.2013.07.020.

[2] A.I. Adetunji, A.O. Olaniran, Treatment of industrial oily wastewater by advanced technologies: a review, Appl Water Sci. 11 (2021) 1–19. https://doi.org/10.1007/s13201-021-01430-4.

[3] J.E.B. Castiblanco, J.C. Carregosa, J.M. Santos, A. Wisniewski, Molecular behavior assessment on initial stages of oil spill in terrestrial environments, Environmental Science and Pollution Research. 28 (2021) 13595–13604. https://doi.org/10.1007/S11356-020-11555-9.

[4] A. Mehmood, F.S.A. Khan, N.M. Mubarak, S.A. Mazari, A.S. Jatoi, M. Khalid, Y.H. Tan, R.R. Karri, R. Walvekar, E.C. Abdullah, S. Nizamuddin, Carbon and polymer-based magnetic nanocomposites for oil-spill remediation—a comprehensive review, Environmental Science and Pollution Research. 28 (2021) 54477–54496. https://doi.org/10.1007/s11356-021-16045-0.

[5] K. Abuhasel, M. Kchaou, M. Alquraish, Y. Munusamy, Y.T. Jeng, Oily Wastewater Treatment: Overview of Conventional and Modern Methods, Challenges, and Future Opportunities, Water 2021, Vol. 13, Page 980. 13 (2021) 980. https://doi.org/10.3390/w13070980.

[6] D.D. Evans, G.W. Mulholland, H.R. Baum, W.D. Walton, K.B. McGrattan, In Situ Burning of Oil Spills, J Res Natl Inst Stand Technol. 106 (2001) 231. https://doi.org/10.6028/jres.106.009.

[7] M.C. Sterling, J.S. Bonner, A.N.S. Ernest, C.A. Page, R.L. Autenrieth, Chemical dispersant effectiveness testing: Influence of droplet coalescence, Mar Pollut Bull. 48 (2004) 969–977. https://doi.org/10.1016/j.marpolbul.2003.12.003.

[8] J.M. Baker, Oil Pollution, Encyclopedia of Ocean Sciences. (2001) 191–199. https://doi.org/10.1016/B978-012374473-9.00055-2.

[9] P. Bobde, A.K. Behera, R.K. Patel, Oil spill treatment using porous materials, Advances in Oil-Water Separation. (2022) 157–173. https://doi.org/10.1016/B978-0-323-89978-9.00005-7.

[10] Z.R. Jiang, J. Ge, Y.X. Zhou, Z.U. Wang, D. Chen, S.H. Yu, H.L. Jiang, Coating sponge with a hydrophobic porous coordination polymer containing a low-energy CF_3-decorated surface for continuous pumping recovery of an oil spill from water, NPG Asia Materials 2016 8:3. 8 (2016) e253–e253. https://doi.org/10.1038/am.2016.22.

[11] G.F. Bennett, R.W. Peters, The removal of oil from wastewater by air flotation: A review, 18 (2009) 189–253. https://doi.org/10.1080/10643388809388348.

[12] E. Nyankson, M.J. Decuir, R.B. Gupta, Soybean Lecithin as a Dispersant for Crude Oil Spills, ACS Sustain Chem Eng. 3 (2015) 920–931. https://doi.org/10.1021/acssuschemeng.5b00027.

[13] Z. Liu, U. Callies, Implications of using chemical dispersants to combat oil spills in the German Bight – Depiction by means of a Bayesian network, Environmental Pollution. 248 (2019) 609–620. https://doi.org/10.1016/j.envpol.2019.02.063.

[14] P. Venkataraman, J. Tang, E. Frenkel, G.L. McPherson, J. He, S.R. Raghavan, V. Kolesnichenko, A. Bose, V.T. John, Attachment of a hydrophobically modified

biopolymer at the oil-water interface in the treatment of oil spills, ACS Appl Mater Interfaces. 5 (2013) 3572–3580. https://doi.org/10.1021/am303000v.

[15] R. Makkar, S. Cameotra, An update on the use of unconventional substrates for biosurfactant production and their new applications, Appl Microbiol Biotechnol. 58 (2002) 428–434. https://doi.org/10.1007/s00253-001-0924-1.

[16] R. Almeda, C. Hyatt, E.J. Buskey, Toxicity of dispersant Corexit 9500A and crude oil to marine microzooplankton, Ecotoxicol Environ Saf. 106 (2014) 76–85. https://doi.org/10.1016/j.ecoenv.2014.04.028.

[17] M.Z. Iqbal, A.A. Abdala, Oil spill cleanup using graphene, Environ Sci and Poll Research. 20 (2013) 3271–3279. https://doi.org/10.1007/s11356-012-1257-6.

[18] R.S. Judson, M.T. Martin, D.M. Reif, K.A. Houck, T.B. Knudsen, D.M. Rotroff, M. Xia, S. Sakamuru, R. Huang, P. Shinn, C.P. Austin, R.J. Kavlock, D.J. Dix, Analysis of eight oil spill dispersants using rapid, in vitro tests for endocrine and other biological activity, Environ Sci Technol. 44 (2010) 5979–5985. https://doi.org/10.1021/es102150z.

[19] Y. Shi, A.M. Roy-Engel, H. Wang, Effects of Corexit Dispersants on Cytotoxicity Parameters in a Cultured Human Bronchial Airway Cells, BEAS-2B, J of Toxico and Environ Health - Part A: Current Issues. 76 (2013) 827–835. https://doi.org/10.1080/15287394.2013.821396.

[20] P.G. Wells, The iconic Torrey Canyon oil spill of 1967 - Marking its legacy, Mar Pollut Bull. 115 (2017) 1–2. https://doi.org/10.1016/j.marpolbul.2016.12.013.

[21] P. Nawavimarn, W. Rongsayamanont, T. Subsanguan, E. Luepromchai, Bio-based dispersants for fuel oil spill remediation based on the Hydrophilic-Lipophilic Deviation

(HLD) concept and Box-Behnken design, Environ Pollution. 285 (2021). https://doi.org/10.1016/j.envpol.2021.117378.

[22] E.S. Okeke, C.O. Okoye, T.P. Chidike Ezeorba, G. Mao, Y. Chen, H. Xu, C. Song, W. Feng, X. Wu, Emerging bio-dispersant and bioremediation technologies as environmentally friendly management responses toward marine oil spill: A comprehensive review, J Environ Manage. 322 (2022). https://doi.org/10.1016/j.jenvman.2022.116123.

[23] N. Das, P. Chandran, Microbial Degradation of Petroleum Hydrocarbon Contaminants: An Overview, Biotechnol Res Int. 2011 (2011) 1–13. https://doi.org/10.4061/2011/941810.

[24] P. Sharma, S. Schiewer, Assessment of crude oil biodegradation in arctic seashore sediments: effects of temperature, salinity, and crude oil concentration, Environ Sci and Poll Research. 23 (2016) 14881–14888. https://doi.org/10.1007/s11356-016-6601-9.

[25] M. Ulbricht, Advanced functional polymer membranes, Polymer. 47 (2006) 2217–2262. https://doi.org/10.1016/j.polymer.2006.01.084.

[26] G.A. Gebreslase, Review on Membranes for the Filtration of Aqueous Based Solution: Oil in Water Emulsion, J Membr Sci Technol. 08 (2018). https://doi.org/10.4172/2155-9589.1000188.

[27] X.L. Cao, F.Y. Zhou, J. Cai, Y. Zhao, M.L. Liu, L. Xu, S.P. Sun, High-permeability and anti-fouling nanofiltration membranes decorated by asymmetric organic phosphate, J Memb Sci. 617 (2021) 118667. https://doi.org/10.1016/j.memsci.2020.118667.

[28] M. Tang, K.S.S. Christie, D. Hou, C. Ding, X. Jia, J. Wang, Fabrication of a novel underwater-superoleophobic/hydrophobic composite membrane for robust anti-oil-

fouling membrane distillation by the facile breath figures templating method, J Memb Sci. 617 (2021) 118666. https://doi.org/10.1016/j.memsci.2020.118666.

[29] J. Zhang, L. Zhu, S. Zhao, D. Wang, Z. Guo, A robust and repairable copper-based superhydrophobic microfiltration membrane for high-efficiency water-in-oil emulsion separation, Sep Purif Technol. 256 (2021) 117751. https://doi.org/10.1016/j.seppur.2020.117751.

[30] M. Al-Maas, A. Hussain, J. Minier Matar, D. Ponnamma, M.K. Hassan, M. al Ali Al-Maadeed, K. Alamgir, S. Adham, Validation and application of a membrane filtration evaluation protocol for oil-water separation, J of Water Process Eng. 43 (2021) 102185. https://doi.org/10.1016/j.jwpe.2021.102185.

[31] M. Cheryan, N. Rajagopalan, Membrane processing of oily streams. Wastewater treatment and waste reduction, J Memb Sci. 151 (1998) 13–28. https://doi.org/10.1016/S0376-7388(98)00190-2.

[32] H.D. Parker, G.D. Pitt, A technical review of the principles of oil-water separation, Pollution Control Instrumentation for Oil and Effluents. (1987) 175–194. https://doi.org/10.1007/978-94-009-3233-3_7.

[33] A.-M. Abdul Aziz, A.R. Adebayo, M.E. Hossain, A sustainable approach to controlling oil spills, J Environ Manage. 113 (2012) 213–227. https://doi.org/10.1016/j.jenvman.2012.07.034.

[34] M.O. Adebajo, R.L. Frost, J.T. Kloprogge, O. Carmody, S. Kokot, Porous Materials for Oil Spills, (2003) 159–170. https://doi.org/10.1023/A:1027484117065.

[35] J. v. Mullin, M.A. Champ, Introduction/Overview to In Situ Burning of Oil Spills, Spill Science & Technology Bulletin. 8 (2003) 323–330. https://doi.org/10.1016/S1353-2561(03)00076-8.

[36] N.P. Ventikos, E. Vergetis, H.N. Psaraftis, G. Triantafyllou, A high-level synthesis of oil spill response equipment and countermeasures, J Hazard Mater. 107 (2004) 51–58. https://doi.org/10.1016/j.jhazmat.2003.11.009.

[37] R. Moosai, R.A. Dawe, Gas attachment of oil droplets for gas flotation for oily wastewater cleanup, Sep Purif Technol. 33 (2003) 303–314. https://doi.org/10.1016/s1383-5866(03)00091-1.

[38] J. Saththasivam, K. Loganathan, S. Sarp, An overview of oil–water separation using gas flotation systems, Chemosphere. 144 (2016) 671–680. https://doi.org/10.1016/j.chemosphere.2015.08.087.

[39] S.A. Nunes, H.L.F. Magalhães, R.S. Gomez, A.F. Vilela, M.J. Figueiredo, R.S. Santos, F.D. Rolim, R.A.A. Souza, S.R. de Farias Neto, A.G.B. Lima, H.L.F.; Gomez, R.S.; Vilela, A.F.; Figueiredo, M.J.; Santos, R.S.; Rolim, F.D.; Souza, R.A.A.; Farias Neto, S.R.D.; Lima, Oily Water Separation Process Using Hydrocyclone of Porous Membrane Wall: A Numerical Investigation, Membranes 11 (2021) 79. https://doi.org/10.3390/membranes11020079.

[40] R.T. Dewling, L.T. McCarthy, Chemical treatment of oil spills, Environ Int. 3 (1980) 155–162. https://doi.org/10.1016/0160-4120(80)90050-1.

[41] Oil spill treating agents, Petroleum Engineer's Guide to Oil Field Chemicals and Fluids. (2015) 695–715. https://doi.org/10.1016/B978-0-12-803734-8.00019-9.

[42] J.C. Athas, K. Jun, C. McCafferty, O. Owoseni, V.T. John, S.R. Raghavan, An effective dispersant for oil spills based on food-grade amphiphiles, Langmuir. 30 (2014) 9285–9294. https://doi.org/10.1021/la502312n.

[43] P. Venkataraman, J. Tang, E. Frenkel, G.L. McPherson, J. He, S.R. Raghavan, V. Kolesnichenko, A. Bose, V.T. John, Attachment of a hydrophobically modified biopolymer at the oil-water interface in the treatment of oil spills, ACS Appl Mater Interfaces. 5 (2013) 3572–3580. https://doi.org/10.1021/am303000v.

[44] B. Chettri, A. Mukherjee, J.S. Langpoklakpam, D. Chattopadhyay, A.K. Singh, Kinetics of nutrient enhanced crude oil degradation by *Pseudomonas aeruginosa* AKS1 and *Bacillus sp*. AKS2 isolated from Guwahati refinery, India, Environ Poll. 216 (2016) 548–558. https://doi.org/10.1016/j.envpol.2016.06.008.

[45] A.J. Pete, B. Bharti, M.G. Benton, Nano-enhanced Bioremediation for Oil Spills: A Review, ACS ES&T Engineering. 1 (2021) 928–946. https://doi.org/10.1021/acsestengg.0c00217.

[46] T.M. Tamer, B.Y. Eweida, A.M. Omer, H.M.A. Soliman, S.M. Ali, A.A. Zaatot, M.S. Mohy-Eldin, Removal of oil spills by novel amphiphilic Chitosan-g-Octanal Schiff base polymer developed by click grafting technique, Journal of Saudi Chemical Society. 25 (2021). https://doi.org/10.1016/j.jscs.2021.101369.

[47] Z. Chen, C. An, Y. Wang, B. Zhang, X. Tian, K. Lee, A green initiative for oiled sand cleanup using chitosan/rhamnolipid complex dispersion with pH-stimulus response, Chemosphere. 288 (2022). https://doi.org/10.1016/j.chemosphere.2021.132628.

[48] A. Wang, Y. Li, X. Yang, M. Bao, H. Cheng, The enhanced stability and biodegradation of dispersed crude oil droplets by Xanthan Gum as an additive of chemical dispersant, Mar Pollut Bull. 118 (2017) 275–280. https://doi.org/10.1016/j.marpolbul.2017.03.001.

[49] G. Pi, Y. Li, M. Bao, L. Mao, H. Gong, Z. Wang, Novel and Environmentally Friendly Oil Spill Dispersant Based on the Synergy of Biopolymer Xanthan Gum and Silica Nanoparticles, ACS Sustain Chem Eng. 4 (2016) 3095–3102. https://doi.org/10.1021/acssuschemeng.6b00063.

[50] B. Bolto, J. Zhang, X. Wu, Z. Xie, A Review on Current Development of Membranes for Oil Removal from Wastewaters, Membranes (Basel). 10 (2020). https://doi.org/10.3390/membranes10040065.

[51] Y. Zhu, D. Wang, L. Jiang, J. Jin, Recent progress in developing advanced membranes for emulsified oil/water separation, NPG Asia Mater. 6 (2014). https://doi.org/10.1038/am.2014.23.

[52] A.E. Mansi, S.M. El-Marsafy, Y. Elhenawy, M. Bassyouni, Assessing the potential and limitations of membrane-based technologies for the treatment of oilfield produced water, Alexandria Eng Journal. 68 (2023) 787–815. https://doi.org/10.1016/j.aej.2022.12.013.

[53] M. Padaki, R. Surya Murali, M.S. Abdullah, N. Misdan, A. Moslehyani, M.A. Kassim, N. Hilal, A.F. Ismail, Membrane technology enhancement in oil-water separation. A review, Desalination. 357 (2015) 197–207. https://doi.org/10.1016/j.desal.2014.11.023.

[54] S. Jamaly, A. Giwa, S.W. Hasan, Recent improvements in oily wastewater treatment: Progress, challenges, and future opportunities, J Environ Sci (China). 37 (2015) 15–30. https://doi.org/10.1016/j.jes.2015.04.011.

[55] S. Mondal, Polymer Nano-Composite Membranes, J Membr Sci Technol. 05 (2015) 5–6. https://doi.org/10.4172/2155-9589.1000134.

[56] J. Zhang, X. Pan, Q. Xue, D. He, L. Zhu, Q. Guo, Antifouling hydrolyzed polyacrylonitrile/graphene oxide membrane with spindle-knotted structure for highly effective separation of oil-water emulsion, J Memb Sci. 532 (2017) 38–46. https://doi.org/10.1016/j.memsci.2017.03.004.

[57] A. Pagidi, R. Saranya, G. Arthanareeswaran, A.F. Ismail, T. Matsuura, Enhanced oil–water separation using polysulfone membranes modified with polymeric additives, Desalination. 344 (2014) 280–288. https://doi.org/10.1016/j.desal.2014.03.033.

[58] T.A. Otitoju, A.L. Ahmad, B.S. Ooi, Polyvinylidene fluoride (PVDF) membrane for oil rejection from oily wastewater: A performance review, J of Water Process Eng. 14 (2016) 41–59. https://doi.org/10.1016/J.JWPE.2016.10.011.

[59] W. Chen, Y. Su, L. Zheng, L. Wang, Z. Jiang, The improved oil/water separation performance of cellulose acetate-graft-polyacrylonitrile membranes, J Memb Sci. 337 (2009) 98–105. https://doi.org/10.1016/j.memsci.2009.03.029.

[60] Y. Yang, A. Raza, F. Banat, K. Wang, The separation of oil in water (O/W) emulsions using polyether sulfone & nitrocellulose microfiltration membranes, J of Water Process Eng. 25 (2018) 113–117. https://doi.org/10.1016/j.jwpe.2018.07.007.

[61] S. Rasouli, N. Rezaei, H. Hamedi, S. Zendehboudi, X. Duan, Superhydrophobic and superoleophilic membranes for oil-water separation application: A comprehensive review, Mater Des. 204 (2021) 109599. https://doi.org/10.1016/j.matdes.2021.109599.

[62] Y. Sun, Y. Zong, N. Yang, N. Zhang, B. Jiang, L. Zhang, X. Xiao, Surface hydrophilic modification of PVDF membranes based on tannin and zwitterionic substance towards effective oil-in-water emulsion separation, Sep Purif Technol. 234 (2020) 116015. https://doi.org/10.1016/j.seppur.2019.116015.

[63] G. Wang, Y. He, H. Wang, L. Zhang, Q. Yu, S. Peng, X. Wu, T. Ren, Z. Zeng, Q. Xue, A cellulose sponge with robust superhydrophilicity and under-water superoleophobicity for highly effective oil/water separation, Green Chemistry. 17 (2015) 3093–3099. https://doi.org/10.1039/c5gc00025d.

[64] S.Z. Zakuwan, I. Ahmad, N.A. Tahrim, F. Mohamed, Functional Hydrophilic Membrane for Oil–Water Separation Based on Modified Bio-Based Chitosan–Gelatin, Polymers 2021, Vol. 13, Page 1176. 13 (2021) 1176. https://doi.org/10.3390/polym13071176.

[65] Y. Zhao, J. Lu, X. Liu, Y. Wang, J. Lin, N. Peng, J. Li, F. Zhao, Performance enhancement of polyvinyl chloride ultrafiltration membrane modified with graphene oxide, J Colloid Interface Sci. 480 (2016) 1–8. https://doi.org/10.1016/j.jcis.2016.06.075.

[66] Y. Zhang, X. Tong, B. Zhang, C. Zhang, H. Zhang, Y. Chen, Enhanced permeation and antifouling performance of polyvinyl chloride (PVC) blend Pluronic F127 ultrafiltration membrane by using salt coagulation bath (SCB), J Memb Sci. 548 (2018) 32–41. https://doi.org/10.1016/j.memsci.2017.11.003.

[67] T. Ahmad, C. Guria, A. Mandal, Optimal synthesis and operation of low-cost polyvinyl chloride/bentonite ultrafiltration membranes for the purification of oilfield produced water, J Memb Sci. 564 (2018) 859–877. https://doi.org/10.1016/j.memsci.2018.07.093.

[68] Y. Zhao, J. Lu, X. Liu, Y. Wang, J. Lin, N. Peng, J. Li, F. Zhao, Performance enhancement of polyvinyl chloride ultrafiltration membrane modified with graphene oxide, J Colloid Interface Sci. 480 (2016) 1–8. https://doi.org/10.1016/j.jcis.2016.06.075.

[69] G. Zhang, F. Gao, Q. Zhang, X. Zhan, F. Chen, Enhanced oil-fouling resistance of poly(ether sulfone) membranes by incorporation of novel amphiphilic zwitterionic copolymers, RSC Adv. 6 (2016) 7532–7543. https://doi.org/10.1039/c5ra23544h.

[70] F. Gao, G. Zhang, Q. Zhang, X. Zhan, F. Chen, Improved Antifouling Properties of Poly(Ether Sulfone) Membrane by Incorporating the Amphiphilic Comb Copolymer with Mixed Poly(Ethylene Glycol) and Poly(Dimethylsiloxane) Brushes, Ind Eng Chem Res. 54 (2015) 8789–8800. https://doi.org/10.1021/acs.iecr.5b02864.

[71] A. Mansourizadeh, A. Javadi Azad, Preparation of blend polyethersulfone/cellulose acetate/polyethylene glycol asymmetric membranes for oil-water separation, J of Pol Research. 21 (2014). https://doi.org/10.1007/s10965-014-0375-x.

[72] Y.Z. Song, X. Kong, X. Yin, Y. Zhang, C.C. Sun, J.J. Yuan, B. Zhu, L.P. Zhu, Tannin-inspired superhydrophilic and underwater superoleophobic polypropylene membrane for effective oil/water emulsions separation, Colloids Surf A Physicochem Eng Asp. 522 (2017) 585–592. https://doi.org/10.1016/j.colsurfa.2017.03.023.

[73] A.M. Kansara, S.G. Chaudhri, P.S. Singh, A facile one-step preparation method of recyclable superhydrophobic polypropylene membrane for oil-water separation, RSC Adv. 6 (2016) 61129–61136. https://doi.org/10.1039/c6ra11008h.

[74] H.C. Yang, J.K. Pi, K.J. Liao, H. Huang, Q.Y. Wu, X.J. Huang, Z.K. Xu, Silica-decorated polypropylene microfiltration membranes with a mussel-inspired intermediate layer for oil-in-water emulsion separation, ACS Appl Mater Interfaces. 6 (2014) 12566–12572. https://doi.org/10.1021/am502490j.

[75] G. Jiang, R. Hu, X. Wang, X. Xi, R. Wang, Z. Wei, X. Li, B. Tang, Preparation of superhydrophobic and superoleophilic polypropylene fibers with application in oil/water

separation, Journal of the Textile Institute. 104 (2013) 790–797. https://doi.org/10.1080/00405000.2012.757008.

[76] N.F. Himma, A.K. Wardani, I.G. Wenten, Preparation of Superhydrophobic Polypropylene Membrane Using Dip-Coating Method: The Effects of Solution and Process Parameters, Polymer - Plastics Technology and Engineering. 56 (2017) 184–194. https://doi.org/10.1080/03602559.2016.1185666.

[77] S.W. Han, K.D. Kim, H.O. Seo, I.H. Kim, C.S. Jeon, J.E. An, J.H. Kim, S. Uhm, Y.D. Kim, Oil–Water Separation Using Superhydrophobic PET Membranes Fabricated Via Simple Dip-Coating Of PDMS–SiO_2 Nanoparticles, Macromol Mater Eng. 302 (2017) 1–10. https://doi.org/10.1002/mame.201700218.

[78] C. Zhang, S. He, D. Wang, F. Xu, F. Zhang, G. Zhang, Facile fabricate a bioinspired Janus membrane with heterogeneous wettability for unidirectional water transfer and controllable oil–water separation, J Mater Sci. 53 (2018) 14398–14411. https://doi.org/10.1007/s10853-018-2659-8.

[79] P.C. Chen, Z.K. Xu, Mineral-coated polymer membranes with superhydrophilicity and underwater superoleophobicity for effective oil/water separation, Sci Rep. 3 (2013) 1–6. https://doi.org/10.1038/srep02776.

[80] P.C. Chen, L.S. Wan, Z.K. Xu, Bio-inspired $CaCO_3$ coating for superhydrophilic hybrid membranes with high water permeability, J Mater Chem. 22 (2012) 22727–22733. https://doi.org/10.1039/c2jm34203k.

[81] C.R. Crick, J.A. Gibbins, I.P. Parkin, Superhydrophobic polymer-coated copper-mesh; Membranes for highly efficient oil-water separation, J Mater Chem A Mater. 1 (2013) 5943–5948. https://doi.org/10.1039/c3ta10636e.

[82] D. Guo, K. Hou, S. Xu, Y. Lin, L. Li, X. Wen, P. Pi, Superhydrophobic–superoleophilic stainless steel meshes by spray-coating of a POSS hybrid acrylic polymer for oil–water separation, J Mater Sci. 53 (2018) 6403–6413. https://doi.org/10.1007/s10853-017-1542-3.

[83] J. Chen, K. Li, H. Zhang, J. Liu, S. Wu, Q. Fan, H. Xue, Highly Efficient and Robust Oil/Water Separation Materials Based on Wire Mesh Coated by Reduced Graphene Oxide, Langmuir. 33 (2017) 9590–9597. https://doi.org/10.1021/acs.langmuir.7b01856

[84] Y.K. Ong, N. Widjojo, T.S. Chung, Fundamentals of semi-crystalline poly(vinylidene fluoride) membrane formation and its prospects for biofuel (ethanol and acetone) separation via pervaporation, J Memb Sci. 378 (2011) 149–162. https://doi.org/10.1016/j.memsci.2011.04.037.

[85] J. Ji, F. Liu, N.A. Hashim, M.R.M. Abed, K. Li, Poly(vinylidene fluoride) (PVDF) membranes for fluid separation, React Funct Polym. 86 (2015) 134–153. https://doi.org/10.1016/j.reactfunctpolym.2014.09.023.

[86] N.G.P. Chew, S. Zhao, C. Malde, R. Wang, Superoleophobic surface modification for robust membrane distillation performance, J Memb Sci. 541 (2017) 162–173. https://doi.org/10.1016/j.memsci.2017.06.089.

[87] D. Hou, J. Wang, X. Sun, Z. Ji, Z. Luan, Preparation and properties of PVDF composite hollow fiber membranes for desalination through direct contact membrane distillation, J Memb Sci. 405–406 (2012) 185–200. https://doi.org/10.1016/j.memsci.2012.03.008.

[88] J. Wu, A. Xie, J. Yang, J. Dai, C. Li, Y. Yan, J. Cui, A facile surface modification of a PVDF membrane via $CaCO_3$ mineralization for efficient oil/water emulsion separation, New Journal of Chemistry. 44 (2020) 20999–21006. https://doi.org/10.1039/d0nj03329d.

[89] J.S. João, A.A. Ribeiro, C.X. Cardoso, Preparation and characterization of PVDF/$CaCO_3$ composites, Materials Science and Engineering: B. 136 (2007) 123–128. https://doi.org/10.1016/j.mseb.2006.09.017.

[90] Z. Zhang, W. Wang, X. Xu, X. Liu, Y. Li, P. Zhang, Enhanced morphology and hydrophilicity of PVDF flat membrane with modified $CaCO_3$@SMA additive via thermally induced phase separation method, J of Indus and Eng Chem. 107 (2022) 444–455. https://doi.org/10.1016/j.jiec.2021.12.016.

[91] J.P. Méricq, J. Mendret, S. Brosillon, C. Faur, High performance PVDF-TiO_2 membranes for water treatment, Chem Eng Sci. 123 (2015) 283–291. https://doi.org/10.1016/j.ces.2014.10.047.

[92] P. Martins, A.C. Lopes, S. Lanceros-Mendez, Electroactive phases of poly(vinylidene fluoride): Determination, processing and applications, Prog Polym Sci. 39 (2014) 683–706. https://doi.org/10.1016/j.progpolymsci.2013.07.006.

[93] K.C. Khulbe, T. Matsuura, Development of Membranes from Biobased Materials and Their Applications, Handbook of Composites from Renewable Materials. 1–8 (2017) 251–281. https://doi.org/10.1002/9781119441632.ch92.

[94] J.E. Lee, Y.E. Shin, G.H. Lee, J. Kim, H. Ko, H.G. Chae, Polyvinylidene fluoride (PVDF)/cellulose nanocrystal (CNC) nanocomposite fiber and triboelectric textile sensors, Compos B Eng. 223 (2021). https://doi.org/10.1016/j.compositesb.2021.109098.

[95] M. Rincón-Iglesias, E. Lizundia, D.M. Correia, C.M. Costa, S. Lanceros-Méndez, The role of CNC surface modification on the structural, thermal and electrical properties of poly(vinylidene fluoride) nanocomposites, Cellulose. 27 (2020) 3821–3834. https://doi.org/10.1007/s10570-020-03067-z.

[96] E. Barnes, J.A. Jefcoat, E.M. Alberts, M.A. McKechnie, H.R. Peel, J.P. Buchanan, C.A. Weiss, K.L. Klaus, L. Christopher Mimun, C.M. Warner, Effect of Cellulose Nanofibrils and TEMPO-mediated Oxidized Cellulose Nanofibrils on the Physical and Mechanical Properties of Poly(vinylidene fluoride)/Cellulose Nanofibril Composites, Polymers 2019, 11 (2019) 1091. https://doi.org/10.3390/polym11071091.

[97] J. Lv, G. Zhang, H. Zhang, C. Zhao, F. Yang, Improvement of antifouling performances for modified PVDF ultrafiltration membrane with hydrophilic cellulose nanocrystal, Appl Surf Sci. 440 (2018) 1091–1100. https://doi.org/10.1016/j.apsusc.2018.01.256.

[98] H.M. Mousa, H.S. Fahmy, R. Abouzeid, G.T. Abdel-Jaber, W.Y. Ali, Polyvinylidene fluoride-cellulose nanocrystals hybrid nanofiber membrane for energy harvesting and oil-water separation applications, Mater Lett. 306 (2022). https://doi.org/10.1016/j.matlet.2021.130965.

[99] X. Huang, W. Wang, Y. Liu, H. Wang, Z. Zhang, W. Fan, L. Li, Treatment of oily waste water by PVP grafted PVDF ultrafiltration membranes, Chem Eng Journal. 273 (2015) 421–429. https://doi.org/10.1016/j.cej.2015.03.086.

[100] M. Obaid, H.O. Mohamed, A.S. Yasin, M.A. Yassin, O.A. Fadali, H.Y. Kim, N.A.M. Barakat, Under-oil superhydrophilic wetted PVDF electrospun modified membrane for continuous gravitational oil/water separation with outstanding flux, Water Res. 123 (2017) 524–535. https://doi.org/10.1016/j.watres.2017.06.079.

[101] T. Li, F. Liu, S. Zhang, H. Lin, J. Wang, C.Y. Tang, Janus Polyvinylidene Fluoride Membrane with Extremely Opposite Wetting Surfaces via One Single-Step Unidirectional Segregation Strategy, ACS Appl Mater Interfaces. 10 (2018) 24947–24954. https://doi.org/10.1021/acsami.8b08278.

[102] L. Yan, S. Hong, M.L. Li, Y.S. Li, Application of the Al_2O_3–PVDF nanocomposite tubular ultrafiltration (UF) membrane for oily wastewater treatment and its antifouling research, Sep Purif Technol. 66 (2009) 347–352. https://doi.org/10.1016/j.seppur.2008.12.015.

[103] J. Kong, K. Li., Oil removal from oil-in-water emulsions using PVDF membranes, Sep Purif Technol. 16 (1999) 83–93. https://doi.org/10.1016/S1383-5866(98)00114-2.

[104] N. Zhang, N. Yang, L. Zhang, B. Jiang, Y. Sun, J. Ma, K. Cheng, F. Peng, Facile hydrophilic modification of PVDF membrane with Ag/EGCG decorated micro/nanostructural surface for efficient oil-in-water emulsion separation, Chem Eng Journal. 402 (2020) 126200. https://doi.org/10.1016/j.cej.2020.126200.

[105] F. Ejaz Ahmed, B.S. Lalia, N. Hilal, R. Hashaikeh, Underwater superoleophobic cellulose/electrospun PVDF–HFP membranes for efficient oil/water separation, Desalination. 344 (2014) 48–54. https://doi.org/10.1016/j.desal.2014.03.010.

[106] C.S. Ong, W.J. Lau, P.S. Goh, B.C. Ng, A.F. Ismail, Investigation of submerged membrane photocatalytic reactor (sMPR) operating parameters during oily wastewater treatment process, Desalination. 353 (2014) 48–56. https://doi.org/10.1016/j.desal.2014.09.008.

[107] K. Valizadeh, A. Heydarinasab, S.S. Hosseini, S. Bazgir, Preparation of modified membrane of polyvinylidene fluoride (PVDF) and evaluation of anti-fouling features and high capability in water/oil emulsion separation, J Taiwan Inst Chem Eng. 126 (2021) 36–49. https://doi.org/10.1016/j.jtice.2021.07.018.

[108] S. Zhang, R. Wang, S. Zhang, G. Li, Y. Zhang, Treatment of wastewater containing oil using phosphorylated silica nanotubes (PSNTs)/polyvinylidene fluoride (PVDF)

composite membrane, Desalination. 332 (2014) 109–116. https://doi.org/10.1016/j.desal.2013.11.008.

[109] X. Zeng, J. Lin, W. Cai, Q. Lu, S. Fu, J. Li, X. Yan, X. Wen, C. Zhou, M. Zhang, Fabrication of superhydrophilic PVDF membranes by one-step modification with eco-friendly phytic acid and polyethyleneimine complex for oil-in-water emulsions separation, Chemosphere. 264 (2021) 128395. https://doi.org/10.1016/j.chemosphere.2020.128395.

[110] Y. Zhang, P. Liu, Preparation of porous ZrO_2 solid superacid shell/void/TiO_2 core particles and effect of doping them on PVDF membranes properties, Chem Eng Sci. 135 (2015) 67–75. https://doi.org/10.1016/j.ces.2015.06.037.

[111] Y. Zhang, M. Cui, Porous YxFeyZr1−x−yO_2 coated TiO_2 solid superacid particles/PVDF hybrid membranes with anti-fouling property, Chem Eng Journal. 301 (2016) 342–352. https://doi.org/10.1016/j.cej.2016.05.002.

[112] F. Chen, X. Shi, X. Chen, W. Chen, An iron (II) phthalocyanine/poly(vinylidene fluoride) composite membrane with antifouling property and catalytic self-cleaning function for high-efficiency oil/water separation, J Memb Sci. 552 (2018) 295–304. https://doi.org/10.1016/j.memsci.2018.02.030.

[113] T. di Pan, Z.J. Li, D.H. Shou, W. Shou, J.T. Fan, X. Liu, Y. Liu, Buoyancy Assisted Janus Membrane Preparation by ZnO Interfacial Deposition for Water Pollution Treatment and Self-cleaning, Adv Mater Interfaces. 6 (2019) 1901130. https://doi.org/10.1002/admi.201901130.

[114] F.U. Ahmed, D. Dhar Purkayastha, PVDF@ZnO membrane for its potential application in oil/water separation, Mater Today Proc. 68 (2022) 177–180. https://doi.org/10.1016/j.matpr.2022.07.236.

[115] Y. Zhu, F. Zhang, D. Wang, X.F. Pei, W. Zhang, J. Jin, A novel zwitterionic polyelectrolyte grafted PVDF membrane for thoroughly separating oil from water with ultrahigh efficiency, J Mater Chem A Mater. 1 (2013) 5758–5765. https://doi.org/10.1039/c3ta01598j.

[116] L. Rao, X. You, B. Chen, L. Shen, Y. Xu, M. Zhang, H. Hong, R. Li, H. Lin, A novel composite membrane for simultaneous separation and catalytic degradation of oil/water emulsion with high performance, Chemosphere. 288 (2022) 132490. https://doi.org/10.1016/j.chemosphere.2021.132490.

[117] P.D. Sutrisna, P.C.B.W. Mustika, R.P. Hadi, Caren, Y.E. Gani, Improved oily wastewater rejection and flux of hydrophobic PVDF membrane after polydopamine-polyethyleneimine co-deposition and modification, S Afr J Chem Eng. 44 (2023) 42–50. https://doi.org/10.1016/j.sajce.2023.01.006.

[118] B.S. Lalia, V. Kochkodan, R. Hashaikeh, N. Hilal, A review on membrane fabrication: Structure, properties and performance relationship, Desalination. 326 (2013) 77–95. https://doi.org/10.1016/j.desal.2013.06.016.

[119] K. Boussu, B. van der Bruggen, C. Vandecasteele, Evaluation of self-made nanoporous polyethersulfone membranes, relative to commercial nanofiltration membranes, Desalination. 200 (2006) 416–418. https://doi.org/10.1016/j.desal.2006.03.353.

[120] Douglas R. Lloyd, Microporus Membrane fromation via thermally induced phase separation, J of Mem Sci. 52 (1990) 239–261. https://doi.org/10.1016/S0376-7388(00)85130-3.

[121] P.D. Graham, A.J. Pervan, A.J. McHugh, The Dynamics of Thermal-Induced Phase Separation in PMMA Solutions, Macromolecules. 30 (1997) 1651–1655. https://doi.org/10.1021/ma961720m.

[122] H. Matsuyama, T. Iwatani, Formation of porous poly (ethylene-co-vinyl alcohol) membrane via thermally induced phase separation, J of Appl Sci. 79 (2001) 2449–2455. https://doi.org/10.1002/1097-4628(20010328)79

[123] R. Pervin, P. Ghosh, M.G. Basavaraj, Tailoring pore distribution in polymer films via evaporation induced phase separation, RSC Adv. 9 (2019) 15593–15605. https://doi.org/10.1039/c9ra01331h.

[124] T. Pasman, D. Baptista, S. van Riet, R.K. Truckenmüller, P.S. Hiemstra, R.J. Rottier, D. Stamatialis, A.A. Poot, Development of Porous and Flexible PTMC Membranes for In Vitro Organ Models Fabricated by Evaporation-Induced Phase Separation, Membranes 10 (2020), 330. https://doi.org/10.3390/membranes10110330.

[125] J. Jia, M. Zhou, D. Liu, M. Li, G. Kang, Y. Cao, Study on two-stage stretching strategy for microstructure improvement of polytetrafluoroethylene hollow fiber membrane, J Appl Polym Sci. 139 (2022) 52216. https://doi.org/10.1002/app.52216.

[126] J. Jia, G. Kang, Y. Cao, Effect of Stretching Parameters on Structure and Properties of Polytetrafluoroethylene Hollow-Fiber Membranes, Chem Eng Technol. 39 (2016) 935–944. https://doi.org/10.1002/ceat.201500690.

[127] F. Tasselli, Membrane Preparation Techniques, Encyclopedia of Membranes. (2014) 1–3. https://doi.org/10.1007/978-3-642-40872-4_1825-1.

[128] X.M. Tan, D. Rodrigue, A Review on Porous Polymeric Membrane Preparation. Part I: Production Techniques with Polysulfone and Poly (Vinylidene Fluoride), Polymers (Basel). 11 (2019). https://doi.org/10.3390/polym11071160.

[129] S. Liu, K. Li, R. Hughes, Preparation of porous aluminium oxide (Al_2O_3) hollow fibre membranes by a combined phase-inversion and sintering method, Ceram Int. 29 (2003) 875–881. https://doi.org/10.1016/S0272-8842(03)00030-0.

[130] S. Remanan, M. Sharma, S. Bose, N.C. Das, Recent Advances in Preparation of Porous Polymeric Membranes by Unique Techniques and Mitigation of Fouling through Surface Modification, Chemistry Select. 3 (2018) 609–633. https://doi.org/10.1002/slct.201702503.

[131] J.A. Lockwood, Nuclear Tracks in Solids (Principles and Applications), Nucl Technol. 30 (1976) 91–92. https://doi.org/10.13182/nt76-a31631.

[132] L.D. Tijing, Y.C. Woo, M. Yao, J. Ren, H.K. Shon, 1.16 Electrospinning for Membrane Fabrication: Strategies and Applications, 2017. https://doi.org/10.1016/b978-0-12-409547-2.12262-0.

[133] P.D. Sutrisna, K.A. Kurnia, U.W.R. Siagian, S. Ismadji, I.G. Wenten, Membrane fouling and fouling mitigation in oil–water separation: A review, J Environ Chem Eng. 10 (2022) 107532. https://doi.org/10.1016/j.jece.2022.107532.

[134] N. Nikooe, E. Saljoughi, Preparation and characterization of novel PVDF nanofiltration membranes with hydrophilic property for filtration of dye aqueous solution, Appl Surf Sci. 413 (2017) 41–49. https://doi.org/10.1016/j.apsusc.2017.04.029.

[135] H.B. Madalosso, R. Machado, D. Hotza, C. Marangoni, Membrane Surface Modification by Electrospinning, Coating, and Plasma for Membrane Distillation Applications: A State-of-the-Art Review, Adv Eng Mater. 23 (2021) 2001456. https://doi.org/10.1002/adem.202001456.

[136] M.C. Cruz, G. Ruano, M. Wolf, D. Hecker, E. Castro Vidaurre, R. Schmittgens, V.B. Rajal, Plasma deposition of silver nanoparticles on ultrafiltration membranes: antibacterial and anti-biofouling properties, Chem Eng Res Des. 94 (2015) 524. https://doi.org/10.1016/j.cherd.2014.09.014.

[137] H.B. Madalosso, R. Machado, D. Hotza, C. Marangoni, Membrane Surface Modification by Electrospinning, Coating, and Plasma for Membrane Distillation Applications: A State-of-the-Art Review, Adv Eng Mater. 23 (2021). https://doi.org/10.1002/adem.202001456.

[138] L. Tjale, H. Richards, O. Mahlangu, L.N. Nthunya, Silica nanoparticle modified polysulfone/polypropylene membrane for separation of oil-water emulsions, Results in Engineering. 16 (2022) 100623. https://doi.org/10.1016/j.rineng.2022.100623.

[139] Y. Yang, W. Fu, L. Chen, C. Hou, X. Chen, X. Zhang, One-step dip-coating method for preparation of ceramic nanofiber membrane with high permeability and low cost, J Eur Ceram Soc. 41 (2021) 358–368. https://doi.org/10.1016/j.jeurceramsoc.2021.09.049.

[140] M. Ebrahim Imanian, M. Kardan-Halvaei, F. Nasrollahi, al, Q. Dai, S. Maloney, W. Chen, P.T. P Aryanti, G. Trilaksono, A. Hotmaida, M.A. Afifah, F.P. Pratiwi, N. Udini, F.A. Nugroho, A. Yani, J. Ters Jend Sudirman, Preparation of Polypropylene/PVDF Composite Membrane by Dip-Coating Method, IOP Conf Ser Mater Sci Eng. 1115 (2021) 012028. https://doi.org/10.1088/1757-899x/1115/1/012028.

[141] N.F. Himma, A.K. Wardani, I.G. Wenten, Preparation of Superhydrophobic Polypropylene Membrane Using Dip-Coating Method: The Effects of Solution and Process Parameters, 56 (2016) 184–194. https://doi.org/10.1080/03602559.2016.1185666.

[142] G.S. Lai, W.J. Lau, P.S. Goh, M. Karaman, M. Gürsoy, A.F. Ismail, Development of thin film nanocomposite membrane incorporated with plasma enhanced chemical vapor deposition-modified hydrous manganese oxide for nanofiltration process, Compos B Eng. 176 (2019) 107328. https://doi.org/10.1016/j.compositesb.2019.107328.

[143] G. de Filpo, E. Pantuso, K. Armentano, P. Formoso, G. di Profio, T. Poerio, E. Fontananova, C. Meringolo, A.I. Mashin, F.P. Nicoletta, Chemical Vapor Deposition of Photocatalyst Nanoparticles on PVDF Membranes for Advanced Oxidation Processes, Membranes (Basel). 8 (2018). https://doi.org/10.3390/membranes8030035.

[144] M.C. Cruz, G. Ruano, M. Wolf, D. Hecker, E. Castro Vidaurre, R. Schmittgens, V.B. Rajal, Plasma deposition of silver nanoparticles on ultrafiltration membranes: antibacterial and anti-biofouling properties, Chem Eng Res Des. 94 (2015) 524. https://doi.org/10.1016/j.cherd.2014.09.014.

[145] H. AbdAllah, M.S. Shalaby, A.M.H. Shaban, Performance and Characterization for Blend Membrane of PES with Manganese (III) Acetylacetonate as Metalorganic Nanoparticles, Int J of Chem Eng. 2015 (2015). https://doi.org/10.1155/2015/896486.

[146] Y. Wen, J. Yuan, X. Ma, S. Wang, Y. Liu, Polymeric nanocomposite membranes for water treatment: a review, Environmental Chemistry Letters 2019 17:4. 17 (2019) 1539–1551. https://doi.org/10.1007/S10311-019-00895-9.

[147] L. Xia, B. Vemuri, S. Saptoka, N. Shrestha, G. Chilkoor, J. Kilduff, V. Gadhamshetty, Antifouling Membranes for Bioelectrochemistry Applications, Biomass, Biofuels, Biochemicals: Microbial Electrochemical Technology: Sustainable Platform for Fuels, Chemicals and Remediation. (2019) 195–224. https://doi.org/10.1016/B978-0-444-64052-9.00008-x.

[148] D.L. Zhao, W.S. Yeung, Q. Zhao, T.S. Chung, Thin-film nanocomposite membranes incorporated with UiO-66-NH_2 nanoparticles for brackish water and seawater desalination, J Memb Sci. 604 (2020) 118039. https://doi.org/10.1016/j.memsci.2020.118039.

[149] A. Bottino, G. Capannelli, V. D'Asti, P. Piaggio, Preparation and properties of novel organic-inorganic porous membranes, Sep Purif Technol. 22–23 (2001) 269–275. https://doi.org/10.1016/S1383-5866(00)00127-1.

[150] T.H. Bae, T.M. Tak, Effect of TiO_2 nanoparticles on fouling mitigation of ultrafiltration membranes for activated sludge filtration, J Memb Sci. 249 (2005) 1–8. https://doi.org/10.1016/j.memsci.2004.09.008.

[151] E.C. Mapunda, B.B. Mamba, T.A.M. Msagati, Carbon nanotube embedded PVDF membranes: Effect of solvent composition on the structural morphology for membrane distillation, Physics and Chemistry of the Earth. 100 (2017) 135–142. https://doi.org/10.1016/j.pce.2017.01.003.

[152] A. Abdel-Karim, J.M. Luque-Alled, S. Leaper, M. Alberto, X. Fan, A. Vijayaraghavan, T.A. Gad-Allah, A.S. El-Kalliny, G. Szekely, S.I.A. Ahmed, S.M. Holmes, P. Gorgojo, PVDF membranes containing reduced graphene oxide: Effect of degree of reduction on membrane distillation performance, Desalination. 452 (2019) 196–207. https://doi.org/10.1016/j.desal.2018.11.014.

[153] J.H. Li, X.S. Shao, Q. Zhou, M.Z. Li, Q.Q. Zhang, The double effects of silver nanoparticles on the PVDF membrane: Surface hydrophilicity and antifouling performance, Appl Surf Sci. 265 (2013) 663–670. https://doi.org/10.1016/j.apsusc.2012.11.072.

[154] P. Jian, H. Yahui, W. Yang, L. Linlin, Preparation of polysulfone-Fe3O4 composite ultrafiltration membrane and its behavior in magnetic field, J Memb Sci. 284 (2006) 9–16. https://doi.org/10.1016/j.memsci.2006.07.052.

[155] A. Bottino, G. Capannelli, A. Comite, Preparation and characterization of novel porous PVDF-ZrO_2 composite membranes, Desalination. 146 (2002) 35–40. https://doi.org/10.1016/s0011-9164(02)00469-1.

[156] L. Yan, Y.S. Li, C.B. Xiang, S. Xianda, Effect of nano-sized Al_2O_3-particle addition on PVDF ultrafiltration membrane performance, J Memb Sci. 276 (2006) 162–167. https://doi.org/10.1016/j.memsci.2005.09.044.

[157] N. Wald, Poly(ethylene oxide)/cellulose-nanocrystal nanocomposites as polymer electrolyte membranes, Master Degree Thesis. (2012).

[158] Y. Huang, H. Li, L. Wang, Y. Qiao, C. Tang, C. Jung, Y. Yoon, S. Li, M. Yu, Ultrafiltration Membranes with Structure-Optimized Graphene-Oxide Coatings for Antifouling Oil/Water Separation, Adv Mater Interfaces. 2 (2015). https://doi.org/10.1002/admi.201400433.

[159] F. Guo, C. Zhang, Q. Wang, W. Hu, J. Cao, J. Yao, L. Jiang, Z. Wu, Modification of poly(vinylidene fluoride) membranes with aluminum oxide nanowires and graphene oxide nanosheets for oil–water separation, J Appl Polym Sci. 136 (2019) 47493. https://doi.org/10.1002/app.47493.

[160] J.A. Prince, S. Bhuvana, V. Anbharasi, N. Ayyanar, K.V.K. Boodhoo, G. Singh, Ultra-wetting graphene-based PES ultrafiltration membrane – A novel approach for successful oil-water separation, Water Res. 103 (2016) 311–318. https://doi.org/10.1016/j.watres.2016.07.042.

[161] Y. Song, J. Lang, J. Guo, Q. Zhang, Q. Han, H. Fan, M. Gao, M. Wei, J. Yang, Z. Sheng, Preparation of carbon cloth membrane with visible light induced self-cleaning performance for oil-water separation, Surf Coat Technol. 403 (2020) 126372. https://doi.org/10.1016/j.surfcoat.2020.126372.

[162] D. Zioui, H. Salazar, L. Aoudjit, P.M. Martins, S. Lanceros-Méndez, Polymer-Based Membranes for Oily Wastewater Remediation, Polymers, 12 (2019) 42. https://doi.org/10.3390/polym12010042.

[163] S.A.D.A.V. Sumithraarachchi, B.D.K.K. Thilakarathna, J. Bandara, TiO_2 encapsulated cross-linked polystyrene-polyacrylic acid membranes for waste oil-water separation, J Environ Chem Eng. 9 (2021) 105394. https://doi.org/10.1016/j.jece.2021.105394.

[164] Z. Xiong, H. Lin, Y. Zhong, Y. Qin, T. Li, F. Liu, Robust superhydrophilic polylactide (PLA) membranes with a TiO_2 nano-particle inlaid surface for oil/water separation, J Mater Chem A Mater. 5 (2017) 6538–6545. https://doi.org/10.1039/c6ta11156d.

[165] Z. Lu, Q. Zia, J. Meng, T. Liu, J. Song, J. Li, Hierarchical porous poly(l-lactic acid)/SiO_2 nanoparticles fibrous membranes for oil/water separation, J Mater Sci. 55 (2020) 16096–16110. https://doi.org/10.1007/S10853-020-05115-2.

[166] Q. Zeng, P. Ma, X. Su, D. Lai, X. Lai, X. Zeng, H. Li, Facile fabrication of superhydrophobic and magnetic poly(lactic acid) nonwoven fabric for oil-water separation, Ind Eng Chem Res. 59 (2020) 9127–9135. https://doi.org/10.1021/acs.iecr.0c01033.

[167] H.M. Mousa, H. Alfadhel, M. Ateia, G.T. Abdel-Jaber, G.A. A, Polysulfone-iron acetate/polyamide nanocomposite membrane for oil-water separation, Environ Nanotechnol Monit Manag. 14 (2020) 100314. https://doi.org/10.1016/j.enmm.2020.100314.

[168] I.S. Al-Husaini, A.R.M. Yusoff, W.J. Lau, A.F. Ismail, M.Z. Al-Abri, M.D.H. Wirzal, Iron oxide nanoparticles incorporated polyethersulfone electrospun nanofibrous membranes for effective oil removal, Chem Eng Research and Design. 148 (2019) 142–154. https://doi.org/10.1016/j.cherd.2019.06.006.

[169] M. Ouda, Y. Ibrahim, F. Banat, S.W. Hasan, Oily wastewater treatment via phase-inverted polyethersulfone-maghemite (PES/γ-Fe_2O_3) composite membranes, J of Water Process Eng. 37 (2020) 101545. https://doi.org/10.1016/j.jwpe.2020.101545.

[170] R.J. Moon, A. Martini, J. Nairn, J. Simonsen, J. Youngblood, Cellulose nanomaterials review: structure, properties and nanocomposites, 2011. https://doi.org/10.1039/c0cs00108b.

[171] Y. Habibi, Key advances in the chemical modification of nanocelluloses, Chem. Soc. Rev. 43 (2014) 1519–1542. https://doi.org/10.1039/c3cs60204d.

[172] Alexis Wells Carpenter, Charles François de Lannoy, Mark R. Wiesner, Cellulose Nanomaterials in Water Treatment Technologies Alexis, Environ Sci Technol. 49 (2015) 209–220. https://doi.org/10.1021/es506351r.

[173] J.-J. Wang, H.-C. Yang, M.-B. Wu, X. Zhang, Z.-K. Xu, Nanofiltration membranes with cellulose nanocrystals as an interlayer for unprecedented performance, J. Mater. Chem. A. 5 (2017) 16289–16295. https://doi.org/10.1039/c7ta00501f.

[174] H. Chang, A.-T. Chien, H.C. Liu, P.-H. Wang, B.A. Newcomb, S. Kumar, Gel Spinning of Polyacrylonitrile/Cellulose Nanocrystal Composite Fibers, ACS Biomater Sci Eng. 1 (2015) 610–616. https://doi.org/10.1021/acsbiomaterials.5b00161.

[175] S. S. Nair, A.P. Mathew, Porous composite membranes based on cellulose acetate and cellulose nanocrystals via electrospinning and electrospraying, Carbohydr Polym. 175 (2017) 149–157. https://doi.org/10.1016/j.carbpol.2017.07.048.

[176] J. Zhou, J. Chen, M. He, J. Yao, Cellulose acetate ultrafiltration membranes reinforced by cellulose nanocrystals: Preparation and characterization, J Appl Polym Sci. 133 (2016) 1–7. https://doi.org/10.1002/app.43946.

[177] Z. Zhang, Q. Wu, K. Song, S. Ren, T. Lei, Q. Zhang, Using cellulose nanocrystals as a sustainable additive to enhance hydrophilicity, mechanical and thermal properties of poly(vinylidene fluoride)/poly(methyl methacrylate) blend, ACS Sustain Chem Eng. 3 (2015) 574–582. https://doi.org/10.1021/sc500792c.

[178] P. Qu, H. Tang, Y. Gao, L.P. Zhang, S. Wang, Polyethersulfone composite membrane blended with cellulose fibrils, Bioresources. 5 (2010) 2323–2336. https://doi.org/10.1016/j.sbspro.2014.01.1130.

[179] D. Trache, M.H. Hussin, M.K.M. Haafiz, V.K. Thakur, Recent progress in cellulose nanocrystals: Sources and production, Nanoscale. 9 (2017) 1763–1786. https://doi.org/10.1039/c6nr09494e.

[180] P. Dhar, V. Katiyar, Thermal degradation kinetics of polylactic acid / acid fabricated cellulose nanocrystal based bionanocomposites, Int J Biol Macromol. 104 (2017) 827–836. https://doi.org/10.1016/j.ijbiomac.2017.06.039.

[181] N. Rajendran, T. Runge, R.D. Bergman, P. Nepal, C. Houtman, Techno-economic analysis and life cycle assessment of cellulose nanocrystals production from wood pulp, Bioresour Technol. 377 (2023). https://doi.org/10.1016/j.biortech.2023.128955.

[182] H. Bai, X. Wang, Y. Zhou, L. Zhang, Preparation and characterization of poly(vinylidene fluoride) composite membranes blended with nano-crystalline cellulose, Progress in Natural Science: Materials International. 22 (2012) 250–257. https://doi.org/10.1016/j.pnsc.2012.04.011.

[183] Z. Karim, A.P. Mathew, M. Grahn, J. Mouzon, K. Oksman, Nanoporous membranes with cellulose nanocrystals as functional entity in chitosan: Removal of dyes from water, Carbohydr Polym. 112 (2014) 668–676. https://doi.org/10.1016/j.carbpol.2014.06.048.

[184] S. Huang, M.B. Wu, C.Y. Zhu, M.Q. Ma, J. Yang, J. Wu, Z.K. Xu, Polyamide Nanofiltration Membranes Incorporated with Cellulose Nanocrystals for Enhanced Water Flux and Chlorine Resistance, ACS Sustain Chem Eng. 7 (2019) 12315–12322. https://doi.org/10.1021/acssuschemeng.9b01651.

[185] M.B. Wu, C. Zhang, J.K. Pi, C. Liu, J. Yang, Z.K. Xu, Cellulose nanocrystals as anti-oil nanomaterials for separating crude oil from aqueous emulsions and mixtures, J Mater Chem A Mater. 7 (2019) 7033–7041. https://doi.org/10.1039/c9ta00420c.

[186] M. Jonoobi, A. Ashori, V. Siracusa, Characterization and properties of polyethersulfone/ modified cellulose nanocrystals nanocomposite membranes, Polym Test. 76 (2019) 333–339. https://doi.org/10.1016/j.polymertesting.2019.03.039.

[187] J.J. Wang, H.C. Yang, M.B. Wu, X. Zhang, Z.K. Xu, Nanofiltration membranes with cellulose nanocrystals as an interlayer for unprecedented performance, J Mater Chem A Mater. 5 (2017) 16289–16295. https://doi.org/10.1039/c7ta00501f.

[188] A. Adeniyi, D. Gonzalez-ortiz, C. Pochat-bohatier, S. Mbakop, M.S. Onyango, Preparation of Nanofiltration Membrane Modified with Sawdust-Derived Cellulose Nanocrystals for Removal of Nitrate from Drinking Water, Membranes (Basel). 12 (2022). https://doi.org/10.3390/membranes12070670.

[189] J. Liu, D. Liu, S. Liu, Z. Li, X. Wei, S. Lin, M. Guo, Preparation and Characterization of Sulfated Cellulose Nanocrystalline and its Composite Membrane for Removal of Tetracycline Hydrochloride in Water, Energy & Environmental Materials. 3 (2020) 209–215. https://doi.org/10.1002/eem2.12055.

[190] C. Xu, W. Chen, H. Gao, X. Xie, Y. Chen, Cellulose nanocrystal/silver (CNC/Ag) thin-film nanocomposite nanofiltration membranes with multifunctional properties, Environ Sci Nano. 7 (2020) 803–816. https://doi.org/10.1039/c9en01367a.

[191] L. Bai, H. Wu, J. Ding, A. Ding, X. Zhang, N. Ren, G. Li, H. Liang, Cellulose nanocrystal-blended polyethersulfone membranes for enhanced removal of natural organic matter and alleviation of membrane fouling, Chem Eng Journal. 382 (2020) 122919. https://doi.org/10.1016/j.cej.2019.122919.

[192] A. Adeniyi, D. Gonzalez-Ortiz, C. Pochat-Bohatier, O. Oyewo, B. Sithole, M. Onyango, Incorporation of Cellulose Nanocrystals (CNC) derived from sawdust into polyamide thin-film composite membranes for enhanced water recovery, Alexandria Engineering Journal. 59 (2020) 4201–4210. https://doi.org/10.1016/j.aej.2020.07.025.

[193] M.L. Hassan, S.M. Fadel, R.E. Abouzeid, W.S. Abou Elseoud, E.A. Hassan, L. Berglund, K. Oksman, Water purification ultrafiltration membranes using nanofibers from unbleached and bleached rice straw, Sci Rep. 10 (2020) 11278. https://doi.org/10.1038/S41598-020-67909-3.

[194] J.C. Jackson, C.H.M. Camargos, V.T. Noronha, A.J. Paula, C.A. Rezende, A.F. Faria, Sustainable Cellulose Nanocrystals for Improved Antimicrobial Properties of Thin Film Composite Membranes, ACS Sustain Chem Eng. 9 (2021) 6534–6540. https://doi.org/10.1021/acssuschemeng.1c02389.

[195] D. Xia, M. Zhang, C. Tong, Z. Wang, H. Liu, L. Zhu, In-situ incorporating zwitterionic nanocellulose into polyamide nanofiltration membrane towards excellent perm-selectivity and antifouling performances, Desalination. 521 (2022) 115397. https://doi.org/10.1016/j.desal.2021.115397.

[196] B.S. Lalia, E. Guillen, H.A. Arafat, R. Hashaikeh, Nanocrystalline cellulose reinforced PVDF-HFP membranes for membrane distillation application, Desalination. 332 (2014) 134–141. https://doi.org/10.1016/j.desal.2013.10.030.

[197] B.S. Lalia, Y.A. Samad, R. Hashaikeh, Nanocrystalline-cellulose-reinforced poly(vinylidenefluoride-co-hexafluoropropylene) nanocomposite films as a separator for lithium ion batteries, J Appl Polym Sci. 126 (2012). https://doi.org/10.1002/app.36783.

[198] H. Voisin, L. Bergström, P. Liu, A.P. Mathew, Nanocellulose-based materials for water purification, Nanomaterials. 7 (2017). https://doi.org/10.3390/nano7030057.

[199] L. Kong, D. Zhang, Z. Shao, B. Han, Y. Lv, K. Gao, X. Peng, Superior effect of TEMPO-oxidized cellulose nanofibrils (TOCNs) on the performance of cellulose triacetate (CTA) ultrafiltration membrane, Desalination. 332 (2014) 117–125. https://doi.org/10.1016/j.desal.2013.11.005.

[200] R. Yang, K.K. Gleason, Ultrathin antifouling coatings with stable surface zwitterionic functionality by initiated chemical vapor deposition (iCVD), Langmuir. 28 (2012) 12266–12274. https://doi.org/10.1021/la302059s.

[201] K.T. Huang, S.B. Yeh, C.J. Huang, Surface Modification for Superhydrophilicity and Underwater Superoleophobicity: Applications in Antifog, Underwater Self-Cleaning, and Oil-Water Separation, ACS Appl Mater Interfaces. 7 (2015) 21021–21029. https://doi.org/10.1021/acsami.5b07362.

[202] C. Ao, W. Yuan, J. Zhao, X. He, X. Zhang, Q. Li, T. Xia, W. Zhang, C. Lu, Superhydrophilic graphene oxide electrospun cellulose nanofiber hybrid membrane for high-efficiency oil/water separation, Carbohydr Polym. 175 (2017) 216–222. https://doi.org/10.1016/j.carbpol.2017.07.085.

[203] W. Kolff, H. Berk, M. Welle, The artificial kidney: A dialyzer with a great area, Acta Med Scand. 117 (1944) 121–134. https://doi.org/10.1016/s0140-6736(14)60870-9.

[204] H.D. Humes, W.H. Fissell, K. Tiranathanagul, The future of hemodialysis membranes, Kidney Int. 69 (2006) 1115–1119. https://doi.org/10.1038/sj.ki.5000204.

[205] H. Ramakrishna, Extracorporeal circulation-from cardiopulmonary bypass to extracorporeal membrane oxygenation and mechanical cardiac assist device therapy: A constant evolution, Ann Card Anaesth. 18 (2015) 133. https://doi.org/10.4103/0971-9784.154460.

[206] A. Arefin, J.H. Huang, D. Platts, V.D. Hypes, J.F. Harris, R. Iyer, P. Nath, Fabrication of flexible thin polyurethane membrane for tissue engineering applications, Biomed Microdevices. 19 (2017). https://doi.org/10.1007/s10544-017-0236-6.

[207] L. de Bartolo, Membrane Bioartificial Organs, in: E. Drioli, L. Giorno (Eds.), Encyclopedia of Membranes, Springer Berlin Heidelberg, Berlin, Heidelberg, 2015: pp. 1–2. https://doi.org/10.1007/978-3-642-40872-4_355-3.

[208] A.F. Jozala, D.C. Geraldes, L.L. Tundisi, V. de A. Feitosa, C.A. Breyer, S.L. Cardoso, P.G. Mazzola, L. de Oliveira-Nascimento, C. de O. Rangel-Yagui, P. de O. Magalhães, M.A. de Oliveira, A. Pessoa, Biopharmaceuticals from microorganisms: from production to purification, Brazilian Journal of Microbiology. 47 (2016) 51–63. https://doi.org/10.1016/j.bjm.2016.10.007.

[209] N. Li, T. Fane, Advanced Membrane Technology and Applications, 2008. https://doi.org/10.1007/s13398-014-0173-7.2.

[210] S. Wang, Q. Feng, J. Sun, F. Gao, W. Fan, Z. Zhang, X. Li, X. Jiang, Nanocrystalline cellulose improves the biocompatibility and reduces the wear debris of ultrahigh molecular weight polyethylene via weak binding, ACS Nano. 10 (2016) 298–306. https://doi.org/10.1021/acsnano.5b04393.

[211] N. Ferraz, D.O. Carlsson, J. Hong, R. Larsson, B. Fellstrom, L. Nyholm, M. Stromme, A. Mihranyan, Haemocompatibility and ion exchange capability of nanocellulose polypyrrole membranes intended for blood purification, J R Soc Interface. 9 (2012) 1943–1955. https://doi.org/10.1098/rsif.2012.0019.

[212] N. Lin, A. Gèze, D. Wouessidjewe, J. Huang, A. Dufresne, Biocompatible Double-Membrane Hydrogels from Cationic Cellulose Nanocrystals and Anionic Alginate as Complexing Drugs Codelivery, ACS Appl Mater Interfaces. (2016). https://doi.org/10.1021/acsami.6b00555.

[213] Z.Q. Huang, F. Zheng, Z. Zhang, H.T. Xu, K.M. Zhou, The performance of the PVDF-Fe_3O_4 ultrafiltration membrane and the effect of a parallel magnetic field used during the membrane formation, Desalination. 292 (2012) 64–72. https://doi.org/10.1016/j.desal.2012.02.010.

[214] Y. Huang, C. fa Xiao, Q. lin Huang, H. liang Liu, J. qiang Hao, L. Song, Magnetic field induced orderly arrangement of Fe_3O_4/GO composite particles for preparation of Fe_3O_4/GO/PVDF membrane, J Memb Sci. 548 (2018) 184–193. https://doi.org/10.1016/j.memsci.2017.11.027.

[215] S. Zinadini, A.A.L. Zinatizadeh, M. Rahimi, V. Vatanpour, Magnetic field-augmented coagulation bath during phase inversion for preparation of $ZnFe_2O_4$/SiO_2/PES

nanofiltration membrane: A novel method for flux enhancement and fouling resistance, J of Indus and Eng Chem. 46 (2017) 9–18. https://doi.org/10.1016/j.jiec.2016.08.005.

[216] H. Zeb, M.A. Hussain, I. Ahmed, M.S. Akram, B. Haider, R. Haider, Z. bin Babar, R.M. Saleem, A. Ahsan, I. Aziz, M. Arif, Study of bleaching of old newsprint recycled paper: reproduction of newspaper material, Mater Res Express. 8 (2021) 085305. https://doi.org/10.1088/2053-1591/ac1ca9.

[217] E. Peşman, M. Parlak, Recycling of colored office paper. Part II: Post bleaching with formamidine sulfinic acid and hydrogen peroxide, Bioresources. 13 (2019) 4841–4855. https://doi.org/10.15376/biores.13.3.4841-4855.

[218] P. Dhar, S.M. Bhasney, A. Kumar, V. Katiyar, Acid functionalized cellulose nanocrystals and its effect on mechanical, thermal, crystallization and surfaces properties of poly (lactic acid) bionanocomposites films: A comprehensive study, Polymer. 101 (2016) 75–92. https://doi.org/10.1016/j.polymer.2016.08.028.

[219] A.K. Pal, V. Katiyar, Nanoamphiphilic Chitosan Dispersed Poly (lactic acid) Bionanocomposite Films with Improved Thermal, Mechanical, and Gas Barrier Properties, 17, 8, (2016) 2603–2618. https://doi.org/10.1021/acs.biomac.6b00619.

[220] J.E. Clarridge 3rd, Impact of 16S rRNA gene sequence analysis for identification of bacteria on clinical microbiology and infectious diseases, Clin Microbiol Rev. 17 (2004) 840–862. https://doi.org/10.1128/cmr.17.4.840-862.2004.

[221] A.C. Darby, S.M. Chandler, S.C. Welburn, A.E. Douglas, Aphid-Symbiotic Bacteria Cultured in Insect Cell Lines, Appl Environ Microbiol. 71 (2005) 4833–4839. https://doi.org/10.1128/aem.71.8.4833-4839.2005.

[222] S.F. Altschul, W. Gish, W. Miller, E.W. Myers, D.J. Lipman, Basic local alignment search tool, J Mol Biol. 215 (1990) 403–410. https://doi.org/https://doi.org/10.1016/s0022-2836(05)80360-2.

[223] D.J. States, W. Gish, S.F. Altschul, Improved sensitivity of nucleic acid database searches using application-specific scoring matrices, Methods. 3 (1991) 66–70. https://doi.org/https://doi.org/10.1016/S1046-2023(05)80165-3.

[224] N. Saitou, M. Nei, The neighbor-joining method: a new method for reconstructing phylogenetic trees., Mol Biol Evol. 4 (1987) 406–425. https://doi.org/10.1093/oxfordjournals.molbev.a040454.

[225] K. Tamura, G. Stecher, D. Peterson, A. Filipski, S. Kumar, MEGA6: Molecular Evolutionary Genetics Analysis version 6.0, Mol Biol Evol. 30 (2013) 2725–2729. https://doi.org/10.1093/molbev/mst197.

[226] J. Dasgupta, S. Chakraborty, J. Sikder, R. Kumar, D. Pal, S. Curcio, E. Drioli, The effects of thermally stable titanium silicon oxide nanoparticles on structure and performance of cellulose acetate ultrafiltration membranes, Sep Purif Technol. 133 (2014) 55–68. https://doi.org/10.1016/j.seppur.2014.06.035.

[227] S. Shenvi, A.F. Ismail, A.M. Isloor, Enhanced Permeation Performance of Cellulose Acetate Ultrafiltration Membranes by Incorporation of Sulfonated Poly (1,4- phenylene ether ether sulfone) and Poly (styrene-co-maleic anhydride), Ind. Eng. Chem. Res., 53, 35, (2014) 13820–13827. https://doi.org/10.1021/ie502310e.

[228] E.W. Washburn, E.W. Washburn, Note on a Method of Determining the Distribution of Pore Sizes in a Porous Material, Proc Natl Acad Sci U S A. 7 (1921) 115. https://doi.org/10.1073/pnas.7.4.115.

[229] T. Ghosh, K. Nakano, V. Katiyar, Curcumin doped functionalized cellulose nanofibers based edible chitosan coating on kiwifruits, Int J Biol Macromol. 184 (2021) 936–945. https://doi.org/10.1016/j.ijbiomac.2021.06.098.

[230] C. Trilokesh, & Kiran, B. Uppuluri, Isolation and characterization of cellulose nanocrystals from jackfruit peel. Scientific Reports 9, (2019) 16709. https://doi.org/10.1038/s41598-019-53412-x.

[231] M.M. Aji, S. Narendren, M.K. Purkait, V. Katiyar, Biopolymer (gum arabic) incorporation in waste polyvinylchloride membrane for the enhancement of hydrophilicity and natural organic matter removal in water, Journal of Water Process Engineering. 38 (2020) 101569. https://doi.org/10.1016/j.jwpe.2020.101569.

[232] F. Lessan, M. Karimi, J.L. Bañuelos, R. Foudazi, Phase separation and performance of polyethersulfone/cellulose nanocrystals membranes, Polymer. 186 (2020). https://doi.org/10.1016/j.polymer.2019.121969.

[233] X. Zhao, Y. Lan, K. Yang, R. Wang, L. Cheng, C. Gao, Antifouling modification of PVDF membranes via in situ mixed-charge copolymerization and TiO_2 mineralization, Appl Surf Sci. 525 (2020) 1–9. https://doi.org/10.1016/j.apsusc.2020.146564.

[234] Z. Chen, G. Chen, H. Xie, Z. Xu, Y. Li, J. Wan, L. Liu, H. Mao, Photocatalytic antifouling properties of novel PVDF membranes improved by incorporation of SnO_2-GO nanocomposite for water treatment, Sep Purif Technol. (2020) 118184. https://doi.org/10.1016/j.seppur.2020.118184.

[235] C. Igathinathane, L.O. Pordesimo, E.P. Columbus, W.D. Batchelor, S.R. Methuku, Shape identification and particles size distribution from basic shape parameters using ImageJ, Comput Electron Agric. 63 (2008) 168–182. https://doi.org/10.1016/j.compag.2008.02.007.

[236] A. Kondyli, W. Schrader, High-resolution GC/MS studies of a light crude oil fraction, Journal of Mass Spectrometry. 54 (2019) 47–54. https://doi.org/10.1002/jms.4306.

[237] R.E. Correa Pabón, C.R. de Souza Filho, Crude oil spectral signatures and empirical models to derive API gravity, Fuel. 237 (2019) 1119–1131. https://doi.org/10.1016/j.fuel.2018.09.098.

[238] B. Oyeneyin, Introduction to the Hydrocarbon Composite Production System, Developments in Petroleum Science. 63 (2015) 11–128. https://doi.org/10.1016/B978-0-444-62637-0.00002-6.

[239] N.K. Kalita, M.K. Nagar, C. Mudenur, A. Kalamdhad, V. Katiyar, Biodegradation of modified Poly(lactic acid) based biocomposite films under thermophilic composting conditions, Polym Test. 76 (2019) 522–536. https://doi.org/https://doi.org/10.1016/j.polymertesting.2019.02.021.

[240] N.K. Kalita, S.M. Bhasney, C. Mudenur, A. Kalamdhad, V. Katiyar, End-of-life evaluation and biodegradation of Poly(lactic acid) (PLA)/Polycaprolactone (PCL)/Microcrystalline cellulose (MCC) polyblends under composting conditions, Chemosphere. 247 (2020) 125875. https://doi.org/https://doi.org/10.1016/j.chemosphere.2020.125875.

[241] S. Faria, C.L. de Oliveira Petkowicz, S.A.L. de Morais, M.G.H. Terrones, M.M. de Resende, F.P. de Frana, V.L. Cardoso, Characterization of xanthan gum produced from sugar cane broth, Carbohydr Polym. 86 (2011) 469–476. https://doi.org/10.1016/j.carbpol.2011.04.063.

[242] B. Gaweł, M. Eftekhardadkhah, G. Øye, Elemental composition and fourier transform infrared spectroscopy analysis of crude oils and their fractions, Energy and Fuels. 28 (2014) 997–1003. https://doi.org/10.1021/ef402286y.

[243] S. Kumar, V. Mahto, Emulsification of Indian heavy crude oil in water for its efficient transportation through offshore pipelines, Chem Eng Research and Design. 115 (2016) 34–43. https://doi.org/10.1016/j.cherd.2016.09.017.

[244] L. v. Castro, F. Vazquez, Fractionation and characterization of Mexican crude oils, in: Energy and Fuels, (2009) 1603–1609. https://doi.org/10.1021/ef8008508.

[245] M. Asemani, A.R. Rabbani, Detailed FTIR spectroscopy characterization of crude oil extracted asphaltenes: Curve resolve of overlapping bands, J Pet Sci Eng. 185 (2020) 106618. https://doi.org/10.1016/j.petrol.2019.106618.

[246] A.K. Pal, S.K. Bhattacharjee, S.S. Gaur, A. Pal, V. Katiyar, Chemomechanical, morphological, and rheological studies of chitosan-graft-lactic acid oligomer reinforced poly(lactic acid) bionanocomposite films, J Appl Polym Sci. 135 (2018). https://doi.org/10.1002/app.45546.

[247] H.S. El-Sheshtawy, M.M. Doheim, Selection of Pseudomonas aeruginosa for biosurfactant production and studies of its antimicrobial activity, Egyptian Journal of Petroleum. 23 (2014) 1–6. https://doi.org/10.1016/j.ejpe.2014.02.001.

[248] W. Sun, W. Cao, M. Jiang, G. Saren, J. Liu, J. Cao, I. Ali, X. Yu, C. Peng, I. Naz, Isolation and characterization of biosurfactant-producing and diesel oil degrading Pseudomonas sp. CQ2 from Changqing oil field, China, RSC Adv. 8 (2018) 39710–39720. https://doi.org/10.1039/c8ra07721e.

[249] F. Guo, D. de Lima Stebbins, R.G. Toomey, N.A. Alcantar, Interfacial Phenomena of Natural Dispersants for Crude Oil Spills, Langmuir. 35 (2019) 15904–15913. https://doi.org/10.1021/acs.langmuir.9b02036.

[250] A.B. Abeer Mohammed, A.A. Tayel, N.M. Elguindy, Production of new rhamnolipids Rha C16-C16 by Burkholderia sp. through biodegradation of diesel and biodiesel, Beni Suef Univ J Basic Appl Sci. 7 (2018) 492–498. https://doi.org/10.1016/j.bjbas.2018.05.003.

[251] G. Pi, L. Mao, M. Bao, Y. Li, H. Gong, J. Zhang, Preparation of Oil-in-Seawater Emulsions Based on Environmentally Benign Nanoparticles and Biosurfactant for Oil Spill Remediation, ACS Sustain Chem Eng. 3 (2015) 2686–2693. https://doi.org/10.1021/acssuschemeng.5b00516.

[252] P. Thakur, N.K. Saini, V.K. Thakur, V.K. Gupta, R. v. Saini, A.K. Saini, Rhamnolipid the Glycolipid Biosurfactant: Emerging trends and promising strategies in the field of biotechnology and biomedicine, Microb Cell Fact. 20 (2021). https://doi.org/10.1186/s12934-020-01497-9.

[253] J.Y. Zhu, U.P. Agarwal, Nanocellulose: Native State, Production, and Characterization, in: L. Hu, F. Jiang, C. Chen (Eds.), Emerging Nanotechnologies in Nanocellulose, Springer International Publishing, Cham, (2023) 1–39. https://doi.org/10.1007/978-3-031-14043-3_1.

[254] Q.Q. Wang, J.Y. Zhu, R.S. Reiner, S.P. Verrill, U. Baxa, S.E. McNeil, Approaching zero cellulose loss in cellulose nanocrystal (CNC) production: Recovery and characterization of cellulosic solid residues (CSR) and CNC, Cellulose. 19 (2012) 2033–2047. https://doi.org/10.1007/s10570-012-9765-6

[255] L. Chen, Q. Wang, K. Hirth, C. Baez, U.P. Agarwal, J.Y. Zhu, Tailoring the yield and characteristics of wood cellulose nanocrystals (CNC) using concentrated acid hydrolysis, Cellulose 22(2015)1753–1762. https://doi.org/10.1007/S10570-015-0615-1.

[256] H. Deng, Q. Chen, F. Xie, C. Zhao, J. Pan, Q. Cheng, C. Zhang, Castor oil-based waterborne polyurethane/tunicate cellulose nanocrystals nanocomposites for wearable strain sensors, Carbohydr Polym. (2022) 120313. https://doi.org/10.1016/j.carbpol.2022.120313.

[257] E.J. Foster, R.J. Moon, U.P. Agarwal, M.J. Bortner, J. Bras, S. Camarero-Espinosa, K.J. Chan, M.J.D. Clift, E.D. Cranston, S.J. Eichhorn, D.M. Fox, W.Y. Hamad, L. Heux, B. Jean, M. Korey, W. Nieh, K.J. Ong, M.S. Reid, S. Renneckar, R. Roberts, J.A. Shatkin, J. Simonsen, K. Stinson-Bagby, N. Wanasekara, J. Youngblood, Current characterization methods for cellulose nanomaterials, Chem Soc Rev. 47 (2018) 2609–2679. https://doi.org/10.1039/c6cs00895j.

[258] S.J. Eichhorn, A. Etale, J. Wang, L.A. Berglund, Y. Li, Y. Cai, C. Chen, E.D. Cranston, M.A. Johns, Z. Fang, G. Li, L. Hu, M. Khandelwal, K.Y. Lee, K. Oksman, S. Pinitsoontorn, F. Quero, A. Sebastian, M.M. Titirici, Z. Xu, S. Vignolini, B. Frka-Petesic, Current international research into cellulose as a functional nanomaterial for advanced applications, J of Mat Sci. 57 (2022) 5697–5767. https://doi.org/10.1007/s10853-022-06903-8.

[259] A. Etale, A.J. Onyianta, S.R. Turner, S.J. Eichhorn, Cellulose: A Review of Water Interactions, Applications in Composites, and Water Treatment, Chem Rev. (2022), 2016–2048. https://doi.org/10.1021/acs.chemrev.2c00477.

[260] Y. Yu, H. Wu, Significant differences in the hydrolysis behavior of amorphous and crystalline portions within microcrystalline cellulose in hot-compressed water, Ind Eng Chem Res. 49 (2010) 3902–3909. https://doi.org/10.1021/ie901925g.

[261] P. Dhar, S. Narendren, S.S. Gaur, S. Sharma, A. Kumar, V. Katiyar, Self-propelled cellulose nanocrystal based catalytic nanomotors for targeted hyperthermia and

pollutant remediation applications, Int J Biol Macromol. 158 (2020) 1020–1036. https://doi.org/10.1016/j.ijbiomac.2020.04.204.

[262] J. Li, L. Zhou, Y. Song, X. Yu, X. Li, Y. Liu, Z. Zhang, Y. Yuan, S. Yan, J. Zhang, Green fabrication of porous microspheres containing cellulose nanocrystal/MnO_2 nanohybrid for efficient dye removal, Carbohydr Polym. 270 (2021) 118340. https://doi.org/10.1016/j.carbpol.2021.118340.

[263] P. Boruah, P. Dhar, V. Katiyar, Nanocellulose-based composites for applications as catalysts and pollutant remediation, Cellulose Nanocrystals. (2020) 229–278. https://doi.org/10.1515/9783110648010-008.

[264] N. Mohammed, N. Grishkewich, K.C. Tam, Cellulose nanomaterials: promising sustainable nanomaterials for application in water/wastewater treatment processes, Environ Sci Nano. 5 (2018) 623–658. https://doi.org/10.1039/c7en01029j.

[265] L. Chen, J.Y. Zhu, C. Baez, P. Kitin, T. Elder, Highly thermal-stable and functional cellulose nanocrystals and nanofibrils produced using fully recyclable organic acids, Green Chemistry. 18 (2016) 3835–3843. https://doi.org/10.1039/c6gc00687f.

[266] A. Sheikhi, S. Safari, H. Yang, T.G.M. van de Ven, Copper removal using electrosterically stabilized nanocrystalline cellulose, ACS Appl Mater Interfaces. 7 (2015) 11301–11308. https://doi.org/10.1021/acsami.5b01619

[267] K.O. Agenson, T. Urase, Change in membrane performance due to organic fouling in nanofiltration (NF)/reverse osmosis (RO) applications, Sep Purif Technol. 55 (2007) 147–156. https://doi.org/10.1016/j.seppur.2006.11.010.

[268] L. Upadhyaya, X. Qian, S. Ranil Wickramasinghe, Chemical modification of membrane surface overview, Curr Opin Chem Eng. 20 (2018) 13–18. https://doi.org/10.1016/j.coche.2018.01.002.

[269] M. Gryta, Surface modification of polypropylene membrane by helium plasma treatment for membrane distillation, J Memb Sci. 628 (2021) 119265. https://doi.org/10.1016/j.memsci.2021.119265.

[270] X.J. Lee, P.L. Show, T. Katsuda, W.H. Chen, J.S. Chang, Surface grafting techniques on the improvement of membrane bioreactor: State-of-the-art advances, Bioresour Technol. 269 (2018) 489–502. https://doi.org/10.1016/j.biortech.2018.08.090.

[271] S.S. Sana, V.R. Badineni, S.K. Arla, V.K.N. Boya, Hydrophilic–hydrophobic polymer based blend membrane for separation of water–isopropanol mixtures by pervaporation, SN Appl Sci. 2 (2020) 1–10. https://doi.org/10.1007/S42452-020-03700-3.

[272] Y.L. Ji, M.J. Yin, Q.F. An, C.J. Gao, Recent developments in polymeric nano-based separation membranes, Fundamental Research. 2 (2022) 254–267. https://doi.org/10.1016/j.fmre.2021.11.029.

[273] S.S. Latthe, R.S. Sutar, T.B. Shinde, S.B. Pawar, T.M. Khot, A.K. Bhosale, K.K. Sadasivuni, R. Xing, L. Mao, S. Liu, Superhydrophobic Leaf Mesh Decorated with SiO_2 Nanoparticle-Polystyrene Nanocomposite for Oil-Water Separation, ACS Appl Nano Mater. 2 (2019) 799–805. https://doi.org/10.1021/acsanm.8b02021.

[274] X. Yi, Y. Zhu, D. Wang, F. Yang, Y. Wang, W. Shi, Adsorption Mechanism of Oil-in-Water on a TiO_2/Al_2O_3-Polyvinylidene Fluoride (PVDF) Ultrafiltration Membrane, Langmuir. 34 (2018) 9907–9916. https://doi.org/10.1021/acs.langmuir.8b01222.

[275] P. Kaspar, D. Sobola, K. Částková, R. Dallaev, E. Šťastná, P. Sedlák, A. Knápek, T. Trčka, V. Holcman, Case study of polyvinylidene fluoride doping by carbon nanotubes, Materials. 14 (2021). https://doi.org/10.3390/ma14061428.

[276] T. Wu, B. Zhou, T. Zhu, J. Shi, Z. Xu, C. Hu, J. Wang, Facile and low-cost approach towards a PVDF ultrafiltration membrane with enhanced hydrophilicity and antifouling performance via graphene oxide/water-bath coagulation, RSC Adv. 5 (2015) 7880–7889. https://doi.org/10.1039/c4ra13476a.

[277] H.S. Barud, T. Regiani, R.F.C. Marques, W.R. Lustri, Y. Messaddeq, S.J.L. Ribeiro, Antimicrobial bacterial cellulose-silver nanoparticles composite membranes, J Nanomater. 2011 (2011). https://doi.org/10.1155/2011/721631.

[278] W. Yu, M. Brown, N.J.D. Graham, Prevention of PVDF ultrafiltration membrane fouling by coating MnO_2 nanoparticles with ozonation, Sci Rep. 6 (2016) 1–12. https://doi.org/10.1038/srep30144.

[279] A. Razmjou, J. Mansouri, V. Chen, The effects of mechanical and chemical modification of TiO_2 nanoparticles on the surface chemistry, structure and fouling performance of PES ultrafiltration membranes, J Memb Sci. 378 (2011) 73–84. https://doi.org/10.1016/j.memsci.2010.10.019.

[280] G. Zhang, J. Lv, F. Yang, Optimized anti-biofouling performance of bactericides/cellulose nanocrystals composites modified PVDF ultrafiltration membrane for micro-polluted source water purification, Water Sci and Tech. 79 (2019) 1437–1446. https://doi.org/10.2166/wst.2019.137.

[281] M. Nuruddin, J. Hamlin, C.M. Clarkson, J.A. Howarter, C.R. Szczepanski, J.P. Youngblood, Processing and Characterization of Food-Grade Plasticizer-Compatibilized Cellulose Nanocrystals and Ethylene Vinyl Alcohol Copolymer

Nanocomposites, ACS Appl Polym Mater. 3 (2021) 5000–5011. https://doi.org/10.1021/acsapm.1c00756.

[282] C. Gomri, M. Cretin, M. Semsarilar, Recent progress on chemical modification of cellulose nanocrystal (CNC) and its application in nanocomposite films and membranes-A comprehensive review, Carbohydr Polym. 294 (2022) 119790. https://doi.org/10.1016/j.carbpol.2022.119790.

[283] W. Lei, C. Fang, X. Zhou, Q. Yin, S. Pan, R. Yang, D. Liu, Y. Ouyang, Cellulose nanocrystals obtained from office waste paper and their potential application in PET packing materials, Carbohydr Polym. 181 (2018) 376–385. https://doi.org/10.1016/j.carbpol.2017.10.059.

[284] M.G. Aguayo, A.F. Pérez, G. Reyes, C. Oviedo, W. Gacitúa, R. Gonzalez, O. Uyarte, Isolation and characterization of cellulose nanocrystals from rejected fibers originated in the Kraft Pulping process, Polymers (Basel). 10 (2018). https://doi.org/10.3390/polym10101145.

[285] S. Manandhar, B. Shrestha, F. Sciortino, K. Ariga, L.K. Shrestha, Recycling Waste Paper for Further Implementation: XRD, FTIR, SEM, and EDS Studies, J Oleo Sci. 71 (2022) 619–626. https://doi.org/10.5650/jos.ess21396.

[286] Inamuddin, H. Abbas Kashmery, Polyvinylidene fluoride/sulfonated graphene oxide blend membrane coated with polypyrrole/platinum electrode for ionic polymer metal composite actuator applications, Sci Rep. 9 (2019) 1–11. https://doi.org/10.1038/s41598-019-46305-6.

[287] M.N. Tamaño-Machiavello, C.M. Costa, J. Molina-Mateo, C. Torregrosa-Cabanilles, J.M. Meseguer-Dueñas, S.N. Kalkura, S. Lanceros-Méndez, R. Sabater I Serra, J.L.G. Ribelles, Phase morphology and crystallinity of poly(vinylidene fluoride)/ poly(ethylene

oxide) piezoelectric blend membranes. Mater. Today Commun. 4 (2015) 214-221. https://doi.org/10.1016/j.mtcomm.2015.08.003

[288] J. Li, Q. Meng, W. Li, Z. Zhang, Influence of crystalline properties on the dielectric and energy storage properties of poly(vinylidene fluoride), J Appl Polym Sci. 122 (2011) 1659–1668. https://doi.org/10.1002/app.34020.

[289] X. Cai, T. Lei, D. Sun, L. Lin, A critical analysis of the α, β and γ phases in poly(vinylidene fluoride) using FTIR, RSC Adv. 7 (2017) 15382–15389. https://doi.org/10.1039/c7ra01267e.

[290] A. Kamtsikakis, G. Delepierre, C. Weder, Cellulose nanocrystals as a tunable nanomaterial for pervaporation membranes with asymmetric transport properties, J Memb Sci. 635 (2021). https://doi.org/10.1016/j.memsci.2021.119473.

[291] Z. Zhang, Q. Wu, K. Song, T. Lei, Y. Wu, Poly(vinylidene fluoride)/cellulose nanocrystals composites: rheological, hydrophilicity, thermal and mechanical properties, Cellulose. 22 (2015) 2431–2441. https://doi.org/10.1007/s10570-015-0634-y.

[292] J. Lv, G. Zhang, H. Zhang, F. Yang, Exploration of permeability and antifouling performance on modified cellulose acetate ultrafiltration membrane with cellulose nanocrystals, Carbohydr Polym. 174 (2017) 190–199. https://doi.org/10.1016/j.carbpol.2017.06.064.

[293] A. Leszczyńska, P. Radzik, E. Szefer, M. Mičušík, M. Omastová, K. Pielichowski, Surface modification of cellulose nanocrystals with succinic anhydride, Polymers (Basel). 11 (2019). https://doi.org/10.3390/polym11050866.

[294] M. Pan, X. Zhou, M. Chen, Cellulose nanowhiskers isolation and properties from acid hydrolysis combined with high pressure homogenization," BioRes. 8(1) (2013), 933-943.

[295] M. Mohammadi Ghaleni, A. al Balushi, S. Kaviani, E. Tavakoli, M. Bavarian, S. Nejati, Fabrication of Janus Membranes for Desalination of Oil-Contaminated Saline Water, ACS Appl Mater Interfaces. 10 (2018) 44871–44879. https://doi.org/10.1021/acsami.8b16621.

[296] E. Lizundia, A. Reizabal, C.M. Costa, A. Maceiras, S. Lanceros-Méndez, Electroactive γ-Phase, Enhanced Thermal and Mechanical Properties and High Ionic Conductivity Response of Poly (Vinylidene Fluoride)/Cellulose Nanocrystal Hybrid Nanocomposites, Materials. 13 (2020). https://doi.org/10.3390/ma13030743.

[297] F. Sun, W. Liu, Z. Dong, Y. Deng, Underwater superoleophobicity cellulose nanofibril aerogel through regioselective sulfonation for oil/water separation, Chemical Engineering Journal. 330 (2017) 774–782. https://doi.org/10.1016/j.cej.2017.07.142.

[298] P. Sukitpaneenit, T.S. Chung, Molecular elucidation of morphology and mechanical properties of PVDF hollow fiber membranes from aspects of phase inversion, crystallization and rheology, J Memb Sci. 340 (2009) 192–205. https://doi.org/10.1016/j.memsci.2009.05.029.

[299] S. Zhang, R. Wang, S. Zhang, G. Li, Y. Zhang, Development of phosphorylated silica nanotubes (PSNTs)/polyvinylidene fluoride (PVDF) composite membranes for wastewater treatment, Chem Eng Journal. 230 (2013) 260–271. https://doi.org/10.1016/j.cej.2013.06.098.

[300] S. Zhang, R. Wang, S. Zhang, G. Li, Y. Zhang, Treatment of wastewater containing oil using phosphorylated silica nanotubes (PSNTs)/polyvinylidene fluoride (PVDF)

composite membrane, Desalination. 332 (2014) 109–116. https://doi.org/10.1016/j.desal.2013.11.008.

[301] Z. Cui, Y. Cheng, K. Xu, J. Yue, Y. Zhou, X. Li, Q. Wang, S.P. Sun, Y. Wang, X. Wang, Z. Wang, Wide liquid-liquid phase separation region enhancing tensile strength of poly(vinylidene fluoride) membranes via TIPS method with a new diluent, Polymer. 141 (2018) 46–53. https://doi.org/10.1016/j.polymer.2018.02.054.

[302] W. Wang, X. Xu, Z. Zhang, P. Zhang, Y. Shi, P. Ding, Study on the improvement of PVDF flat ultrafiltration membrane with MWCNTs-OH as the additive and the influence of different MWCNTs-OH scales, Colloid Interface Sci Commun. 43 (2021) 100433. https://doi.org/10.1016/j.colcom.2021.100433.

[303] H. Gong, H. Pang, M. Du, Z. Chen, Fabrication of a superhydrophobic mixed matrix PVDF-SiO_2-HDTMS hollow fiber membrane for membrane contact carbon dioxide absorption, Clean Eng Technol. 5 (2021) 100278. https://doi.org/10.1016/j.clet.2021.100278.

[304] Q. Xu, Y. Chen, T. Xiao, X. Yang, A Facile Method to Control Pore Structure of PVDF/SiO_2 Composite Membranes for Efficient Oil/Water Purification, Membranes, 11 (2021) 803. https://doi.org/10.3390/membranes11110803.

[305] M.S. Nasution, A. Mataram, I. Yani, G.D. Septano, Characteristics of a PVDF-Tin Dioxide Membrane Assisted by Electric Field Treatment, Membranes, 12 (2022) 772. https://doi.org/10.3390/membranes12080772.

[306] K. Wang, A.A. Abdalla, M.A. Khaleel, N. Hilal, M.K. Khraisheh, Mechanical properties of water desalination and wastewater treatment membranes, Desalination. 401 (2017) 190–205. https://doi.org/10.1016/j.desal.2016.06.032.

[307] S. Rajesh, K.H. Shobana, S. Anitharaj, D.R. Mohan, Preparation, morphology, performance, and hydrophilicity studies of poly(amide-imide) incorporated cellulose acetate ultrafiltration membranes, Ind Eng Chem Res. 50 (2011) 5550–5564. https://doi.org/10.1021/ie1019613.

[308] M. Pinto, P.S.F. Ramalho, N.F.F. Moreira, A.G. Gonçalves, O.C. Nunes, M.F.R. Pereira, O.S.G.P. Soares, Application of magnetic nanoparticles for water purification, Environmental Advances. 2 (2020) 100010. https://doi.org/10.1016/j.envadv.2020.100010.

[309] M. Gui, J.K. Papp, A.S. Colburn, N.D. Meeks, B. Weaver, I. Wilf, D. Bhattacharyya, Engineered Iron/Iron Oxide Functionalized Membranes for Selenium and Other Toxic Metal Removal from Power Plant Scrubber Water, J Memb Sci. 488 (2015) 79. https://doi.org/10.1016/j.memsci.2015.03.089.

[310] I. Koyuncu, B. Yavuzturk Gul, M.S. Esmaeili, E. Pekgenc, O. Orhun Teber, G. Tuncay, H. Karimi, S. Parvaz, A. Maleki, V. Vatanpour, Modification of PVDF membranes by incorporation Fe_3O_4@Xanthan gum to improve anti-fouling, anti-bacterial, and separation performance, J Environ Chem Eng. 10 (2022) 107784. https://doi.org/10.1016/j.jece.2022.107784.

[311] S. Palchoudhury, J.R. Lead, A facile and cost-effective method for separation of oil-water mixtures using polymer-coated iron oxide nanoparticles, Environ Sci Technol. 48 (2014) 14558–14563. https://doi.org/10.1021/es5037755.

[312] S.M. Moatmed, M.H. Khedr, S.I. El-Dek, H.Y. Kim, A.G. El-Deen, Highly efficient and reusable superhydrophobic/superoleophilic polystyrene@ Fe_3O_4 nanofiber membrane for high-performance oil/water separation, J Environ Chem Eng. 7 (2019) 103508. https://doi.org/10.1016/j.jece.2019.103508.

[313] W. Yu, L. Xu, N. Graham, J. Qu, Contribution of Fe_3O_4 nanoparticles to the fouling of ultrafiltration with coagulation pre-treatment, Scientific Reports 2015 5:1. 5 (2015) 1–13. https://doi.org/10.1038/srep13067.

[314] X. Yang, Y. Liu, S. Hu, F. Yu, Z. He, G. Zeng, Z. Feng, A. Sengupta, Construction of Fe_3O_4@MXene composite nanofiltration membrane for heavy metal ions removal from wastewater, Polym Adv Technol. 32 (2021) 1000–1010. https://doi.org/10.1002/pat.5148.

[315] L. Li, F. Wang, Y. Lv, J. Liu, D. Zhang, Z. Shao, Halloysite nanotubes and Fe_3O_4 nanoparticles enhanced adsorption removal of heavy metal using electrospun membranes, Appl Clay Sci. 161 (2018) 225–234. https://doi.org/10.1016/j.clay.2018.04.002.

[316] T.A. Aragaw, F.M. Bogale, B.A. Aragaw, Iron-based nanoparticles in wastewater treatment: A review on synthesis methods, applications, and removal mechanisms, Journal of Saudi Chemical Society. 25 (2021) 101280. https://doi.org/10.1016/j.jscs.2021.101280.

[317] Z.H. Huang, X. Zhang, Y.X. Wang, J.Y. Sun, H. Zhang, W.L. Liu, M.P. Li, X.H. Ma, Z.L. Xu, Fe_3O_4/PVDF catalytic membrane treatment organic wastewater with simultaneously improved permeability, catalytic property and anti-fouling, Environ Res. 187 (2020) 109617. https://doi.org/10.1016/j.envres.2020.109617.

[318] W.F. Elmobarak, F. Almomani, Application of magnetic nanoparticles for the removal of oil from oil-in-water emulsion: Regeneration/reuse of spent particles, J Pet Sci Eng. 203 (2021) 108591. https://doi.org/10.1016/j.petrol.2021.108591.

[319] S. Mirshahghassemi, B. Cai, J.R. Lead, Evaluation of polymer-coated magnetic nanoparticles for oil separation under environmentally relevant conditions: effect of

ionic strength and natural organic macromolecules, Environ Sci Nano. 3 (2016) 780–787. https://doi.org/10.1039/c5en00282f.

[320] N.S.M. Nawi, W.J. Lau, N. Yusof, A.F. Ismail, The Impacts of Iron Oxide Nanoparticles on Membrane Properties for Water and Wastewater Applications: a Review, Arabian Journal for Science and Engineering. 47 (2021) 5443–5464. https://doi.org/10.1007/s13369-021-06373-1.

[321] A. Rabajczyk, M. Zielecka, K. Cygańczuk, Ł. Pastuszka, L. Jurecki, Nanometals-Containing Polymeric Membranes for Purification Processes, Materials. 14 (2021) 1–30. https://doi.org/10.3390/ma14030513.

[322] M.G. Aguayo, A.F. Pérez, G. Reyes, C. Oviedo, W. Gacitúa, R. Gonzalez, O. Uyarte, Isolation and Characterization of Cellulose Nanocrystals from Rejected Fibers Originated in the Kraft Pulping Process. 10 (2018) 1145. https://doi.org/10.3390/polym10101145.

[323] A. G. Nene, M. Takahashi, P. R. Somani, Fe_3O_4 and Fe Nanoparticles by Chemical Reduction of $Fe(acac)_3$ by Ascorbic Acid: Role of Water, World Journal of Nano Science and Engineering. 06 (2016) 20–28. https://doi.org/10.4236/wjnse.2016.61002.

[324] G. Bhargava, I. Gouzman, C.M. Chun, T.A. Ramanarayanan, S.L. Bernasek, Characterization of the “native” surface thin film on pure polycrystalline iron: A high resolution XPS and TEM study, Appl Surf Sci. 253 (2007) 4322–4329. https://doi.org/10.1016/j.apsusc.2006.09.047.

[325] N.T.T. Van, A.N. Phan, V.C. Cuong, N.T.T. Van, H.G.T. Thanh, N.Q. Khai, N. Tri, T.T. Nguyen, X.T. Bui, K.P.H. Huynh, Enhanced heterogeneous Fenton degradation of p-nitrophenol by Fe_3O_4 nanoparticles decorated cellulose aerogel from banana stem, Environ Technol Innov. 30 (2023). https://doi.org/10.1016/j.eti.2023.103041.

[326] Q. Ai, Z. Yuan, R. Huang, C. Yang, G. Jiang, J. Xiong, Z. Huang, S. Yuan, One-pot co-precipitation synthesis of Fe_3O_4 nanoparticles embedded in 3D carbonaceous matrix as anode for lithium ion batteries, J Mater Sci. 54 (2019) 4212–4224. https://doi.org/10.1007/s10853-018-3141-3.

[327] Q. An, F. Lv, Q. Liu, C. Han, K. Zhao, J. Sheng, Q. Wei, M. Yan, L. Mai, Amorphous vanadium oxide matrixes supporting hierarchical porous Fe_3O_4/graphene nanowires as a high-rate lithium storage anode, Nano Lett. 14 (2014) 6250–6256. https://doi.org/10.1021/nl5025694.

[328] C. Tan, N. Gao, Y. Deng, J. Deng, S. Zhou, J. Li, X. Xin, Radical induced degradation of acetaminophen with Fe_3O_4 magnetic nanoparticles as heterogeneous activator of peroxymonosulfate, J Hazard Mater. 276 (2014) 452–460. https://doi.org/10.1016/j.jhazmat.2014.05.068.

[329] P. Dhar, A. Kumar, V. Katiyar, Magnetic Cellulose Nanocrystal Based Anisotropic Polylactic Acid Nanocomposite Films: Influence on Electrical, Magnetic, Thermal, and Mechanical Properties, ACS Appl Mater Interfaces. 8 (2016) 18393–18409. https://doi.org/10.1021/acsami.6b02828.

[330] A. Norouzian Baghani, A.H. Mahvi, M. Gholami, N. Rastkari, M. Delikhoon, One-Pot synthesis, characterization and adsorption studies of amine-functionalized magnetite nanoparticles for removal of Cr (VI) and Ni (II) ions from aqueous solution: kinetic, isotherm and thermodynamic studies, J Environ Health Sci Eng. 14 (2016). https://doi.org/10.1186/s40201-016-0252-0.

[331] J. Lv, G. Zhang, H. Zhang, F. Yang, Exploration of permeability and antifouling performance on modified cellulose acetate ultrafiltration membrane with cellulose

nanocrystals, Carbohydr Polym. 174 (2017) 190–199. https://doi.org/10.1016/j.carbpol.2017.06.064.

[332] L. Bai, N. Bossa, F. Qu, J. Winglee, G. Li, K. Sun, H. Liang, M.R. Wiesner, Comparison of Hydrophilicity and Mechanical Properties of Nanocomposite Membranes with Cellulose Nanocrystals and Carbon Nanotubes, Environ Sci Technol. 51 (2017) 253–262. https://doi.org/10.1021/acs.est.6b04280.

[333] A. Moslehyani, A.F. Ismail, M.H.D. Othman, T. Matsuura, Design and performance study of hybrid photocatalytic reactor-PVDF/MWCNT nanocomposite membrane system for treatment of petroleum refinery wastewater, Desalination. 363 (2015) 99–111. https://doi.org/10.1016/j.desal.2015.01.044.

[334] S. Zhang, R. Wang, S. Zhang, G. Li, Y. Zhang, Development of phosphorylated silica nanotubes (PSNTs)/polyvinylidene fluoride (PVDF) composite membranes for wastewater treatment, Chem Eng Journal. 230 (2013) 260–271. https://doi.org/10.1016/j.cej.2013.06.098.

[335] L.Y. Susan, S. Ismail, B.S. Ooi, H. Mustapa, Surface morphology of PVDF membrane and its fouling phenomenon by crude oil emulsion, J of Water Process Eng. 15 (2017) 55–61. https://doi.org/10.1016/j.jwpe.2016.05.013.

[336] M.A. Masuelli, Ultrafiltration of oil/water emulsions using PVDF/PC blend membranes, Desalination Water Treat. 53 (2015) 569–578. https://doi.org/10.1080/19443994.2013.846539.

[337] T. Rajasekhar, M. Trinadh, P. Veera Babu, A.V.S. Sainath, A.V.R. Reddy, Oil–water emulsion separation using ultrafiltration membranes based on novel blends of poly(vinylidene fluoride) and amphiphilic tri-block copolymer containing carboxylic

acid functional group, J Memb Sci. 481 (2015) 82–93. https://doi.org/10.1016/j.memsci.2015.01.030.

[338] Y. Wang, X. Chen, J. Zhang, J. Yin, H. Wang, Investigation of microfiltration for treatment of emulsified oily wastewater from the processing of petroleum products, Desalination. 249 (2009) 1223–1227. https://doi.org/10.1016/j.desal.2009.06.033.

[339] X.S. Yi, S.L. Yu, W.X. Shi, S. Wang, L.M. Jin, N. Sun, C. Ma, L.P. Sun, Separation of oil/water emulsion using nano-particle (TiO_2/Al_2O_3) modified PVDF ultrafiltration membranes and evaluation of fouling mechanism, Water Sci and Tech. 67 (2013) 477–484. https://doi.org/10.2166/wst.2012.565.

[340] S. Zinadini, A.A.L. Zinatizadeh, M. Rahimi, V. Vatanpour, Magnetic field-augmented coagulation bath during phase inversion for preparation of $ZnFe_2O_4$/SiO_2/PES nanofiltration membrane: A novel method for flux enhancement and fouling resistance, J of Indus and Eng Chem. 46 (2017) 9–18. https://doi.org/10.1016/j.jiec.2016.08.005.

[341] T. Sun, Y. Liu, L. Shen, Y. Xu, R. Li, L. Huang, H. Lin, Magnetic field assisted arrangement of photocatalytic TiO_2 particles on membrane surface to enhance membrane antifouling performance for water treatment, J Colloid Interface Sci. 570 (2020) 273–285. https://doi.org/10.1016/j.jcis.2020.03.008.

[342] J. Dasgupta, S. Chakraborty, J. Sikder, R. Kumar, D. Pal, S. Curcio, E. Drioli, The effects of thermally stable titanium silicon oxide nanoparticles on structure and performance of cellulose acetate ultrafiltration membranes, Sep Purif Technol. 133 (2014) 55–68. https://doi.org/10.1016/j.seppur.2014.06.035.

Appendix I

The basic cost estimation for the fabrication of 1 m^2 of PVDF/CNC/ and PVDF/FeCNC membrane is presented here. Rajendran N. et al. [14] carried out a detailed techno-economic analysis and life cycle assessment of CNC production from a wood-based source by acid hydrolysis method. Their results indicated that CNC fabricated using acid recovery process was economically more profitable than without the acid recovery process, and the total cost of CNC was found to be approximately Rs 800/kg. Considering this cost of CNC for further calculations, the cost of FeCNC was found to be Rs 9135/kg.

Table A1: Approximate Market cost of different raw materials used for fabrication of FeCNC and membrane.

Raw materials	**Approximate Cost (Rs)**
PVDF	1200/kg
CNC	800/kg
FeCNC	9100/kg
PEG	100/kg
DMF	70/L
$FeCl_3$	30/kg
$FeCl_2$	150/kg
NH_3 solution	20/L

Table A2: Cost of chemicals to convert 1kg CNC to FeCNC

	Rate (Rs)	**Amount of chemicals required to convert 1 kg CNC to FeCNC**	**Amount (Rs)**
CNC	800/kg	1 kg	800
$FeCl_3$	30/kg	2 kg	60
$FeCl_2$	150/kg	0.5 kg	75
NH3 solution	20/L	50 L	1000
Total Cost required			**1935**

The total amount required for 1 kg of chemicals (PVDF, CNC, DMF and PEG) required for the fabrication of PVDF/CNC membrane is Rs 228.1, and the PVDF/FeCNC membrane is Rs 477.1.

Table A3: Total cost of 1 kg of chemicals required to fabricate PVDF/CNC and PVDF/FeCNC membranes

Basis: 1 kg					
Composition (wt%)	**PVDF (12%)**	**CNC/FeCNC (3%)**	**DMF (83%)**	**PEG (2%)**	**Total**
Quantity (g)	120	30	830	20	1000
Cost of PVDF/CNC membrane (Rs)	144	24	2	58.1	228.1
Cost of PVDF/FeCNC membrane (Rs)	144	273	2	58.1	477.1

A membrane of size 0.1 m^2 and 100 µm thickness can be produced from ~20 g of solution. Therefore, 200 g is required to produce a 1 m^2 thickness of 100 µm PVDF/CNC membrane, amounting to Rs 45.62 and Rs 95.42 for PVDF/FeCNC membrane.

Table A4: Total cost of production for 1 m^2 of PVDF/CNC and PVDF/FeCNC membrane

Total amount of Chemical (g)	**PVDF/CNC membrane, Cost (Rs)**	**PVDF/FeCNC membrane, Cost (Rs)**
1000	228.1	477.1
200	45.62	95.42

A basic cost estimation, considering the raw material cost only, is mentioned in the above discussion. However, the total cost estimation involves the consideration of various factors like cost associated with raw materials, manpower, power consumption, equipment and many other associated factors, which may vary at large scales. This needs to be evaluated at the pilot and industrial scales to predict the actual cost, which can be a scope for future research.